

STUDIES ON DRIVEN DUST VORTEX FLOW DYNAMICS IN DUSTY PLASMA

By

LAISHRAM MODHUCHANDRA SINGH

PHYS06201204008

Institute for Plasma Research, HBNI, Gujarat, India

A thesis submitted to the

Board of Studies in Physical Sciences

In partial fulfillment of requirements

for the Degree of

DOCTOR OF PHILOSOPHY

of

HOMI BHABHA NATIONAL INSTITUTE

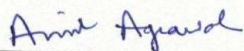


December 2017

Homi Bhabha National Institute

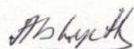
Recommendations of the Viva Voice Committee

As members of the Viva Voice Committee, we certify that we have read the dissertation prepared by **Laishram Modhuchandra Singh** entitled "STUDIES ON DRIVEN DUST VORTEX FLOW DYNAMICS IN DUSTY PLASMA" and recommend that it may be accepted as fulfilling the dissertation requirement for the award of Degree of Doctor of Philosophy.



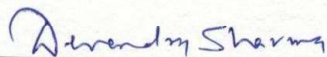
Examiner - Prof. Amit Agrawal

Date : 26 December 2017



Chairman - Prof. Abhijit Sen

Date : 26 December 2017



Guide/Convener - Dr. Devendra Sharma

Date : 26 December 2017



Member - Prof. Subroto Mukherjee

Date : 26 December 2017



Member - Prof. Prabal K. Chattopadhyay

Date : 26 December 2017

Final approval and acceptance of this dissertation is contingent upon the candidate's submission of the final copies of the thesis to HBNI.

I hereby certify that I have read this dissertation prepared under my direction and recommend that it may be accepted as fulfilling the thesis requirement.

Date: 26/12/2017

Place: Gandhinagar



Guide

STATEMENT BY AUTHOR

This dissertation has been submitted in partial fulfillment of requirements for an advanced degree at Homi Bhabha National Institute (HBNI) and is deposited in the Library to be made available to borrowers under rules of the HBNI.

Brief quotations from this dissertation are allowable without special permission, provided that accurate acknowledgement of source is made. Requests for permission for extended quotation from or reproduction of this manuscript in whole or in part may be granted by the Competent Authority of HBNI when in his or her judgement the proposed use of the material is in the interests of scholarship. In all other instances, however, permission must be obtained from the author.



Laishram Modhuchandra Singh

DECLARATION

I, hereby declare that the investigation presented in the thesis has been carried out by me. The work is original and has not been submitted earlier as a whole or in part for a degree / diploma at this or any other Institution / University.



Laishram Modhuchandra Singh

List of publications arising from the thesis

Peered reviewed Journal publications

1. *Dynamics of a confined dusty fluid in a sheared ion flow*,
M. Laishram, D. Sharma and P. K. Kaw, *Physics of Plasmas* 21, 073703 (2014).
2. *Analytic structure of a drag-driven confined dust vortex flow in plasma*,
M. Laishram, D. Sharma and P. K. Kaw, *Phys. Rev. E* 91, 063110 (2015).
3. *Nonlinear effects in the bounded dust-vortex flow in plasma*,
M. Laishram, D. Sharma, Prabal K. Chattopadhyay and P. K. Kaw,
Phys. Rev. E 95, 033204 (2017).

Peered reviewed conference publications

1. *Flow characteristics of bounded self-organized dust vortex in complex plasma*,
M. Laishram, D. Sharma, Prabal K. Chattopadhyay and P. K. Kaw,
(*AIP Conference Proceedings* (2017), accepted, In press).

To be submitted for publications

1. *Sequential equilibrium of co-rotating dust vortices in sheared streaming flow of plasma*, M. Laishram, D. Sharma, and P. K. Kaw, (*draft under preparation*).



Laishram Modhuchandra Singh

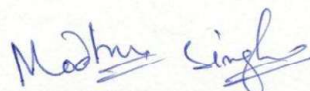
List of Conference/Schools participated :

International Conferences :-

1. 33th International Conference on Phenomena in Ionized Gases (ICPIG), from 9 to 14 July 2017, Estoril, Portugal.
2. 8th International Conference on the Physics of Dusty Plasmas- ICPDP, May-2017, Prague, Czech Republic.
3. EMN meeting on Microfluidics and Nanofludics, April-2016, World Trade Center, Dubai, UAE.
4. Asian Plasma Fusion Association(APFA) meeting, Ahmadabad, December-2015, Gujarat, India.
5. CPP-IPR workshop on linear Tokamak Diverter Simulations, November-2014, Guwahati, India.
6. 7th International Conference on the Physics of Dusty Plasmas - ICPDP, 2014, Delhi, India.

National Conferences :-

1. National Symposium on Plasma Science and Technology, December- 2016, Tamil-Nadu, India.
2. National Symposium on Plasma Science and Technology, December-2015, Kolkata, India.
3. DST-SERB School on Tokamak and Magnetized Plasma Fusion, February-2013, IPR, Gujarat, India.
4. National Symposium, Indian Physics and Mega Projects, February-2009, Delhi University, Delhi, India.



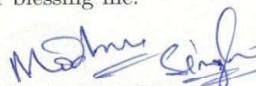
Laishram Modhuchandra Singh

DEDICATIONS

*Dedicated to
my family
and
friends*

ACKNOWLEDGEMENTS

I wish to thank my advisers Dr. Devendra Sharma for his invaluable guidance, intellectual support, encouragement, inspiration and enthusiasm, which made this research work possible. I am indebted to late Prof. P. K. Kaw for his continuous encouragement and providing me with an invaluable insight of the subject of my entire research work. I am always greatfull to both my guides for their tremendous supports, suggestions and guidances. I also would like to thank my Doctoral Committee members Prof. Abhijit Sen, Prof. P. K. Chattopadhyay and Prof. S. Mukherjee for tremendous valuable discussions and supports up to now. I also would like to thank Prof. S. Mukherjee, Prof. R. Ganesh, Prof. Sudip, Prof. Joydeep, Dr. A Chattopadhyay, Dr. M Kundu, Dr. Mainak, Dr. V. P. Anita, Dr. Santanu Karkari, Dr. G.Ravi and Dr. Ramasubramanian and other academic members for their encouragement, advises and supports in academic affairs since the interaction during the first year course work. Their experiences, friendly and spirited support and guidances has been the inspiration in IPR. I convey my thanks to the library staff, computer center staff, canteen staff, medical support, security staff and whole administrative staff of IPR for their kind cooperation through the research career. I will always remember those wonderful days in IPR Hostel, well maintaining facilities with greenly environment, various sport facilities through out the years which help me maintaining energetic and healthy dynamic life during stay in IPR. The hostel life with the football team, the volleyball team, the evening tea party with my friends and colleagues will be memories for years. I sincerely thanks you all for being well wishers and invaluable supports during last five years. At last, I would like to thank my family for their continuous support, wishes and encouragement all the time. This thesis would not have been possible without their love, support and confidence on me. I thank God for blessing me.


Laishram Modhuchandra Singh

Contents

Synopsis	5
List of Figures	13
1 Introduction	19
1.1 Introduction to dusty plasmas and driven dust vortices	24
1.1.1 Dusty plasmas	25
1.1.2 Phases of dusty plasma medium	26
1.1.3 Occurrence and applications of dusty plasmas	28
1.2 Confined dust flow as driven complex system	30
1.2.1 Experimental recovery of driven dust vortex solutions . . .	31
1.2.2 Dynamical equivalence with natural complex flows	32
1.3 Brief review of studies of existing dust vortex flow in plasma	33
1.4 The hydrodynamic approaches to dust-fluid dynamics	36
1.4.1 Governing equations in the Navier-Stokes fluid regime	36
1.4.2 Governing equations in the viscoelastic fluid regime	37
1.5 Thesis outline	38
2 Hydrodynamic formulation of dust vortex flow in plasma	45
2.1 Introduction	45
2.2 2-D Hydrodynamic formulation	48
2.2.1 Model setup relevant to laboratory dusty plasma experi- ments	49
2.2.2 Conservation equations in 2D cylindrical setup	50
2.2.3 The streamfunction formulation in curvilinear setup	52
2.2.4 Boundary conditions	55
2.2.5 Normalization, Scaling and Parameter regimes	56
2.3 Bounded dust flow equilibria: monotonic drive	57

2.3.1	Dust circulation driven by cosine flow field of the ions . . .	58
2.3.2	Dust Streamfunction and streamlines	59
2.3.3	Effect of ion drag coefficient ξ on the dust circulation strength	61
2.3.4	Effect of neutral friction ν on dust circulation	63
2.3.5	Effect of kinematic viscosity μ on dust vortex motion	64
2.3.6	Dust boundary layer and its characterization	65
2.4	Bounded dust flow equilibria: non-monotonic drive	68
2.4.1	Drive by a localized Gaussian plasma stream	68
2.4.2	Multiple counter-rotating dust vortex formation	69
2.4.3	Radial shift and emergence of a counter rotating vortex . .	71
2.5	Summary and conclusions	73
3	Analytic structure of confined and driven dust vortex flows	79
3.1	Introduction	79
3.2	2D hydrodynamic dust vortex formulation	82
3.2.1	Construction of analytic boundary value problem	85
3.2.2	Boundary conditions and appropriate eigenvectors	85
3.2.3	Eigenvalues of the operator F	87
3.2.4	Analytic form of the boundary conditions and spectral limit	90
3.3	Solutions of the flow field eigenvalue problem	91
3.3.1	Radial eigenmodes of the driver field	92
3.3.2	Dust streamfunction and streamlines	93
3.3.3	Dust vortex flow with increasing radial driver mode number	95
3.3.4	Radial mode spectrum and its characteristics	97
3.4	Dust boundary layer and parameters affects	100
3.4.1	Characterization of dust boundary layer width	100
3.4.2	Characterization of the Reynolds number	101
3.4.3	Scaling laws for dust boundary phenomena	102
3.5	Summary and conclusions	106

4	Nonlinear effects in the bounded dust vortex flow in plasma	111
4.1	Introduction	111
4.2	2D nonlinear hydrodynamic approach to dust vortex flow	113
4.2.1	Definition and mapping of the boundary segments	114
4.2.2	Nonlinear conservation equations in curvilinear set up	116
4.3	Iterative numerical solution procedure	118
4.3.1	The technique of successive over-relaxation	118
4.3.2	Benchmark of the numerical formulation	121
4.3.3	Emerging nonlinear characteristics of the vortex flow	125
4.4	Nonlinear dust vortex flow solutions	126
4.4.1	Persistent uniform vorticity solutions at high Re	130
4.4.2	Boundary layer separation and secondary vortices	131
4.4.3	Boundary separation as structural bifurcation	135
4.4.4	Velocimetric prescription of the dust viscosity	138
4.5	Summary and conclusions	140
5	Co-rotating multiple vortex equilibria in nonlinear regime	143
5.1	Introduction	143
5.2	Vortex flow at higher domain aspect ratio	146
5.2.1	Vortex structure replication for domain aspect ratio L_z :	
	$L_r = 2$	147
5.2.2	Critical topological modification of 2D vortex structures	149
5.3	Generation of co-rotating vortex sequence for higher aspect ratio	150
5.3.1	Recovery of multiple co-rotating vortices in the experiments	152
5.4	Characteristics of driven dust flow with fractional domain aspect ratio	155
5.4.1	Dependence on changing domain aspect ratio	155
5.5	Continued stability by structural bifurcation	158
5.6	Summary and conclusions	160

6	Conclusion and future work	165
6.1	Main conclusions of the thesis	166
6.2	Future work	177
	Appendix	179
A	Introduction to relevant fluid and flow properties	181
A.1	Equations for fluid dynamics	183
A.2	Viscoelastic fluids	184
A.3	Incompressible hydrodynamics	184
A.4	Vortex structures and vorticity	186
A.5	Potential flow and streamfunction.	187
B	Overview of complex (dusty) plasmas	191
B.1	Various forces on dust particles	196
B.1.1	Force of gravity	197
B.1.2	Thermophoretic Force	197
B.1.3	Ion-Dragging Force	198
B.1.4	Neutral-Collision Force	199
B.1.5	Electromagnetic Force	200
B.2	Descriptive methods for dusty plasma	201
	Bibliography	216

Synopsis

The dust clouds electrostatically suspended in a quasineutral plasma show characteristics of various phases of matter, ranging from crystalline to fluids, depending on the parameter of coupling between dust grains ($\Gamma = \text{Potential Energy} / \text{Kinetic Energy}$) and the screening parameter ($\kappa = d/\lambda_D$) which is the ratio of average inter particles separation to the plasma Debye length [1–4]. Dusty plasmas with coupling parameters of $10 \leq \Gamma \leq 100$ over a range of fixed screening parameter κ behave like complex fluids [4–6]. When confined by an effective potential and subjected to external drivers of fluid flow, the suspended dust medium exhibits various self organized flow patterns like vortex and shear layer formation apart from collective dust excitations extensively studied in the existing dusty plasma literature [7–13]. Such patterned steady-state equilibria of the complex dust fluid represent a large category of driven-dissipative complex dynamical systems that continuously operate away from their thermodynamic equilibrium [14, 15]. The flow dynamics of dusty plasmas is therefore an attractive and accessible means studying of many complex system. This is in addition to the fact that the steady state low Reynolds number flow of the dust medium also shares its dynamical regime with a variety of natural flow systems, including, swimming of micro-organisms, bacterial turbulence, flow of viscoelastic fluids [16–18], as well as many robust life-saving biotechnology applications based on networks of microchannels to achieve enhanced rates of mixing, reactions, and conduction of fluid flows, essentially in the absence of the macroscopic turbulence [19–21]. Whether the spectacular dust flow dynamics observed in a variety of recent dusty plasma experiments, often accessible by velocimetric techniques [12, 13], can be employed to study complex nonequilibrium thermodynamic systems is subject to availability of a systematic formulation of the dusty plasma in its fluid-like dynamical regime. The focus of studies presented in this thesis is therefore on the aspects of fluid-dynamical analysis of a driven confined

dust fluid suspended in a quasineutral plasma.

Provided below is a more systematic chapter-wise analysis of the vortex motion of the dust clouds and its characteristics addressed in the present thesis.

Chapter-1: Introduction

This chapter introduces the fundamental concepts of dusty plasmas which, sometime, are also addressed as complex plasmas [22]. An overview of topics of research in dusty plasmas, which are of close relevance to the present study, is also presented in this part of the chapter [23]. The subsequent sections provides a detail report of literature survey on the topics of the relevant research and general motivations of the present study. The content of the chapter covers discussion on experimental as well as theoretical research work on the dust flow dynamics and a road-map for the present studies carried out on this subject. Based on the existing body of work on the subject referred in the first part of the chapter, the conclusion of the chapter lists certain outstanding issues in the subject and describes the issues that are addressable within the scope of the present work. The chapter also provides brief chapter-wise summary of the study covered in the thesis and summary of the main results presented in rest of the chapters.

Chapter-2: Hydrodynamic formulation of dust vortex flow in plasma

In this chapter we developed and analyzed a hydrodynamic formulation, considering a more relevant cylindrical setup with boundaries in \hat{z} direction, for the driven flow of the dust fluid confined in an effective 2-D potential well and in dynamic equilibrium with a combination of an unconfined streaming flow of driving fluid and a stationary background fluid resisting the driven flow. The analytic form of the hydrodynamic model comprising the Navier-Stokes equation [23] and dust fluid continuity equation is provided and the conditions for its applicability are discussed obtaining an simplified essential model for the confined dust setup [24].

The vorticity-streamfunction formulation, suitable for analyzing vortex flows, is introduced in curvilinear setup relevant to experimental configurations where dust flow dynamics with a special toroidal symmetry is recovered [11, 12]. The 2D solutions obtained for an azimuthally symmetric cylindrical setup are presented for the driving flow profiles having both spatially distributed and localized flows and their associated shear intensities. The solutions show a finite circulation in the driven flow field of the dust coupled to a driving flow field, having finite vorticity, via a mutual drag. The solutions of the hydrodynamic formulation are obtained with appropriate boundary conditions applied to the confined dust fluid [24]. A detailed analysis is presented of the dependence of dust dynamics and flow field on the various parameters, namely, dust viscosity μ , coefficient of ion drag on the dust particles ξ and the coefficient of friction between dust and the neutral gas ν .

Two cases, (i) with profiles of the driving plasma flow having a nonlocal distributed shear and (ii) having a localized intensity and shear, were analyzed by obtaining solutions that show finite circulations and boundary layer effects. The solutions with a localized driver flow intensity are further explored to show that the shift in the localization of the driving flow at various smaller to larger radius features a transition from single to multiple vortex structures with due flux conservation properties in the cylindrical geometry [12, 24]. The cases analyzed in the present study highlight the situations in systems where a dynamic flow equilibrium exists in a cylindrical geometry with boundaries in the z direction. This includes dusty plasma setups where such 2D dust confining boundaries are present due to an effective potential, generated by a combination of gravity and electrostatic effects, and where an unbounded (streaming) driving plasma flow exists, either in the form of a wider beam or in a filamented state, across the boundaries. The case-wise analysis shows that the appearance and properties of boundary layers in dust flow are subject to the structure of the boundary as well as its capacity to interact with or influence the dust flow adjacent to the boundary and in the

interior via the momentum diffusion.

Chapter-3: Analytic structure of confined and driven dust vortex flows

In this chapter we have addressed certain analytical aspects of the majority of bounded setups of the dust medium suspended in the plasmas and subjected to neutral friction. We mainly address the issues that for the dust dynamics subjected to a background high Reynolds number driving plasma flow, (i) what are the characteristic mathematical attributes of the formulation and its 2D driven dust flow structure solutions in the linear limit which admits low to moderate dust flow Reynolds numbers, and (ii) how do the spectral properties of the driver flow influence equilibrium mode number spectrum of the driven dust flow when it is subjected to important boundary phenomena. For the analysis of driven confined dust fluid vortex flow, a boundary value problem is constructed in a nonplanar, cylindrical geometry in terms of dust flow streamfunction [25].

The presented analytic treatment uses the description of the vorticity of both the dust and of the driving plasma in terms of strength of eigenmodes of a curvilinear bounded setup in the modenumber space. The analytic solutions for the dust flow are obtained by treating the boundary value formulation as an eigenvalue problem, and using the linearly independent set of Bessel functions as eigenmodes that allows both driving and driven flows to follow valid flux conservation and have a multiple scale vorticity spectrum [25]. This choice allows a multiple scale plasma flow field to produce a vorticity scale spectrum for the driven dust flow field, essentially non-identical to the driver and the one that accommodates the effects of boundary with the stationary dust. The spectral characteristics of dust vorticity at higher mode numbers is shown to be determined predominantly by the boundary effects that have additional impact when combined with variation in the usual physical parameters of the dust medium, including the kinematic viscosity and the coefficients of neutral friction and ion drag acting on the dust fluid.

Among these effects is the formation of a boundary layer whose width depends on the viscosity and allows the dust flow to be in low Reynolds number regime up to considerably smaller values of the coefficient of the dust viscosity.

With the effect of increasing complexity in the driver setup resolved in the orthogonal eigenfunctions and characterized individually with increasing mode number, the independence of effects associated with boundary could be identified and shown to have definite exponents of variation with respect to the medium viscosity μ . While the effective boundary layer width is recovered to scale with $\mu^{1/3}$, the effective Reynolds number for the setup is recovered to scale with $\mu^{-2/3}$ [25]. Both these orderings are seen to be obscured by an increasing spatial complexity of the driving mechanism. The degree of the impact of this complexity is estimated by systematically characterizing the effect of individual driver flow modes in various cases with increasing value of the cylindrical mode number. The chapter concludes by discussing the limitations of linear solutions. Also discussed are the aspect that how and why with the availability of the linear streamfunction formulation and its solutions, an interesting but nontrivial extension to non-linear limit highly relevant to a variety of natural systems, must be technically accessed.

Chapter-4: Nonlinear effects in the bounded dust vortex flow in plasma

In this chapter the nontrivial extension is made to the nonlinear regime of the dust vortex flow formulation. By producing the nonlinear solutions using a 2D iterative numerical procedure, the nonlinear properties of a volumetrically driven 2D dust vortex flow of a confined dust fluid suspended in a plasma are studied. Motivated by toroidally symmetric flow formation in experiments and signatures of nonlinear nature of poloidal flow dynamics at higher dust velocities therein [11, 12], 2D nonlinear equilibrium solutions of the vortex flow are obtained in a toroidally symmetric domain [26]. The relevance of the nonlinear solution is described to a large number of observations in dusty plasmas setups where a vigorous dust vortex

flow dynamics is observed with flow velocities attaining moderate to high Reynolds number values. The high Reynolds number limit confirms with the experiments where localized dust vortex are seen surrounded by regions of relatively moderate or negligible dynamical activity [26] usually absent in the linear limit of solutions for the equivalent setups [24, 25].

In agreement to observations of a dust torus where poloidal dust flow is recoverable with considerably uniform vorticity, the driven primary vortex in the present solutions is formed with almost uniform vorticity in the core, surrounded by region a strong variation of vorticity value and oscillatory nature of streamfunction. The relationship between vorticity ω and product $r\psi$ is examined in the small and large Reynolds number regimes to recover independence of ω from $r\psi$ in the uniform vorticity core formed at large Reynolds number. In this limit, the core vorticity follows the curvilinear form of an integral condition given by Batchelor [27] on the regions of closed streamlines where boundary conditions are no longer usable for determination of ω in high Reynolds number regime and its analytic value remains largely indeterminate.

In presence of 2D heterogeneous boundary conditions applied to dust flow in a curvilinear coordinate system, the major nonlinear effects cause the boundary layer to separate from the domain boundary [26]. This causes the vorticity generated from the interaction with the no-slip, or frictional, boundaries to be convected away with strong flows of the primary vortices. The separation allows dynamic isolation of the regions scaling with the dimensions of small scale features of the boundary (e.g., spatial modulations or the sharp corners) and development of secondary vortices in these regions. The development of separated boundary layer is investigated as a structural bifurcation [26] where the kinematic viscosity μ assumes the role of the bifurcation parameter and the separation coincides with the bifurcation at a critical value μ^* . The bifurcation is shown to occur when the vorticity profile approaches its first zero value along the boundary at the point

where its minimum is located. This critical behavior and signatures of equivalent nonlinear vortex states in experiments indicates capacity of confined dusty plasma vortex structures to represent a class of systems that can self-stabilize by making a critical transition to a self-similar state, for example, biophysical transition during the biological cells undergoing mitosis [28]. The nonlinear scaling of the boundary layer parameters with kinematic viscosity μ is obtained and the critical value μ^* demarcating transition to nonlinear regime is identified. These two factors are shown to allow estimation of viscosity of charged fluids using appropriate scaling by identifying a structural change in flow patterns in experiments. The nonlinear dust vortex dynamics developed in this study thus offers quantitative insight and analytic framework to a number of natural systems that dusty plasmas emulate.

Chapter-5: Co-rotating multiple vortex equilibria in nonlinear regime

This chapter explores the extendibility of nonlinear solutions produced in Chapter 4 to newer regimes where the characteristics of dusty plasma flow dynamics correspond to experimentally observed dynamics of the dusty plasma vortices [13, 29, 30]. The nonlinear solutions are obtained and presented in this chapter with variation in the aspect ratio of the cross-section of the toroidal dust confinement domain (L_z/L_r). In another parameter variation, the Reynolds number of the dust flow is varied by variation in the values of the dust kinematic viscosity μ . Among the most important observations made, upon increasing the domain aspect ratio beyond $L_z/L_r = 1$ at higher Reynolds number, the smaller corotating secondary vortex produced with a scale size ratio of $1 : \sqrt{2} - 1$ with respect to larger primary core vortex, grows in its dimension and attains a size ratio $1 : 1$ as $L_z/L_r \rightarrow 2$. This dynamic replication of the original vortices is noted as a recurring process during variation of L_z/L_r , where a series of vortex replication is noted with increasing value of L_z/L_r . The correspondence between this observation and a similar observation of series of corotating vortices forming in a very

recent dusty plasma experiment [13] is described. The multiplicity of corotating vortex is discussed along with its limitation due to increasing momentum diffusion across the streamlines by increase in the aspect ratio from smaller to larger values with respect to unity. The chapter also discusses correspondence of the linear and nonlinear vortex solutions recovered in this work to the various natural flow and dynamical processes ranging from microscopic to very large scale size systems [28, 31], many of which operating away from their thermodynamic equilibrium [14] and well represented by driven-dissipative nature of the dusty plasma systems under consideration.

Chapter-6: Conclusion and future work

This chapter provides brief summary of the complete study presented in the thesis and main conclusions drawn from the results obtained in this study. The few results from the linear and nonlinear regimes of the present studies are discussed in the perspective of existing experimental and theoretical studies on the subject. The content of this chapter further identify and describe the potential areas of interest in which the present research can lead and contribute. The discussion also covers possibility of extension of applied techniques and numerical approaches for addressing more detailed and readily accessible regimes of the present formulation. Certain experimental studies are suggested for possible experimental realization of the predictions made in the present studies and verification of various theoretical estimates provided in the present study using experimental means, for example, estimate of dust dynamical viscosity using velocimetric techniques obtained in Chapter 4. Finally, the implications of present results and their applicability to address certain outstanding fundamental issues related to nonequilibrium systems and a statistical approach to their study are discussed.

List of Figures

1.1	Dust clouds with poloidal circulation in the laboratory dusty plasma experiment at IPR, by M. Kaur <i>et al.</i> , Phys. Plasmas 22 , 033703 (2015).	22
1.2	Vortex formation in the dusty plasma cloud in microgravity condition on board the International Space Station (ISS) by V. N. Tsytovich <i>et al.</i> , New Journal of Physics 5 , 66 (2003).	22
1.3	Γ and κ relation showing dusty plasma can exist at different state of matter by changing coupling parameter Γ and κ , by S. Hamaguchi <i>et al.</i> Phys. Rev. E 56 4(1997).	27
1.4	Γ and ν^* relation for various screening parameters κ showing gases and liquid phases of fluids by V. E. Fortov <i>et al.</i> Phys. Rev. Lett. 109 055002 (2012).	27
2.1	Toroidal dust cloud with poloidal circulation in the laboratory dusty plasma experiment by M. Kaur <i>et al.</i> Phys. Plasmas 22 , 033703 (2015).	49
2.2	Schematic representation of dust confined toroidally by $V(r, z)$ and driven by shear flow field $v_s(r)$ through the domain.	49
2.3	(a) Streamfunction potential and (b) corresponding streamlines or contours of $r\psi$ of the driven dust flow in rz -cross section of aspect ratio $L_z/L_r = 5$.	60
2.4	Radial profiles passing through center of circulation (r_0, z_0) for (c) Driver cosine ion flow velocity v_z , (d) Dust stream-function ψ , (e) Dust flow velocity u_r and (f) Dust flow velocity u_z for no-slip and perfect-slip boundary conditions.	61
2.5	Radial profiles at $z = z_0$ for (a) Driver cosine ion flow velocity v_z , (b) Corresponding vorticity ω_s , (c) Varying dust stream-function ψ and (d) Dust flow velocity u_z for $\xi = 0.1, 0.4, 0.7$ and $1.0 \times 10^{-5} U_0/L_r$.	62
2.6	Streamlines for the dust fluid flow in r - z cross section for varying ions dragging frequency $\xi =$ (a) 0.1, (b) 0.4, (c) 0.7, and (d) $1.0 \times 10^{-5} U_0/L_r$ and fixed $\mu = 10^{-3} U_0 L_r$, $\nu = 10^{-1} U_0/L_r$.	62
2.7	Radial profiles at $z = z_0$ for (a) Driver cosine ion flow velocity v_z , (b) Corresponding vorticity ω_s , (c) Varying dust stream-function ψ and (d) Dust flow velocity u_z for $\nu = 0.5, 2.0, 3.5$ and $5.0 \times 10^{-1} U_0/L_r$.	64

2.8	Streamlines for the dust fluid flow in r - z plane for varying neutral collision frequency $\nu =$ (a) 0.5, (b) 2.0, (c) 3.5, and (d) $5.0 \times 10^{-1} U_0/L_r$ and fixed $\mu = 10^{-3} U_0 L_r$, $\xi = 10^{-5} U_0/L_r$	64
2.9	Radial profiles at $z = z_0$ for (a) Driver cosine ion flow velocity v_z , (b) Corresponding vorticity ω_s , (c) Varying dust stream-function ψ and (d) Dust flow velocity u_z for $\mu = 0.1, 0.4, 0.7$ and $1.0 \times 10^{-3} U_0 L_r$	66
2.10	Streamlines for the dust fluid flow in r - z plane for varying kinematic viscosity $\mu =$ (a) 0.1, (b) 0.4, (c) 0.7, and (d) $1.0 \times 10^{-3} U_0 L_r$ and fixed $\xi = 10^{-5} U_0/L_r$, $\nu = 10^{-1} U_0/L_r$	66
2.11	Dependence of the separation Δr_b on the parameter μ for (a) $\xi = 0.2, 0.4, 0.6, 0.8$ and $1 U_0/L_r$ and (b) $\xi = 0.2, 0.4, 0.6, 0.8$ and $1.0 \times 10^{-4} U_0/L_r$	67
2.12	Radial profiles at $z = z_0$ for (a) Driver cosine ion flow velocity v_z , (b) Corresponding vorticity ω_s , (c) Varying dust stream-function ψ and (d) Dust flow velocity u_z for $\xi = 0.1, 0.4, 0.7$ and $1.0 \times 10^{-5} U_0/L_r$	70
2.13	Streamlines for the dust fluid flow in r - z plane for varying ions dragging frequency $\xi =$ (a) 0.1, (b) 0.4, (c) 0.7, and (d) $1.0 \times 10^{-5} U_0/L_r$ and fixed $\mu = 10^{-3} [U_0 L_r]$, $\nu = 10^{-1} U_0/L_r$	70
2.14	Radial profiles at $z = z_0$ for (a) Driver cosine ion flow velocity v_z with various peak locations r_0 . (b) Corresponding vorticity ω_s . (c) Varying dust stream-function ψ and (d) Dust flow velocity u_z for $r_0 = 0.0, 0.24, 0.42$ and $0.60 L_r$	72
2.15	Streamlines for the dust fluid flow in r - z plane for localized Gaussian ion flow at $r_0 =$ (a) 0.0, (b) 0.24, (c) 0.42, and (d) $0.60 [L_r]$ for fixed $\mu = 10^{-3} U_0 L_r$, $\xi = 10^{-5} U_0/L_r$, and $\nu = 10^{-1} U_0/L_r$	72
3.1	Schematic of the setup in the cylindrical geometry. Surface plot of an example effective confining potential $V(r, z)$ for the dust fluid (surface) is presented along with the flux conserving velocity field vector \mathbf{v} of the unconfined driving fluid in the r - z plane (arrows) and radial profile of its z -component $v_z(r)$ (2D plot).	83
3.2	Bessel function reconstruction of a known function $\omega_{sr}(r)$ with increasing number m of modes.	86

3.3	(a) 2D dust streamfunction $\psi(r, z)$ (colorbar), and corresponding dust flow streamlines, or the contours of the product $r\psi$. (b) Driver velocity v_z and corresponding Driver vorticity ω_s for single eigenmode source vorticity with $I = 1$. (c) Dust streamfunction ψ , (d) dust flow velocity u_r and (e) dust flow velocity u_z for set of fixed parameters $\mu = 0.1 U_0 L_r$, $\xi = 10^{-5} U_0 / L_r$ and $\nu = 0.1 U_0 / L_r$	94
3.4	2D dust streamfunction $\psi(r, z)$ for single eigenmode source vorticity with (a) $I = 1$ (c) $I = 3$ and (e) $I = 5$. Dust flow streamlines, or the contours of the product $r\psi$, for single eigenmode source vorticity with (b) $I = 1$ (d) $I = 3$ and (f) $I = 5$	96
3.5	Source flow velocity profile at $z = 0$ for (a) $I = 1$ (d) $I = 3$ and (g) $I = 5$. Dust flow velocity profile at $z = 0$ for (b) $I = 1$ (e) $I = 3$ and (h) $I = 5$. Intensity spectrum for the range of mode-number m at $z = 0$ for (c) $I = 1$ (f) $I = 3$ and (i) $I = 5$	96
3.6	Radial profiles of dust velocity u normalized to the corresponding maximum values u_{\max} appearing at the the edge of the boundary layer whose width shrinks with decreasing μ values, ranging from 10^{-1} to $10^{-7} U_0 L_r$ arranged on a logarithmic scale.	98
3.7	Intensity spectrum for the solutions with $I = 1$, normalized to the intensity a_1^2 of the dust vorticity mode-number $m = 1$ for the cases with the value of viscosity coefficient $\mu = 10^{-1}, 10^{-3}, 10^{-5}$ and $10^{-7} U_0 L_r$	98
3.8	(a) Width Δr_b of the boundary layer and (b) values of the Reynolds number Re , for $I = 1$ and the cases with various values of ξ	100
3.9	(a) Dependence on μ of width Δr_b of the boundary layer with various values of ξ for the cases with the driver mode number (a) $I = 1$ (b) $I = 3$ and (c) $I = 5$. The broken line represents the dependence $\Delta r_b \propto \mu^{1/3}$	103
3.10	(a) Dependence on μ of the Reynolds number Re with various values of ξ for the cases with the driver mode number (a) $I = 1$ (b) $I = 3$ and (c) $I = 5$. The broken line represents the dependence $\text{Re} \propto \mu^{-2/3}$	103
4.1	(a) Toroidal dust cloud with poloidal circulation in the laboratory dusty plasma experiment by M. Kaur <i>et al.</i> Phys. Plasmas 22 , 093702 (2015). (b) the dust flow velocity distribution and (c) the dust flow vorticity distribution, obtained from the Particle Imaging Velocimetry (PIV) analysis of the image data.	115

4.2	Schematic representation of the toroidal dust cloud with vortex motion and mapping of the boundary of its cross-section to a toroidal domain of rectangular cross-section accommodated in the cylindrical geometry of the present nonlinear solutions. Segments AB , BC , CD and DA , of the cloud map to the corresponding sides of the rectangle $ABCD$	115
4.3	(a) Single axial mode driver velocity profile $J_0(\alpha_1 r/R)$ at $z = 0$, (b) 2D dust streamfunction $\psi(r, z)$, and (c) Corresponding streamlines for the dust fluid flow in r - z plane with $\mu = 1 \times 10^{-3} U_0 L_r$, $\xi = 1 \times 10^{-5} U_0/L_r$ and $\nu = 1 \times 10^{-1} U_0/L_r$	123
4.4	Comparison between Analytic and Numerical results of $u_r(r_0, z)$, $u_z(r, z_0)$ for fixed system parameters, $\xi = 1 \times 10^{-5} U_0/L_r$, $\nu = 1 \times 10^{-1} U_0/L_r$, fixed single axial mode radial $I = 1$ driving field and varying $\mu = 10^{-1}$ to $10^{-5} U_0 L_r$ in low Reynolds numbers linear regime $\text{Re} \ll 1$	123
4.5	(a) Single axial mode driver velocity profile $J_0(\alpha_1 r/R)$ at $z = 0$. And corresponding streamlines for the dust fluid flow in r - z plane with aspect ratio ($L_z/L_r = 2$) for (b) $\mu = 1 \times 10^{-3} U_0 L_r$ and (c) $\mu = 3 \times 10^{-5} U_0 L_r$, having fixed other system parameters at $\xi = 1 \times 10^{-5} U_0/L_r$ and $\nu = 1 \times 10^{-1} U_0/L_r$	125
4.6	Profiles of the (a) driver velocity v , and (b) driver vorticity ω_s which are uniform along \hat{z} and $\hat{\phi}$	127
4.7	(a) Dust flow streamlines, strength of (b) diffusive term $\nabla^2 \omega$ and (c) nonlinear term $\mathbf{u} \cdot \nabla \omega$ plotted from top to bottom for the values of dust viscosity $\mu = 1 \times 10^{-3}$, 1×10^{-4} , 1×10^{-5} and $8 \times 10^{-7} U_0 L_r$, respectively, where the values $\nu = 0.01 U_0/L_r$ and $\xi = 0.001 U_0/L_r$ are used for other fixed parameters.	128
4.8	(a) Dust flow streamlines superimposed by straight lines and contours used to draw profiles of ω as function of $r\psi$ (b) vorticity ω as function of $r\psi$ along the straight line segments joining vortex center to domain vortices and (c) that along the indicated contours. The profiles correspond to $\mu = 10^{-3} U_0 L_r$, $\xi = 0.001 U_0/L_r$ and $\nu = 0.01 U_0/L_r$	132

4.9	(a) Dust flow streamlines superimposed by straight lines and contours used to draw profiles of ω as function of $r\psi$ (b) vorticity ω as function of $r\psi$ along the straight line segments joining vortex center to domain vortices and (c) that along the indicated contours. The profiles correspond to $\mu = 8 \times 10^{-7} U_0 L_r$, $\xi = 0.001 U_0/L_r$ and $\nu = 0.01 U_0/L_r$	132
4.10	(a) Magnitude of the diffusion term and (b) Magnitude of the nonlinear term plotted for $\mu = 8 \times 10^{-7} U_0 L_r$, $\xi = 0.001 U_0/L_r$ and $\nu = 0.01 U_0/L_r$ in a domain confinement limited to larger r values.	134
4.11	The vorticity surface plots for values of parameter (a) $\mu = 10^{-3}$, (b) 10^{-4} , (c) 10^{-5} and (d) $10^{-6} U_0 L_r$. The developing points of separation are indicated by arrows on segments AB and BC	135
4.12	(a) The normalized vorticity profile along the no-slip boundary BC for various values of parameter μ . The point of separation and associated bifurcation is indicated by an arrow where profile corresponding to critical value $\mu^* \sim 10^{-5} U_0 L_r$ has a single degenerate singular point. (b) The nonlinear boundary layer scaling with dust viscosity μ . The profile shows a change of regime at the critical μ^*	137
4.13	characterization of μ dependence on the boundary layer flow velocity u and the characteristic length scale along the streamlines $L_{ }$	139
5.1	Schematic representation of the toroidal dust cloud with vortex motion and mapping of the boundary of its cross-section to a toroidal domain of rectangular cross-section accommodated in the cylindrical geometry of the present nonlinear solutions. Segments AB , BC , CD and DA , of the cloud map to the corresponding sides of the rectangle $ABCD$	145
5.2	[Effect of varying viscosity at $L_z : Lr = 2$] Streamlines for the dust fluid flow in r - z plane for varying (a) $\mu = 10^{-3} U_0 L_r$, (b) $\mu = 3 \times 10^{-5} U_0 L_r$ (c) $\mu = 1.8 \times 10^{-5} U_0 L_r$ and (d) $\mu = 9 \times 10^{-6} U_0 L_r$ respectively having fixed other parameters $\xi = 10^{-4} U_0/L_r$, $\nu = 10^{-3} U_0/L_r$. The corresponding cross-section profiles for (e) $r\psi(r, z_0)$, (f) $u_z(r, z_0)$ and (g) $u_r(r_0, z)$ passing through the center of the primary vortex (r_0, z_0)	148

5.3	[Shifting effect in (r_0, z_0) with varying ξ , ν and μ] Shifting in center of circulation (r_0, z_0) with changes in (a) ion dragging co-efficient ξ , (b) neutral collision frequency ν . And (c) Shifting in center of circulation (r_0, z_0) , and changes in boundary layer thickness Δr_b with varying kinematic viscosity μ	149
5.4	[Effect of varying viscosity at $L_z : L_r = 3$] Streamlines for the dust fluid flow in r - z plane, correspond to varying (a) $\mu = 10^{-3}U_0L_r$, (b) $\mu = 10^{-4}U_0L_r$, (c) $\mu = 10^{-5}U_0L_r$ respectively having fixed other parameters $\xi = 10^{-4}U_0/L_r$, $\nu = 10^{-3}U_0/L_r$	151
5.5	Uniform vorticity core region surrounded by very sharp and localized shear flows observed in toroidal dust cloud with poloidal circulation in the laboratory dusty plasma experiment by M. Kaur <i>et al.</i> Phys. Plasmas 22 , 033703 (2015)[12].	153
5.6	Steady equilibrium co-rotating vortices observed in dusty Phys. Plasmas 24 , 033703(2017) [13]. The number of vortex structures depends on the position of the observed cross-section away from the source region and the variation in input power as shown in upper and lower rows.	154
5.7	[Effect of varying viscosity at $L_z : L_r = 0.5$] Streamlines for the dust fluid flow in $r - z$ plane, correspond to varying (a) $\mu = 10^{-3}U_0L_r$, (b) $\mu = 10^{-5}U_0L_r$ and (c) $\mu = 3 \times 10^{-6}U_0L_r$ respectively having fixed other system parameters $\xi = 10^{-4}U_0/L_r$, $\nu = 10^{-3}U_0/L_r$	156
5.8	[Effect of varying system size $L_z : L_r$] Streamlines for the dust fluid flow in r - z plane, correspond to fixed $\mu = 3 \times 10^{-6}U_0L_r$, $\xi = 10^{-4}U_0/L_r$, $\nu = 10^{-3}U_0/L_r$ and varying aspect ratio (a) $L_z : L_r = 0.25$, (b) $L_z : L_r = 0.2$ and (c) $L_z : L_r = 0.125$ respectively. The corresponding cross-section profile for (d) $r\psi(r, z_0)$, (e) $u_z(r, z_0)$ and (f) $u_r(r_0, z)$ passing through the center of primary vortex (r_0, z_0)	157
5.9	Schematic of an autonomous system with vortex nonlinearity controlled periodic replication and growth of vortex.	159
B.1	Various forces on a dust particle [32].	198

1

Introduction

Complex systems are identified by their nonintuitive response to external stimuli and their capacity to adapt to their surrounding for enhanced stability and longevity. Macroscopic behavior of most of the soft matter and fluids, having rather intricate microscopic or molecular level structure, often displays complex phenomena. Studies in this thesis are conducted to formulate and analyze the fluid-like dynamics of clouds of microscopic dust particles electrostatically suspended in plasmas and capable of displaying a range of complex phenomena in various laboratory and natural settings.

Fluids, depending on their microscopic texture and constitution, let their macroscopic dynamics being described by formulations of increasing mathematical rigor (related to underlying kinetic closure and subsequent moment description [33–40]). Dust particles introduced in a plasma that tend to get heavily charged and can, in turn, be electrostatically suspended in a plasma, constitute a range of interesting fluid-phases where this microscopic inter-particle ordering is largely determined by only a limited number of externally controllable parameters of the background suspending plasma medium, often maintained in laboratories using ordinary electrical

instrumentation. The dusty plasmas therefore offer a highly customizable and easily diagnosed medium (e.g., via particle imaging velocimetry [41, 42]), realizable in rather simpler laboratory setups, for investigating many fundamental aspects of complex fluids as well as of many other extremely exotic phases of matter in the universe [22].

Out of these exotic and not so exotic possibilities, certain readily realizable phases in common dusty plasma experiments already display characteristics of many well known classes of complex systems. Apart from formulating dust vortex flow dynamics recovered in experiments, the present thesis focuses on one such class of systems in which the systems are driven to enduring nonequilibrium states by a continuing source of free energy and serve as paradigm for a wide range of living and nonliving systems [43–45]. Nonequilibrium systems of this kind form stimulated and stable patterns, and recover, as a result of interventions from surrounding to show first formal signatures of being responsive (*alive*) in clear distinction from their nonliving or purely entropy maximizing counterparts, like most museum exhibits that simply follow the Clausius’ principle [45].

These responsive systems show a vast dynamic memory by their capacity and range of response to a continuum of stimuli from their surrounding, each of which may invoke a unique response, like making them erupt into a unique pattern. In its simplest form, a behavioral transition to such a state occurs, for example, in a system of Brownian particles irreversibly diffusing through a medium [46] when they are additionally subjected to a drive by a streaming medium and simultaneously restricted in space by a confining potential or boundary. This results in a variety of their particle distributions for respective combinations of potential, boundary and flow topologies [14]. A more correlated fluid-like phase of charged micro-particles, well represented by the dust particles suspended in the plasma state of matter (or a dusty plasma) [3, 6, 47–49], shows an even larger range of patterned response both in its linear [11, 12, 24, 25] and nonlinear [26, 50] regime

of dynamics, analyzed systematically in the studies present in this thesis.

While microscopic characteristics of dusty plasmas are well-known to resemble the crystalline [51–53] to viscoelastic fluid-like media [18, 54] the overall macroscopic dynamics of its fluid-like phase represents vortex activity in many volumetrically driven complex and biophysical fluids at much accessible scales. This dynamical range potentially covers low Reynolds number life supporting dynamics of intracellular fluid or microcirculation of blood in lymphatic capillaries ($Re < 1$) [55], to high Reynolds number enormous scale circulations like Jovian great red spot ($Re > 10^2$) [31, 56]. Presented in the first part of this thesis is the first application of a 2D hydrodynamic model to these volumetrically driven spatially confined dust vortices [24] observable in many of the dusty plasma experiments. The detailed hydrodynamic analysis is done to systematically formulate the vortex dynamics of dusty plasmas observed in normal laboratory conditions (see Fig. 1.1) as well as in microgravity condition, for example, on board the international space station (ISS) [9] (see Fig. 1.2). The results obtained in the first, linear part, of the study, mainly done by numerical solutions of the developed linear model, successfully predicted and interpreted experimentally observed multiplicity of vortex in a series of observations by M. Kaur et al. [11, 24]. A more systematic and analytic approach to various advanced aspects of linear dust vortex dynamics also outlines basic scaling of boundary effect at low to moderate Reynolds number [25]. The second part of the study presented in this thesis addresses a further advanced and complete nonlinear regime of the dust vortex flows. The nonlinear studies complement the linear studies by addressing the still left out nontrivial physics of often noted transition to nonlinear regime of these vortices and extends the limits of valuable analytic prescriptions of estimates and scaling recoverable from rather easily diagnosed flow dynamics of the dust, to high Reynolds number nonlinear regimes. The remarkable aspect of a continued stability of spatially extended vortex structures via a structural bifurcation is analyzed by means of finding non-

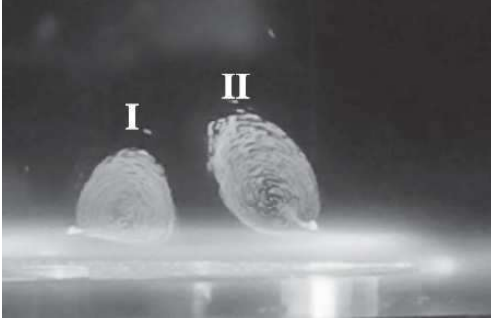


Figure 1.1: Dust clouds with poloidal circulation in the laboratory dusty plasma experiment at IPR, by M. Kaur *et al.*, Phys. Plasmas **22**, 033703 (2015).

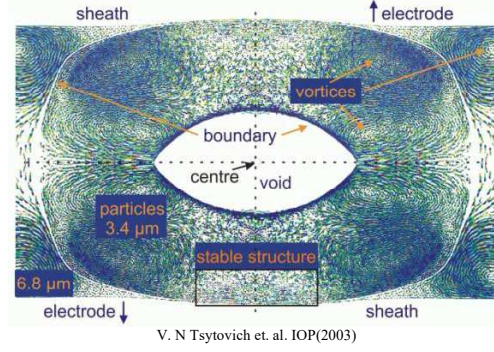


Figure 1.2: Vortex formation in the dusty plasma cloud in microgravity condition on board the International Space Station (ISS) by V. N. Tsytovich *et al.*, New Journal of Physics **5**, 66 (2003).

linear co-rotating multiple vortex solutions of the formulation, highlighting also their recovery in recent experiments, showing an identical transition.

Among the strong motivations for the nonlinear studies are the recently observed compelling nonlinear features of dust vortex dynamics [11] which promise to shed light on several less understood aspects of natural flows. For example, a nearly uniform vorticity in the core of a toroidal dust cloud observed in higher flow velocity limit resembled high Reynolds number flow phenomena at gigantic scales, such as the anticyclonic circulation associated with the Jovian great red spot [31, 56]. In a very distinct kind of nonlinear effect recovered in the advanced nonlinear solutions of the present studies, and simultaneously observed in the experiments, is generation of a sequence of multiple co-rotating vortex in the solutions of nonlinear formulation when the dust kinematic viscosity exceeds a critical threshold value. In the associated experiments reported by M. Choudhary *et al.* [13] the phenomenon strikes when total input power to the exceeds a threshold limit or when dust cloud is moved in a region of stronger plasma wind [13].

Most noticeable, from the view point of applicability to complex systems, is the fact that the nonlinear phenomena of the form displayed also by the critical dust

dynamics analyzed in this study are proving to be natural timing mechanism for biological systems with growing evidence that processes like cell division are timed by critical transitions on approaching a threshold size rather than a preprogrammed linear evolution [57]. For example, the low Reynolds number intracellular mitotic activity taking place in cytoplasmic medium examined in budding yeast shows that the cells born smaller than normal size spend longer duration in initial G1 phase until they reach a critical size for division, reproducing normal size offspring [58]. Nonlinear critical transitions thus provide a potential mechanism that monitors cell size and uses this information to regulate progression through events of the cell cycle, determining cell size and age, effectively, the fundamental limiting factors for overall evolution of the carbon based life [57, 59].

With the prime requirement of being externally driven fulfilled, an important class of complex systems is suitably represented by a fluid-like phase of the suspended dust that obeys a rather simpler microscopic ordering, for example, the one underlying an incompressible Navier-Stokes hydrodynamic model [23]. While this has been the central model for the studies presented in this thesis and the basis of successful interpretation of a series of recent experimental observations related to dust vortex flows, in the Section 1.4 of this chapter we also introduce the essential elements of microscopic structure of the dusty plasma in other regimes of its existence and suitable approaches to its respective dynamics in them. We begin this chapter by presenting in the Sec. 1.1 a brief introduction to dusty plasmas while making its sufficient detail available in Appendix B. The concept of confined dust vortex flow as paradigm for driven complex systems, mainly explored in the nonlinear part of the present studies, is introduced in Sec.1.2. A brief review of the existing studies on the subject of dust vortex dynamics is presented in Sec. 1.3. The chapter concludes by presenting, in Sec. 1.5, a chapter-wise summary of the work presented in this thesis.

1.1 Introduction to dusty plasmas and driven dust vortices

Plasma is one of the four fundamental states of matter, the others being solid, liquid, and gas. Most plasmas are the ionized form of the matter with three different components, i.e, electrons, ions and neutrals. Plasmas are formally defined as partially or fully ionized media which are electrically quasineutral and show collective behavior [60]. The plasma state of matter is generally characterized by certain parameters, such as temperature T_j , that represent the equilibrium distribution of j^{th} species with average kinetic energy $E \sim K_B T_j$, the number density n_j and the mass m_j associated with the different species in the system. The length scale given by Debye length $\lambda_{Dj} = (T_j/4\pi n_j e^2)^{1/2}$, time scale given by inverse of plasma frequency $\omega_j = (n_j e^2/m_j \epsilon_0)^{1/2}$, and a speed $c_s = \lambda_{Dj} \omega_j$ known as speed acoustic are rather more useful parameters and scales of a plasma system. Here e is the electronic charge, λ_{Dj} is Debye length which is measure of distance over which the influence of the electric field of an individual charged particle of j^{th} species is felt by other charged particles inside the plasma. Plasma frequency indicates that the internal space charge potential of j^{th} species oscillates with a characteristic frequency ω_j by virtue of its inertia. The other important characteristic frequencies are associated with the collisions of the plasma particles (electrons and ions) with stationary neutrals, ϵ_0 is the permittivity of free space. Plasmas are of various kinds based on the properties of constituent species, namely, electrons, ions and neutrals. When $T_e \sim T_i$ and $n_e \sim n_i$, a plasma is classified as hot plasma (or a thermal plasma) where the collisional rate between $e - e$, $ion - ion$ and $e - ion$ species are equal and they are in thermal equilibrium with $\lambda_{De} \sim \lambda_{Di}$. On the other hand, plasmas with $T_e \gg T_i$ are called cold plasmas (or non-thermal plasma) where the collision rate among ions or among electrons ($e - e$, $ion - ion$) is larger then the

rate of collisions between an ion and an electron ($e - ion$) [60, 61].

1.1.1 Dusty plasmas

Complex (dusty) plasmas are plasmas with four different components, which, in addition to the usual plasma components i.e, electrons, ions and neutrals, contain micron sized particles, also called grains or dust. The dust grains are intrinsically neutral, relatively heavy and large sized particles mostly dielectric or conducting in nature and therefore introduce many peculiar phenomena in the system. Once the grains are introduced in a conventional electron-ion plasma, they get bombarded with heavy flux of (highly mobile) electrons, relative to ions, on its surface. They therefore collect a high electron population and mostly get negatively charged [22]. In some cases, when the dust particles undergo emission of electrons because of radiation sources like ultraviolet lights, secondary electron emission, thermionic emission, field emission etc., and the dust grains may also be found to be positively charged [62]. Thus, one has the possibility of having dust grains charged both negatively and positively.

The dust particles acquire large electric charge, and exhibit many collective phenomena through long-range coulomb interactions. The charges on dust species can additionally fluctuated because of the electrons/ions may leave the surface of dust grains in course of collision with other ions or dust grains, specially in streaming plasma, or because of thermal effects, or other radiative processes in the plasma [63]. A dusty plasma is significantly different from a multiple-ion-species plasma, because the presence of massive charged dust grains it produces a new collective phenomenon on a different time and length scale. The inclusion of charged dust species makes the plasma becomes even richer, physically, with several additional modes arising solely due to introduction of new scales or additional instabilities. Thus these extra component of macro-particles increases the complexity of the system even further. The dynamics of dusty plasma is very similar to many com-

plex fluids that have multiple phases of dust particles introducing multiple length and time scales in the system. This is why a dusty plasma is sometime called as “complex plasma” [22, 64].

1.1.2 Phases of dusty plasma medium

Instead of using the multiple parameters, such as the species temperature T_j , the number density n_j and various length scales and time scales, it is possible to represent the characteristic features of a dusty plasma in term of only two key parameters, the screening parameter κ and the Coulomb coupling parameter Γ . The ratio of inter-dust-particle separation to the plasma Debye length, a_d/λ_D , is known as screening parameter κ which takes care of density and shielding due to background plasma. Coupling parameter Γ measures the degree of interactions over the thermal motion of the ensemble of dust particles for fixed inter particle separation and background shielding κ [1, 22, 65, 66]. Mathematically, Γ is given by the ratio of average coulomb potential energy (including the shielding effect) to average kinetic energy of particle in the dust system.

$$\Gamma = \frac{(Z_d e)^2}{4\pi\epsilon_0 a_d K_b T_d} \exp\left(-\frac{a_d}{\lambda_D}\right) \quad (1.1)$$

where $a_d = (3/4\pi n_d)^{1/3}$ is the Wigner-Seitz radius or mean inter-dust separation, n_d is the particle number density, $Q_d = Z_d e$ is the dust particle charge, and T_d is the equilibrium temperature. As Γ increases, the dust system changes from a nearly collisionless, or only occasionally experiencing binary collisions, to a gaseous regime for $\Gamma \ll 10$, through an increasingly correlated liquid-like regime for $10 \leq \Gamma \ll 175$, to undergoing a Wigner crystallization into a lattice near $\Gamma_m \geq 175$, as shown in Fig. (1.3). The high dust charge (typically $Q \sim 10^5 e$) even at low dust temperature makes the coupling parameter $\Gamma > 1$ even at lower dust density. Thus the dusty plasmas could be found in gaseous, liquid as well as ordered crystalline phase.

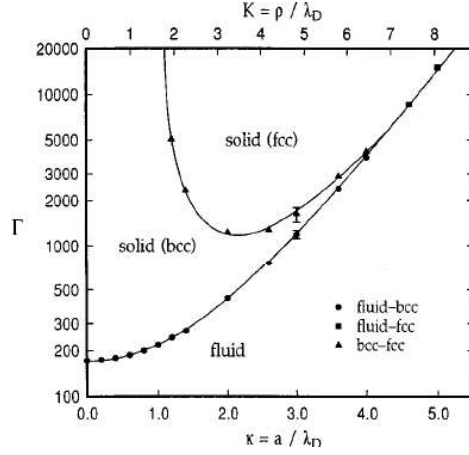


Figure 1.3: Γ and κ relation showing dusty plasma can exist at different state of matter by changing coupling parameter Γ and κ , by S. Hamaguchi *et al. Phys. Rev. E* **56** 4(1997).

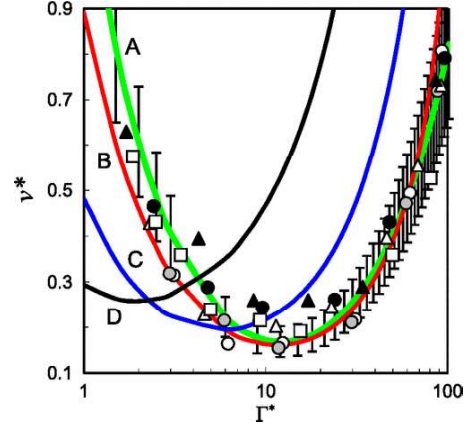


Figure 1.4: Γ and ν^* relation for various screening parameters κ showing gases and liquid phases of fluids by V. E. Fortov *et al. Phys. Rev. Lett.* **109** 055002 (2012).

The phase transitions occur under suitable physical conditions of the dust system. Statistically, the local density around a given particle as a function of the distance from this particle, is smooth in gaseous phase $\Gamma \ll 10$, and rapidly vanishes for small r because of the repulsion between the particles with same sign of charge. As Γ increases, positions of neighboring particles are more and more correlated, leading to a modulation of local density around a given particle. At $\Gamma \geq \Gamma_m$, the modulation or fluctuation in local density grows spontaneously into full long-range order, characteristic of a periodic crystalline structure [67, 68]. The kinematic viscosity which is a fundamental property of a fluid flows, correlates with the coupling parameters Γ and screening parameter κ for a dust fluid flows [5, 69, 70]. Fortunately, most of the routinely accessible dusty plasmas are in fluid regime and thus well known fluid model can be used for their flow dynamics. As shown in Fig. (1.4), the regions where kinematic viscosity ν^* increases with decreasing Γ , is in gaseous regime while the regions with ν^* increasing with Γ is in liquid state of the dust fluid. Dusty plasma, therefore, is an attractive field of research because of

several of its unique features, for example, its existence in various states of matter and its ability to display the kinetic level dynamics of dust particles at easily observable scales, that make it a versatile medium supporting various collective phenomena as well as useful for study of many fundamental physical aspects of the nature.

1.1.3 Occurrence and applications of dusty plasmas

Dusty plasmas are ubiquitous in different parts of our universe, such as in diffused interstellar clouds, in the planetary ring system, in Jupiter's moon, in the comet tails, in circumpolar rings and interplanetary medium, in supernova remnants, and in interstellar molecular clouds etc [71, 72]. Presence of dust particles in lower part of Earth's ionosphere is already known. On the Earth, the most common occurrence of dusty plasmas are artificial ones, whether it be in experimental laboratory, in lighting technology, in fusion reactors and in various plasma processing techniques. In many of these systems, dust can seriously disturb the system or even change the characteristics of the system. For example, in fusion reactors, dust can either grow inside the plasma or be evaporated or sputtered from the walls when plasma-surface interaction take place [73–75]. On the other hand, the dust can be radioactive and damage the reactor blanket. Presence of dust could pose a threat to the operation of the fusion reactor by increases the plasma resistivity, leading to increased voltages needed for start-up [76]. This might becomes a serious hindrance for the experimental or reactor grade devices, like ITER [77], which is currently under construction in France. However proper placement of dust in fusion reactors can be a useful tool for improving its performance. Introduction of dust shield in SOL region can be used to protect the wall by absorbing and preventing most of convection heat flux to the wall [78]. The effect of naturally present and externally injected dusts have been recently reported as effective controlling edge plasma condition and mitigating disruption with comparatively higher effi-

ciently then the conventional technique [79]. In revolution of technology, addition of nanoparticles in manufacturing plasmas device have beneficial effects such as, the performance of solar cells can be improved, carbon-structures can be grown in plasmas, and the deposition rates in plasma enhanced chemical vapor deposition and plasma surfacing can be enhanced using dust [80].

Complex plasma posses a unique combination of properties due to its relatively large mass, larger size and highly charged collection compare to background plasma. There are strong similarity and differences of dynamics between the colloidal dispersion, biological flows, astronomical flow systems and the dusty plasmas [81]. Like colloids, complex plasmas form solid and liquid-like structures with long range correlations and exhibit phase transitions and self organized patterns formation like vortex or circulating flows [1, 12]. Unlike colloids, they also exhibit a range of dynamic phenomena such as particle-mediated linear and nonlinear waves, soliton, shocks, wake formation and instabilities etc. The dynamics of dust particles in such system can be observed at the atomistic level [82]. Thus dusty plasma become a versatile medium that support many fundamental physics of nature. This become an excellent model system for studying phenomena such as phase transitions, particle transport, waves, instability, collective behaviors vortex or circulating flows etc. [24, 25, 82, 83]. It is also known that many phenomena in dusty plasmas have analogues and applications in many different fields of science and technology such as plasma physics, fusion, solid state physics, fluid dynamics, acoustics, optics, material science, nanoscience, nanotechnology, biological complex flows, environment protection, space exploration and astrophysics. The detailed study of complex flows in this system will be useful to understand various fundamental characteristics of various relevant natural flow processes.

1.2 Confined dust flow as driven complex system

Dust particles are heavily charged and are therefore easily confined in the localized electrostatic potential wells (regions of low potential) present in common laboratory and natural plasmas [12, 13]. In laboratory dusty plasmas the bulk plasma stays at a higher positive potential than its negatively charged confining boundaries and provides a natural strong potential well such that dust is often seen levitated in the bulk plasma. In many cases this levitated dust medium is additionally observed to display a spectacular flow dynamics. When the dust clouds are extended in considerable plasma volume, they show characteristics like a fluid with a very well defined flow field equilibrium in the region of confinement with definite mass-density conservation.

In setups with more than one dimension, the spatial boundaries of such dust fluid must acquire the shape of the equipotential contours (in a 2D equilibrium) or surfaces (in a 3D equilibrium) of the potential well, and the dust thus remains confined by the surrounding 2 or 3-dimensional potential barrier which this unperturbed dust fluid is unable to overcome. The dust flow along this boundary can therefore only be parallel to the boundary. In inviscid and isolated conditions, an isolated incompressible fluid contained in any such volume has a variety of equilibrium flow field solutions that essentially need to satisfy only the appropriate boundary conditions [23]. However, in the conditions where an external momentum source or driver is present, specific equilibrium flow solutions are attainable only in presence of a friction and/or viscosity, either with boundaries or with a more spatially distributed sink of the momentum. This sink can be present in the form, for example, of a third fluid capable of generating a friction and thereby dissipating the energy of the driven fluid, leading the system to a dynamical equi-

librium state. A dust fluid which is electrostatically suspended in a plasma and confined by an effective potential well represents a setup where both of these elements may be available in the form of a quasineutral plasma (ion) flow and a stationary background of neutral gas, respectively. The confined dust flow therefore presents an excellent example of a complete volumetrically driven-dissipative complex system that although stays in mechanical equilibrium (steady-state), operates continuously away from a thermodynamic equilibrium.

1.2.1 Experimental recovery of driven dust vortex solutions

As an important and realizable consequence of the analogy described above between driven confined dust flow and complex driven systems, the confined dust flow structures in dusty plasmas are expected to show a range of nonlinear effects, including the robust and continued stability of solutions that destabilize by bifurcating at critical points. A transition of this class in drives system ensures that system simultaneously makes transition to regime of stability of an alternate solution [84]. The temporal and spatial interval between successive bifurcations in such system might yield the essential temporal and structural limitations for the continued stability that appear to be the characteristics of responsive and self replicating complex systems. In an important achievement, while the nonlinear analysis presented in Chapter 5 of this thesis (and in Ref. [26]) recovers such dynamics, an identical experimental effect is simultaneously detected in a recent, completely independent, dusty plasma experiment by another group of workers in our laboratory [13]. The above experimental validation is apart from a series of experimental verification of the linear results presented in Chapters 2 and 3, describing the vortex multiplicity and counter-rotating pairing from a nonmonotonic drive [24, 25], which were predicted by our analysis presented in Chapters 3

and 4 and were simultaneously detected by a separate set of experiments examining confined dusty plasma vortex structures in our laboratory [11, 12].

1.2.2 Dynamical equivalence with natural complex flows

A drive by streaming fluid relates the confined dusty plasma vortex flow motion to many other natural flow setups of high importance. Consider that a typical laboratory dusty plasma setup has an assembly of negatively charged dust particles electrostatically levitated against the gravity by the electronegative sheath formed on the electrode at the bottom (e.g., see Fig. 4.1), allowing a supersonic plasma to continuously filter through it in order to let the latter reach the electrode. This arrangement, given a much slower time scale of response of the dust in comparison to plasma species and very low Reynolds number of dust flow, resembles a number of physical and bio-physical set ups, for example, a microscopic semipermeable mixing chamber that allows a colloidal solute to gradually dissolve into a solvent filtering through it at a comparatively high Reynolds number. Another example is a developing, localized, artery/vessel congestion by a cohesive lipid (e.g., cholesterol), producing blockade to a cardiac passage that would permit the blood flow of only higher Reynolds number [85]. The lipid must steadily dissolve in the blood flow in order to check the blockade growth. As one of its significant related effects, atherosclerosis, a leading cause of death from myocardial infarction (heart attack), remains a geometrically focal disease, preferentially affecting the outer edges of vessel bifurcations. In these predisposed areas, hemodynamic shear stress, i.e., the frictional force acting on the endothelial cell surface as a result of blood flow, is weaker than in protected regions, rendering endothelium (interior surface of blood vessels) more susceptible to pathogenic stimuli of injury, cell adhesion, cell proliferation, and lipid uptake [86].

1.3 Brief review of studies of existing dust vortex flow in plasma

A wealth of theoretical and experimental knowledge is available from a variety of dusty plasma experiments performed, analyzed and reported in the present literature where dust circulation or dust vortex formation is observed. Vortex or circulation is among the self organized patterns or collective behaviors other than crystallization, waves and instability, shocks or soliton formed in dusty plasma due to its long range coulomb interactions. Vortex or circulation of dust in plasma has been observed in various laboratory experiments and computation simulations either in presence or absence of magnetic field.

The experiment by Y. Saitou *et al.* [8] and M. Puttscher *et al.* [87] in RF discharge plasma demonstrated the dust circulation in presence of magnetic field. Subsequent analysis by P. K. Kaw *et al.* [88] proposed a theoretical model that explained the causes of dust vortex in magnetized dusty plasma as a spontaneous response to ion rotation generated by the electromagnetic field. There have been investigations in magnetized dusty plasmas where electromagnetic Lorentz force induces ion species rotation, which, in turn, causes the levitated dust particles to circulate in azimuthal direction [89–91]. The main difficulty realized in such cases is that the dust grains are relatively heavy and require strong magnetic field ($B \geq 3$ Tesla) to get magnetized in a plasma. A Magnetized Dusty Plasma Experiment (MDPX) achieving this limit is presently being developed by E. Thomas *et al.* [92, 93] to perform some of interesting experiment in magnetized dusty plasma regime.

Dust vortex in absence of magnetic field are also observed in various experiments, for example, dust vortex are observed forming in laboratory dusty plasmas by Vaulina *et al.* [7], Saitou *et al.* [8], and in microgravity conditions (space station, ISS) in a dust cloud surrounding a void as reported by H. M. Thomas *et al.* [9].

Experimental observations include a very recent observation, in our laboratory by M. Kaur *et al.* [11], of the formation of a complete toroidal dust structure in a glow discharge plasma with a poloidal dust flow, and steady equilibrium co-rotating vortex system by M. Choudhary *et al.* [13]. The mechanisms underlying the vortex motion in these experiments include a range of possibilities that result into nonuniform forces on the suspended dust clouds, either from its direct or indirect interaction with the surrounding plasma as reported by H. M. Thomas *et al.* [9] or by external means including boundaries as reported by G. Uchida *et al.* [94], by radiation using two laser beams that apply variable torque on a dust cluster in experiment studies by M. Klindworth *et al.* [95] and T. Miksch *et al.* [96]. Further, the momentum transfer from drifting ions to gas molecules and resulting compact vortex structures containing a large number of coagulating dust particles and dense dust clouds evolving in time are studied in experiment by V. I. Vladimirov *et al.* [97]. In the experiment the motion of ions is induced by the external electric field as well as by the intense recombination of ions and electrons on dust particles, which might cause the emergence of large concentration gradients and additional flows of plasma particles. Also, the dust rotation in dusty plasma experiment was observed to be induced by a biased probe immersed in plasma by Law *et al.* [98]. The origin of the circulation are attributed to the formation of a nonuniform electric field in the crystal region by the induced probe. In inhomogeneous plasmas, dust charge gradient can drive instabilities that lead to the vortex formation as reported in some of the theoretical and numerical studies by O. S. Vaulina *et al.* [99–101]. Further, in a dc glow discharge plasma, a two-dimensional dust vortex flow near the edge of a metal plate could be generated due to an unbalanced ion drag force near the metal plate as observed by G. Uchida *et al.* [94]. It has also been observed that convection of neutral gas by thermal creeping exhibits a global convective motion of dusts as similar to Rayleigh-Benard convection of fluids in various experimental work by M. Schwabe *et al.* [102], V.N.

Tsyтовich *et al.* [103] and S. Mitic *et al.* [104]. Moreover, the role of a drag force from sheared flow of ions in the formation of dust vortices is discussed in T. Bockwoldt *et al.* [105], Laishram *et al.* [24–26] and M. Kaur *et al.* [11, 12]. In these various works, self-excited large-scale vortices are observed due to non-zero curl of various forces such as the ion drag force.

Among some of the recent investigations of vortex flows in dusty plasmas is experimental work by Kil-Byoung Chai *et al.* [106] where dust grain poloidal vortices with two adjacent co-rotating poloidal vortices have been observed due to ion density gradient and the gradient of the magnitude of the ion ambipolar velocity. In another recent experiment carried out at our Institute (IPR) by M. Choudhary *et al.* [13], it has been observed that steady equilibrium dust flow undergoes a transition from a single to multiple co-rotating vortices with varying input power. The occurrence of these vortices is explained on the basis of the charge gradient of dust particles, which is orthogonal to the ion drag force.

The observed or analyzed vortices in the above dusty plasma studies are also relevant to various natural processes involving rotational flow of matter, other than in laboratory dusty plasmas, ranging from those at the astronomical scales, like galactic star formation [107], Great Red spot and white ovals of Jupiter [31, 56], Saturn’s ring, nebulae [108] to small-scale natural fluids including colloidal suspensions, emulsions, foams, polymer melts and solutions, liquid crystals, swimming of bacteria or microorganism and whole blood samples etc. [109–111] as well as at the micro- or nano-scales like mixing/separation of heterogeneous fluids, biological flows [112, 113]. Thus, besides the central objectives of this thesis, i.e., developing a working approach for analyzing dust vortex dynamics in experiments and its application to complex systems, the study of dust vortices and determining its characteristics have multiple alternate applications. This subject therefore continues to be an active area of research for understanding a host of relevant physics of many natural flow systems.

1.4 The hydrodynamic approaches to dust-fluid dynamics

Limited to a normal fluid limit $\Gamma < 100$, suitably represented by the Navier-Stokes regime of the hydrodynamic model, the present studies are done in this simplistic regime considering the incompressible and normal fluid-like characteristics observed of the dust fluid in the parameter regime of interest. Below, we however introduce both, the Navier-Stokes hydrodynamic model, mainly applicable to the laboratory dust under analysis, and the viscoelastic fluid model, applicable largely to more exotic, strongly coupled phase of the dusty plasmas. Additional detail of formulation in these regimes are described further in Appendix [A](#) and [B](#), respectively.

1.4.1 Governing equations in the Navier-Stokes fluid regime

The macroscopic fluid dynamics description is based on some fundamental laws of nature that essentially take into account the conservation of mass (continuum flow), conservation of momentum (Newton's second law of motion) and conservation of energy (first law of the thermodynamics). Following these fundamental laws in a fixed volume of the space occupied by the fluid (Eulerian approach), the governing differential equations representing the complete dynamics of a fluid flow system can be derived using a rather simple diffusive transport modelled by Gaussian processes in the species phase space [[114](#), [115](#)],

$$\frac{\partial \rho}{\partial t} + \nabla \cdot (\rho \mathbf{u}) = 0, \quad (1.2)$$

$$\frac{\partial \mathbf{u}}{\partial t} + \mathbf{u} \cdot \nabla \mathbf{u} = g - \frac{\nabla p}{\rho} + \mu \nabla^2 \mathbf{u} - \frac{2}{3} \mu (\nabla \cdot (\nabla \cdot \mathbf{u}) \mathbf{I}) + \mathbf{f}_{\text{friction}}, \quad (1.3)$$

$$\rho \left(\frac{\partial \mathbf{e}}{\partial t} + \mathbf{u} \cdot \nabla \mathbf{e} \right) = k \nabla^2 T + \Phi - p \nabla \cdot \mathbf{u}. \quad (1.4)$$

Here ρ , \mathbf{u} , p and μ are the dust density, velocity, pressure and kinematic viscosity of the dust. Quantities g and f_{friction} represent gravitational and frictional forces acting on the dust. e , T , and Φ are internal energy, Temperature and viscous dissipation rate of the flow system [114, 115]. These coupled differential equations of fluid dynamics, representing the above fundamental laws, are known as the Navier-Stokes equations. In the above set of equations however has larger number of unknowns variables than the numbers of equations and therefore require more equations for perfect closure of the set. Generally, the density(ρ) relates to pressure and temperature, my means of a relationship given by the so called equation of state $p = c\rho^\gamma$, where $\gamma = c_p/c_v$. Its simplest form is $p = \rho RT$ (ideal gas equation). Quantities $dh = c_p dT$ and $de = c_v dT$ allow expressing enthalpy and internal energy, respectively, in terms of temperature. The equation of state provides the required closure for normal fluids, allowing to solve the set for generating solutions, in a bounded region by additionally prescribing the boundary conditions.

1.4.2 Governing equations in the viscoelastic fluid regime

The strongly couple complex fluids, such as biological systems or dusty plasmas having coupling parameter in the range ($100 \leq \Gamma \leq \Gamma_c$), behave like visco-elastic fluids. For such flows, both the viscous and elastic effects need to be effectively incorporated in the flow characteristics. One of the means to achieve this is via augmenting the usual hydrodynamic description by a phenomenological visco-elastic term to account for the strong coupling correlations. A generalized momentum balance equation obtained by this approach in the regime of its applicability is written as follows [116],

$$\left[1 + \tau_m \left(\frac{\partial}{\partial t} + \mathbf{u} \cdot \nabla\right)\right] \left[\left(\frac{\partial}{\partial t} + \mathbf{u} \cdot \nabla\right) \mathbf{u} + \frac{\nabla p}{\rho} - \nabla V\right] = \eta \nabla^2 \mathbf{u} + \left(\frac{\mu}{3} + \zeta\right) \nabla(\nabla \cdot \mathbf{u}), \quad (1.5)$$

where τ_m is the newly introduced relaxation parameter, V is potential and ζ is bulk viscosity of the dusty plasma. The evolution of \mathbf{u} in (1.5) incorporates characteristic traits associated with strongly coupled matter through a relaxation parameter τ_m . For time scales longer than τ_m the medium behaves like a viscous liquid, whereas at shorter time scales the memory effect persists and the system shows solid like elastic properties. A detailed description of dusty plasma's physical structure and regimes of its operation corresponding to a complete range of in key parameters is provided in Appendix B.

Considering the intended regime of present study to be weakly coupled and normal fluid-like, the present time independent approach to steady-state vortex flows is limited to making use of the model (1.3) for first application of velocity potential based 2D hydrodynamics to bounded and driven dust vortex flow described in further detail in Chapter 2 and 3. The general introduction to features of 2D hydrodynamics relevant to present study are detailed in the Appendix A.

1.5 Thesis outline

The description provided in the preceding sections indicate the great variety of dynamics exhibited by the dusty plasmas and its potential to display characteristics of various states of matter in the nature depending on largely externally controllable parameter in simple laboratory experiments. Whether the spectacular dust flow dynamics observed in a variety of recent dusty plasma experiments, often accessible by velocimetric techniques [117], can be employed to study complex systems operating far from thermodynamic equilibrium, is subject to availability of a systematic formulation of the dusty plasma in its simplest, fluid-like, dynamical regime. The focus of studies presented in this thesis is therefore on the aspects of fluid-dynamical analysis of a driven confined dust fluid suspended in a quasineutral plasma.

Presented in the first half of this thesis is the first application of a 2D hydrodynamic model to these volumetrically driven spatially confined dust vortices [24] observable in many of the dusty plasma experiments. Besides predicting and interpreting experimentally observed multiplicity of vortex in a series of observations by means of numerical solutions, a more systematic and analytic approach to various advanced aspects of linear dust vortex dynamics also outlines basic scaling of boundary phenomena at low to moderate Reynolds number [25]. The second part of the study presented in this thesis addresses a further advanced and complete nonlinear regime of the dust vortex flows. Besides interpreting nontrivial physics of often noted transition to nonlinear regime of these vortices in the recent experiment the nonlinear analysis extends the limits of valuable analytic prescriptions of estimates and scaling recoverable from rather easily diagnosed flow dynamics of the dust, to high Reynolds number nonlinear regimes. The remarkable aspect of a continued stability of spatially extended vortex structures via a structural bifurcation is analyzed by means of finding nonlinear co-rotating multiple vortex solutions of the formulation, highlighting also their recovery in recent experiments showing an identical transition.

Provided below is a systematic chapter-wise analysis of the vortex motion of the dust clouds and its characteristics addressed in the present thesis.

In **chapter 2**, addressing the requirement of a formulation for study of vortices forming in dusty plasmas as motivation, the first application of 2D hydrodynamic formulation is done in the linear, low Reynolds number, limit to confined dust clouds electrostatically suspended in a laboratory plasma. As a first approximation, the nearly incompressible dust flow dynamics is treated as governed by the 2D Navier-Stokes equations in which the drive produced by the ion drag and the friction produced by the stationary neutral fluid can be suitably accounted for in a steady-state. The dust vortex formulation is developed based on the stream-function approach in fully curvilinear setup which inherently accounts for the in-

compressibility of the dust flow and produces characterizable solutions in terms of dust streamlines, as functions of measurable parameters and relevant boundary conditions. In the applicable regime of interest, the formulation produces scaled solutions with system relevant normalizations allowing to obtain and characterize the Bounded dust flow equilibria. The formulation modelling an open system admits dust drive by a number of external sources of vorticity by allowing to specify them by means of a source term. The dust flow equilibria are analyzed in two important cases of sheared ion flow profiles, first in the where the driving ion flow field is considered having a monotonic profile with shear, and in the second case with a nonmonotonic variation in the flow profile, having a localized shear. The solutions relevant to observation of dust vortex flow in many experiments are recovered, including a prescription to obtain counter-rotating multiple vortices within the linear limit as subsequently recovered in the experiments.

In **chapter 3**, we have continued exploring the linear regime of the dust flow by analytically addressing the issues that in presence of a background high Reynolds number driving plasma flow, what are the characteristics of the 2D driven flow structure, and how do the spectral properties of the driver flow influence equilibrium mode number spectrum of the driven flow when it is subjected to important boundary phenomena. For the analysis of driven confined dust fluid vortex flow a boundary value problem is constructed in a nonplanar, cylindrical geometry in terms of dust flow streamfunction. The analytic solutions for the dust flow are obtained by treating the boundary value formulation as an eigenvalue problem, and using the linearly independent set of Bessel functions as eigenmodes that allows both driving and driven flows to follow valid flux conservation and have a multiple scale vorticity spectrum. The spectral characteristics of dust vorticity at higher mode numbers is shown to be determined predominantly by the boundary effects that have additional impact when combined with variation in the usual physical parameters of the dust medium, including the kinematic viscosity and the coeffi-

cients of neutral friction and ion drag acting on the dust fluid. Both the boundary layer thickness and the dust Reynolds number are shown to have definite exponents of variation with respect to the medium viscosity μ . While the effective boundary layer width is recovered to scale with $\mu^{1/3}$, the effective Reynolds number for the setup is recovered to scale with $\mu^{-2/3}$. Both these orderings are seen to be obscured by an increasing spatial complexity of the driving mechanism. The degree of the impact of this complexity is estimated by systematically characterizing the effect of individual driver flow modes in various cases with increasing value of the cylindrical mode number.

In **chapter 4**, the nonlinear properties of a volumetrically driven 2D dust vortex flow of a confined dust fluid suspended in a plasma are studied. Motivated by toroidally symmetric flow formation and signatures of nonlinear nature of its flow dynamics at higher dust velocities, 2D nonlinear equilibrium solutions of the vortex flow are obtained in a toroidally symmetric domain. The solutions obtained in present treatment are relevant to a large number of observations in dusty plasmas setups where a vigorous dust vortex flow dynamics is observed with flow velocities approaching the nonlinear limit. In presence of 2D heterogeneous boundary conditions applied to dust flow in a curvilinear coordinate system, the major nonlinear effects cause the boundary layer to separate from the domain boundary. This causes the vorticity generated from the interaction with the no-slip, or frictional, boundaries to be convected away with strong flows of the primary vortices. The development of separated boundary layer is investigated as a structural bifurcation where the kinematic viscosity assumes role of the bifurcation parameter and the separation coincides with the bifurcation. The bifurcation is shown to occur when the vorticity profile approaches its first zero value along the boundary at the point where its minimum is located. This critical behavior and signatures of equivalent nonlinear vortex states in experiments indicates capacity of confined dusty plasma vortex structures to represent a class of systems that can self-stabilize by making a

critical transition to a self similar state, for example, biophysical transition during cells undergoing mitosis. The nonlinear scaling of the boundary layer parameters with kinematic viscosity μ is obtained that shows a velocity independent linear estimate of kinematic viscosity to modify and additionally depend up on the flow velocity and its gradient scale length along the streamlines as $\mu = \Delta r_b^2 \frac{u}{L_{\parallel}}$. Similarly existence of a critical values μ^* demarcating transition to nonlinear regime is identified. These two factors allow estimation of viscosity of charged fluids using appropriate scaling by identifying a structural change in flow patterns in experiments.

In **chapter 5**, we present the solutions of 2D nonlinear hydrodynamic formulation of confined, volumetrically driven dust cells with variation in the confinement domain's aspect ratio and its impact on the formation of vortices and their number. The bifurcation predicted in Chapter 4 for a dusty plasma 2D flow cell is discussed in the light of its close resemblance to bifurcation transition in more complex biophysical processes, for example, in certain approaches to model the process of cell division or mitosis. The advanced numerical analysis done examined more diverse aspect ratio values, including those exceeding 2 and smaller than unity. It is discussed that the cases with aspect ratio larger than 2 and more, a complete sequence of identical co-rotating vortices is recovered with number of identical vortices equal to the value of the aspect ratio. This result is discussed in the light of recovery of similar results in the dusty plasma experiments by M. Choudhary *et al.* [13] where, in close agreement with our nonlinear results, a dust cloud with aspect ratio exceeding unity is indeed seen to develop a series of multiple co-rotating vortices with stronger drive, or larger Reynolds number. It is formally shown that achieving a periodic frequency of bifurcation in autonomously growing vortex flow cells might be possible by introducing an dependence of the a cell dimension via a time-integral relationship with the increasing area of an unsaturated vortex cell. The possibility of an exact implementation and solution of the prescribed model is

highlighted as a future extension of the present model and computational analysis, for recovering a nonlinearity controlled continued replication and generation of a spatially periodic sequence of vortex structures.

Finally, **chapter 6.1** provides brief summary of the overall study presented in the thesis and main conclusions drawn from the results obtained in this research work. Few results from the linear and nonlinear regimes of the present studies are discussed in the perspective of existing experimental and theoretical studies on the subject. The content of this chapter further identify and describe the potential areas of interest in which the present research can lead and contribute. The discussion also covers possibility of extension of applied techniques and numerical approaches for addressing more detailed and readily accessible regimes of the present formulation. Options to explore certain statistical aspects related to dust vortex equilibria are also suggested. Certain experimental studies are suggested for possible experimental realization of the predictions made in the present studies and verification of various theoretical estimates provided in the present work, for example, estimate of dust dynamical viscosity using velocimetric techniques obtained in **chapter 4**.

2

Hydrodynamic formulation of dust vortex flow in plasma

2.1 Introduction

The systematic analysis of complex systems in nature essentially requires investigating their less complex and more accessible forms to serve as paradigm. The simple driven systems that display a range of stable states away from thermodynamic equilibrium form attractive models to study the behavior their more complex driven counterparts exhibit. Vortex structures forming in various dusty plasma present such an example which have also shown their accessibility in very simpler systems, at much realistic scales and via equally simple forms of diagnostics. In a wide variety of laboratory experiments involving dusty plasma, the levitated dust medium is observed to display a spectacular flow dynamics. In many cases the dust clouds are extended in considerable plasma volume and show characteristics like a fluid with a very well defined flow field equilibrium in the region of confinement with definite mass-density conservation. Such fluid-like dynamic equilibria

indicate applicability of the hydrodynamic approach to the dust medium within a finite range of its phase-diagram. The physical regime for the dusty plasma to be in a normal Navier-Stokes like fluid regime is determined specifically by such a phase-diagram presented in Chapter 1.

As already discussed in larger detail in Chapter 1, the main objective of this first part of study is to model the basic behavior of dust flow dynamics in a range of experiments where a vortex-like dust flow is observed. Such observations are available in the experiments performed both in normal laboratory Dusty plasma [7, 8, 11] and in microgravity conditions, for example in International Space Station (ISS) where the vortex formed in the dust cloud surrounding a void [9]. Keeping in view the above observations, it is quite relevant to consider situations where, a high enough dust particle population, localized in a limited volume by an effective confining potential, strongly interacts with, and comes to an equilibrium with, the effective confining potential. The dust particles must uniformly fill the region of low potential, or the bottom of the potential well. For the cases in which the average kinetic energy of the dust particles either exceeds or is comparable to the energy of their mutual interaction [118], this formation of a dust cloud can suitably be treated by an incompressible hydrodynamic formulation. The corresponding fluid equations can be employed as a first approximation for obtaining time independent flow-field distributions in space or for analyzing processes with the characteristic timescales longer than the inverse of dust acoustic frequency, ω_d^{-1} [119].

In setups with more than one dimension, the spatial boundaries of such dust fluid must acquire the shape of the equipotential contours (in a 2D equilibrium) or surfaces (in a 3D equilibrium) of the potential well, and the dust thus remains confined by the surrounding 2 or 3-dimensional potential barrier which this unperturbed dust fluid is unable to overcome. The dust flow along this boundary can therefore only be parallel to the boundary. In inviscid conditions, an isolated incompressible fluid contained in any such volume has a variety of equilibrium

flow field solutions that essentially need to satisfy only the appropriate boundary conditions [23]. However in the conditions where an external momentum source is present, specific equilibrium flow solutions are attainable only in presence of a friction, either with boundaries or with a more spatially distributed sink of the momentum. This sink can be present in the form, for example, of a third fluid capable of generating a friction and thereby dissipating the energy of the driven fluid, leading the system to an equilibrium dynamical state. A dust fluid which is electrostatically suspended in a plasma and confined by an effective potential well represents a setup where both of these elements may be available in the form of a quasineutral plasma (ion) flow and a stationary background of neutral gas, respectively.

The setup considered in this chapter, and throughout this thesis, is therefore highly relevant to a dust fluid suspended in the plasma which is spatially confined/localized, effectively by a combination of electrostatic and gravitational fields. A 2D or 3D conservative field $\mathbf{F}_c = -\nabla V$ confining the dust fluid can however be produced by various means as achieved in many complex plasma setups. For example, by using an electrode with parabolic trough to achieve the required horizontal confinement that results in a parabolic potential well [95]. The other means include potential caused by special geometry of the containing surfaces [30, 120, 121] or even the effect of thermophoretic force due to heated electrodes which in combination with other factors could generate a 3D harmonic confining potential [122]. Since the boundary provided by an effective potential may be structureless ($k_{\parallel} \rightarrow 0$, where the subscript \parallel represents direction parallel to the boundary) the friction with the boundary may vanish preventing the microturbulence at the boundary and the associated entropy production [123]. The considered boundaries can therefore be treated with various boundary conditions, namely, no-slip, complete slip or partial slip boundary flow of the dust, providing a finite or zero boundary layer width, respectively, though the dust fluid has a finite viscos-

ity and flows with very small Reynolds number. In the present analysis we have used a combination of no-slip and complete-slip dust flow at various sections of the enclosing boundary, motivated by situations of more practical interest.

In this chapter the dust fluid setup described above are analyzed by means of a hydrodynamic formulation and its solutions. Various flow equilibria are obtained between a dust fluid confined by an effective confining potential and a streaming plasma flow, in presence of a stagnant neutral fluid in the background providing a frictional resistance to the dust motion. For most of the practical cases of interest the effective confining potential is likely to have spatial nonuniformities and flux conservation in the Cartesian coordinates may be valid only locally, making it difficult to include effects of the boundaries which essentially have global character, as they must enclose the entire volume of the interest. The formulation and the solutions here therefore are worked out in a cylindrical setup that allows to account for finite curvature and nonlinearity in the spatial configuration of the setup and the boundaries. In this chapter, in Sec. 2.2 we present the hydrodynamic formulation in a 2-dimensional, cylindrical set-up. In Sec. 2.3 the solutions of the model are presented and discussed, including a detailed characterization of the dust flow in terms of the basic parameters, namely, dust viscosity, coefficient of ion drag on the dust particles and the coefficient of friction between dust and the neutral gas. Two cases, with profiles of the driving plasma flow having a monotonic variation (modelled by a cosine radial distribution) and a non-monotonic variation (modelled by a spatially localized Gaussian radial distribution), are presented in Sec. 2.3.1 and Sec. 2.4, respectively. Summary and conclusions are presented in Sec. 2.5.

2.2 2-D Hydrodynamic formulation

The geometry of confined dust fluid considered in present formulation is identical to the recent experiments in the laboratory at Institute for Plasma Research (IPR-

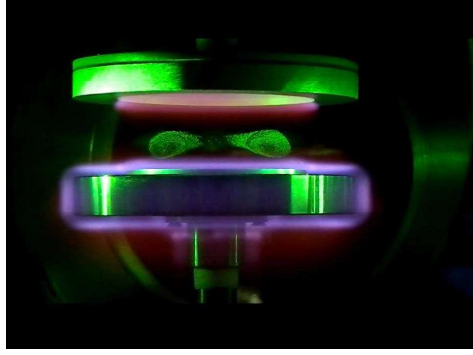


Figure 2.1: Toroidal dust cloud with poloidal circulation in the laboratory dusty plasma experiment by M. Kaur *et al.* Phys. Plasmas **22**, 033703 (2015).

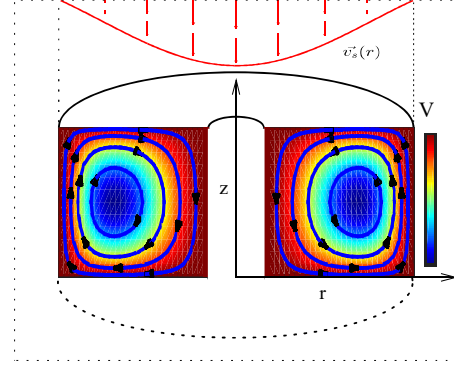


Figure 2.2: Schematic representation of dust confined toroidally by $V(r, z)$ and driven by shear flow field $v_s(r)$ through the domain.

India) where a toroidal dust structure forms having a poloidal circulating flow in a glow discharge plasma [11] as shown in Fig. 2.1. The steady-state nature of dust-fluid flow in such experiments indicate an almost time-independent distribution of electrostatic potential in the plasma which could subsequently be measured by the careful probe diagnostics in absence of dust. In order to treat these quite realizable driven dust vortex structures as a paradigm for natural driven-dissipative complex systems their dynamics is modelled by a simplistic limit of the hydrodynamic approach in the relevant curvilinear coordinate system introduced in the following sections.

2.2.1 Model setup relevant to laboratory dusty plasma experiments

For theoretical formulation, we consider a setup where dust fluid is confined by an effective potential V_b and its associated conservative force field $\mathbf{F}_c = -\nabla V_b$ as shown in Fig. 2.2. The confined dust cloud is in dynamic equilibrium with an unbounded streaming flux of ions which drives the dust fluid dynamics and a

stationary neutral fluid that resists the dust flow. In the associated azimuthally symmetric experimental setup Fig. 2.1, the dust fills volume of a torus which generally acquires a non-regularly shaped cross-section determined by the effective confining potential. For analytic or computational simplicity, however, this cross section of the torus is approximated in the present treatment as a rectangle, as illustrated schematically in Fig. 2.2. Accordingly, using cylindrical co-ordinates to accommodate the azimuthal symmetry, the toroidal dust fluid is considered confined by the effective potential $V_b(r, z)$ within the boundaries of a finite section of an infinite cylinder of flowing plasma, or in the region where $0 < r/L_r < 1$ and $-1 < z/L_z < 1$, with no variation along the azimuthal dimension $0 < \phi < 2\pi$. The potential at the boundary of this region jumps to a very high value at the r and z boundaries of this region, producing a high barrier for the dust particles to ensure a zero flow across this boundary. Since in the limit of dust parameters considered here the dust fluid tends to settle at the bottom of the potential well, and for smaller quantity of the dust fluid the boundary should assume the shape of equipotential contours in the r - z plane while continuing to have a periodic structure along $\hat{\phi}$. For the present treatment, however, the dust fluid is assumed to fill the complete region covering the volume up to the outermost contour and the intersection of the dust volume by an r - z plane is a rectangle.

2.2.2 Conservation equations in 2D cylindrical setup

For the azimuthally symmetric bounded dust flow that follows incompressibility condition and has a finite viscosity, the dynamics is governed by the 2D Navier-Stokes equation in which the drive produced by the ion drag and the friction produced by the stationary neutral fluid can be suitably accounted for,

$$\frac{\partial \mathbf{u}}{\partial t} + (\mathbf{u} \cdot \nabla) \mathbf{u} = -\frac{\nabla P}{\rho} - \nabla V + \mu \nabla^2 \mathbf{u} - \xi(\mathbf{u} - \mathbf{v}) - \nu(\mathbf{u} - \mathbf{w}), \quad (2.1)$$

where \mathbf{u} is the dust flow velocity, \mathbf{v} is the ion flow velocity and \mathbf{w} is the flow velocity of the neutral fluid. P and ρ are the pressure and mass density of the dust fluid, V is the effective confining potential, μ is kinematic viscosity, ξ is coefficient of ion drag acting on the dust and ν is the coefficient of friction with the neutral fluid [124–126]. Accordingly, the components of flow equation (2.1) in the r-z plane are written as follows [23],

$$\frac{\partial u_r}{\partial t} + u_r \frac{\partial u_r}{\partial r} + u_z \frac{\partial u_r}{\partial z} = -\frac{1}{\rho} \frac{\partial P}{\partial r} - \frac{\partial V}{\partial r} + \mu \nabla^2 u_r - \xi(u_r - v_r) - \nu(u_r - w_r), \quad (2.2)$$

$$\frac{\partial u_z}{\partial t} + u_r \frac{\partial u_z}{\partial r} + u_z \frac{\partial u_z}{\partial z} = -\frac{1}{\rho} \frac{\partial P}{\partial z} - \frac{\partial V}{\partial z} + \mu \nabla^2 u_z - \xi(u_z - v_z) - \nu(u_z - w_z), \quad (2.3)$$

along with the equation of continuity for the incompressible dust fluid, $\nabla \cdot \mathbf{u} = 0$, written in r-z plane following the cylindrical coordinates as,

$$\frac{1}{r} \frac{\partial(r u_r)}{\partial r} + \frac{\partial u_z}{\partial z} = 0. \quad (2.4)$$

A more detailed description of these simplified conservation equations is provided in Sec. 1.4 and in appendix A. In the limit of small Reynolds number ($\text{Re} \approx Lu/\mu \ll 1$), the nonlinear advective transport in the left hand sides of Eq. (2.2) and (2.3) are negligible compared to the diffusive transport in the right hand side. Further in the steady-state equilibrium flow limit, the first term comprising the time derivative is also negligible and the ions and neutral flows maintain equilibrium distribution over the duration where fluctuations have a vanishing average over the slow dust time scale. Assuming this linear, or low Reynolds number, steady flows limit, and operating (2.2) and (2.3) with $\partial/\partial z$ and $\partial/\partial r$, respectively, both equations can be combined to yield dynamic equation in term of dust vorticity, $\omega = \nabla \times \mathbf{u}$, as

follows,

$$\mu \nabla^2 \omega - (\xi + \nu) \omega + \xi \omega_s = 0, \quad (2.5)$$

where ω_s is the vorticity of the source, or that of the driving fluid (plasma ions) in the present case. The coefficient of various terms i.e., ξ , ν and μ are generally functions of system parameters as in standard dusty plasma modelling procedures, for example that presented by Barnes and Kharapak [124–126]. Note that the source of vorticity ω_s in Eq. 2.5 might account for a variety of sources arising from various finite contributions in circulation (curl operating on a momentum source), for example, ion or neutral drag ($\nabla \times v_{i,n}$), nonuniformity of dust charge density ($\nabla Q_d \times E$), nonuniformity of plasma/neutral flow and density ($\nabla v_{i,n} \times \nabla n_{i,n}$) and nonuniformities of the ion or neutral temperatures ($\nabla T_{i,n} \times \nabla n_{i,n}$) are among the possible mechanisms in many dusty plasma systems. For simplicity, however, we treat the source of vorticity from ion drag $\omega_s = (\nabla \times \mathbf{v}_i)$ as the representative source mechanism among these possible sources, for the present study.

2.2.3 The streamfunction formulation in curvilinear setup

For the subsonic dust flow ($\mathbf{u}/c_s \ll 1$), where c_s is dust acoustic velocity, the flow field is considered incompressible in nature, or satisfying $\nabla \cdot \mathbf{u} = 0$. This allows introducing a velocity potential or streamfunction Ψ such that $\mathbf{u} = \nabla \times \Psi$ satisfies the incompressibility condition. However, for azimuthally symmetric flow system the dust motion can suitably be treated in the 2-dimensional r - z plane such that the dust vorticity vector $\omega = \nabla \times \mathbf{u}$ is directed purely along $\hat{\phi}$. Then the streamfunction and vorticity behave as a scalar potential giving two dimensional flow velocity as $\mathbf{u} = \nabla \times (\psi \hat{\phi})$. Thus the r and z components of the velocity

become expressible in term of scalar streamfunction as,

$$u_r = -\frac{\partial\psi}{\partial z}, \quad u_z = \frac{1}{r} \frac{\partial(r\psi)}{\partial r} \quad (2.6)$$

and the corresponding vorticity ω in term of ψ is given by,

$$\omega = -\left(\frac{\partial^2\psi}{\partial r^2} + \frac{1}{r} \frac{\partial\psi}{\partial r} - \frac{\psi}{r^2} + \frac{\partial^2\psi}{\partial z^2}\right). \quad (2.7)$$

The advantage of such potential instead of dealing with vector field of of system has discussed explicitly in section 2.2.3. Now using (2.5) and (2.7) we obtain the equation governing streamfunction of the dust fluid as

$$\begin{aligned} \frac{\partial^4\psi}{\partial r^4} + \frac{2}{r} \frac{\partial^3\psi}{\partial r^3} - \left[\left(\frac{3}{r^2} + K_1\right) - \frac{2\partial^2}{\partial z^2}\right] \frac{\partial^2\psi}{\partial r^2} + \left[\left(\frac{3}{r^3} - \frac{K_1}{r}\right) + \frac{2}{r} \frac{\partial^2}{\partial z^2}\right] \frac{\partial\psi}{\partial r} \\ - \left[\frac{3}{r^4} - \frac{K_1}{r^2} + \left(\frac{2}{r^2} + K_1\right) \frac{\partial^2}{\partial z^2} - \frac{\partial^4}{\partial z^4}\right] \psi - K_2\omega_s = 0, \end{aligned} \quad (2.8)$$

where $K_1 = (\xi + \nu)/\mu$ and $K_2 = \xi/\mu$. The coefficients in (2.8) are independent of z , we therefore treat dependence on z in ψ via a separable function $\psi_z(z)$ that allows ψ to be expressed in the form of the product $\psi = \psi_r(r)\psi_z(z)$ and the Eq. (2.8) to be written as,

$$\begin{aligned} \frac{\partial^4\psi_r}{\partial r^4} + \frac{2}{r} \frac{\partial^3\psi_r}{\partial r^3} - \left[\left(\frac{3}{r^2} + K_1\right) - \frac{2\psi_z''}{\psi_z}\right] \frac{\partial^2\psi_r}{\partial r^2} + \left[\left(\frac{3}{r^3} - \frac{K_1}{r}\right) + \frac{2}{r} \frac{\psi_z''}{\psi_z}\right] \frac{\partial\psi_r}{\partial r} \\ - \left[\left(\frac{3}{r^4} - \frac{K_1}{r^2}\right) + \left(\frac{2}{r^2} + K_1\right) \frac{\psi_z''}{\psi_z} - \frac{\psi_z''''}{\psi_z}\right] \psi_r - K_2 \frac{\omega_s}{\psi_z} = 0 \end{aligned} \quad (2.9)$$

where prime denotes differentiation with respect to z . Based on the homogeneous boundaries along axial direction, the same consideration further allows us to resolve the z dependent factor of the function, $\psi_z(z)$, in its Fourier components along \hat{z} . The choice of axial scale k_z set as the scale length associated with the confinement

domain,

$$\psi_z = a_z \cos(k_z z), \quad k_z = (\pi/2L_z). \quad (2.10)$$

This chosen scale enables ψ to satisfy the boundary conditions at the top and bottom boundaries ($z = \pm L_z$), ensuring no dust flow across these boundaries. The ion flow however is unbounded and allowed to be an arbitrary function of r and z , therefore encompassing all possible length scales in ω_s . The associated stream function for ions thus has a wider spectrum of Fourier modes with an arbitrary range of k_{sz} values, and is expressible more generally as,

$$\psi_s = \sum_{n=1}^{\infty} b_n \psi_{sr} \cos(k_{szn} z). \quad (2.11)$$

Then, substituting (2.10) and (2.11) in (2.9) and using (2.7) couples vorticity of the dust to any arbitrary scale of the vorticity of the driving fluid. The coupling between individual Fourier modes of variation along axial \hat{z} of the vorticities of the two fluids is linear and effectively corresponds to the choice $k_{szn} = k_z$ for which Eq. (2.9) reduces to a simpler form, independent of ψ_z ,

$$\begin{aligned} \frac{\partial^4 \psi_r}{\partial r^4} + \frac{2}{r} \frac{\partial^3 \psi_r}{\partial r^3} - \left[\left(\frac{3}{r^2} + K_1 \right) - \frac{2\psi_z''}{\psi_z} \right] \frac{\partial^2 \psi_r}{\partial r^2} + \left[\left(\frac{3}{r^3} - \frac{K_1}{r} \right) + \frac{2}{r} \frac{\psi_z''}{\psi_z} \right] \frac{\partial \psi_r}{\partial r} \\ - \left[\left(\frac{3}{r^4} - \frac{K_1}{r^2} \right) + \left(\frac{2}{r^2} + K_1 \right) \frac{\psi_z''}{\psi_z} - \frac{\psi_z''''}{\psi_z} \right] \psi_r - K_2 \omega_{sr} = 0, \end{aligned} \quad (2.12)$$

where the prime denotes integration with respect to z . Eq. 2.12 represents the equations to be solved for the dust flow system in order to recover the basic characteristics of the dust circulations as functions of parameters ξ , μ and ν motivated by the dusty plasma experiments. For its simpler numerical solutions using standard numerical procedures [127–129], the fourth order differential equation (2.12) can be resolved into four coupled first order linear ordinary differential equations

as follows,

$$\begin{aligned}
 \partial\psi_r/\partial r &= \psi_r^{(1)}, \\
 \partial\psi_r^{(1)}/\partial r &= \psi_r^{(2)}, \\
 \partial\psi_r^{(2)}/\partial r &= \psi_r^{(3)}, \\
 \text{and} \quad \partial\psi_r^{(3)}/\partial r &= f\left(\psi_r, \psi_r^{(1)}, \psi_r^{(2)}, \psi_r^{(3)}, \omega_{sr}\right).
 \end{aligned} \tag{2.13}$$

Here, the source vorticity ω_{sr} is determined by the form of the 2-D external unbounded background driver velocity field $v_s(r, z)$. Thus, the Eq. (2.13) couples circulations in the unbounded ion flow with finite vorticity on scale L_z to that of the dust fluid confined within the boundaries $-L_z < z < L_z$ and $0 < r < L_r$ while allowing the existence of ion flow circulations of varying scales along both along r and z . The above set of coupled linear partial differential equations is solved numerically by applying boundary conditions described below, obtaining 2D equilibrium flow field for the dust fluid in the region of confinement.

2.2.4 Boundary conditions

The boundaries for the dust flow in the present treatment are defined by the effective potential that allows no dust flow across a sharp potential step where the potential V_b for dust jumps from a small accessible value to a large value at the boundaries. Thus the dust velocity normal to the boundaries is zero ($u_\perp = 0$), consequently the dust is well confined in a finite section of a cylinder that accommodates the torus having a rectangular cross-section in r - z plane with azimuthally symmetry. For a boundary with no spatial structures or roughness ($k \rightarrow 0$), the dust fluid can be considered to flow with arbitrary velocity along the boundary using a perfect slip boundary flow, free from a dissipation or entropy generation. The flow parallel to the boundary in such cases is determined purely by the driving ion

flow. On the other hand, when the boundary is considered to produce a frictional dissipation in the flow, a partial or no-slip boundary flow ($u_{\parallel} = 0$) needs to be imposed and a boundary layer is expected to result in the solutions of Eq. (2.13). The boundary conditions are motivated by the experimental configurations where the driver is localized in a narrow region of the domain, and in the region of domain far from the influence of the driver the dust experiences strong friction such that velocities there are considerably small Ref. [11]. Depending on the above factors, various categories of solutions are obtained using the corresponding boundary conditions that are expressed in term of value of the streamfunction potential at the boundaries. Since the velocity is described by spatial derivatives of the streamfunction ψ as determined by Eq. (2.6), gradients of ψ is controlled along r and z directions at the boundaries. Clearly, fixing an equal velocity potential along any boundary section ensures flow purely along the boundary. Accordingly, a constant value $\psi = 0$ is set along the entire confining boundary of the domain. Further, the gradient normal to the boundary is set equal to zero along the sections of the boundary where no slip, or zero parallel velocity needs to be set. Such boundaries include all the sections of boundary with $r > 0$, namely, the top, right and bottom sections of the boundary. On the left boundary, on the other hand, which is the boundary section having $r = 0$, no control of the normal gradient of ψ is used, effectively allowing purely the driver to determine the flow velocity at the center of the domain.

2.2.5 Normalization, Scaling and Parameter regimes

Identifying the radial width of the region L_r and the ion flow velocity at the center U_0 as the ideal normalization for the lengths and velocities in our system, respectively, the quantities in governing fluid dynamic Eq. (2.13) is nondimensionalized and normalized in the present approach. We have thus used the transformations, $\psi \rightarrow \psi/[U_0 L_r]$, $\omega \rightarrow \omega/[U_0/L_r]$, $\mathbf{u} \rightarrow \mathbf{u}/[U_0]$, $\omega_s \rightarrow \omega_s/[U_0/L_r]$, $\mu \rightarrow \mu/[U_0 L_r]$,

$\xi \rightarrow \xi/[U_0/L_r]$ and $\nu \rightarrow \nu/[U_0/L_r]$. These normalization factors serve as the units in our numerical solutions presented in the following sections.

Considering a typical laboratory glow discharge argon plasma with micron size dust and the plasma parameters, $n = 10^{12} \text{ cm}^{-3}$, $T_e = 3 \text{ eV}$, $T_i = 1 \text{ eV}$, we assume the conditions where ions are streaming into the bottom electrode with a flow velocity U_0 equivalent to fraction of the ion acoustic velocity $c_s = \sqrt{T_e/m_i}$. For such plasma conditions the value of ion drag coefficient is estimated to be $\xi \sim 1.0 \times 10^{-5} U_0/L_r$ and neutral collision frequency to be $\nu \sim 1.0 \times 10^{-1} U_0/L_r$ [124–126]. For a typical system size, $L_r \sim 10 \text{ cm}$, the range of kinematic viscosity μ can similarly be chosen $\mu \sim 1 \times 10^{-6} U_0 L_r$ which corresponds to small Reynolds number ($\text{Re} \simeq 1$) of the dust flow, consistent with many dusty plasma experiments and simulations results [4, 130]. The variation in ranges about these values of parameters is therefore made in the present treatment for the characterization of the dust flow dynamics relevant to various experiments.

2.3 Bounded dust flow equilibria: monotonic drive

The Eq. (2.13) is solved numerically obtaining the 2-D distribution of the stream-function ψ of the dust flow in the confined region $0 < r/L_r < 1$ and $-1 < z/L_z < 1$ using a range of system parameters, with fixed boundaries and the driving fluid's vorticity ω_s . In this and the following section, we have analyzed dust flow equilibrium in two important cases of sheared ion flow profiles, first in the subsection 2.3.1 where the driving field is considered having a monotonic profile with shear, using a cosine like radial variation in velocity at $z = 0$ that peaks at the center ($r = 0$) but drops to minimum value at the boundary at $r = L_r$. In the following section 2.4, the driving field is considered having a localized shear where flow

velocity value has a narrow peak at an intermediate radial location and remains minimum both at the center and at the boundary $r = L_r$. The nature of dust flow field and its characterization with respect to various system parameters is described systematically in the following subsections.

2.3.1 Dust circulation driven by cosine flow field of the ions

For simple flow structure, let us consider the shear driver velocity profile as a single cosine mode for radial as well as axial direction such that the intensity of ion flow is maximum at the center but drops to minimum value at the outer boundary $r = L_r$. We begin by choosing the driver velocity profile corresponding to the single axial Fourier mode of the vorticity coupling to the confined dust fluid dimension as follows,

$$v_z(r, z) = A_m \cos\left(\frac{\pi r}{2L_r}\right) \cos\left(\frac{\pi z}{2L_z}\right). \quad (2.14)$$

Here A_m are magnitude of the sheared streaming external driving fields. For obtaining the corresponding source function ω_{sr} , we adapt the stream function for the ions in the following form as desired,

$$\psi_s = \psi_{sr} \cos\left(\frac{\pi z}{2L_z}\right), \quad (2.15)$$

The corresponding velocity component $v_r = -\partial\psi_s/\partial z$ can readily be written as,

$$v_r(r, z) = \left(\frac{\pi}{2L_z}\right) \psi_{sr} \sin\left(\frac{\pi z}{2L_z}\right). \quad (2.16)$$

which, upon using (2.14) and (2.16), yields,

$$\omega_{sr} = A_m \left(\frac{\pi}{2L_r} \right) \sin \left(\frac{\pi r}{2L_r} \right) + \left(\frac{\pi}{2L_z} \right)^2 \psi_{sr}. \quad (2.17)$$

Now, using $v_z = \frac{1}{r} \frac{\partial(r\psi_s)}{\partial r}$, the unknown function ψ_{sr} can be determined by using v_z from (2.14) which yields a linear equation,

$$\frac{\partial \psi_{sr}}{\partial r} + \frac{\psi_{sr}}{r} = A_m \cos \left(\frac{\pi r}{2L_r} \right), \quad (2.18)$$

that can be solved analytically to obtain,

$$\psi_{sr} = \frac{A_m}{r(\pi/2L_r)^2} \left[r \left(\frac{\pi}{2L_r} \right) \sin \left(\frac{\pi r}{2L_r} \right) + \cos \left(\frac{\pi r}{2L_r} \right) - 1 \right].$$

Substituting the above expression for ψ_{sr} in (2.17) we obtain the value of ω_{sr} as,

$$\omega_{sr} = A_m \left[\left(\frac{\pi}{2L_r} \right) \sin \left(\frac{\pi r}{2L_r} \right) + \frac{1}{r} \left(\frac{L_r}{L_z} \right)^2 \left\{ r \left(\frac{\pi}{2L_r} \right) \sin \left(\frac{\pi r}{2L_r} \right) + \cos \left(\frac{\pi r}{2L_r} \right) - 1 \right\} \right] \quad (2.19)$$

The value of ω_{sr} is used in Eq. (2.13), which couples circulations of an unbounded ion flow with finite vorticity of axial scale L_z to that of the confined dust fluid. The solutions in terms of dust streamfunction $\psi = \psi_r \psi_z$ are now determined using (2.19) as the known driver vorticity consistent with the monotonically varying cosine radial profile (2.14) of the driver flow velocity.

2.3.2 Dust Streamfunction and streamlines

The advantage of employing with scalar potential streamfunction, ψ , instead of the vector fields in two dimensional flow problem is already introduced in sec. 2.2.3. The complete 2D solution of the formulated numerical model yielding the streamfunction $\psi(r, z)$, and its corresponding streamlines, i.e., the contours of the product $r\psi$ are presented in Fig. 2.3 (a) and (b), respectively, for a set of relevant system

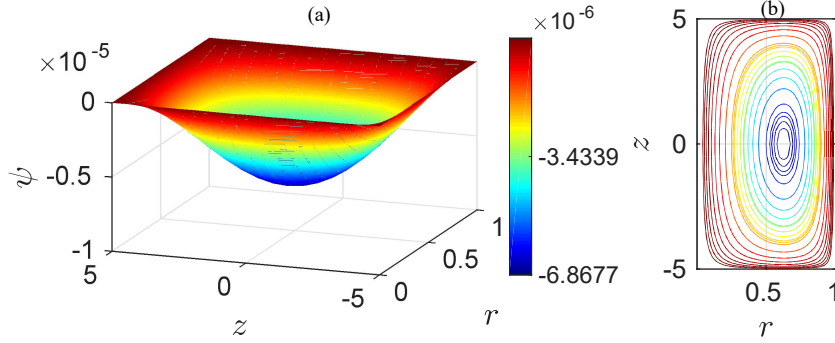


Figure 2.3: (a) Streamfunction potential and (b) corresponding streamlines or contours of $r\psi$ of the driven dust flow in rz -cross section of aspect ratio $L_z/L_r = 5$.

parameters $\mu = 10^{-3}U_0L_r$, $\xi = 10^{-5}U_0/L_r$ and $\nu = 10^{-1}U_0/L_r$ in the linear viscous regimes of the confined dust flow described by the Eq. (2.12). The streamlines show characteristic features of flow circulations confirming to the boundary geometry in the linear regimes when the Reynolds number approaches zero ($\text{Re} \ll 1$). The radial profile of the sheared driver flow field is shown in Fig. 2.4(a), and that of streamfunction ψ through the axial center of circulation z_0 on one of the azimuthally symmetric r - z planes is shown in Fig. 2.4(b). The resulting radial and axial profiles of the dust flow velocity, i.e., $u_z(r, z_0)$ and $u_r(r_0, z)$ on this plane through the corresponding centers of the circulation z_0 and r_0 of the 2D r - z plane are shown in Fig. 2.4(c) and (d), respectively. The variations in cross-section profile of streamfunction and velocity profiles for two different types of boundary conditions, namely no-slip ($u_{\parallel} = 0$) and perfect slip applied at the outer radial boundary $r = 1$, are compared in the figure 2.4(c) to (d). Note that the no-slip boundary introduces friction between the stationary dust at the boundary and the internal dust flow field such that a strong shear develops allowing the velocity at the boundary to drop to zero at $r = 1$. This finite region adjacent to the external boundary where a strong viscous diffusive stress develops is seen extended up to certain characteristic radial width that can be identified as the boundary layer thickness. This thickness of the boundary layer is seen depending systematically

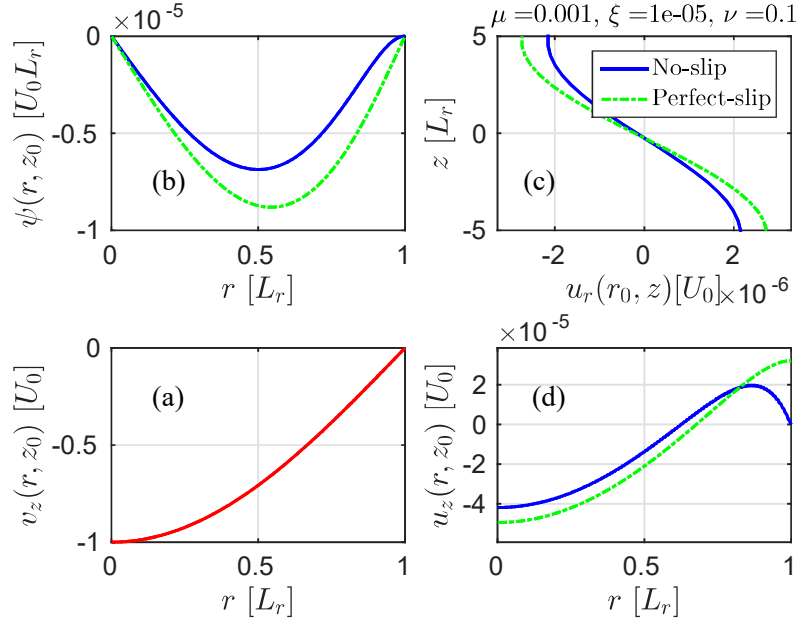


Figure 2.4: Radial profiles passing through center of circulation (r_0, z_0) for (c) Driver cosine ion flow velocity v_z , (d) Dust stream-function ψ , (e) Dust flow velocity u_r and (f) Dust flow velocity u_z for no-slip and perfect-slip boundary conditions.

on various system parameters, and is discussed in further detail in the analysis presented in the section 2.3.6.

2.3.3 Effect of ion drag coefficient ξ on the dust circulation strength

The dynamics of a confined dusty cloud in a sheared streaming plasma depends on changes in many system parameters such as the kinematic viscosity μ , coefficient of ion drag force on the dust ξ , the neutral-dust collision frequency ν , the form $v(r, z)$ of the unbounded driver field and the nature of the confining boundaries. In the present analysis the effect of ion drag co-efficient ξ , on the equilibrium between the two flows is explored by fixing the other system parameters in the linear or small Reynolds number ($Re \leq 1$) regimes of the dust flow and varying the value of ion drag coefficient to take the values $\xi = 0.1, 0.4, 0.7$ and $1.0 \times 10^{-5} U_0 / L_r$.

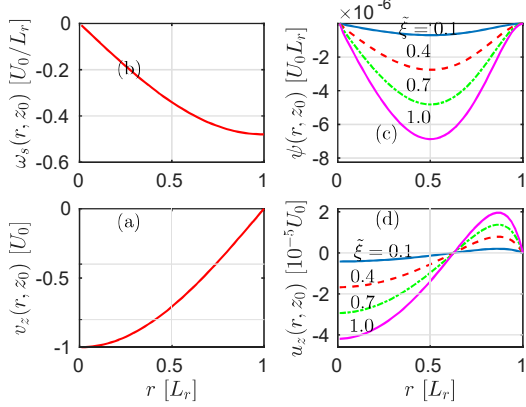


Figure 2.5: Radial profiles at $z = z_0$ for (a) Driver cosine ion flow velocity v_z , (b) Corresponding vorticity ω_s , (c) Varying dust stream-function ψ and (d) Dust flow velocity u_z for $\xi = 0.1, 0.4, 0.7$ and $1.0 \times 10^{-5} U_0/L_r$.

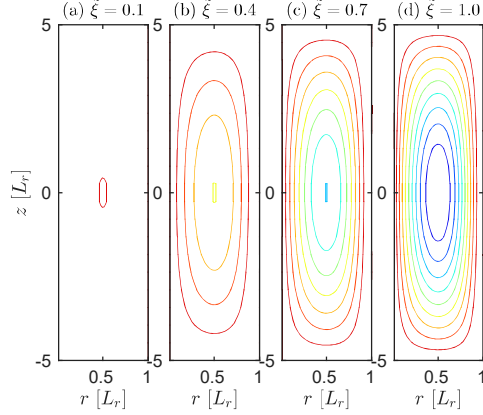


Figure 2.6: Streamlines for the dust fluid flow in r - z cross section for varying ions dragging frequency $\xi =$ (a) 0.1, (b) 0.4, (c) 0.7, and (d) $1.0 \times 10^{-5} U_0/L_r$ and fixed $\mu = 10^{-3} U_0 L_r$, $\nu = 10^{-1} U_0/L_r$.

The used radial profile of the flow velocity of the driver fluid, ions, is plotted in Fig. 2.5(a) at $z = z_0$ along with the corresponding source vorticity ω_s in Fig. 2.5(b). The resulting radial profiles of the stream-function ψ and the dust flow u_z for above values of ξ are presented in Fig. 2.5(c) and (d) respectively. As seen in Fig. 2.5(a) and 2.5(d), when the unbounded ion fluid flows from the top to bottom (i.e., along $-\hat{z}$) at all r values with a monotonic shear, the net flux of confined dust across the location $z = z_0$ remains zero since the dust flow, driven by the ion drag, undergoes only a circular flow in the volume as it is confined by the boundaries of the region satisfying the continuity equation (2.4). Across the location $z = z_0$, the direction of the dust flow is downward (i.e., $-\hat{z}$) at all radial locations up to $r = r_0$. The dust flow however changes sign at an intermediate radial location ($r > r_0$) in order to satisfy the continuity of the dust flow, Eq. (2.4). The downward flowing flux of dust at small $r < r_0$ values balances the upward flowing dust flux at large $r > r_0$. Clearly, the dust flow is along the ion flow where ion flow is stronger and is capable of dragging the dust along, while the flow of dust fluid is against the ion flow at

the large r locations where the downward ion flow is rather weak. As plotted in Fig. 2.5(d), at small values of drag coefficient ξ the radial profiles of dust flow is almost uniform, it however tends to acquire the radial variation (or shear) almost identical to that of the driver fluid when a larger drag coefficient is present with appropriate modification near the external boundaries to satisfy imposed boundary conditions. The corresponding streamline patterns are plotted in Fig. 2.6(a)-(d) for the values of $\xi = 0.1, 0.4, 0.7$ and $1 \times 10^{-5} U_0/L_r$ showing the characteristics changes in flow patterns. For a small value of ion drag co-efficient ξ , the local loss of momentum to neutral is equalized with the local momentum gain from interaction with ions without requiring significant transport across streamlines and thus the dust circulation is negligible or cease in the recovered steady-state equilibrium. However, the gradual strengthening of the dust circulation is observed with increasing ξ and fixed value of μ and ν .

2.3.4 Effect of neutral friction ν on dust circulation

The background neutral medium acts as a volumetric sink of the momentum or vorticity in the system of dust driven by ions and maintain a dynamic equilibrium steady-state flow of the dust fluid. To study the effect of dust-neutral collision frequency ν , the equilibrium flow is explored for a wide range of this frequency, $\nu = 0.5, 2.0, 3.5$ and $5.0 \times 10^{-1} U_0/L_r$, respectively. The above flow characteristics in terms of resulting variation in the dust streamfunction $\psi(r, z_0)$ are presented in Fig. 2.7(c) while the corresponding velocity profiles $u_z(r, z_0)$ are plotted in Fig. 2.7(d). These flow characteristics show significant reduction in the strength of flow potential and corresponding flow velocities with increasing neutral collisions coefficient ν . Note that neutrals are uniformly distributed through out the confined flow domain and act against the flow, thus affecting the Reynolds number indirectly through collisions. The effect on the strength of the circulations of the confined dust driven by unbounded sheared driving field Fig. 2.7(a) and (b),

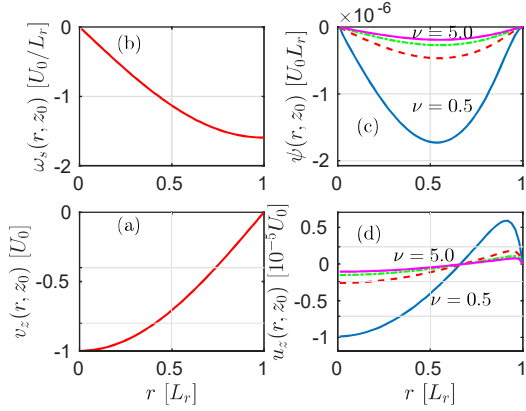


Figure 2.7: Radial profiles at $z = z_0$ for (a) Driver cosine ion flow velocity v_z , (b) Corresponding vorticity ω_s , (c) Varying dust stream-function ψ and (d) Dust flow velocity u_z for $\nu = 0.5, 2.0, 3.5$ and $5.0 \times 10^{-1} U_0/L_r$.

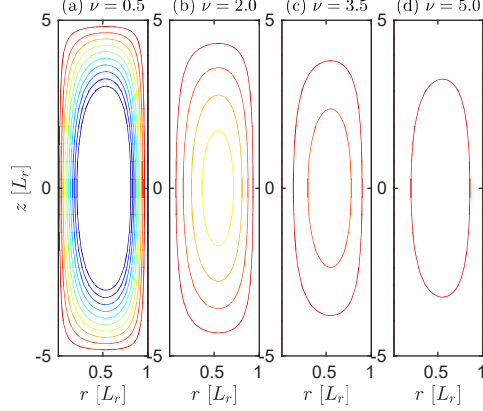


Figure 2.8: Streamlines for the dust fluid flow in r - z plane for varying neutral collision frequency $\nu = (a) 0.5, (b) 2.0, (c) 3.5$, and $(d) 5.0 \times 10^{-1} U_0/L_r$ and fixed $\mu = 10^{-3} U_0 L_r$, $\xi = 10^{-5} U_0/L_r$.

are again characterized in term of changes in streamlines patterns with increasing neutral collision frequency, as presented in Fig. 2.8.

The weakening of strength of streamline patterns with increasing neutral collision frequency ν shows the characteristics changes of dust circulations with varying neutral collision frequency. Dust dynamics can cease at extremely high neutral collision frequency. In both sets of characterization, namely, by changing ξ as shown in Fig. 2.5 and by changing ν as shown in Fig. 2.7, the center of circulation remains fixed at a particular location (r_0, z_0) .

2.3.5 Effect of kinematic viscosity μ on dust vortex motion

In order to study the effect produced by changing kinematic viscosity μ , the dynamic equilibrium of the dust flow is again explored for a finite ranges of dust kinematic viscosity μ , while fixing the other parameters, including the strength of unbounded driving field, as presented in Figs. 2.9(a) and 2.9(b). The corresponding variations in cross-section profiles for streamfunction and velocity profiles are

shown in Fig. 2.9(c) and (d), showing a negligible reduction in flow strength, but change in position of the center of circulation and increase in the width of the boundary layer, Δr_b , developed on the boundaries with increasing dust viscosity using the values $\mu = 0.1, 0.4, 0.7$ and $1.0 \times 10^{-3} U_0 L_r$. This shows that the diffusive stress at the boundaries is distributed over a larger radial extension with increasing viscosity of the fluids. The characterization also reveals that more viscous fluid develops slightly smaller flow velocity than the less viscous fluid under same external driving field. The variations in streamlines as shown in Fig. 2.10 reveal that any change in kinematic viscosity μ in linear (low Re) regime, although has no strong effect on the overall strength of the circulations of the confined and driven dust flows but strongly affects its spatial distribution close to the boundaries. The characteristic effects of change in kinematic viscosity are quite different from that of ion drag co-efficient ξ and neutral collision frequency ν . The central circulations appear with same level of strength at all possible μ values and the μ -variation shows only small change in nature of the core region while significant changes appear in boundary regions. The effect of kinematic viscosity in the boundary region in linear (low Re) regimes is further discussed in following sections. Although not representable in the limit of linear solutions presented in this and the next chapter, it is clear that effect of kinematic viscosity will be an important factor in nonlinear (high Re) flow regimes where the relative strength of advective transport and diffusive transport depends mainly on kinematic viscosity μ . These effects of system parameters μ , ξ and ν at nonlinear (high Re) flow regime are addressed in sufficient detail in complete nonlinear treatment done in chapters 4 and 5.

2.3.6 Dust boundary layer and its characterization

The dust flow at the boundary remains parallel to the boundary surface, however the flow velocity parallel to the boundary changes in magnitude depending on the nature of boundary. Considering the no-slip boundary condition applied at the

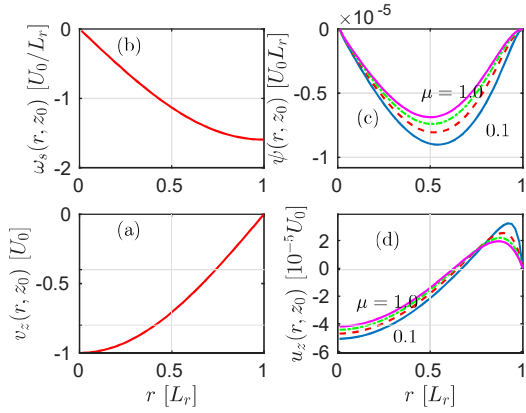


Figure 2.9: Radial profiles at $z = z_0$ for (a) Driver cosine ion flow velocity v_z , (b) Corresponding vorticity ω_s , (c) Varying dust stream-function ψ and (d) Dust flow velocity u_z for $\mu = 0.1, 0.4, 0.7$ and $1.0 \times 10^{-3} U_0 L_r$.

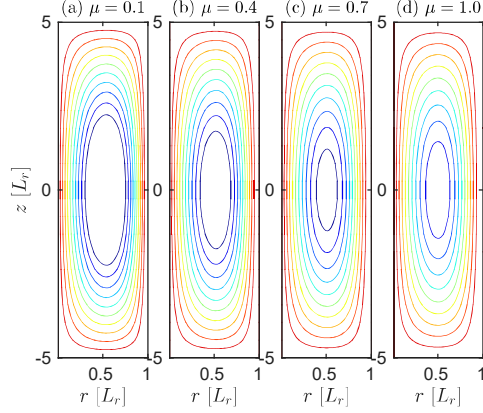


Figure 2.10: Streamlines for the dust fluid flow in r - z plane for varying kinematic viscosity $\mu =$ (a) 0.1, (b) 0.4, (c) 0.7, and (d) $1.0 \times 10^{-3} U_0 L_r$ and fixed $\xi = 10^{-5} U_0/L_r$, $\nu = 10^{-1} U_0/L_r$.

external cylinder surface $r = L_r$ and a perfect-slip at the boundary at $r = 0$, the dust flow velocity the latter is determined purely by the driver flow and the dust viscosity μ . As plotted in Fig. 2.3(f), the dust flow velocity u is obtained to be maximum at $r = 0$ and along the direction of the driving flow. At large r ($r \rightarrow L_r$) it changes sign and the dust flows against the driving field. Further, after attaining a maximum value against the ion flow at large r , it again drops to zero at its approach to outer radial boundary $r = L_r$ of the confined domain. The region near the boundaries where the viscous shear introduced by the no-slip boundaries is significant is identified as a boundary layer. Since the velocity at the boundary must drop to zero because of no-slip boundary condition, a maximum value appears in the velocity profiles close to the boundary and the separation of this maximum from the boundary, Δr_b , can be a good measure of the boundary layer thickness in most cases of interest. We analyze dependence of this separation both on the dust viscosity μ and coefficient of ion drag force ξ as shown in Fig. 2.11. We note that this characteristic length scale Δr_b increases with increasing viscosity μ .

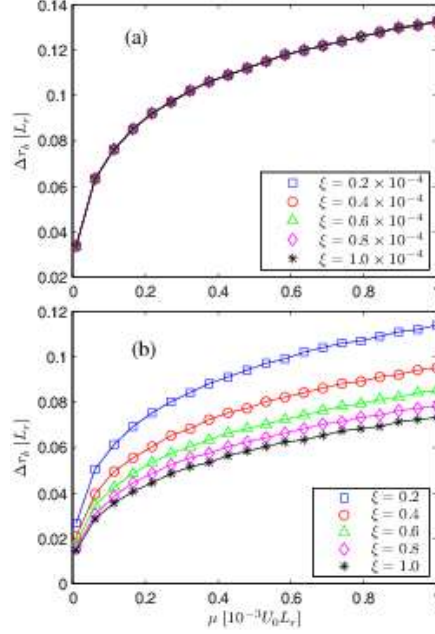


Figure 2.11: Dependence of the separation Δr_b on the parameter μ for (a) $\xi = 0.2, 0.4, 0.6, 0.8$ and $1 U_0/L_r$ and (b) $\xi = 0.2, 0.4, 0.6, 0.8$ and $1.0 \times 10^{-4} U_0/L_r$.

The dependence on ξ over a wide range of small values of ξ is negligible. However, in the cases with large enough ξ values plotted in Fig. 2.11(b), Δr_b value is sensitive to ξ and relatively smaller for higher ion drag coefficients ξ , therefore effectively smaller for larger dust flow velocities. The above dependence shows increasing impact, in the interior, of the boundaries that resist the dust motion at larger dust viscosity with ξ . Dependence on ξ indicates that this impact of boundary reduces at higher dust velocity in the interior. The complementary effects of these two quantities thus relate to the scale independence of the dust flow setup analogous to flow with a particular Reynolds number, $Re = Lu/\mu$, given a combination of velocity in the interior, $u(r = 0)$, and the length scale L_r . The dependence of Δr_b on various system parameters is different for different regime of the flows based on combination of the various system parameters. This correlation will be discuss in detail in the following chapters 3 and 4.

2.4 Bounded dust flow equilibria: non-monotonic drive

The solutions discussed in Sec. 2.3 presented the cases where an uncomplicated monotonic shear is present in a system with sufficiently large size which also determines the upper limit on the structure size. Presence of multiple driver length scales however generalizes this setup where structures of multiple scales might appear allowing to determine the lowest structure size that may be allowable by the diffusion process. Self-consistent appearance of the multiple scale structures is however not expected in the present linear regime of the formulation. This aspect is addressed in Chapter 3 and 4 where the nonlinear regime of the setup is analyzed. The numerical solutions with non-monotonic driver presented in this section however addresses the linear counter-rotating class of the system of multiple vortices and highlights the rich analytic character of this class, addressed further, in Chapter 2, using an analytic approach to the linear solutions presented

2.4.1 Drive by a localized Gaussian plasma stream

In order to use driver having scales distinct from the radial dimension L_r , we now examine the dust flow characteristics in the cases where ion flow is localized in the region around a fixed value of the radius, $r = r_0$ and therefore the associated shear is also confined to thin layers surrounding this region. A profile of the driving ion flow has been chosen for this purpose having the following form,

$$v_z(r, z) = A_m \exp \left[- \left(\frac{r - r_0}{\Delta L} \right)^2 \right] \cos \left(\frac{\pi z}{2L_z} \right). \quad (2.20)$$

Here A_m is magnitude of the streaming sheared driving fields, and ΔL is the width of the localized flow velocity profile. Following a procedure similar to that

in Sec. 2.3.1 results into a linear equation analogous to Eq. (2.18),

$$\frac{\partial \psi_{sr}}{\partial r} + \frac{\psi_{sr}}{r} = A_m \exp \left[- \left(\frac{r - r_0}{\Delta L} \right)^2 \right] \quad (2.21)$$

that has the following solution for the ψ_{sr} ,

$$\psi_{sr} = \frac{A_m}{r} \left[-\frac{\Delta L^2}{2} \exp \left\{ - \left(\frac{r - r_0}{\Delta L} \right)^2 \right\} + r_0 \int_0^r \exp \left\{ - \left(\frac{s - r_0}{\Delta L} \right)^2 \right\} ds + \frac{\Delta L^2}{2} \exp \left\{ - \left(\frac{r_0}{\Delta L} \right)^2 \right\} \right]$$

where s is the spatial variable of integration from the inner boundary to the location r . The radial dependence of ion vorticity, ω_{sr} , in the region is thus obtained in this case as,

$$\omega_{sr} = 2A_m \frac{(r - r_0)}{\Delta L^2} \exp \left\{ - \left(\frac{r - r_0}{\Delta L} \right)^2 \right\} + \left(\frac{\pi}{2L_z} \right)^2 \psi_{sr} \quad (2.22)$$

The value of ω_{sr} is used in Eq. (2.13), which couples circulations of an unbounded ion flow with localized sheared vorticity to that of the confined dust fluid and solved for streamfunction of the dust flows.

2.4.2 Multiple counter-rotating dust vortex formation

The radial profiles for the dust flow driven by the sheared ion flow localized at a radial location $r_0 = 0.5L_r$, or the center of the zone, are presented in Fig. 2.12 with values of drag coefficient $\xi = 0.1, 0.4, 0.7$ and $1.0 \times 10^{-5}U_0/L_r$, respectively, where the normalized parameter $\tilde{\xi} = \xi/(10^{-5}U_0/L_r)$ is used for simplicity of the representation. The corresponding change in streamline patterns are shown in Fig. 2.13. By choosing the width of ion flow profile $\Delta L = 0.1L_r$ the solutions are obtained where the dust flow profiles in the interior $r < L_r$ as well as the center $r = 0$ are determined by the driving ion flow. At the outer boundary $r = L_r$ the dust flow velocity is however set to be zero. The solutions for the dust streamfunction in this case are seen divided, about the location $r = r_0 \sim 0.5L_r$,

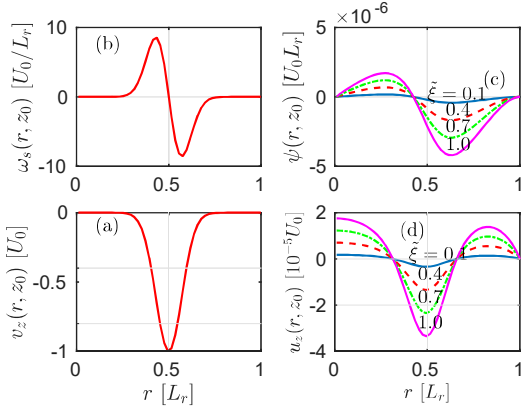


Figure 2.12: Radial profiles at $z = z_0$ for (a) Driver cosine ion flow velocity v_z , (b) Corresponding vorticity ω_s , (c) Varying dust stream-function ψ and (d) Dust flow velocity u_z for $\xi = 0.1, 0.4, 0.7$ and $1.0 \times 10^{-5} U_0/L_r$.

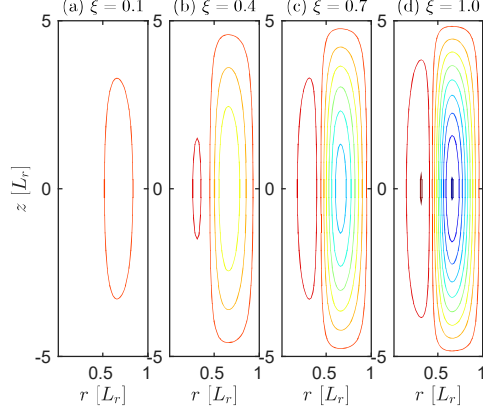


Figure 2.13: Streamlines for the dust fluid flow in $r-z$ plane for varying ions dragging frequency $\xi =$ (a) 0.1, (b) 0.4, (c) 0.7, and (d) $1.0 \times 10^{-5} U_0/L_r$ and fixed $\mu = 10^{-3} [U_0 L_r]$, $\nu = 10^{-1} U_0/L_r$.

in two separate zones, forming two counter-circulating dust flow vortex. A finite asymmetry in the two zones corresponding $r < r_0$ and $r > r_0$, results from, (i) the boundary in the outer zone where u_z must approach to zero in contrast to that at $r = 0$, and (ii) from the characteristics of the cylindrical setup where smaller area is available at smaller radius and flow velocity must increase in order to balance the upward directed flux at the larger radius as the net flow across $z = 0$ for the confined dust must be zero unlike the ion fluid. Note that though the depth of streamfunction curve is higher for the outer zone $r > r_0$, the peak value of u_z in this zone is smaller than that in the inner zone at $r < r_0$ for all the values of ξ as seen from Fig. 2.12(c) and 2.12(d) respectively. This observed flow characteristics are very relevant to the vortices observed in laser heating driven dust flow in laboratory experiments [131]. This prediction of multiple vortices [24] also motivated the recovery of similar kind of multiple counter-rotating vortices in laboratory dusty plasma experiment at IPR-India by Manjit *et al.* [12], where non-monotonic radial density profile was introduced in the background ions. This

was achieved experimentally by a specially designed cathode structure that has a concentric metallic disk and ring of different radii on the bottom electrode (see Fig. 2.1) acting as cathode.

2.4.3 Radial shift and emergence of a counter rotating vortex

Further we have analyzed the cases where we varied the value of r_0 in order to examine the effect of radial location of the peak of the localized source profile and its impact in the present cylindrical geometry where the flux associated with a constant density has a natural r dependence. These results in term of cross section profile are presented in Fig. 2.14 and streamline patterns in Fig. 2.15 respectively. This can be seen that the localization of the driving flow at various small to large radial values features a transition from single to multiple vortex structures. In the cases presented here, the driving flow is considered localized at larger to smaller radius, including at the center $r_0 = 0$. In the case where source is localized at the center ($r_0 = 0$) the strong downward driven flux of dust fluid present at the center is balanced by a less stronger upward directed flux at the large r locations. A single dust vortex with strong downward directed flow, concentrated close to the center $r = 0$ can be seen in this case while the flow away from the center and in the region close to outer boundary has negligible intensity. It can however be noted that a visibly larger area under the negative part of the flow velocity curve contributes an equivalent downward flux close to the $r = 0$ due to reduction in the area element $2\pi r dr$ with reducing r in the present cylindrical geometry. When the location of the driving flux peak is moved at larger r values the downward directed dust flux at the center gradually reduces in the magnitude and at a sufficiently large r_0 the flow at the center changes the sign by producing a net upward flow. Emergence of this new route in the flux conserving flow set up corresponds to a transition from

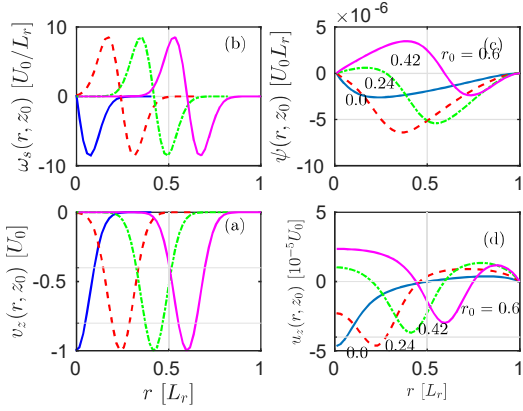


Figure 2.14: Radial profiles at $z = z_0$ for (a) Driver cosine ion flow velocity v_z with various peak locations r_0 . (b) Corresponding vorticity ω_s . (c) Varying dust stream-function ψ and (d) Dust flow velocity u_z for $r_0 = 0.0, 0.24, 0.42$ and $0.60 L_r$.

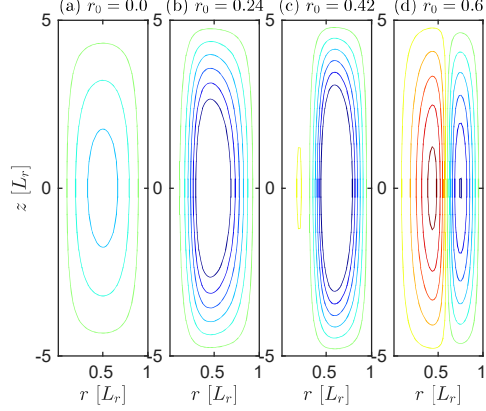


Figure 2.15: Streamlines for the dust fluid flow in $r-z$ plane for localized Gaussian ion flow at $r_0 =$ (a) 0.0, (b) 0.24, (c) 0.42, and (d) 0.60 L_r for fixed $\mu = 10^{-3} U_0 L_r$, $\xi = 10^{-5} U_0/L_r$, and $\nu = 10^{-1} U_0/L_r$.

a single to multiple vortex regime where the upward moving dust flux balances the downward driven flux via two disjoint regions in the $r-\phi$ plane, producing two counter circulating vortex in the $r-z$ plane as visible in the streamlines presented in Fig 2.15(a)-(d) that feature such a transition beyond $r_0 = 0.24$, between Fig 2.15(b) and Fig 2.15(c). Although the solutions with a single localized flow structure are presented here, the multiple vortex solution must emerge when a complex source structure with multiple localized shear layers is used as external driver. For a fixed system size, however, the radial scale length of the vortices must reduce in such situation allowing the details of viscous dissipation or nonlinear effects of vorticity convection to become important at sufficiently larger k values, where a viscous cutoff, k_d , may exist and determine the smallest sustainable spatial scale of the observable vortex [132, 133].

2.5 Summary and conclusions

The dust vortex structures, routinely recovered in dusty plasma experiments in normal laboratory conditions and in microgravity conditions present an attractive and accessible paradigm for a range of driven-dissipative complex system apart from numerous small Reynolds number natural flow systems that can be modelled by dusty plasma vortices on much more accessible scales. With requirement of a formulation for study of vortices forming in dusty plasmas as motivation, the first application of 2D hydrodynamic formulation is done to confined dust clouds electrostatically suspended in a laboratory plasma. As a first approximation, the nearly incompressible dust flow dynamics is treated as governed by the 2D Navier-Stokes equations in which the drive produced by the ion drag and the friction produced by the stationary neutral fluid can be suitably accounted for in a steady-state. The dust vortex formulation is developed based on the streamfunction approach in fully curvilinear setup which inherently accounts for the incompressibility of the dust flow and produces characterizable solutions in terms of dust streamlines, as functions of measurable parameters and relevant boundary conditions.

Beginning from the conservation equations in 2D cylindrical setup the formulation introduces the dust streamfunction and its relationship with the 2D dust flow field components. Reducible in to a set of multiple coupled first order partial differential equations, the model can be suitably solved for dust streamfunction, subject to appropriate boundary conditions that are transformed in terms of the dust streamfunction and its derivatives. In the applicable regime of interest, the formulation produces scaled solutions with system relevant normalizations allowing to obtain and characterize the bounded dust flow equilibria. The formulation modelling an open system admits dust drive by a number of external sources of vorticity by allowing to specify them by means of a source term. Describing a number of possible sources, the solutions obtained here consider the vorticity sup-

plied by a streaming sheared flow of ions, exerting a drag force on the dust, as a representative driving mechanism. The dust flow equilibria are analyzed in two important cases of sheared ion flow profiles, first in the case where the driving ion flow field is considered having a monotonic profile with shear, using a cosine like radial variation in velocity at $z = 0$ that peaks at the center ($r = 0$) but drops to minimum value at the boundary located at $r = L_r$. In the second case, the driving field is considered having a localized shear where flow velocity value has a narrow peak at an intermediate radial location and remains minimum both at the center and at the boundary $r = L_r$.

By means of treatment in the first monotonic drive case, a detailed characterization was done in terms of the effects of (i) ion drag coefficient ξ , (ii) neutral friction ν and (iii) kinematic viscosity μ , on the dust circulation or dust vortex structure properties. Demonstrating the desired applicability to the dust vortex formation observed in a number of experimental conditions, this first characterization in terms of dust streamfunction solutions yielded the following characteristic observations and conclusions:

- The complete 2D profiles of the dust streamfunction $\psi(r, z)$ produce corresponding streamlines, represented, in the present curvilinear geometry, by the contours of the product $r\psi$ in the domain of the solutions.
- The no-slip boundary used at finite boundary section introduces friction between: the stationary dust medium it represents at the boundary, and the internal dust flow field, such that a strong shear develops allowing the velocity at the boundary to drop to small values at the corresponding boundary sections.
- This finite region adjacent to the resisting boundary where a strong viscous diffusive stress develops is seen extended up to certain characteristic width that can be identified as the boundary layer thickness.

- The net flux of confined dust across the vertical symmetry location $z = z_0$ remains zero since the dust flow, driven by the ion drag, undergoes only a circular flow in the volume as it is confined by the boundaries of the region satisfying the continuity equation.
- For the ion flow profile which is unidirectional, because of the confinement the dust flow is along the ion flow where ion flow is stronger and is capable of dragging the dust along. It however turns against the ion flow at the large r locations where the downward ion flow is rather weak, resulting in its steady circulation.
- At small values of drag coefficient ξ the radial profiles of dust flow at symmetry plane is almost uniform, it however tends to acquire the radial variation (or shear) almost identical to that of the driver fluid when a larger drag coefficient is present with appropriate modification near the external boundaries to satisfy imposed boundary conditions.
- For a small value of ion drag co-efficient ξ the dust circulation is negligible. However, the gradual strengthening of the dust circulation is observed with increasing ξ and fixed value of μ and ν .
- The weakening of strength of streamline patterns with increasing neutral collision frequency ν shows the characteristics change of dust circulations with varying neutral collision frequency. Dust dynamics can cease at extremely high neutral collision frequency.
- Increase in the dust viscosity coefficient μ although results only in a negligible reduction in the flow strength, it changes position of the center of circulation and increases the width, Δr_b , of the boundary layer developed on the resisting boundaries with increasing dust viscosity

- The dust flow at the boundary remains parallel to the boundary surface, however the flow velocity parallel to the boundary changes in magnitude depending on the nature of boundary.
- Since the velocity at the boundary with stationary dust must drop to zero (the no-slip boundary condition), a maximum value appears in the velocity profiles close to the boundary and the separation of this maximum from the boundary, Δr_b , can be a good measure of the boundary layer thickness in most cases of interest. As already noticed, this characteristic length scale increases with increasing viscosity μ .
- The dependence of Δr_b on ξ over a wide range of small values of ξ ($\sim 10^{-4}U_0/L_r$) is negligible. However, in the cases with large enough ξ values ($\sim 1 U_0/L_r$), the Δr_b value is sensitive to ξ and relatively smaller for higher ion drag coefficients ξ , and therefore smaller for larger dust flow velocities.
- The streamfunction solutions were presented in additional cases of nonmonotonic shear in the streaming plasma flow. When a narrow stream of plasma $\Delta L = 0.1L_r$ is used as a driver localized at radial center $r = L_r/2$ of the domain, the dust streamfunction presents a solution that divides the domain in two separate zones, forming two counter-circulating dust flow vortices about the location of the stream.
- The flow characteristics recovered for the case of monotonic driver are found quite relevant to the vortices observed in the experimental setups where localized source of momentum is present, e.g, in the laser heated driven dust flow in a laboratory experiments [131]. This prediction of multiple vortices [24] also motivated the subsequent recovery of similar multiple counter-rotating vortices in laboratory dusty plasma experiment at IPR-India by Manjit *et al.* [12], up on introducing non-monotonic radial density profile of the back-

ground ions.

- Gradual development of a counter-rotating vortex was studied by introducing an increasing shift in the localized stream of ions. Transition from a single to multiple vortex regime is recovered where the upward moving dust flux balances the downward driven flux via two disjoint regions in the r - ϕ plane, producing two counter circulating vortex in the r - z plane.
- With respect to multiple vortex solutions it is generally noted that they must emerge when a complex source structure with multiple localized shear layers is used as external driver. For a fixed system size, however, the radial scale length of the vortices must reduce in such situation allowing the viscous dissipation or nonlinear effects of vorticity convection to become important at sufficiently larger k values, where a viscous cutoff, k_d , may exist and determine the smallest sustainable spatial scale of the observable vortex [132, 133].

In conclusion, the hydrodynamic formulation developed in this chapter has allowed modelling the basic characteristics of the laboratory dusty plasma vortices. A more analytic approach to solutions of the formulation might allow investigating the scalings and spectral properties of the dust vortices within the linear regime of their dynamics. Such an analytic approach is presented in the next chapter with a discussion on its application to many natural flow set ups and driven complex systems.

3

Analytic structure of confined and driven dust vortex flows

3.1 Introduction

A number of low Reynolds number flow processes in nature involving flow relative to boundaries share dynamical regime with fluid-like phase of electrostatically suspended highly charged dust particles in plasmas. Some examples of them include, swimming of microorganisms [16], bacterial turbulence [17], flow of viscoelastic fluids [18], as well as many robust life-saving biotechnology applications based on network of microchannels to achieve enhanced rates of, mixing, reactions and conduction of fluid flows [19, 20] essentially in the absence of the usual macroscopic turbulence [21]. A distinct mathematical structure is also associated with the dynamics of confined dust fluid which is driven, volumetrically, by a streaming unbounded plasma fundamental to a different class of flow setups. Consider that a typical laboratory dusty plasma setup has an assembly of negatively charged dust particles electrostatically levitated against the gravity by the electronegative

sheath formed on the electrode at the bottom, allowing a supersonic plasma to continuously filter through it in order to let the latter reach the electrode. This arrangement, given a much slower time scale of response of the dust in comparison to plasma species and very low Reynolds number of dust flow, resembles a number of physical and bio-physical set ups, for example, a microscopic semipermeable mixing chamber that allows a colloidal solute to gradually dissolve into a solvent filtering through it at a comparatively high Reynolds number. Another example is a developing, localized, artery congestion by a cohesive lipid (e.g., cholesterol) producing blockade to a cardiac valve that would permit the blood flow of higher Reynolds number [85]. The lump, in the latter, must steadily dissolve in the blood flow in order to check the blockade growth. As one of its significant related effects, atherosclerosis, a leading cause of death from myocardial infarction (heart attack), remains a geometrically focal disease, preferentially affecting the outer edges of vessel bifurcations. In these predisposed areas, hemodynamic shear stress, the frictional force acting on the endothelial cell surface as a result of blood flow, is weaker than in protected regions, rendering endothelium (interior surface of blood vessels) more susceptible to pathogenic stimuli of injury, cell adhesion, cell proliferation, and lipid uptake [86].

Under a systematic hydrodynamic formulation of the dust medium suspended in the plasma, studying the analytic structure of the dust vortex flow equilibria driven, volumetrically, by a high Reynolds number plasma flow ($Re \sim 10^6$ and above [134]), allows addressing many issues [24] relevant to above categories of complex fluid flow systems, including certain subtle implications of interaction of dust flow with limiting boundaries. The fact that though such boundary phenomena are essential to many natural dynamical processes but difficult to analyze in ordinary laboratory experiments, given the complexity or the inaccessible scale of original set up, makes the dusty fluid suspended in a plasma an ideal means of their study apart from being a complex medium often displaying spectacular flow

dynamics in various laboratory experiments. Harnessing this considerable analytic potential of the emerging field of dusty plasmas requires more accessible analytic version of the characterization done in Chapter 2 of this thesis and presented by Laishram *et al.* [24] with rather simple motivation of obtaining first 2D solutions to describe the dust vortex flow observed in the experiments carried out in normal laboratory conditions e.g., Ref. [11]) as well as in the international space station (ISS) under microgravity conditions [9]. These first systematic numerical solutions of the formulation, apart from describing the observable basic dynamics, demonstrated that various fundamental analytic aspects of the dust flow dynamics can indeed be exploited or examined more deterministically by means of the adopted formulation if the analytic version of such solutions presenting the vortex flow can be obtained. For example, the scale of the shear observable in the dust vortex motion relates to the (often overlooked) physics of the boundary phenomena and must follow a definite scaling with respect to the fundamental parameters of the dynamics, e.g., the kinematic viscosity μ of the medium displaying them.

Unlike the usual driven flow setups, the boundaries confining dust in plasma are exclusively seen by the dust medium while the medium providing the direct volumetric drive is allowed to have a global flow profile. This unique physics aspect of the dusty plasma systems, apart from making it relevant to numerous microscopic semipermeable flow setups in the nature, defines the basic mathematical structure of the formulation. Its solution, in turn, encompass the inhomogeneity introduced by the driver modes that are not essentially the eigen modes of the confined dust flow. The analytic characteristics of the solutions recovered in this chapter show that the shear in the dust vortex flow observable in the experiments follows a definite scaling with respect to the kinematic viscosity of the dust medium over a substantially wide range of the latter. This quantifies the considerable capacity of the dusty plasma setups to represent a wide range of low Reynolds number of natural flow processes with sufficient flexibility. It is additionally shown here that the

driven flow of the dust medium in a plasma conveniently lies in the linear regime ($\text{Re} \leq 1$) of the formalism over a substantially wide parameter range. This property is usually desired in the microscopic flow systems where the fundamental processes of mixing, reactions and convection must take place with sufficient efficiency without a turbulent dynamics [21] that necessitates dominance of the nonlinear effects and introduces interaction between the normal modes of the dynamics.

Addressing the above analytic issues in this chapter, in Sec. 3.2 we revisit the hydrodynamic formulation introduced in Chapter 2 highlighting the analytic eigenvalue structure of the problem and its solutions. In Sec. 3.2.1 the boundary value problem is constructed for a dust flow driven by a background plasma flow field having a prescribed eigenmode spectrum of the flow shear. The analytic solutions of the hydrodynamic model are obtained in Sec. 3.3 by treating the boundary value formulation as an eigenvalue problem and by expressing the eigenmodes in terms of linearly independent set of Bessel modes where both driving and driven flows follow valid flux conservation. The solutions that admit use of a driving plasma flow field with a multiple scale vorticity spectrum allow coupling of a multiple scale plasma flow field to produce an associated, but essentially non-identical, vorticity scale spectrum for the driven dust flow field. The deviation of spectral characteristics of dust vorticity from that of the driver is analyzed as determined largely by the boundary effects and a set of physical parameters, including the dust kinematic viscosity, the coefficient of neutral friction, and that of the ion drag acting on the dust fluid. The results and conclusions are summarized in Sec. 3.5.

3.2 2D hydrodynamic dust vortex formulation

We once again consider the dust dynamics within the Navier-Stokes regime and begin from using the momentum and particle conservation equations (2.2) and (2.4), respectively. The problem is once again best described by the curvilinear

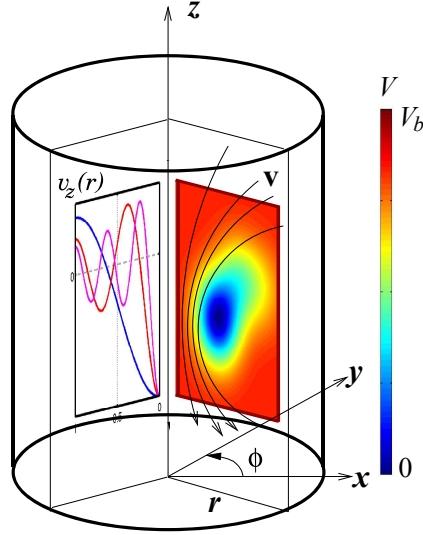


Figure 3.1: Schematic of the setup in the cylindrical geometry. Surface plot of an example effective confining potential $V(r, z)$ for the dust fluid (surface) is presented along with the flux conserving velocity field vector \mathbf{v} of the unconfined driving fluid in the r - z plane (arrows) and radial profile of its z -component $v_z(r)$ (2D plot).

set up similar to the schematic 2.2 presented in Chapter 2, we however reproduce it here in Fig. 3.1 to additionally emphasize on the structure of the driver flow expressible rather in terms of the appropriate radial eigenmodes of the system as considered in the this chapter and schematically drawn in Fig. 3.1 in the left-hand side rectangular cross-section of the toroidal dust cloud.

Following the streamfunction formulation provided in Sec-2.3.2, the dust vorticity ω is expressed in term of streamfunction ψ in the azimuthally symmetric cylindrical set up as,

$$\omega = - \left(\frac{\partial^2 \psi}{\partial r^2} + \frac{1}{r} \frac{\partial \psi}{\partial r} - \frac{\psi}{r^2} + \frac{\partial^2 \psi}{\partial z^2} \right). \quad (3.1)$$

Based on the spatial independence of coefficients of the governing Navier-Stokes equation (2.1), when ψ is assumed separable in r and z with its z -dependence described by a single Fourier mode $\psi_z = \cos(k_z z)$, a single vortex along z in agree-

ment with experiments [11, 12] represented by the choice $k_z = (2\pi/L_z)$ and ψ is expressible in the form of the product $\psi = \psi_r(r)\psi_z(z)$ [24]. When the effective coupling between individual Fourier modes of ψ_z with the axial mode of the driver vorticity ω_s is considered over the region, the Eq. (2.9) reduces in a form independent of ψ_z [24],

$$\begin{aligned} \frac{\partial^4 \psi_r}{\partial r^4} + \frac{2}{r} \frac{\partial^3 \psi_r}{\partial r^3} - \left[\left(\frac{3}{r^2} + K_1 \right) - 2k_z^2 \right] \frac{\partial^2 \psi_r}{\partial r^2} + \left[\left(\frac{3}{r^3} - \frac{K_1}{r} \right) + \frac{2k_z^2}{r} \right] \frac{\partial \psi_r}{\partial r} \\ - \left[\left(\frac{3}{r^4} - \frac{K_1}{r^2} \right) + \left(\frac{2}{r^2} + K_1 \right) k_z^2 - k_z^4 \right] \psi_r - K_2 \omega_{sr} = 0 \end{aligned} \quad (3.2)$$

where $K_1 = (\xi + \nu)/\mu$, $K_2 = (\xi/\mu)$ and the source vorticity ω_{sr} is determined by the form of the 2-D velocity field $v(r, z)$ of the background ion flow. The contribution from the modes other than the axial eigenmodes, due to its origin in the inhomogeneity of the formulation, is recoverable as a particular integral over the continuum of the Fourier modes for the cases where the circulations with scale larger than L_z are accounted for. This continuum contribution must however drop very fast in the interior when a sufficiently large number of Fourier eigenmodes are included. The Eq. (3.2) thus couples circulations in an unbounded ion flow of finite vorticity on scale L_z to that of the dust fluid confined within the boundaries $-L_z < z < L_z$ and $0 < r < L_r$ while allowing the existence of ion flow circulations of scales larger than L_z . Limiting the analysis to $\langle k_r \rangle \gg \langle k_z \rangle$, however, a single axial mode is assumed in present solutions providing a purely downward streaming driver plasma flow at $z = 0$ allowing it to turn radial at the distant top and bottom boundaries because of $L_z \gg L_r$. A complete multiple radial mode analysis is done as presented in rest of this chapter.

3.2.1 Construction of analytic boundary value problem

In order to construct the radial solutions bounded in the region $0 < r < L_r$ we begin by casting the Eq. (3.2) as an eigenvalue problem, with an associated set of eigenfunctions φ_m which satisfy the desired boundary conditions and can be assembled in linear combinations to construct the radial parts of the driven fluid streamfunction and the driving fluid vorticity or corresponding streamfunction,

$$\psi_r = \sum_{m=1}^{\infty} a_m \varphi_m \quad \text{and} \quad \omega_{sr} = \sum_{m=1}^{\infty} b_m \varphi_m, \quad (3.3)$$

respectively, such that the Eq. (3.2) is transformed into

$$F \sum_{m=1}^{\infty} a_m \varphi_m = K_2 \sum_{m=1}^{\infty} b_m \varphi_m, \quad (3.4)$$

with the operator F representing,

$$F = \frac{\partial^4}{\partial r^4} + \frac{2}{r} \frac{\partial^3}{\partial r^3} - \left[\left(\frac{3}{r^2} + K_1 \right) - 2k_z^2 \right] \frac{\partial^2}{\partial r^2} + \left[\left(\frac{3}{r^3} - \frac{K_1}{r} \right) + \frac{2k_z^2}{r} \right] \frac{\partial}{\partial r} - \left[\left(\frac{3}{r^4} - \frac{K_1}{r^2} \right) + \left(\frac{2}{r^2} + K_1 \right) k_z^2 - k_z^4 \right]. \quad (3.5)$$

Note that since the driver vorticity ω_{sr} is prescribed, the coefficients b_m are known. Hence, if the eigenvalues of the operator F corresponding to functions φ_m are known, the coefficients a_m can be determined from (3.4), producing, in turn, the desired solution (3.3).

3.2.2 Boundary conditions and appropriate eigenvectors

The solution procedure requires (i) selection of appropriate of eigenvectors φ_m that satisfy the boundary conditions as well as continuity equation for both, the dust and the ion fluid, and (ii) subsequent expansion of the prescribed source

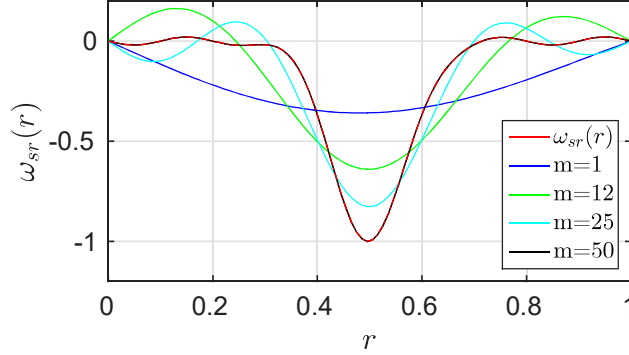


Figure 3.2: Bessel function reconstruction of a known function $\omega_{sr}(r)$ with increasing number m of modes.

vorticity ω_{sr} in the linear combination of eigenvectors φ_m . Note that, however, the solutions are sought for the streamfunction ψ , the physical boundary conditions are essentially defined on the $u_{||}$, i.e., the z component of the flow velocity field in the dust confinement domain, obtainable from the relation,

$$u_z = \frac{1}{r} \frac{\partial(r\psi)}{\partial r}. \quad (3.6)$$

The relation (3.6) ensured that the radial gradient of the eigenfunctions can govern the value of the u_z at the boundaries while in the interior $0 < r < L_r$ it is governed by the source, effectively via the Eq. (3.2). From physical considerations, in absence of any physical boundary at $r = 0$ the flow velocity value there is again determined by the driver and only its gradient can be set to zero by symmetry argument. On the other hand, at the outer boundary ($r = L_r$) the choice, for example, of a no-slip flow can be made by setting $u_z(r = L_r) = 0$. This latter choice is made in the present analysis in order to allow and study the formation of a boundary layer at this boundary.

For most suitable imposition, as discussed below, of the above physical boundary conditions in the present cylindrical setup, we choose to express the streamfunction of both the dust and the background ion flow in terms of linear combinations

of functions φ_m that represent to a set of Bessel functions,

$$\psi_r = \sum_{m=1}^{\infty} a_m J_n \left(\alpha_m \frac{r}{R} \right), \quad \omega_{sr} = \sum_{m=1}^{\infty} b_m J_n \left(\alpha_m \frac{r}{R} \right). \quad (3.7)$$

The set $J_n(\alpha_m r/R)$ can additionally be a diagonalized set of eigenvectors by ensuring that the α_m are Bessel zeros, such that the functions φ_m satisfy the orthogonality condition,

$$\int_0^R r J_n \left(\alpha_i \frac{r}{R} \right) J_n \left(\alpha_j \frac{r}{R} \right) dr = \delta_{ij}. \quad (3.8)$$

Further, since the radial boundary must confine the dust with vanishing velocity normal to the boundary, $u_{\perp} = 0$, the relation (2.6) prescribes that streamfunction ψ must be a constant along boundaries at $r = L_r$, while the radial derivative of the streamfunction can be controlled to impose an appropriate boundary value of the velocity u_z at this boundary using (3.6). Accordingly, we choose the set of first order Bessel functions J_1 (i.e., $n = 1$) as eigenfunctions φ_m that satisfy the $J_n(\alpha_m r/R) = 0$ at both the radial boundaries, $r \approx 0$ and $r \approx R(= L_r)$ while its derivative J_1' can be determined under the following formulation to achieve the solutions with desired boundary flow values. The optimum number of modes m in Bessel series expansion of the desired solutions and source must be used in Eq. (3.7) for computational efficiency as shown via a representative example in Fig. 3.2.

3.2.3 Eigenvalues of the operator F

In order to evaluate the eigenvalues λ_m of F we write the associated eigenvalue equation,

$$(F - \lambda_m) J_1(x_m) = 0, \quad (3.9)$$

where $x_m = \alpha_m r / R$. Substituting F from (3.5) in Eq. (3.9) we get,

$$x_m^4 J_1''''(x_m) + 2x_m^3 J_1'''(x_m) - [3 + K_1 r^2 - 2r^2 k_z^2] x_m^2 J_1''(x_m) + [3 - K_1 r^2 + 2r^2 k_z^2] x_m J_1'(x_m) + [-3 + K_1 r^2 - r^4(2/r^2 + K_1)k_z^2 + r^4 k_z^4] J_1(x_m) = r^4 \lambda_m J_1(x_m), \quad (3.10)$$

where the prime denotes differentiation with respect to r . Eq. (3.10), up on using the appropriate recurrence relations for the Bessel derivatives and eliminating J_0 and J_2 , yields the desired eigenvalues of the operator F ,

$$\lambda_m = \left(\frac{\alpha_m}{R}\right)^4 + K_1 \left(\frac{\alpha_m}{R}\right)^2 - \left[2 \left(\frac{\alpha_m}{R}\right)^2 + K_1\right] k_z^2 + k_z^4. \quad (3.11)$$

Combining Eq. (3.4), (3.9) and (3.11) produces the equation for the unknown coefficients a_m required for the solutions for the dust flow field in terms of the radial dust streamfunction ψ_r given by Eq. (3.7),

$$\sum_{m=1}^{\infty} (\lambda_m a_m - K_2 b_m) J_n(x_m) = 0. \quad (3.12)$$

Representing sufficiently small scales of the radial variation requires a large number $m = M$ of the eigenfunctions $J_n(x_m)$ for the streamfunction ψ_r . For the choice of orthogonal set of finite number of eigenvectors satisfying (3.8) and a common, non-zero boundary condition for J_1 , the coefficients a_m can be determined generally as,

$$a_m = \frac{K_2 b_m}{\lambda_m}, \quad (3.13)$$

whereas the particular boundary conditions can be applied by substituting the value of x_m corresponding to the boundary in the Eq. (3.12). For the general set of eigenfunctions, independent of condition (3.8), it is however clear that substituting a chosen value $r = r_i$ in Eq. (3.12) produces a single equation containing total

M unknown coefficients a_m . A set of minimum M values, r_i , must therefore be selected to construct a complete set of M simultaneous equations for obtaining the coefficients a_m ,

$$\begin{aligned}
 \sum_{m=1}^M (\lambda_m a_m - K_2 b_m) J_n(\alpha_m r_1/R) &= 0, \\
 \sum_{m=1}^M (\lambda_m a_m - K_2 b_m) J_n(\alpha_m r_2/R) &= 0, \\
 &\dots\dots\dots \\
 &\dots\dots\dots \\
 \sum_{m=1}^M (\lambda_m a_m - K_2 b_m) J_n(\alpha_m r_M/R) &= 0.
 \end{aligned} \tag{3.14}$$

The set of Eqs. (3.14) can be rearranged in a more familiar form,

$$\begin{bmatrix} A_{11} & A_{12} & \dots & A_{1M} \\ A_{21} & A_{22} & \dots & A_{2M} \\ \vdots & \vdots & \ddots & \vdots \\ A_{M1} & A_{M2} & \dots & A_{MM} \end{bmatrix} \begin{bmatrix} a_1 \\ a_2 \\ \vdots \\ a_M \end{bmatrix} = \begin{bmatrix} B_1 \\ B_2 \\ \vdots \\ B_M \end{bmatrix} \tag{3.15}$$

where,

$$A_{ij} = \lambda_j J_n(\alpha_j r_i/R) \tag{3.16}$$

$$\text{and } B_i = K_2 \sum_{j=1}^M b_j J_n(\alpha_j r_i/R). \tag{3.17}$$

The value a_m determined by solution of the set (3.15) corresponds to the weight of the contribution of m^{th} Bessel mode to the eigenmode spectrum of the dust streamfunction ψ_r .

3.2.4 Analytic form of the boundary conditions and spectral limit

Since the fourth order Eq. (3.4) is solved in terms of eigenfunctions that already satisfy two of the required boundary conditions $\psi_r = 0$ at the boundaries $r = 0$ and $r = R$ of the cylindrical region, the rest of the procedure clearly admits only two additional boundary conditions which need to be specified in terms of the radial derivatives of the streamfunction ψ_r at the two radial boundary locations. Note that the cylindrical symmetry of the present setup also results in the eigenmodes J_1 which naturally obey the condition that the radial derivatives of all the physical variables, e.g. that of the velocity u_z , must vanish at $r = 0$. With dust flow velocity at $r = 0$ purely determined by the driving source no conditions are imposed at this boundary on the u_z value and, in turn, the only remaining boundary condition is applied at $r = R$. Imposing the latter as a no-slip boundary condition, such that the dust flow velocity $u_z = 0$ at $r = R$, and requiring that the solutions must show no oscillations at the scales comparable to the grid resolution, Δr ($> d$, where d is the average particle separation), effectively produces the following two additional equations to replace two equations from the set of Eqs. (3.14), corresponding, respectively, to r_{M-1} and r_M ,

$$\sum_{m=1}^M a_m \frac{\alpha_m}{R} J_{n-1} \left(\alpha_m \frac{r_{M-1}}{R} \right) - \sum_{m=1}^M a_m \left(\frac{\alpha_m}{R} \right)^2 \times (r_M - r_{M-1}) J_n \left(\alpha_m \frac{r_{M-1}}{R} \right) = 0 \quad (3.18)$$

$$\text{and} \quad \sum_{m=1}^M a_m \frac{\alpha_m}{R} J_{n-1} \left(\alpha_m \frac{r_M}{R} \right) = 0, \quad (3.19)$$

with the corresponding matrix coefficients,

$$\begin{aligned} A_{M-1,j} &= \left(\frac{\alpha_j}{R} \right) J_{n-1} \left(\alpha_j \frac{r_{M-1}}{R} \right) - \left(\frac{\alpha_j}{R} \right)^2 (r_M - r_{M-1}) J_n \left(\alpha_j \frac{r_{M-1}}{R} \right), \\ B_{M-1} &= 0, \end{aligned} \quad (3.20)$$

and

$$A_{M,j} = \left(\frac{\alpha_j}{R} \right) J_{n-1} \left(\alpha_j \frac{r_M}{R} \right), \quad (3.21)$$

$$B_M = 0. \quad (3.22)$$

The desired matrix of Bessel coefficients \mathbf{a} for ψ_r can thus be evaluated as,

$$\mathbf{a} = \mathbf{A}^{-1} \mathbf{B}. \quad (3.23)$$

Determination of \mathbf{a} for a flux conserving plasma flow, which in the present analytic formulation can be prescribed in terms of the source streamfunction ψ_{sr} or the vorticity ω_{sr} , is thus possible by simply ensuring that the source flow velocities are pure eigenfunctions of the geometric setup.

3.3 Solutions of the flow field eigenvalue problem

The analytic solutions in terms of linear combinations of orthonormal Bessel modes representing the dust streamfunction can now be obtained provided that the prescribed driving plasma flow field $\omega_{sr}(r)$ is expressed in terms of the same set of orthonormal functions such that the known coefficients b_m , determine the matrix B in Eq. (3.23). The present analytic formulation reproduces the arbitrary source vorticity functions as a linear combination of the eigenmodes $J_1(x_m)$ represented by Eq. (3.7). Considering that for a known function $\omega_{sr}(r)$, the set of coefficients b_m can be obtained using the Orthonormality condition (3.8) of the Bessel functions as,

$$b_m = \frac{2}{R^2 [J_{n+1}(\alpha_m)]^2} \int_0^R r \omega_{sr}(r) J_n \left(\alpha_m \frac{r}{R} \right) dr, \quad (3.24)$$

once the co-efficient b_m are known, the corresponding set of desired coefficients a_m can be determined using (3.23) for recovering, for example, the solutions with two kinds of driver velocity profiles presented in sections 2.3 and 2.4, respectively, and in Ref. [24]

3.3.1 Radial eigenmodes of the driver field

In the present analysis, however, we limit ourselves to the source velocity $v_z(r, z)$ that are pure eigenfunctions of the cylindrical setup, i.e., the Bessel mode with monotonic shear as follows,

$$v_z(r, z) = \sum_m A_m J_0\left(\alpha_m \frac{r}{R}\right) \cos\left(\frac{\pi}{2L_z} z\right). \quad (3.25)$$

Here A_m is magnitude and α_m are the zeros of corresponding Bessel eigenmodes $J_0(\alpha_m r/R)$ of the ion velocity profile, such that the outermost zero coincides with the external boundary location $L_r = R$. Note that using a single radial eigenmode driver field might still produce a multiple mode radial structure of the dust vorticity field in the confinement zone as the resulting dust flow must additionally satisfy the no-slip boundary condition at the boundary $r = R$, requiring additional short scale radial eigenmodes to be excited in order to accommodate a sharper boundary layer structure. The signatures of an associated multiple vorticity scale eigenmode spectrum of the dust flow generated in the resulting boundary layer can thus be analyzed effectively by means of the present analytic eigenmode solutions. In this bounded setup the diffusive effects included in Eqs. (2.2) and (2.4) cause a finite magnitude of the dust flow velocity u in the bulk to reduce in the boundary region and approach zero at the boundary $r = R$. This is despite the flow velocity v of the driving plasma which is finite at the boundary. The corresponding solutions for Eq. (3.23), in terms of coefficients a_m , using this unbounded external field ω_{sr} allow examining the spectral properties of the dust flow fields.

3.3.2 Dust streamfunction and streamlines

The present cases with single, I^{th} , eigenmode structure of the driving plasma flow vorticity ω_{sr} correspond to the choice, in Eq. (3.25),

$$b_m = \begin{cases} A_I & \text{if } m = I; \\ 0 & \text{if } m \neq I, \end{cases} \quad (3.26)$$

of the ion velocity while the use of a large number ($m = 200$) of eigenmodes is made to express the resulting dust streamfunction (ψ). The first set of analytic solutions in term of the streamfunction potential, streamlines in the axis symmetric cylindrical r - z cross-section and its corresponding profiles for two different boundary conditions (no-slip and perfect-slip) are presented in Fig. 3.3 as similar to Sec.2.3.2. Here the driver as plotted in Fig. 3.3(b), corresponds to the choice $I = 1$ such that the boundary $r = R$ of the confinement zone corresponds to the first zero α_1 of the single eigenmode $J_1(\alpha_1 r/R)$ chosen to represent the vorticity (and streamfunction) field of the driver. The scales in Fig. 3.3(a) to Fig. 3.3(e) are based on the system size $L_r = R$ and fraction of ion acoustic velocity U_0 as units of lengths and velocities, respectively. The results with variation of parameters ξ , ν , μ are discussed further in Sec.2.2.5, and the corresponding results as relevant to the experimental observations [11] where a toroidal dust structure having a poloidal circulating flow are observed.

For the parameter values, $\mu = 0.1 U_0 L_r$, $\xi = 10^{-5} U_0 / L_r$ and $\nu = 0.1 U_0 / L_r$, the 2D solution in terms of dust streamfunction $\psi(r, z)$ (in the form of colorbar) and corresponding streamlines, effectively the contours of the product $r\psi$, are presented in Fig. 3.3(a) which show characteristic features of the linear streamline flow aligned with the boundaries in the low Reynolds number regime ($\text{Re} \ll 1$). The radial profiles of the stream function ψ through the central axial location z_0 of the circulation on one of the r - z planes of the azimuthally symmetric toroidal

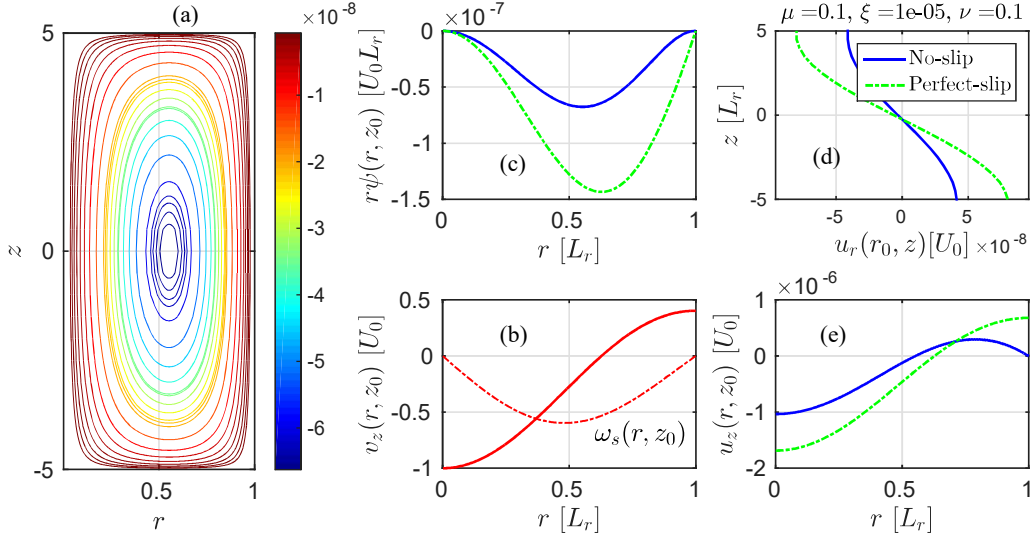


Figure 3.3: (a) 2D dust streamfunction $\psi(r, z)$ (colorbar), and corresponding dust flow streamlines, or the contours of the product $r\psi$. (b) Driver velocity v_z and corresponding Driver vorticity ω_s for single eigenmode source vorticity with $I = 1$. (c) Dust streamfunction ψ , (d) dust flow velocity u_r and (e) dust flow velocity u_z for set of fixed parameters $\mu = 0.1 U_0 L_r$, $\xi = 10^{-5} U_0 / L_r$ and $\nu = 0.1 U_0 / L_r$.

dust cloud are shown in Fig. 3.3(c) for the cases of no-slip and perfect-slip boundary conditions. The corresponding profiles of the r and z components of the flow velocity of the dust, $u_r(r_0, z)$ and $u_z(r, z_0)$ are plotted in Fig. 3.3(d) and (e) respectively. Considering a set of plasma parameters described in Sec.2.2.5 such that the streaming ion flow velocity is of the order of ion acoustic velocity ($U_0 \sim 2.5 \times 10^5$ cm s $^{-1}$), the resulting profiles of components of dust velocity are presented in Fig. 3.3(d) and (e) which agree with observation of $u \sim 0.1 - 1$ mm s $^{-1}$ in a typical dust vortex flow experiment [11].

The no-slip boundary condition with zero dust flow velocity at the outer radial boundary, $u_z(R) = 0$, is ensured by the Eqs. (3.18) and (3.19), as plotted in the Fig. 3.3(e). This boundary condition directly corresponds to the vanishing radial derivative of dust streamfunction, as plotted in Fig. 3.3(c), that approaches zero at the boundary $r = R$ for the no-slip case. The variations in the radial profile of

streamfunction and velocity profiles for two different boundary conditions, no-slip and perfect slip cases are compared in the figure 3.3. No-slip boundary introduces additional shear with the flow and strong shear developed so that the velocity at the boundary reduce to zero. In analysis of boundary flow, as originally introduced in Sec. 2.3.6, the regions of radially decreasing flow velocity magnitude near the boundaries where the viscous diffusive stress is very high, is identified as boundary layer. Its thickness here is further recovered to have a definite analytic form as discussed in detail in Sec. 3.4 of this chapter.

3.3.3 Dust vortex flow with increasing radial driver mode number

The expression of the driver flow field in the form of system eigenmodes (3.26) allows studying the dynamic equilibrium between the two flows with increasing radial mode number of the driving field. This is observed to introduce smaller scales in the dust flow and a corresponding limit on the smallest of the vortex flow scale. The 2D streamfunction solutions are presented in Fig. 3.4(a), (c) and (e) for the radial mode-numbers $I = 1, 3$ and 5 of the driving plasma vorticity ω_s . These values correspond to the cases where the first, third and fifth zeros of the chosen eigenmode, J_1 , coincide with the boundary location L_r , respectively.

Note that similar to $I = 1$ case presented in Fig. 3.3, while the radial derivative of the dust streamfunction also approaches zero ensuring a zero z -component of the dust flow velocity, $u_z = 0$, at the boundary for all I values, a uniform boundary value of the ψ along \hat{z} also ensures a zero r -component for them, such that the dust fluid does not cross the radial boundary and is confined in the domain $r < L_r$. The confinement in the region $-L_z < z < L_z$ is similarly ensured by the uniformity of $\psi(\sim 0)$ along r at the top and bottom boundaries, $z = \pm L_z$, respectively. The alternate depression and bulges in the surface plots in Fig. 3.4(a), (c) and

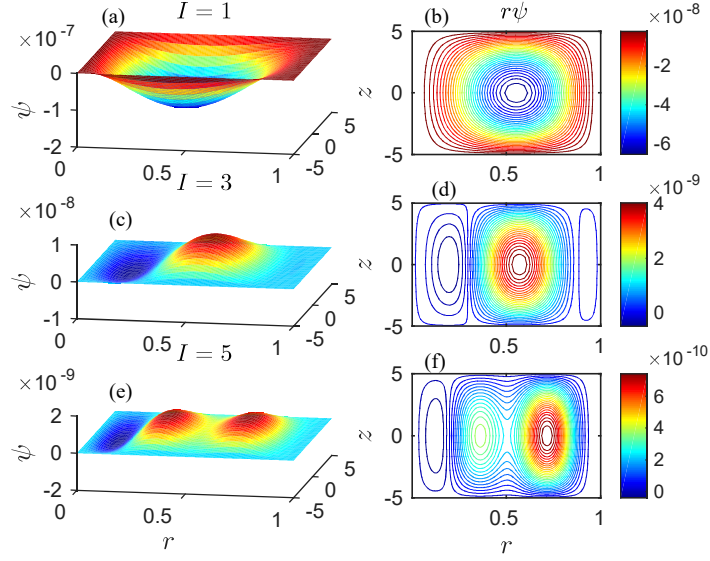


Figure 3.4: 2D dust streamfunction $\psi(r, z)$ for single eigenmode source vorticity with (a) $I = 1$ (c) $I = 3$ and (e) $I = 5$. Dust flow streamlines, or the contours of the product $r\psi$, for single eigenmode source vorticity with (b) $I = 1$ (d) $I = 3$ and (f) $I = 5$.

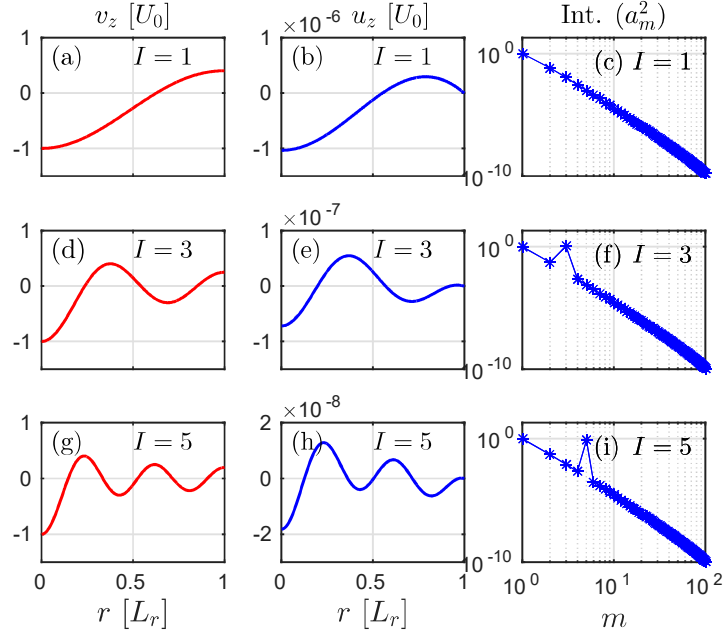


Figure 3.5: Source flow velocity profile at $z = 0$ for (a) $I = 1$ (d) $I = 3$ and (g) $I = 5$. Dust flow velocity profile at $z = 0$ for (b) $I = 1$ (e) $I = 3$ and (h) $I = 5$. Intensity spectrum for the range of mode-number m at $z = 0$ for (c) $I = 1$ (f) $I = 3$ and (i) $I = 5$.

(e) indicate development of multiple vortices structure in the flow field of the dust fluid. These vortices correspond to appearance of circulations in the corresponding streamlines of the dust flow given by the contours of the quantity $r\psi$ that are presented for these cases with $I = 1, 3$ and 5 in Fig. 3.4(b), (d) and (f), respectively.

3.3.4 Radial mode spectrum and its characteristics

The radial profiles of the driver and the dust velocities at $z = z_0$ with increasing value of individual driver mode-number I are plotted in Fig. 3.5 in the left and the middle columns, respectively. This variations of velocities profile near the external no-slip boundary show that the dust dynamics involved new scale introduced by the boundaries other then the driving external fields. The range of scales present in the system can be visualized from the corresponding intensity spectrum of the constituent modes of the driven dust flow vorticity profiles, $\text{Int}(m) = a_m^2$, which is plotted in right most column of Fig. 3.5 as a function of the corresponding mode number m . Although a most dominant mode, with the mode-number $m = I$ of the driver vorticity ω_s , can be seen in the dust fluid mode-number spectrum in each of the cases with $I = 1, 3$ and 5 of the source plotted in Fig. 3.5(c), (f) and (i), respectively, a finite intensity at other m values is also recovered in the spectrum of the dust flow. This finite intensity for $m \neq I$ dust modes, unlike source intensity $\text{Int}(m) = \delta_{mI}$, originates from the additional spatial variation of the dust velocity profiles (b), (e) and (h) introduced by the no-slip boundary condition, forcing the dust flow velocity to drop to zero at $r = L_r$. The influence of increasing spatial variation, related to the appearance of a boundary layer, on the dust vorticity spectrum $\text{Int}(m)$ characterizes the correlation between the dust parameters and the intensity of the additional modes with a range of length scales.

The width of boundary layer, effectively the radial interval between the dust flow velocity maximum and the boundary location, reduces gradually with reducing value of dust viscosity μ as visible in the radial variation of the dust flow velocity

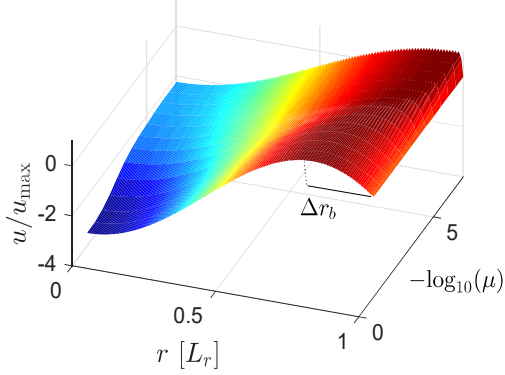


Figure 3.6: Radial profiles of dust velocity u normalized to the corresponding maximum values u_{\max} appearing at the edge of the boundary layer whose width shrinks with decreasing μ values, ranging from 10^{-1} to $10^{-7}U_0L_r$ arranged on a logarithmic scale.

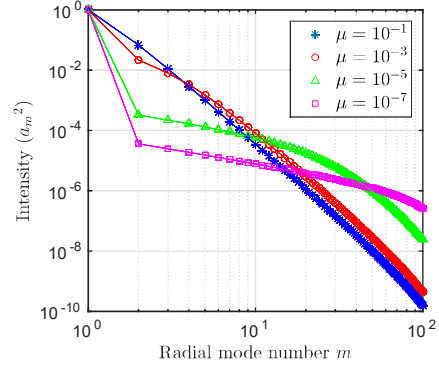


Figure 3.7: Intensity spectrum for the solutions with $I = 1$, normalized to the intensity a_1^2 of the dust vorticity mode-number $m = 1$ for the cases with the value of viscosity coefficient $\mu = 10^{-1}, 10^{-3}, 10^{-5}$ and $10^{-7}U_0L_r$.

profile plotted in Fig. 3.6 for $I = 1$ and wide range of kinematic viscosity μ . The location of the maximum of the normalized velocity is accordingly seen shifting close to the radial boundary $r = L_r$ for the smaller μ , indicating that the boundary layer region shrinks and becomes steeper at smaller values of μ , presented in Fig. 3.6 using a logarithmic scale variation. The complete intensity spectrum of the constituent modes and effect of shrinking width of the boundary layer associated with additional short scale modes, that it generates in the intensity spectrum, can now be analyzed explicitly. The intensity spectrum $\text{Int}(m)$ is plotted in Fig. 3.7 for the case $I = 1$ and values of coefficient of viscosity $\mu = 10^{-1}, 10^{-3}, 10^{-5}$ and $10^{-7}U_0L_r$. As seen from Fig. 3.6 and Fig. 3.7, steepening of the flow velocity variation near the boundary with decreasing μ corresponds to an increase in the contribution of the radial modes with higher mode number m in the vorticity spectrum. Note, for example, that for the case with $\mu = 0.1$ (plotted with ‘*’ in Fig. 3.7), where the width of the boundary region approximately corresponds to the scaled interval between the zeros of $m = 2$ mode, there is a considerable intensity of $m = 2$ mode

in the spectrum. This intensity of $m = 2$ mode however can be seen to drop with reduction in the μ values, whereas the corresponding intensity of the modes with large $m (\gg 10)$ increases. This transition is seen accompanied by a proportional reduction in the width of the boundary layer that rather corresponds to the shorter scale lengths associated with the large m modes ($m \gg 10$) whose intensity, relative to $m = 2$ mode, indeed grows for smaller μ values. The mode-number spectrum for varying values of μ , displaying a dominant intensity of resonant scale and a continuum of small scales, features a single exponent for large values of μ but two distinct exponents for small μ values. This indicates that in the regime when boundary layer is wider and has scale length comparable to that of the driver flow, the driver flow introduces a set of structures in the flow having a definite power law with single exponent. However, in the regime where a thin boundary layer emerges, the boundary may introduce a set of intermediate scales with an exponent which can be significantly different from that of the set of modes generated by the driver flow. Very small length scales, that are either comparable or finer than the average inter-dust-element separation, d , are obviously disallowed in the existing macroscopic model by the conditions (3.18) and (3.19). In presence of viscoelastic effects, with possibility of finite stochasticity at microscopic level, such finer scales are likely to be populated by modes with a power-law that in the recent first-principle computer simulations have been predicted to follow a Kolmogorov like turbulent scaling [135]. However, how these resulting finer-scales structures must interact with the boundary layer that forms at the similar scales, remains an interesting question for analytically determining the nature of the spectrum at such finer scales. Correctly addressing this region of spectrum under the hydrodynamic formulation would therefore require extending the present Navier-Stokes model to a generalized hydrodynamic model by including the essential viscoelastic effects.

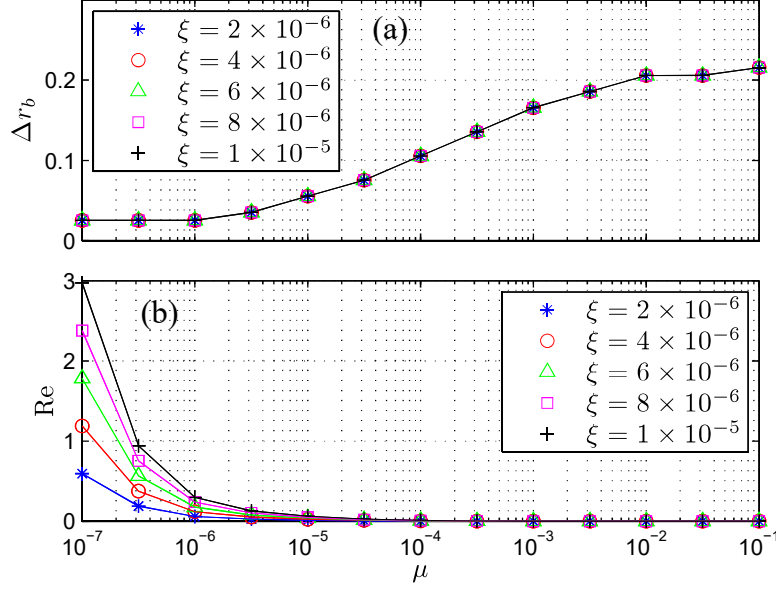


Figure 3.8: (a) Width Δr_b of the boundary layer and (b) values of the Reynolds number Re , for $I = 1$ and the cases with various values of ξ .

3.4 Dust boundary layer and parameters affects

The dependence of both, the boundary layer width Δr_b and the dust flow Reynolds number Re on various system parameters such as ξ and μ introduced and discussed in Sec. 2.3.6 is further examined here for specific radial mode numbers of the driver and over wider range of the parameters.

3.4.1 Characterization of dust boundary layer width

As obtained from the variation in velocity profile with system parameters shown in Fig. 3.6, the width of the boundary layer Δr_b is plotted as function of μ for a wide range of ξ values in Fig. 3.8(a) and the corresponding dependence of an effective Reynolds number, discussed further below, is plotted in Fig. 3.8(b). The boundary

layer thickness for this wide range of μ value is also found to be almost independent of the coefficient of ion drag ξ (or ν) as evident from Fig. 3.8(a) where profiles of $\Delta r_b(\mu)$ evaluated with various ξ values are seen to be overlapping. The shear scale length is, in turn, not sensitive to the ξ (or ν) and the driver strength remains largely decoupled with the characteristics of the dust dynamics in the linear (low Re) flow regimes. This behavior shows the neutrality of the dust dynamics with respect to the driving mechanism and its strength. However for very large value of ξ , the increase in flow strength were observed as similar to the numerical results discussed in chapter 2, section 2.3.6.

3.4.2 Characterization of the Reynolds number

Another important quantity that can additionally be estimated and examined as function of μ and ξ is the Reynolds number (Re). Considering the recovery of boundary layer width as effective characteristic length Δr_b , that allows defining and estimating the effective Reynolds number, $\text{Re} = u_b \Delta r_b / \mu$ for various cases, where $u_b = u(r \approx L_r - \Delta r_b)$. In view of the large range of the parameter μ ($1 < \mu < 10^{-7} U_0 L_r$) explored in the present analysis covering the low Re flow regimes, the ratio $u_b \Delta r_b / \mu$ might shoot up unless a corresponding variation is recovered in the product $u_b \Delta r_b$ appearing in the numerator. Using the values of u_b and Δr_b , both of which are the output of the present analysis, it can now be examined whether the values of Re associated with the results presented above are well within the linear limit $\text{Re} < 1$ of the Eqs. (2.2) and (2.4) as required in order to re-confirm the applicability of the analysis to the considered low Reynolds number setups. The estimated values of Re are plotted in Fig. 3.8(b) for the range of the parameters μ and ξ relevant to the general laboratory dusty plasma and other low Reynolds number setups considered in the present analysis. The domain $\text{Re} < 1$ in Fig. 3.8(b) can thus be considered representing to the linear limit, suitably covered by the present analysis. While sufficiently large values of drag coefficient

ξ are admissible at large μ without losing the self-similarity of the solutions, for smaller value of μ a corresponding limiting ξ value can be estimated by finding the curve $\text{Re}(\mu)$ that intersects the horizontal line $\text{Re} = 1$ at the chosen μ .

3.4.3 Scaling laws for dust boundary phenomena

In contrast to absence of its sensitivity to variation in ξ visible from Fig. 3.8(a), the shear scale length does however show a strong response to the non-uniformity or the presence of spatial stochasticity in the plasma. This is further examined us by means of characterizing the boundary layer width in the cases of higher driver mode numbers, $I = 3$ and 5, besides the smallest value $I = 1$ as plotted using logarithmic scale in Fig. 3.9. It is evident that the regions of separate exponents of μ are present in every case. The boundary layer width is recovered clearly following a definite exponent $\Delta r_b \propto \mu^{1/3}$ in the small to intermediate orders of μ values, e.g., ranging from 10^{-6} - $10^{-2}[U_0 L_r]$ for the case of $I = 1$. The range of μ exhibiting this definite power law is however found to be rather limited in the cases of higher driver mode numbers, for example in the cases $I = 3$ and 5 presented in Fig 3.9(b) and (c), respectively. The origin of the observed scaling lies in the dust momentum diffusivity largely balancing the momentum source from the driver in the narrow boundary layer, in which the net dissipation via neutrals approaches marginal values. The Eq. (2.5) at the boundary layer therefore takes the following limiting form,

$$\mu \nabla^2 (\nabla \times \mathbf{u}) \simeq \xi \nabla \times \mathbf{v}. \quad (3.27)$$

Considering, for $I = 1$ for example, that in the boundary layer region the radial scale length of variation in the driver plasma velocity is comparable to system size, $|\mathbf{v}|/|\nabla \times \mathbf{v}| = v_z/v'_z \sim L_r$ while that of the dust velocity variation approaches the effective boundary layer width, $|\mathbf{u}|/|\nabla \times \mathbf{u}| = u/u' \sim L_\perp \sim \Delta r_b$, in order to achieve

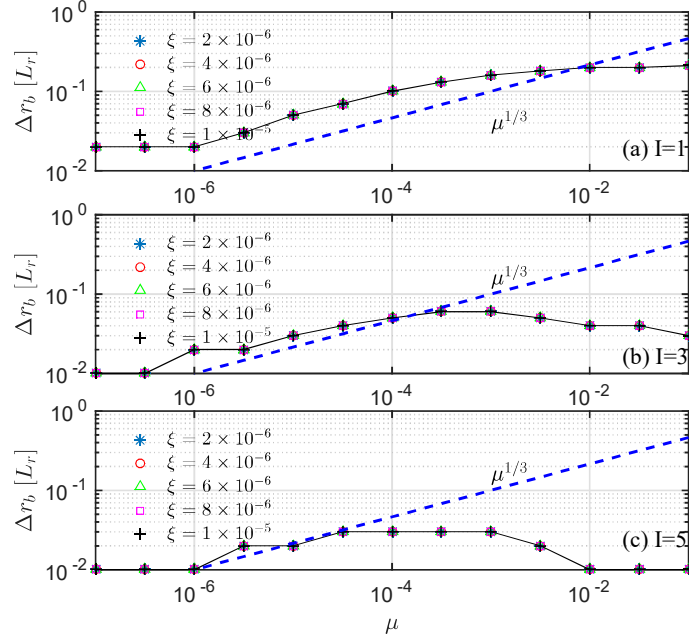


Figure 3.9: (a) Dependence on μ of width Δr_b of the boundary layer with various values of ξ for the cases with the driver mode number (a) $I = 1$ (b) $I = 3$ and (c) $I = 5$. The broken line represents the dependence $\Delta r_b \propto \mu^{1/3}$.

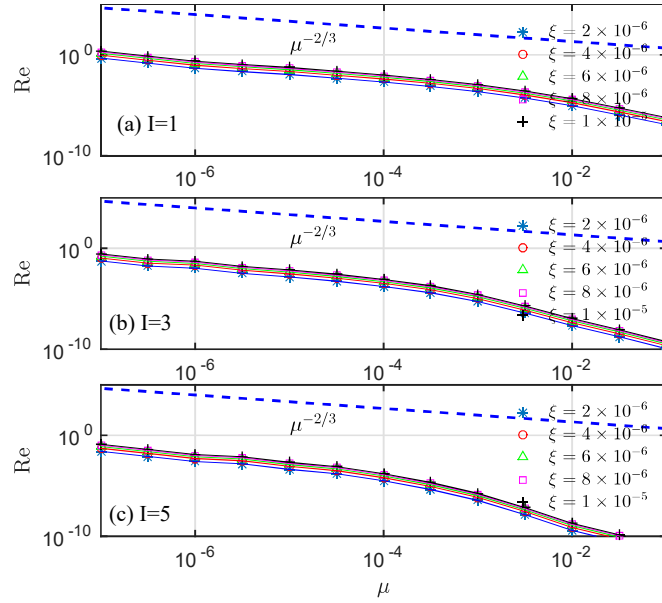


Figure 3.10: (a) Dependence on μ of the Reynolds number Re with various values of ξ for the cases with the driver mode number (a) $I = 1$ (b) $I = 3$ and (c) $I = 5$. The broken line represents the dependence $Re \propto \mu^{-2/3}$.

the dust flow velocity $u_b \sim u_0$ at the onset of boundary layer using (3.27) requires,

$$\frac{\mu u_0}{\Delta r_b^3} \simeq \frac{\xi v}{L_r}. \quad (3.28)$$

Therefore, treating the quantities ξ, u_0, v and L_r as parameters would yield the scaling observed in the above characterization,

$$\Delta r_b \simeq \mu^{1/3}. \quad (3.29)$$

Estimated for $I = 1$, the scaling (3.29) is however obscured by an increasing value of I as seen from Fig. 3.9, mainly because of the reduction in the values of u_b in comparison to u_0 for $I > 1$ (see Fig. 3.5 (b), (e) and (h) for example). The mode-wise dependence of (3.29) on μ obtained in the present analysis makes it convenient to determine, from the spectral properties of the driver flow spatial variation present in a particular case, the range in which a corresponding modification of the scaling (3.29) must be applied. In simpler terms, the considerable range of driven setups where the driver background remains largely free of spatial nonuniformities corresponds to class of systems analytically more tractable by (3.29) in comparison to those where the flows may rather be driven by autonomous mechanisms for the vortex dynamics, for example those involving temperature or charge density variations within the structure region with sharper gradients. The regime of (3.29) suitably covers alternate drivers like a thermophoretic force, translating into a force $\gamma_n \omega_n$ by the neutral vorticity field which frictionally couples to dust particles via coefficient γ_n , and other generic mechanisms [29] that effectively yield a non conservative force field capable of entering Eq. (2.5).

A corresponding dependence is recovered in $\text{Re} < 1$ profiles over the viscosity μ with a definite exponent where $\text{Re} \propto \mu^{-2/3}$ that suitably follows from the scaling (3.29), as $\text{Re} = u_b \Delta r_b / \mu$, hence $\text{Re} \sim \mu^{-2/3}$. This dependence, as presented in the logarithmic plots in Fig. 3.10, is once again pronounced in a longer range of μ

values for the small mode numbers (e.g., $I = 1$) and the profiles show this definite ordering to be obscured by the increasing spatial fluctuation in the driver for larger μ values, for example in the cases of $I = 3$ and 5. A rather step-wise change in the profiles at small and large μ values in Fig. 3.9 are caused by the spatial resolution, which is analytically limited by the maximum number M of the dust eigenmodes in use, getting highlighted over the logarithmic scale. It is estimated that for the cases of relatively higher dust charge densities ($\sim 4 \times 10^4 e^-$) and moderate dust flow velocities ($\sim 0.5 \text{ cm s}^{-1}$) achievable in the existing systems displaying vortex dynamics, the lowest μ value used in the present analysis ($10^{-7} U_0 L_r \equiv 0.26 \text{ cm}^2 \text{s}^{-1}$) approaches the results of the computer simulations yielding the shear viscosity η for the Yukawa systems (e.g., $\mu = \eta/mn \sim 0.5\sqrt{3}\omega_E a^2 \equiv 0.21 \text{ cm}^2 \text{s}^{-1}$ [69, 130], where m and n are dust mass and particle density, respectively, ω_E is the Einstein frequency, and a , the average inter-dust separation) using the present dusty plasma parameters [11]. For these μ values, the effective $\text{Re} = u_b \Delta r_b / \mu \sim 1$ (using $r_b = 0.5 \text{ cm}$ and $u_b = 0.5 \text{ cm s}^{-1}$) indicates that the associated cases having $\text{Re} < 1$ can suitably be treated with the present results.

Although a very rich nonlinear regime is excluded by the linear treatment presented in this chapter, as a lowest order approach already implemented with appropriate set up and boundary conditions and characterized, the present linear treatment highlights a relatively straight but non trivial extension of the present treatment to nonlinear regime. This is possible, for example, by inclusion of the originally existing nonlinear convective terms that are excluded from the the present model for simplicity, for the similar flow, boundary and driver configuration, but exploring them over an enhanced, nonlinear, parameter regime. Such first nontrivial extension to nonlinear limit, for investigating advanced aspects of the confined dust vortex flow is step-wise implemented and presented in following Chapters 4 and 5 of this thesis.

3.5 Summary and conclusions

For the majority of bounded setups of the dust medium suspended in the plasmas with boundaries and friction, we have analytically addressed the issue that in presence of a background high Reynolds number driving plasma flow, what are the characteristics of the 2D driven flow structure, and how do the spectral properties of the driver flow influence equilibrium mode number spectrum of the driven flow when it is subjected to important boundary phenomena. For the analysis of driven confined dust fluid vortex flow a boundary value problem was constructed in a nonplanar, cylindrical geometry in terms of dust flow streamfunction.

The presented analytic treatment used the description of the vorticity of both the dust and of the driving plasma in terms of strength of eigenmodes of a curvilinear bounded setup in the mode number space. The analytic solutions for the dust flow are obtained by treating the boundary value formulation as an eigenvalue problem, and using the linearly independent set of Bessel functions as eigenmodes that allows both driving and driven flows to follow valid flux conservation and have a multiple scale vorticity spectrum. This choice allows a multiple scale plasma flow field to produce a vorticity scale spectrum for the driven dust flow field, essentially nonidentical to the driver and the one that accommodates the effects of boundary with the stationary dust. The spectral characteristics of dust vorticity at higher mode numbers is shown to be determined predominantly by the boundary effects that have additional impact when combined with variation in the usual physical parameters of the dust medium, including the kinematic viscosity and the coefficients of neutral friction and ion drag acting on the dust fluid. Among these effects is the formation of a boundary layer whose width depends on the viscosity and allows the dust flow to be in low Reynolds number regime up to considerably smaller values of the coefficient of the dust viscosity.

The adopted analytic approach involving definition of a radial eigenvalue prob-

lem for the 2D confined dust fluid setup essentially outlined that, (i) with prescribed boundary conditions and known analytic structure of the driver field, a set of orthogonal eigen functions can represent both driver and dust solutions allowing to determine desired coefficients to determine the dust streamfunction solutions in the confinement domain. (ii) Although the solutions are sought in terms of the streamfunction ψ , the physical boundary conditions can be defined on the velocity components and their gradients based on the symmetry of the set up and the associated eigenfunctions. (iii) For the hydrodynamic formulation the spectral limit associated with shorted scale length resolved is determined by the condition that the spatial resolution of the solution, Δr , must exceed the average dust particle separation d over which a valid continuum dust density can be defined.

With respect to the solutions of the 2D formulation obtained here, the first set of dust vortex flow solutions obtained for the characterization show that for a typical set of laboratory dusty plasma parameters described in Sec.2.2.5, where the streaming ion flow velocity is of the order of ion acoustic velocity ($U_0 \sim 2.5 \times 10^5$ cm s⁻¹), the magnitude of resulting profiles of components of dust velocity agrees with observation of $u \sim 0.1 - 1$ mm s⁻¹ in a typical dust vortex flow experiment [11].

The expression of the driver flow field in the form of system eigenmodes (3.26) allows studying the dynamic equilibrium between the two flows with systematically increasing radial mode number of the driving field. This increase is observed to introduce smaller gradient scales in the dust flow and yield a corresponding limit on the smallness of the vortex flow scale, effectively because of the presence of finite dust viscosity.

The variation of the dust velocity profile near the external no-slip boundary shows that the dust dynamics involved new scale introduced by the boundaries other than the driving external fields. The range of scales present in the system can be visualized from the corresponding intensity spectrum of the constituent modes

of the driven dust flow vorticity profiles, $\text{Int}(m) = a_m^2$ (where a are the coefficients of the dust eigenmodes). This spectral dependence could be characterized in the analysis as a function of mode number m for increasing value of radial mode number of source vorticity I .

In respect to the smallest scale analyzable by the largely macroscopic hydrodynamic formulation, very small length scales in the boundary layer, that are either comparable or finer than the average inter-dust-element separation, d , are obviously disallowed in the existing macroscopic model by the special conditions used for limiting the minimum scale of flow gradients in the present solution procedure. With finite possibility of finite stochasticity at microscopic (molecular) level, such finer scales are likely to be populated by modes with a power-law that in the some of the first-principle computer simulations have been predicted to follow a Kolmogorov-like turbulent scaling [135]. However, how these resulting finer-scales structures must interact with the boundary layer that forms at the similar scales, remains an interesting question for analytically determining the nature of the spectrum at such finer scales. Correctly addressing this region of spectrum under the hydrodynamic formulation would therefore require extending the present Navier-Stokes model to a generalized hydrodynamic model, by including the essential viscoelastic effects [116].

The boundary layer thickness for a wide range of μ value is found to be almost independent of the coefficient of ion drag ξ such that profiles of $\Delta r_b(\mu)$ evaluated with various ξ values are seen to be overlapping. The shear scale length is, in turn, not sensitive to the ξ and the driver strength remains largely decoupled with the characteristics of the dust dynamics in the linear (low Re) flow regimes. This behavior shows the neutrality of the dust dynamics with respect to the driving mechanism and its strength.

With the effect of increasing complexity in the driver setup resolved in the orthogonal eigenfunctions and characterized individually for increasing value of

radial mode number, a scale independence of effects associated with boundary could be identified. Both the boundary layer thickness and the dust Reynolds number are shown to have definite exponents of variation with respect to the medium viscosity μ . While the effective boundary layer width is recovered to scale with $\mu^{1/3}$, the effective Reynolds number for the setup is recovered to scale with $\mu^{-2/3}$. Both these orderings are seen to be obscured by an increasing spatial complexity of the driving mechanism. The degree of the impact of this complexity is estimated by systematically characterizing the effect of individual driver flow modes in various cases with increasing value of the cylindrical mode number.

We conclude by discussing that while the regime relevant to present results includes the low Reynolds number processes driven by the factors involving spatial complexity and the microscopic setups that are dominated by the boundary effect, following the present implementation of the 2D model, the analysis of additional regimes covered by dusty plasmas must now be more accessible. This is possible, for example, by inclusion of the originally existing nonlinear convective terms (that are excluded from the the present model for simplicity) for the similar flow, boundary and driver configuration, but exploring them over an enhanced, nonlinear, parameter regime. Such first nontrivial extension to nonlinear limit, for investigating advanced aspects of the confined dust vortex flow is systematically implemented and presented in following Chapters 4 and 5 of this thesis.

4

Nonlinear effects in the bounded dust vortex flow in plasma

4.1 Introduction

The driven-dissipative systems show a vast dynamic memory by their capacity and range of response to a continuum of stimuli from their surrounding, each of which may invoke a unique response, like making them erupt into a unique pattern. In its simplest form, a behavioral transition to such a state occurs, for example, in a system of Brownian particles irreversibly diffusing through a medium [46] when they are additionally subjected to a drive by a streaming medium and restricted in space by a confining potential or boundary. This results in a variety of their particle distributions for respective combinations of potential, boundary and flow topologies [14]. The fluid-like phase of dust particles suspended in plasma [3, 6, 47–49], which is subject of the present study shows an even larger range of patterned response already in the linear regime of its dynamics [11, 12, 24, 25] as a more realistic and rich nonlinear regime of it remains yet unexplored [50].

While the results of the linear studies presented in Chapter 2 and 3 successfully predicted the multiplicity of vortex [12, 24] and outlined basic scaling of boundary effect at low to moderate Reynolds number [25], exploring the nonlinear regime of this system can potentially address the nontrivial physics of often noted transition from linear to nonlinear regime of these vortices. Recently observed compelling nonlinear features of dust vortex dynamics [11] promise to shed light on several less understood aspects of the dusty plasmas as well as a variety of dynamically equivalent natural flows. For example, a nearly uniform vorticity in the core of a toroidal dust cloud observed in higher flow velocity limit resembled high Reynolds number flow phenomena of the Jovian great red spot [31, 56]. More noticeably, nonlinear phenomena, displayed also by dust dynamics, are proving to be natural timing mechanism for biological systems with growing evidence that processes like cell division are timed by critical transitions on approaching a threshold size rather than a preprogrammed linear evolution [57]. For example, the low Reynolds number intracellular mitotic activity taking place in cytoplasmic medium examined in budding yeast shows that the cells born smaller than normal size spend longer duration in initial G1 phase until they reach a critical size for division, reproducing normal size offspring [58]. Nonlinear critical transitions thus provide a potential mechanism that monitors cell size and uses this information to regulate progression through events of the cell cycle, determining cell size and age, namely, the fundamental limiting factors for overall evolution of the carbon based life [57, 59].

Equating the influence of chemical inhibitors of protein synthesis and polymerization by that of the inertial flow in a dusty plasma vortex, both of which must undergo criticality for continued stabilization by diffusion dominated viscous transport at optimum scale, one gets a very primitive model for size regulation of a biophysical cell via a nonlinear threshold [28]. The equilibrium dusty vortex dimension in nonlinear operating regime are similarly asserted by the dynamics at a critical separation threshold rather than governed by the boundary geometry.

Such a meaningful isomorphism between complex systems and suspended dust-fluid is however quantifiable only by a systematic nonlinear formulation of the dusty plasma vortex dynamics. The present Chapter approaches this advanced objective by extension, to nonlinear regime, of the hydrodynamic formulation developed and applied to linearly regime in preceding chapters. In the Chapter in Sec. 4.2 we have revisited the essential two dimensional toroidally symmetric, axially and radially bounded setup considered in the present formulation from the view point of nonlinear treatment. The methodology of nonlinear solutions is presented in Sec. 4.3, followed by the characterization of solutions in Sec 4.4. The signature of nonlinearity in the form of uniform vorticity in the vortex core is discussed in Sec 4.4 where this uniformity is additionally shown confirming with gigantic scale circulations like the great Jovian red spot. In Sec. 4.4.3 the phenomena of the boundary layer separation is investigated as a structural bifurcation of the 2D nondivergent vector fields with kinematic dust viscosity μ acquiring the role of a bifurcation parameter. Sec. 4.4.4 provides a nonlinear scaling, allowing to estimate μ using velocimetric parameters of dust vortex flow. Summary and conclusions are presented in Sec. 4.5

4.2 2D nonlinear hydrodynamic approach to dust vortex flow

The definition of toroidal dust-fluid set up considered both in Chapter 2 and 3, confirming with the experimental arrangement, is further enriched for the treatment presented in this chapter in order to address the signatures of nonlinearity noticed in the dust vortex flow experiments in the plasma. Figure 4.1(a) shows a pair of counter-rotating dust circulations developed by a special arrangement of the bottom electrodes producing a non-monotonically sheared density profile

correlated to the vortex pair location. As recovered in a post-experimental particle image velocimetry analysis of the dust vortex flow field by M. Kaur *et al.*, the 2-dimensional, azimuthally symmetric, poloidal dust vortex flow displays an almost circular region of nearly uniform dust flow vorticity as shown in Fig. 4.1(c). The associated dust flow velocity, as plotted in Fig. 4.1(b), is clearly seen having a corresponding nearly linear radial drop, with reference to the vortex center (r_0, z_0) .

4.2.1 Definition and mapping of the boundary segments

In order to describe the results of the formulation more systematically, the schematic of dust vortex flow set up geometry presented in Fig. 4.1 is provided in this chapter with additional definition of the all the four boundary segments of the rectangular dust confinement domain. Accordingly, using cylindrical co-ordinates to accommodate the azimuthal symmetry, as used in Chapters 2 and 3, the toroidal dust fluid is considered confined by an effective potential $V(r, z)$ within the boundaries defined by points $ABCD$ of a finite section of an infinite cylinder of flowing plasma. The boundary $ABCS$ thus encloses the region where $0 < r/L_r < 1$ and $-1 < z/L_z < 1$, with no variation along the azimuthal dimension $0 < \phi < 2\pi$. More specifically, the curved boundary segments AB , BC , CD and DA , of the cloud are schematically indicated to map to the, bottom, inner radial, top and outer radial boundaries of the rectangular domain $ABCD$, respectively, as drawn in Fig. 4.2 using line segments of the corresponding colours surrounding both the domains. It is once again assumed that the confining potential jumps from a constant value V_0 to a very high value at the rectangular boundary $ABCD$ providing a rectangular contour for perfect confinement.

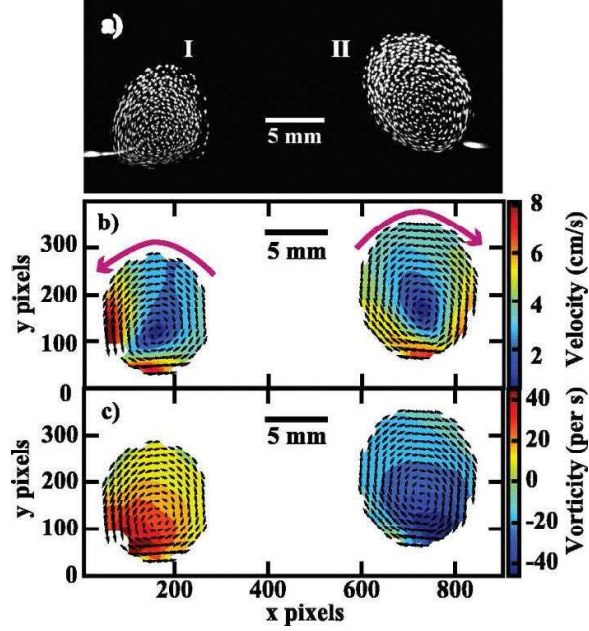


Figure 4.1: (a) Toroidal dust cloud with poloidal circulation in the laboratory dusty plasma experiment by M. Kaur *et al.* Phys. Plasmas **22**, 093702 (2015). (b) the dust flow velocity distribution and (c) the dust flow vorticity distribution, obtained from the Particle Imaging Velocimetry (PIV) analysis of the image data.

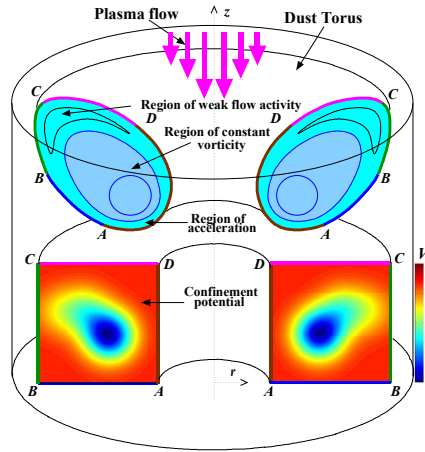


Figure 4.2: Schematic representation of the toroidal dust cloud with vortex motion and mapping of the boundary of its cross-section to a toroidal domain of rectangular cross-section accommodated in the cylindrical geometry of the present nonlinear solutions. Segments AB , BC , CD and DA , of the cloud map to the corresponding sides of the rectangle $ABCD$.

4.2.2 Nonlinear conservation equations in curvilinear set up

For the dust flow that follows incompressibility condition and has a finite viscosity, the dynamics is governed by the Navier-Stokes equation in which the drive produced by the ion drag and the friction produced by the stationary neutral fluid can be suitably accounted for [23],

$$\frac{\partial \mathbf{u}}{\partial t} + (\mathbf{u} \cdot \nabla) \mathbf{u} = -\frac{\nabla P}{\rho} - \nabla V + \mu \nabla^2 \mathbf{u} - \xi(\mathbf{u} - \mathbf{v}) - \nu(\mathbf{u} - \mathbf{w}). \quad (4.1)$$

Here \mathbf{u} , \mathbf{v} and \mathbf{w} are the flow velocities of the dust, ion and neutral fluids, respectively. P and ρ are the pressure and mass density of the dust fluid, respectively, $V(r, z)$ is the confining potential, μ is kinematic viscosity, ξ is coefficient of ion drag acting on the dust and ν is the coefficient of friction generated by the stationary neutral fluid [124–126]. The overall combination of charged dust and background plasma is quasineutral and the electrons are in thermal equilibrium with the streaming ions and the confined dust. The incompressibility of the confined dust component is enforced by the expression

$$\nabla \cdot \mathbf{u} = 0, \quad (4.2)$$

which allows defining a streamfunction ψ such that $\mathbf{u} = \nabla \times (\psi \hat{\phi})$, with corresponding velocity components,

$$u_r = -\partial \psi / \partial z \quad \text{and} \quad u_z = \frac{1}{r} \frac{\partial(r\psi)}{\partial r}. \quad (4.3)$$

In case of an azimuthally symmetric dust flow the dust motion can suitably be treated in the 2-dimensional r - z plane such that the dust vorticity vector $\vec{\omega} = \nabla \times \mathbf{u}$

is directed purely along $\hat{\phi}$. Using these definitions in Eqs. (4.1)-(4.2) and stationary neutrals ($\mathbf{w} = 0$), we obtain for a time independent force equilibrium of dust flow field,

$$\nabla^2 \psi = -\omega, \quad (4.4)$$

$$(\mathbf{u} \cdot \nabla) \omega = \mu \nabla^2 \omega - (\xi + \nu) \omega + \xi \omega_s, \quad (4.5)$$

where ω_s is the vorticity of the ion fluid. In Chapter 2 and 3 the 2D solutions of (4.4)-(4.5) were obtained in the linear regime, or the low Reynolds number regime ($\text{Re} = Lu/\mu \rightarrow 0$) where the the inertial effects are dominated by the diffusive transport and nonlinear term in the left hand side of the Eq. (4.5) could be neglected. Among the additional approximations, a separable streamfunction dependence on the orthogonal directions r and z was used with a single mode analysis along the axial direction while doing a multiple mode analysis only along the radial dependence via Bessel eigenfunction representation. These approximations forced an up-down symmetry of the vortex structure about the center Z_0 of the domain and also disallowed use of an axially uniform driver field since an identical axial mode structure (single mode) was implemented for both driving ion and driven dust vorticities, valid for cases with $k_z \ll k_r$ in which the top and bottom boundaries are at sufficiently large distances from the center. The linear results thus allowed analysis of the almost laminar dust vortex structures involving slow dust motion in the recent laboratory experiments where various single and multiple dust vortex form driven by nonuniformity of the plasma flows and parameters. Interestingly, a detailed nonlinear regime of strong dust vortex flow is routinely observable in these experiments where driven vortices with strong circulations are surrounded in the region of weak drive either by secondary vortices that are co- and counter-circulating, or the stagnant regions of almost no circulation such that very sharp and localized flow velocity gradients are maintained inside the dust vol-

ume [11]. Usually termed as more complex dust flow patterns and excluded from the simpler interpretations, we show that these configurations are well represented by the nonlinear solutions of the system (4.4)-(4.5) as obtained in the following section.

4.3 Iterative numerical solution procedure

The Eqs. (4.4)-(4.5) are solved in the present work by retaining the nonlinear term in the left hand side of the Eq. (4.5) which becomes comparable to the source and diffusion terms in the right hand side in the limit of large flow velocity. The Eq. (4.5) in linear limit admits standard solution procedures where integration is possible for individual modes of the dust vorticity interacting with those of the driver. As presented in Chapter 3 and Ref. [25], such first 2D linear solutions excluding the nonlinear term were obtained by constructing an eigenvalue problem and representing the dust and source streamfunctions in terms of a set of orthogonal eigenfunctions that satisfy the appropriate boundary conditions. Free from most of the approximations made in Chapter 3, the Eqs. (4.4)-(4.5) in this chapter are solved rather exactly (limited by the finite spatial resolution) with explicit effect of multiple axial mode structure of downstreaming flow of both, the streaming driver and the confined dust. The nonlinear solutions are however nontrivial and even a numerical approach to them in 2-dimensions must involve an iterative procedure as adopted in the present study.

4.3.1 The technique of successive over-relaxation

In the first step, Eqs. (4.4)-(4.5) written using the appropriate dimensionless variables and parameters, introduced in section 2.2.5 and adopted in Chapter 2 and

3, are rewritten in the following equilibrium representation,

$$0 = \nabla^2 \psi + \omega, \quad (4.6)$$

$$0 = \nabla^2 \omega - \frac{1}{\mu} (\mathbf{u} \cdot \nabla) \omega - \frac{(\xi + \nu)}{\mu} \omega + \frac{\xi}{\mu} \omega_s. \quad (4.7)$$

They can now be cast in the form suitable for obtaining numerical solutions with enough accuracy. This objective is achieved by beginning with an approximate solution ψ^0, ω^0 (where superscript corresponds to the number of iterations finished) and ensuring that the two residues, R_1 and R_2 , defined, respectively, as,

$$R_1 \approx \frac{\Delta \psi}{\Delta L^2} = \frac{\psi^{n+1} - \psi^n}{\Delta L^2} = \nabla^2 \psi^n + \omega^n, \quad (4.8)$$

$$R_2 \approx \frac{\Delta \omega}{\Delta L^2} = \frac{\omega^{n+1} - \omega^n}{\Delta L^2} = \nabla^2 \omega^n - \frac{1}{\mu} (\mathbf{u}^n \cdot \nabla) \omega^n - \frac{(\xi + \nu)}{\mu} \omega^n + \frac{\xi}{\mu} \omega_s. \quad (4.9)$$

are sufficiently smaller than a physically determined tolerance after $n+1$ successive iterations. Considering once again the bounded set up described in Fig. 4.2 that uses azimuthally symmetric cylindrical coordinates (r, ϕ, z) having all variations only in the r - z plane, the equations (4.8) and (4.9) reduce to,

$$\psi^{n+1} = \psi^n + \Delta L^2 \left(\frac{\partial^2}{\partial r^2} + \frac{1}{r} \frac{\partial}{\partial r} - \frac{1}{r^2} + \frac{\partial^2}{\partial z^2} \right) \psi^n + \Delta L^2 \omega^n, \quad (4.10)$$

$$\begin{aligned} \omega^{n+1} = \omega^n + \Delta L^2 \left(\frac{\partial^2}{\partial r^2} + \frac{1}{r} \frac{\partial}{\partial r} - \frac{1}{r^2} + \frac{\partial^2}{\partial z^2} \right) \omega^n - \frac{\Delta L^2}{\mu} \left(u_r \frac{\partial \omega}{\partial r} \right)^n \\ - \frac{\Delta L^2}{\mu} \left(u_z \frac{\partial \omega}{\partial z} \right)^n - \Delta L^2 K_1 \omega^n + \Delta L^2 K_2 \omega_s, \end{aligned} \quad (4.11)$$

where $\Delta \psi \equiv \psi^{n+1} - \psi^n$, $K_1 = (\xi + \nu)/\mu$ and $K_2 = \xi/\mu$ and the integer n represents the index of the iteration. Since $\psi^{n+1} \rightarrow \psi^n$ for the steady equilibrium solution,

the above equations can be rearranged as follows,

$$\begin{aligned} \left[1 - \Delta L^2 \left(\frac{\partial^2}{\partial r^2} + \frac{1}{r} \frac{\partial}{\partial r} + \frac{\partial^2}{\partial z^2} \right)\right] \psi^{n+1} &= \psi^n + \Delta L^2 \omega^n - \frac{\Delta L^2}{r^2} \psi^n, \\ \left[1 - \Delta L^2 \left(\frac{\partial^2}{\partial r^2} + \frac{1}{r} \frac{\partial}{\partial r} + \frac{\partial^2}{\partial z^2} \right)\right] \omega^{n+1} &= \omega^n - \frac{\Delta L^2}{\mu} \left(u_r \frac{\partial \omega}{\partial r} \right)^n - \frac{\Delta L^2}{\mu} \left(u_z \frac{\partial \omega}{\partial z} \right)^n \\ &\quad - \frac{\Delta L^2}{r^2} \omega^n - \Delta L^2 K_1 \omega^n + \Delta L^2 K_2 \omega_s. \end{aligned} \quad (4.12)$$

Again for numerical efficiency and suitable for iterative determination for ψ and ω , the above equations are split into two operator form where each operators has only one directional derivatives as follows,

$$\begin{aligned} \left[1 - \Delta L^2 \left(\frac{\partial^2}{\partial r^2} + \frac{1}{r} \frac{\partial}{\partial r} \right)\right] \left[1 - \Delta L^2 \frac{\partial^2}{\partial z^2}\right] \psi^{n+1} &= \psi^n + \Delta L^2 \omega^n - \frac{\Delta L^2}{r^2} \psi^n \\ &\quad + \Delta L^4 \left(\frac{\partial^2}{\partial r^2} + \frac{1}{r} \frac{\partial}{\partial r} \right) \left(\frac{\partial^2}{\partial z^2} \right) \psi^n \end{aligned} \quad (4.13)$$

$$\begin{aligned} \left[1 - \Delta L^2 \left(\frac{\partial^2}{\partial r^2} + \frac{1}{r} \frac{\partial}{\partial r} + \frac{1}{\mu} \frac{\partial \psi^n}{\partial z} \frac{\partial}{\partial r} \right)\right] \left[1 - \Delta L^2 \left(\frac{\partial^2}{\partial z^2} - \frac{1}{\mu} \left(\frac{\partial \psi^n}{\partial r} + \frac{\psi^n}{r} \right) \frac{\partial}{\partial z} \right)\right] \omega^{n+1} \\ = \omega^n - \left(\frac{\Delta L^2}{r^2} \right) \omega^n - \Delta L^2 K_1 \omega^n + \Delta L^2 K_2 \omega_s^n \\ + \Delta L^4 \left(\frac{\partial^2}{\partial r^2} + \frac{1}{r} \frac{\partial}{\partial r} + \frac{1}{\mu} \frac{\partial \psi^n}{\partial z} \frac{\partial}{\partial r} \right) \left(\frac{\partial^2}{\partial z^2} - \frac{1}{\mu} \left(\frac{\partial \psi^n}{\partial r} + \frac{\psi^n}{r} \right) \frac{\partial}{\partial z} \right) \omega^n \end{aligned} \quad (4.14)$$

In order to compute the solutions on a two dimensional grid, an initial guess ψ_{ij}^1 and ω_{ij}^1 is made for streamfunction and vorticity respectively, by additionally imposing the desired boundary conditions. In each iteration with index n , beginning from $n = 1$, the Eq. (4.13) is first solved for radial (r -operator) part on A_{ij}^{n+1} which formally represents the result of the second factor (z -operator) in the LHS of

Eq. (4.13) operating on the desire updated streamfunction values ψ^{n+1} , i.e.,

$$\left[1 - \Delta L^2 \frac{\partial^2}{\partial z^2}\right] \psi_{ij}^{n+1} = A_{ij}^{n+1}. \quad (4.15)$$

The computed radial (r -operator) part A_{ij}^{n+1} values allow determination of ψ_{ij}^{n+1} by solving axial (z -operator) part, i.e., by inverting, in Eq. (4.15), the matrix operating on ψ_{ij}^{n+1} , where A_{ij}^{n+1} are known from the similar inversion of the original equation (4.13) solvable for A_{ij}^{n+1} using the known source at the right hand side. An identical procedure is applied for determining ω_{ij}^{n+1} from Eq. 4.14 by defining,

$$\left[1 - \Delta L^2 \left(\frac{\partial^2}{\partial z^2} - \frac{1}{\mu} \left(\frac{\partial \psi^n}{\partial r} + \frac{\psi^n}{r} \right) \frac{\partial}{\partial z} \right)\right] \omega_{ij}^{n+1} = B_{ij}^{n+1}, \quad (4.16)$$

and first solving Eq. (4.14) for B_{ij}^{n+1} with known source, which allows Eq. (4.16) to be solved for ω_{ij}^{n+1} . The updated ψ_{ij}^{n+1} values are used in second half of the iteration to compute B_{ij}^{n+1} and ω_{ij}^{n+1} , rather than the old values ψ_{ij}^n , which concludes the n^{th} iteration. The iterations are made updating the ω and ψ fields until the maximum values of the residues R_1 and R_2 below a reasonable tolerance are achieved. The iteration parameter ΔL^2 and grid size Δr are the parameters which affects the speed of convergence and numerical stability. It is important to follow CFL [129], condition $\Delta L^2 \leq \frac{\Delta r^2}{4}$, as stability criteria for 2D numerical solution, also larger values of ΔL^2 cause the iterations to become unstable and diverge.

4.3.2 Benchmark of the numerical formulation

The capacity of the fully nonlinear 2D numerical procedure developed is utilized in rest of the analysis in this chapter and in Chapter 5 for the characterization of the nonlinear effects in the 2D dust vortex solutions. We however begin this analysis by benchmarking this procedure to recover from it the solutions in the limiting case of the low Reynolds number, linear regime.

For the ready comparison with the analytic solutions presented in Chapter 3,

we have used the identical conditions, specifically a driver vorticity with a single axial mode as well as a single radial Bessel mode corresponding to $I = 1$ in Eqs. (3.25)-(3.26). At axial location $z = z_0 = 0$, the chosen radial profile of the z -component of the driver velocity, v_z , is presented in Fig. 4.3(a) showing that the radial variation of v_z confirms with a natural eigenmode of the set up, i.e., a single Bessel function mode. This dependence ensures that the corresponding streamfunction and vorticity profiles approach zero value at the radial boundaries of the domain at the location z_0 . Note that further choosing a single separable axial mode of the vorticity requires the streamfunction to drop to zero also at the top and bottom boundaries, requiring that the source streamfunction be zero along the entire boundary $ABCD$ of the domain. The vortex flow solutions for this set up in the low Reynolds number obtainable by both, the previous linear approach as well as the present nonlinear numerical approach, can now be compared to check the reduction of the numerical solutions in to the analytic (series) solutions in the appropriate low Reynolds number limit. For typical system parameters considered in Sec. 2.2.5, we have plotted the numerically converged dust streamfunction and streamlines in Fig. 4.3(b) and Fig. 4.3(c), respectively. It can be noticed that the main characteristic features of the linear model are recovered in this limit as expected in a single axial mode driven set up used for the benchmark. These characteristics include the vortex flow where (i) streamlines for this low Reynolds number case remain aligned to the boundary in the region adjacent to boundaries (ensuring vorticity transport purely by diffusion orthogonal to the streamlines) and (ii) a top-bottom symmetry of the single vortex flow, are recovered as expected in this single axial mode driven set up.

A more quantitative validation is possible by comparing the flow velocity component profiles obtained numerically and those obtained by means of analytic solutions in linear regime in Chapter 3. The flow solutions from both numerical and analytic approaches are compared by varying μ while using the same set of system

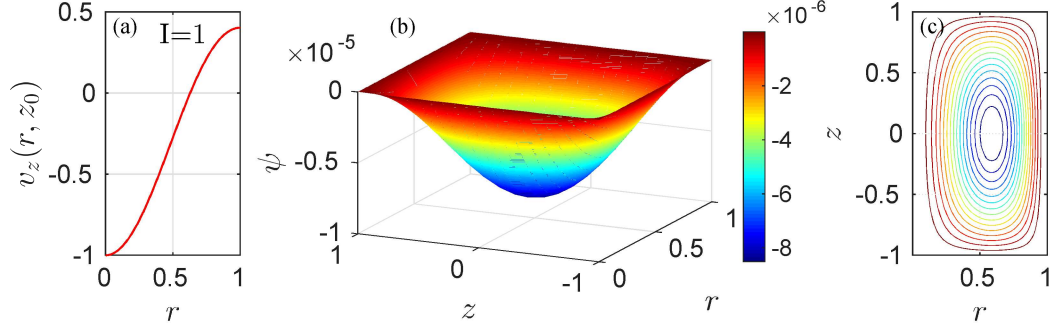


Figure 4.3: (a) Single axial mode driver velocity profile $J_0(\alpha_1 r/R)$ at $z = 0$, (b) 2D dust streamfunction $\psi(r, z)$, and (c) Corresponding streamlines for the dust fluid flow in r - z plane with $\mu = 1 \times 10^{-3} U_0 L_r$, $\xi = 1 \times 10^{-5} U_0/L_r$ and $\nu = 1 \times 10^{-1} U_0/L_r$.

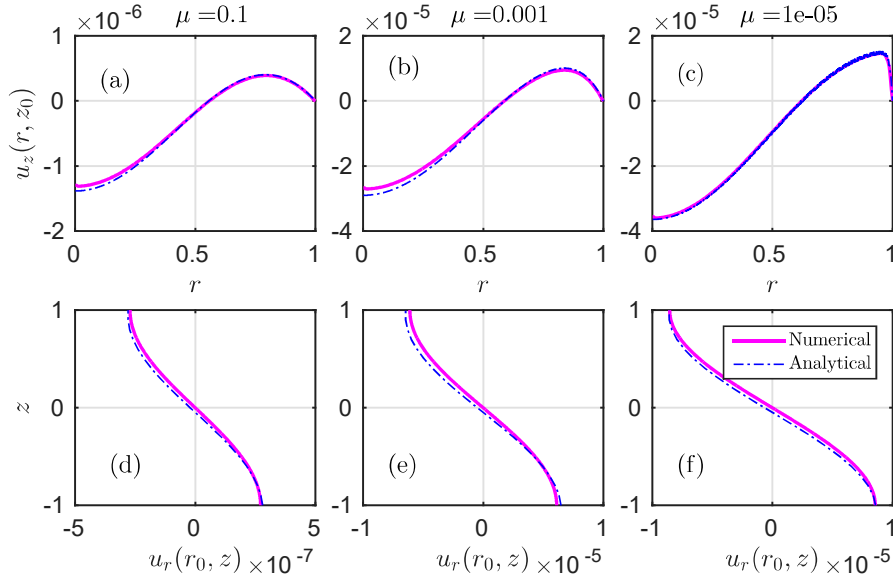


Figure 4.4: Comparison between Analytic and Numerical results of $u_r(r_0, z)$, $u_z(r, z_0)$ for fixed system parameters, $\xi = 1 \times 10^{-5} U_0/L_r$, $\nu = 1 \times 10^{-1} U_0/L_r$, fixed single axial mode radial $I = 1$ driving field and varying $\mu = 10^{-1}$ to $10^{-5} U_0 L_r$ in low Reynolds numbers linear regime $\text{Re} \ll 1$.

parameters, L_z/L_r , ξ , ν and the same single axial mode driver field $v_z = J_0(\alpha_I r/R)$ with $I = 1$, as shown in Fig. 4.3(a). Note that the value $I = 1$ corresponds to the case where zero of the corresponding streamfunction/vorticity coincides with the outer radial boundary located at $r = L_r$. The kinematic viscosity is varied from $\mu = 10^{-1}$ to $10^{-5}U_0L_r$ producing the flow over a large range of different Reynolds number from $\text{Re} \sim 10^{-5}$ to 10^{-1} which is well within the linear viscous regimes ($\text{Re} \ll 1$). The profiles of the dust flow velocity components, $u_z(r, z_0)$ and $u_r(r_0, z)$, are plotted in Fig. 4.4 top and bottom rows, respectively, as obtained from both the approaches for comparison by varying kinematic viscosity value μ .

The numerical profiles of the velocity show only a slight deviation from analytic results at highly viscous regime up to $\mu = 10^{-3}U_0L_r$ or more as shown in Fig. 4.4(a), (d) and Fig. 4.4(b), (e). However the deviation is negligibly small at lower viscous regimes as shown in Fig. 4.4(c), (f). Thus the analytic and numerical results are recovered to be in good agreement with each other, validating the numerical method and motivating the analysis of the dust flow for higher Reynolds numbers nonlinear flow regimes which is inaccessible by the analytic linear approach.

The varying in velocity profile for $u_r(r_0, z)$ and $u_z(r, z_0)$ near the boundaries shows the impact of difference in boundary conditions and demonstrated the boundary layer formation take place near the no-slip boundaries. Boundary layers are formed due to effective viscous stress of the flow near the boundaries. The thickness of the boundary layer is decreasing with decrease in kinematic viscosity as shown in Fig. 4.4(d)-(f). Thus at higher Reynolds number, the thickness of boundary layer formed is negligibly small, follows $\Delta r_b \simeq \mu^{1/3}$, and reduces to very thin layer giving sharp deviation in velocity profile as shown in Fig. 4.4(f). There are no boundary layers formation near other confining boundaries where perfect slip is used as boundary conditions which does not introduce any additional viscous stress on the bounded dust flow.

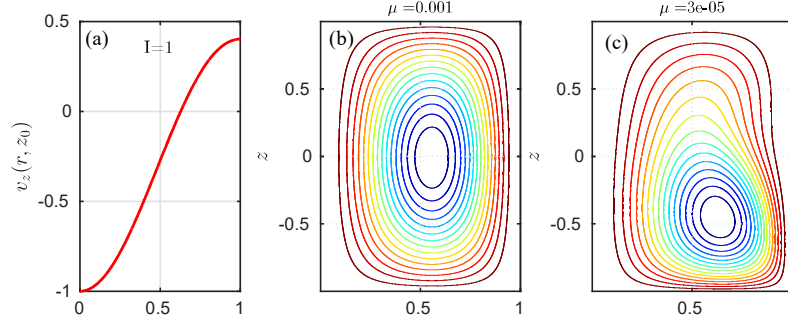


Figure 4.5: (a) Single axial mode driver velocity profile $J_0(\alpha_1 r/R)$ at $z = 0$. And corresponding streamlines for the dust fluid flow in r - z plane with aspect ratio ($L_z/L_r = 2$) for (b) $\mu = 1 \times 10^{-3} U_0 L_r$ and (c) $\mu = 3 \times 10^{-5} U_0 L_r$, having fixed other system parameters at $\xi = 1 \times 10^{-5} U_0/L_r$ and $\nu = 1 \times 10^{-1} U_0/L_r$.

4.3.3 Emerging nonlinear characteristics of the vortex flow

The above analysis of the bounded driven dust dynamics is extended in to high Re regime where the nonlinear convective transport $(\mathbf{u} \cdot \nabla)\mathbf{u}$ is either equivalent or dominant over the diffusive transport process. The flow structure of the confined dust fluid which is symmetric about z_0 in the low Reynolds number ($\text{Re} \ll 1$) regime as shown in Fig. 4.5(b) begins to turn asymmetric about z_0 in higher Reynolds number ($\text{Re} \gg 1$) regime as shown in Fig. 4.5(c). The flow structure in nonlinear (high Re) regime is also found to be dependent on the aspect ratio (L_z/L_r) of the dust confinement domain. In the following analysis, the converged solutions are obtained for the confined dust in the toroidal domain having a rectangular cross-section with aspect ratio of unity ($L_z/L_r = 1$) while a detailed analysis of cases with aspect ratio other than unity is done in Chapter 5. Certain remarkable impacts of these nonlinear characteristics on the physics of dust vortex flow and other dynamically identical natural systems are analyzed in the following sections.

4.4 Nonlinear dust vortex flow solutions

The converged solutions are obtained for the confined dust in the toroidal domain having a rectangular cross-section where the driving plasma flow velocity v is directed along $-\hat{z}$ and has only a radial variation of the form of Bessel function j_0 as presented in Fig. 4.6(a) with associated source vorticity ω_s plotted in Fig. 4.6(b). Driven by this plasma flow field in the domain of confinement, the dust stream function is determined iteratively by imposing the boundary conditions such that the dust velocity normal to the boundaries is zero. Consequently, the dust is well confined in a finite section of a cylinder that accommodates the torus having a rectangular cross-section in r - z plane. The boundary conditions are motivated by the high shear experimental configurations where the driver is localized in a narrow region of the domain and in the region of domain far from the influence of the driver the dust experiences strong friction such that velocities there are considerably small (see schematic Fig. 4.2 and Ref. [11]). Accordingly, the dust velocity follows no slip boundary conditions for all the physical boundaries confining the dust. However, at the vertical boundary imposed by symmetry at the cylinder center ($r \rightarrow 0$), where the driving ion flow velocity is strongest, the magnitude of the dust velocity is not controlled by the boundary condition. A governing factor, all the derivatives at $r = 0$ vanish owing to the cylindrical symmetry of the domain and radial component of the dust velocity vanishes at this boundary by natural symmetry of the cylindrical setup.

The complete nonlinear solutions describing the driven dust dynamics in terms of 2D flow streamlines and corresponding ψ and ω fields are presented for small to high Reynolds number regimes in Fig. 4.7. The length and velocities in the present analysis are scaled to the system length or the domain dimension $L \equiv L_r = L_z$ and vertically downward streaming ion velocity magnitude U_0 , respectively. The parameters ξ , μ and ν accordingly have units derived from these scales. The entire

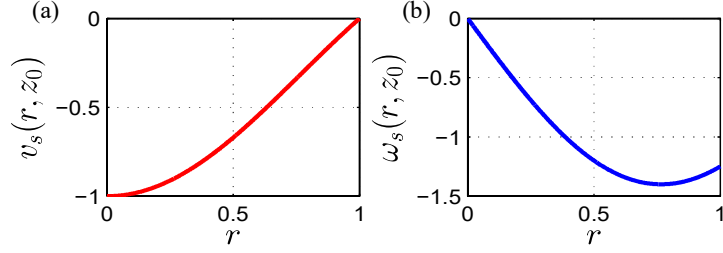


Figure 4.6: Profiles of the (a) driver velocity v , and (b) driver vorticity ω_s which are uniform along \hat{z} and $\hat{\phi}$.

analysis is done using a common combination of driver velocity and corresponding vorticity profiles presented in Fig. 4.6(a) and (b), respectively. Considering a typical laboratory glow discharge argon plasma with micron size dust with parameters, $n \simeq 10^9 \text{ cm}^{-3}$, $T_e \simeq 3\text{eV}$, $T_i \simeq 1\text{eV}$, largely at the sheath entrance where ions are streaming with a flow velocity U_0 equivalent to the a fraction of the ion acoustic velocity $c_s = \sqrt{T_e/m_i}$. The value of ion drag coefficient can be estimated as $\xi \sim 10^{-4} U_0/L$, neutral collision frequency can be $\nu \sim 10^{-2} U_0/L$ [124–126]. For a typical system size, $L \sim 10 \text{ cm}$, the range of kinematic viscosity μ can similarly be chosen $\mu \sim 6 \times 10^{-4} U_0 L$ which correspond to small Reynolds numbers ($\text{Re} \simeq 1$) of the dust flow consistent with the linear viscous regime.

The dust flow streamlines, which in cylindrical setup are the equal height contours of the product $r\psi$ in the r - z plane, are plotted in the first column of frames in Fig. 4.7 for the parameters $\xi = 0.001U_0/L$ and $\nu = 0.01U_0/L$. The effect of change in the dust kinematic viscosity, from a higher value $\mu = 1 \times 10^{-3}U_0L$ to a lower value $\mu = 8 \times 10^{-7}U_0L$ is visible on examining the results plotted from top to bottom row of frames in Fig. 4.7 where μ reduces taking the values 1×10^{-3} , 1×10^{-4} , 1×10^{-5} and $8 \times 10^{-7}U_0L$, respectively. Also shown in the second and third columns of Fig. 4.7 are the strengths of most dominant term $\nabla^2\omega$ and the nonlinear term $-\mathbf{u} \cdot \nabla\omega/\mu$, respectively, showing the increasing strength of the nonlinearity which is increasingly balanced by the viscous diffusion at decreasing

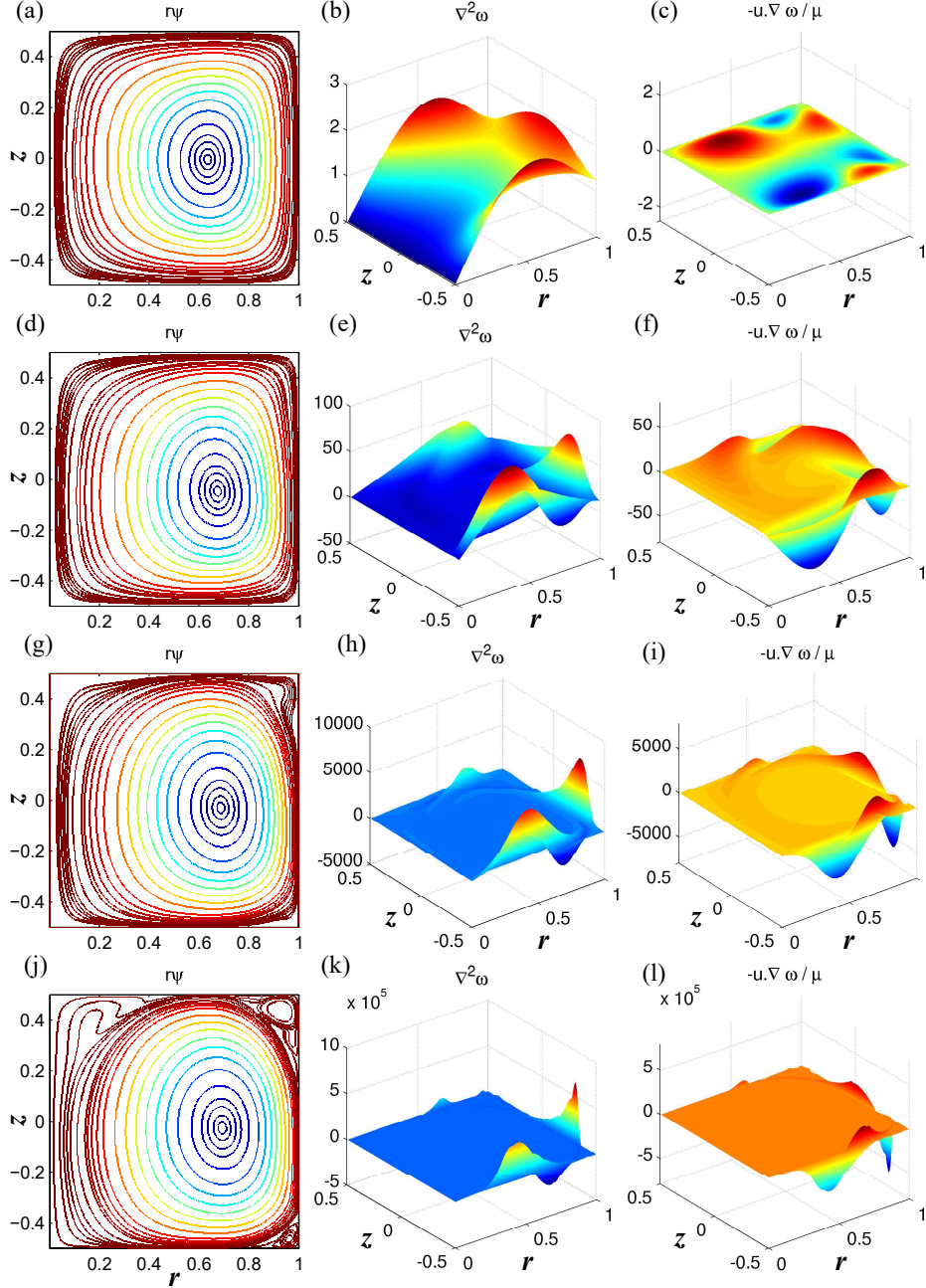


Figure 4.7: (a) Dust flow streamlines, strength of (b) diffusive term $\nabla^2 \omega$ and (c) nonlinear term $\mathbf{u} \cdot \nabla \omega$ plotted from top to bottom for the values of dust viscosity $\mu = 1 \times 10^{-3}$, 1×10^{-4} , 1×10^{-5} and $8 \times 10^{-7} U_0 L_r$, respectively, where the values $\nu = 0.01 U_0 / L_r$ and $\xi = 0.001 U_0 / L_r$ are used for other fixed parameters.

Table 4.1: Parameters μ and resulting values of u_b , Δr_b and Re in the analysis.

μ [$U_0 L_r$]	u_b [U_0]	Δr_b [L_r]	Re
1×10^{-3}	0.0024	0.1387	0.336
1×10^{-4}	0.0116	0.1030	11.961
1×10^{-5}	0.0217	0.0456	99.141
1×10^{-6}	0.0254	0.0198	503.705
8×10^{-7}	0.0252	0.0178	561.600

μ values. For example, as clearly visible from Fig. 4.7 the diffusive term is much larger and entirely uncorrelated to nonlinear terms for large μ values, or in the frames (b) and (c). For small μ value cases presented in frames (k) and (l) the most interesting variation is present in boundary regions of the solution of the Eq. (4.5) which is produced entirely by the balance $\nabla^2 \omega - \mathbf{u} \cdot \nabla \omega / \mu \sim 0$ as the contribution of other terms remains nearly negligible. As we analyze in the following sections, the boundary in this regime provides the strongest source of vorticity at smaller scales which can be dissipated in the domain volume at a relatively slower rate than linear case after being convected away in the interior along the streamlines.

For the system (4.4)-(4.5) with applied boundaries, the values of width Δr_b of boundary region, bulk flow velocity u_b and Re are provided in Table 4.1 in the range of transition corresponding to the range of μ values used in the present analysis. Note that the saturation of the width Δr_b is in departure from the linear boundary layer scaling $\Delta r_b \propto \mu^{1/3}$ [25] and relates to nonlocal diffusion of vorticity convected along streamlines. This convection governs a number of nonlinear aspects of the dust vortex flow addressable under the present formulations. The dominant nonlinear features of high Re solutions described below include, (i) a persistent uniform vorticity core of the vortex, (ii) development of separated convective boundary layer via a critical phenomenon analogous to certain biophysical processes, and (iii) a nonlinear boundary layer scaling prescribing velocimetric determination of the dust viscosity.

4.4.1 Persistent uniform vorticity solutions at high Re

The strength of the nonlinear term $\mathbf{u} \cdot \nabla \omega$ in Eq. (4.11) can be examined for our solutions based on the properties of dependence $\omega(\psi)$ in a 2D setups. For ω purely a function of ψ the term must vanish as can be shown by substituting the definitions $\mathbf{u} = \nabla \times \psi \hat{\phi}$ and a formal solution $\omega = f(\psi)$ of $\nabla^2 \psi = -\omega$ in $\mathbf{u} \cdot \nabla \omega$,

$$\mathbf{u} \cdot \nabla \omega = (\hat{\phi} \times \nabla \psi) \cdot \nabla (f(\psi)). \quad (4.17)$$

Note that the right hand side represents a dot product of two orthogonal vectors which must vanish for all ψ , implying that the nonlinear term $\mathbf{u} \cdot \nabla \omega$ must vanish where ω is either a pure function ψ or uniform. For application to present cylindrical set up where the contour parameter is $r\psi$ rather than ψ , this result readily transforms in the condition that the nonlinear convection vanishes when ω is purely a function of $r\psi$. For our solutions it is noted that at high μ , although the nonlinear term has a small magnitude it remains finite since ω shows a dependence on the product $r\psi$ as well as on r and z . For the low μ (high Re) solutions, however, the vorticity ω remains almost independent of r and z in the interior and is purely a function of $r\psi$, except in (and beyond) a thin boundary layer region.

This dependence is characterized in Figs. 4.8 and 4.9 for high and low μ cases, respectively. The contours of $r\psi$ are plotted in subplot (a) of Figs. 4.8 and 4.9. The dependence $\omega(r\psi)$ is examined by plotting variation of ω in space both when $r\psi$ is allowed to change (across streamlines, by following the solid lines, in subplot (b)) and when $r\psi$ is kept constant (along streamlines, by following the dashed contours, in subplot (c)). The strong variation in boundary region of low μ case (Fig. 4.9) shows that the function of nonlinear term is to prevent the diffusion of externally produced large vorticity to the interior region, by convecting it away along the streamlines in the boundary layer. The constant net vorticity of the core region is hence conserved. This nonlinear balance allows setup of a nearly rigid

body like motion of the vortex core with $v \propto r$ and a constant vorticity both in laboratory experiments and in natural flows.

We are now in position to compare both low and high μ limits accessible in a laboratory experiments with vortex formation in nature at phenomenally different scales than those of ordinary dusty plasma experiments. Highly persistent vortex structure like the Jovian great red spot (GRS), Jupiter's largest anticyclonic vortex, measuring approximately 22,000 by 11,000 km, for example, displays zonal eastward velocity profiles [31] in close agreement with the large Re (small μ) case plotted in Fig. 4.9 where a uniform vorticity core is surrounded by zones of sharp vorticity gradients. The similar velocity profiles are observed in relatively younger, year 1939 originated, pair of anticyclonic Jovian white ovals that are separated by teardrop shaped cyclonic vortex. In the interior region of closed streamlines the additional uniformity of ω with respect to the product $r\psi$ in low μ case (Fig. 4.9) is in confirmation of a toroidal analog of the integral condition obtained by Batchelor [27],

$$\frac{\partial \omega}{\partial(r\psi)} \oint r(u_r \hat{r} + u_z \hat{z}) \cdot d\mathbf{l} = 0,$$

which applies to the streamlines in the interior region as the integral evaluated along these closed streamlines vanishes for these solutions requiring ω to be independent of the product $r\omega$ in the core.

4.4.2 Boundary layer separation and secondary vortices

For our high μ case solutions, the boundary layer forms all along the domain boundary where no slip condition is applied and ψ remains monotonic in the direction orthogonal to streamlines. In low μ cases, however, the flow in the regions of sharp corners features an arrangement of smaller co- and counter-rotating vortices and ψ shows oscillatory spatial variation orthogonal to streamlines with a variety of

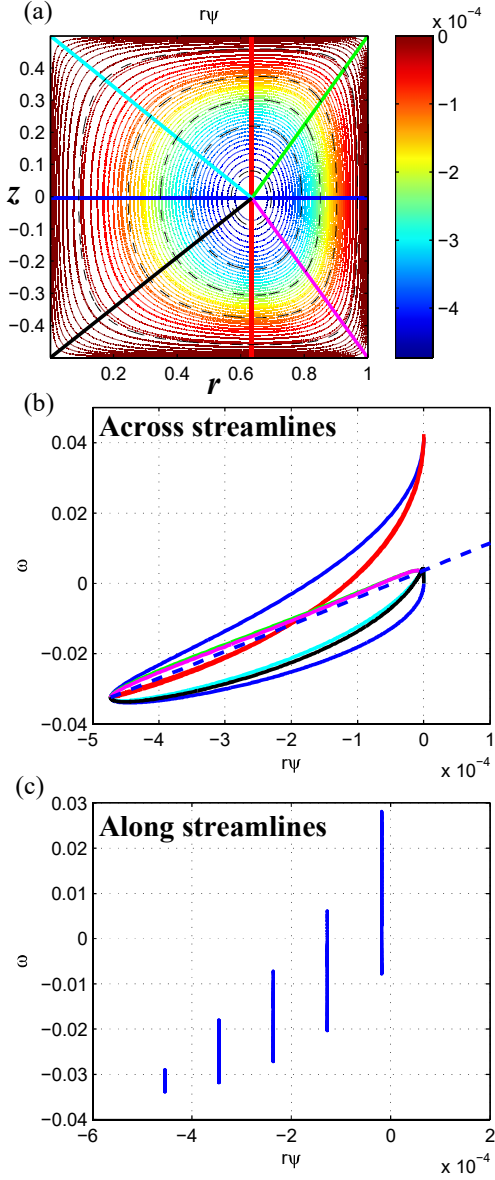


Figure 4.8: (a) Dust flow streamlines superimposed by straight lines and contours used to draw profiles of ω as function of $r\psi$ (b) vorticity ω as function of $r\psi$ along the straight line segments joining vortex center to domain vortices and (c) that along the indicated contours. The profiles correspond to $\mu = 10^{-3} U_0 L_r$, $\xi = 0.001 U_0/L_r$ and $\nu = 0.01 U_0/L_r$.

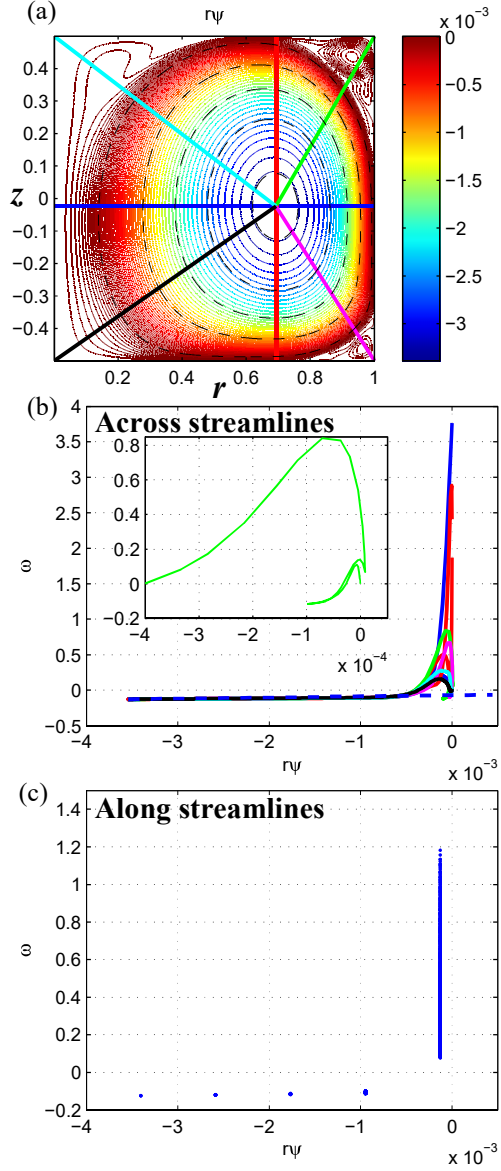


Figure 4.9: (a) Dust flow streamlines superimposed by straight lines and contours used to draw profiles of ω as function of $r\psi$ (b) vorticity ω as function of $r\psi$ along the straight line segments joining vortex center to domain vortices and (c) that along the indicated contours. The profiles correspond to $\mu = 8 \times 10^{-7} U_0 L_r$, $\xi = 0.001 U_0/L_r$ and $\nu = 0.01 U_0/L_r$.

scales as highlighted in the subplot drawn in Fig. 4.9(b). When driven at the same scale, the scale length of the largest vortex in this regime is still determined by the dimension L of the domain while the surrounding secondary co-rotating vortex have a smaller spatial scale length $\sim (\sqrt{2} - 1)L$. This factor corresponds to the corner zones of a square domain which accommodates a primary vortex of diameter $\sim L$. The region between two co-rotating vortices is further populated by somewhat elongated and weak counter-rotating teardrop-like vortices as shown in Fig. 4.9(a). The strength of the secondary small scale vortex structures is however subject to the magnitude of the dust viscosity. At higher dust viscosity the large momentum diffusivity begins to prevent the formation of small scale structures as presented in Fig. 4.8(a) and (b) where the dust flow streamlines and ω values are plotted, respectively, using $\mu = 10^{-3}U_0L$.

For a low μ case Fig. 4.10(a) and 4.10(b) present strengths of diffusive and nonlinear source terms for vorticity, respectively, in a set of solutions obtained for a confinement domain limited to larger r values ($0.5 < r < 0.1$) for clarity. The interface of the central vortex with the domain boundary is strongly localized at a few points (indicated as **a**, **b** and **c**) of closest approach from the center, ($\sim L/2$). while elsewhere it is only via a nearly circular shear layer running along the rest of the boundary of the strongest vortex. The vorticity generated by interaction of the central vortex with the no-slip domain boundary is being convected away from points **a**, **b** and **c** along the streamlines in Fig. 4.10(b) as the convective nonlinear term has large positive value along these streamline. This convected vorticity is, in turn, diffused away steadily across the streamlines, owing to sharp velocity gradient, by the diffusion term which displays an identical variation but with negative magnitude. Although the velocity gradients and diffusion are higher along the shear layer they are relatively much moderate as compared to the those required in the linear model where convection channel is unavailable and a sharp boundary layer must exist in order to diffuse the vorticity generated at the no-slip

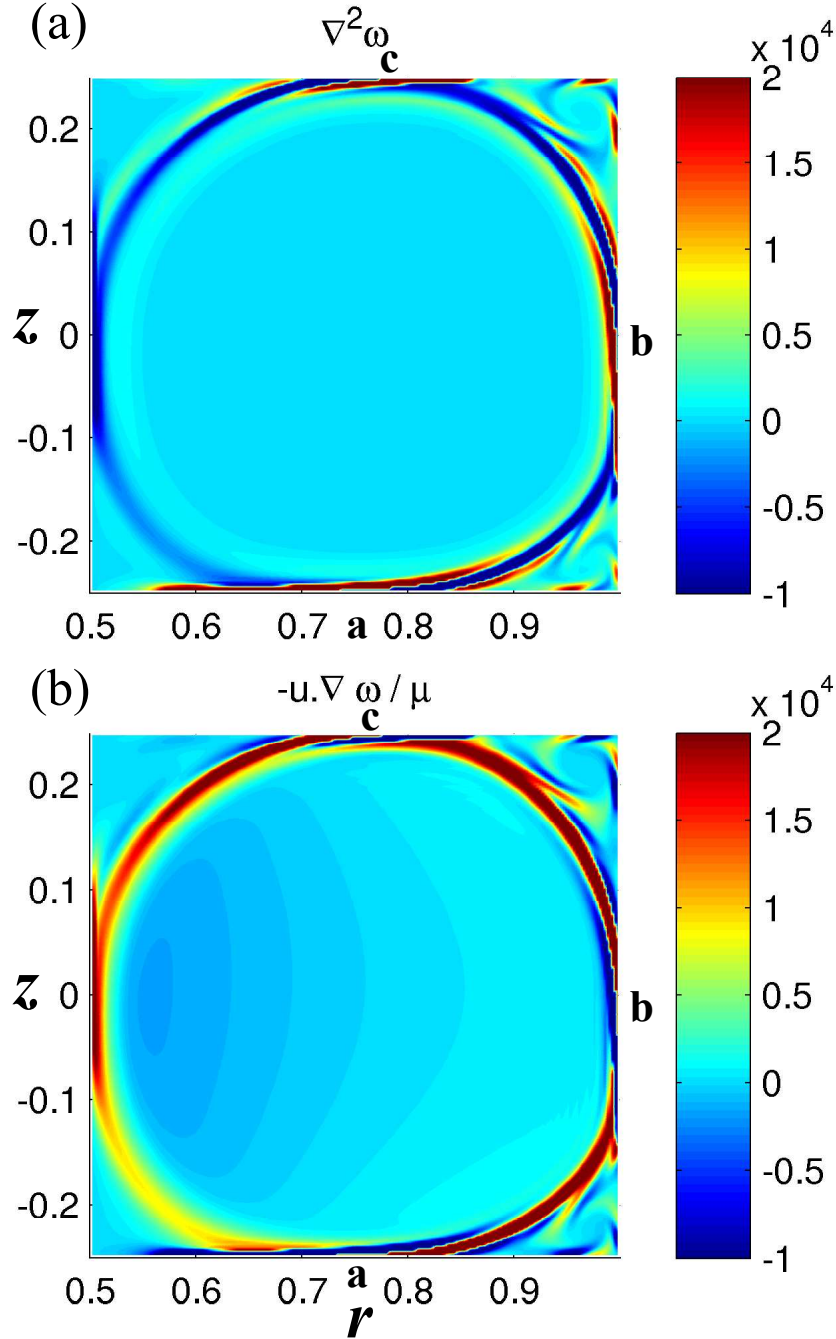


Figure 4.10: (a) Magnitude of the diffusion term and (b) Magnitude of the non-linear term plotted for $\mu = 8 \times 10^{-7} U_0 L_r$, $\xi = 0.001 U_0 / L_r$ and $\nu = 0.01 U_0 / L_r$ in a domain confinement limited to larger r values.

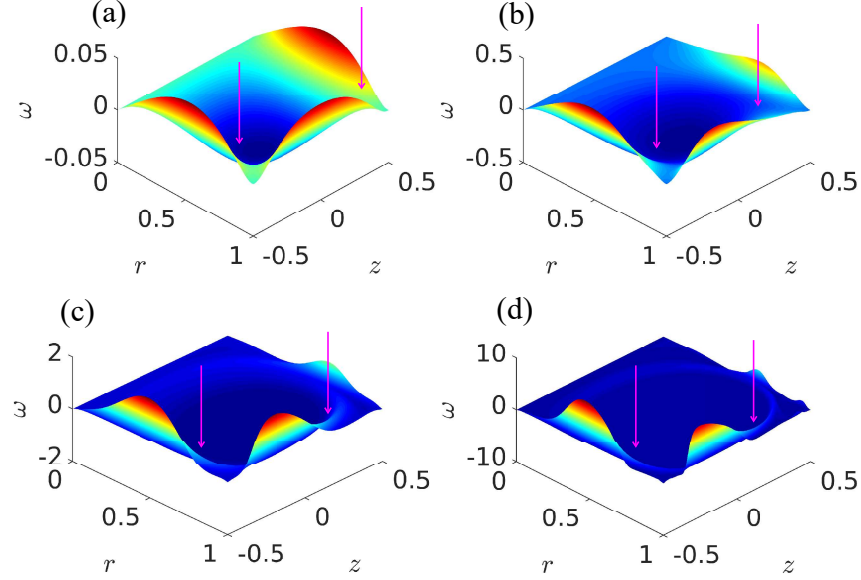


Figure 4.11: The vorticity surface plots for values of parameter (a) $\mu = 10^{-3}$, (b) 10^{-4} , (c) 10^{-5} and (d) $10^{-6}U_0L_r$. The developing points of separation are indicated by arrows on segments AB and BC .

boundary purely across the streamlines.

4.4.3 Boundary separation as structural bifurcation

We now address the nonuniformity of the flow structure along the domain boundary at high μ . Although the ideas related to Prandtl-Batchelor boundary flows and their breakdown in various limits long existed and thoroughly reviewed [136], it is only somewhat recently that development of such nonuniformity and transition to a separated boundary layer was shown to be a structural bifurcation of the 2D flow characteristics [137, 138]. For time dependent or turbulent flows this bifurcation was identified to take place at a critical value of time $t = T^*$ that corresponds to the breakdown of monotone vorticity profile in the boundary layer. We note that in our steady-state flow formulation the kinematic viscosity μ assumes the role of bifurcation parameter and this transition in our solutions takes place at a critical

μ value. This criticality allows the bounded dust vortex setup to represent a class of systems that can self-stabilize by making a critical transition to a self-similar state [28].

As discussed in [137] the solutions of the set formed by the Navier-Stokes and the incompressibility condition,

$$\frac{\partial \mathbf{u}}{\partial t} + (\mathbf{u} \cdot \nabla) \mathbf{u} = -\nabla \frac{P}{\rho} + \mu \nabla^2 \mathbf{u} \quad (4.18)$$

$$\text{and} \quad \nabla \cdot \mathbf{u} = 0 \quad (4.19)$$

with a no-slip boundary ∂M of a compact manifold M can be viewed as one-parameter families of divergence-free vector fields with parameter t . For such a family of divergence-free vector fields $\mathbf{u}(t)$ a structural bifurcation, or a change in topological equivalence class, occurs at a point in the spatial and parameter space if the normal derivative of the velocity field $\mathbf{u}_n = \partial \mathbf{u} / \partial \mathbf{n}$ has a degenerate singular point on the boundary segment ∂M such that \mathbf{u}_n there is a finite function of the parameter t , or $\partial \mathbf{u}_n / \partial t \neq 0$. Since the point of separation is also a spatially local extremum for the vorticity, it was concluded by applying the Hopf Lemma that the vorticity gradient is directed outward or inward at this point. The presence of an adverse pressure gradient required for the separation in such divergence-free field systems follows directly from the fact that the tangential derivative of the pressure is exactly the normal derivative of the vorticity. Based on this relationship, the above bifurcation condition was shown in [137] to translate in terms of vorticity at the boundary ∂M , which essentially required that the vorticity profile must reach its first zero value along ∂M at a local minimum point while evolving with respect to the bifurcation parameter.

In Fig. 4.11 where ω is plotted for range of μ examined in our analysis we show that this condition holds for our solutions at the frictional boundaries $\partial M \equiv AB, BC$, and CD (indicated by arrows at two of the boundaries visible in the

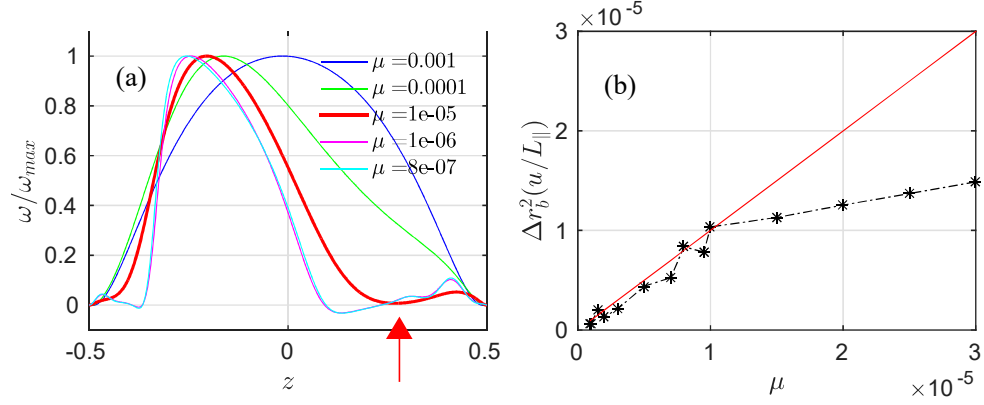


Figure 4.12: (a) The normalized vorticity profile along the no-slip boundary BC for various values of parameter μ . The point of separation and associated bifurcation is indicated by an arrow where profile corresponding to critical value $\mu^* \sim 10^{-5}U_0L_r$ has a single degenerate singular point. (b) The nonlinear boundary layer scaling with dust viscosity μ . The profile shows a change of regime at the critical μ^* .

figure) where such boundary layer separation takes place following interaction with boundary of the primary vortex at points **a**, **b** and **c** in our solutions (as marked in Fig. 4.10). For clarity, in Fig. 4.12(a) we present the profiles of vorticity along the boundary segment BC for various values of μ where the first zero value of vorticity coincides with the local minima of vorticity at a critical value $\mu^* \approx 1 \times 10^{-5}U_0L$ for our analysis. This location, $z \sim 0.29$, at the boundary BC is indicated by an arrow in Fig. 4.12(a). At this value $\mu = \mu^*$ the profile has a degenerate singular point that bifurcates, at lower μ values, into a set of two isolated points since the profile begins to intersect the axis $\omega = 0$ at two points above its minimum. Similarly, the values for μ^* for the separation at the boundaries, AB and CD were noted to be $\approx 3 \times 10^{-5}U_0L$ and $\approx 2 \times 10^{-6}U_0L$, respectively, meaning that the separation is triggered at the highest μ value at the boundary AB , followed by the boundaries BC and CD . These values demarcate the range beyond which nonlinear prescription needs to be applied for the local estimates. This critical behavior, accompanied by emergence of self-similar secondary structures, highlights capacity of confined dusty plasma vortex structures to represent the complexity of biophysical processes where

replication must follow a bifurcation [57]. The transition in our square shaped setup produces an identical structure only with a scale ratio of $\sim 1 : (\sqrt{2} - 1)$. Interestingly, a recent experiment [13] with dust vortices has indeed shown a transition resulting into secondary dust vortices with scale ratio of unity, which is isomorphic to the process of cell mitosis triggered by a bifurcation and is being addressed by a distinct parameter regime of our formulation.

4.4.4 Velocimetric prescription of the dust viscosity

We finally note that beyond the boundary layer separation (BLS) transition at μ^* , a very simple relationship exists between the velocimetrically obtainable quantities and dust viscosity. This should allow one to estimate the dust viscosity using velocimetry techniques, for example computer aided particle imaging velocimetry (PIV) which provides local velocity and vorticity in the vortex [11, 41, 42]. Since we observe from the characterization of nonlinear solution that the vorticity diffusion across the streamlines is nearly balanced by the nonlinear convection of the vorticity, the balance (4.5) in the convection dominated boundary layer reads,

$$\mu \nabla^2 \omega = \mathbf{u} \cdot \nabla \omega. \quad (4.20)$$

Note that the right hand side involved convective derivative of the vorticity ω parallel to streamlines while the left hand side has a diffusion purely orthogonal to the streamlines. At any given point in the boundary layer the balance (4.20) therefore has a simple form,

$$\mu \frac{\omega}{\Delta r_b^2} = u \frac{\omega}{L_{\parallel}}. \quad (4.21)$$

where Δr_b is the velocity gradient scale length, or approximately the boundary layer width, and $L_{\parallel} = u/u'$ is the gradient scale length of the velocity along

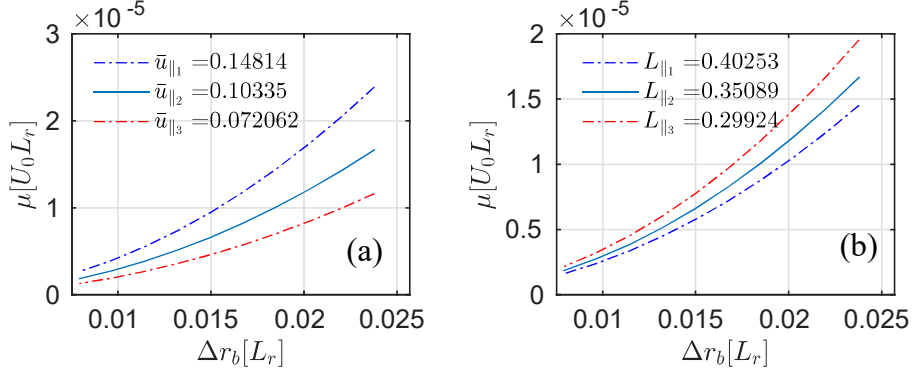


Figure 4.13: characterization of μ dependence on the boundary layer flow velocity u and the characteristic length scale along the streamlines $L_{||}$.

the streamlines (with prime indicating derivative along the streamlines). This readily provides the nonlinear version of the boundary layer width scaling with the viscosity μ as,

$$\mu = \Delta r_b^2 \frac{u}{L_{||}}. \quad (4.22)$$

indicating that in the BLS regime, the dust viscosity may be evaluated from the experimentally determinable quantities, namely, boundary layer width, dust velocity and its gradient length along the streamlines. In Fig. 4.12(b) we have plotted the quantity $\Delta r_b^2 u / L_{||}$ as a function of viscosity μ showing that beyond the BLS transition ($\mu < \mu^* \sim 1 \times 10^{-5} U_0 L$ on segment BC) this quantity is equal to the viscosity μ . However the a clear disagreement is triggered below the critical BLS transition and at larger μ the linear scaling [25] can be recovered.

The scaling (4.22) is further characterized for various parameters in Fig. 4.13 for the typical experimental conditions outlined in Sec. 4.4 for estimation of the kinematic viscosity μ which is normalized to the product $U_0 L_r$. The formal dependence of μ on the boundary layer width Δr_b , flow velocity u and the characteristic length scale of variation along the streamlines $L_{||}$ is described further in Fig. 4.13(a) and Fig. 4.13(b), respectively, to indicate the sense of its variation with respect to

these two parameters.

4.5 Summary and conclusions

In this chapter, the nonlinear properties of a volumetrically driven 2D dust vortex flow of a confined dust fluid suspended in a plasma are studied. Motivated by toroidally symmetric flow formation and signatures of nonlinear nature of its flow dynamics at higher dust velocities, 2D nonlinear equilibrium solutions of the vortex flow are obtained in a toroidally symmetric domain. The solutions obtained in present treatment are relevant to a large number of observations in dusty plasmas setups where a vigorous dust vortex flow dynamics is observed with flow velocities approaching the nonlinear limit. The solutions are in confirmation with a variety of characteristics observed in the experiments, for example observation by M. Kaur *et al.* [11], where localized dust vortex with relatively uniform core vorticity are seen surrounded by regions with strong variation, featuring very vigorous to relatively moderate or negligible dynamical activity.

In terms of completeness of the solutions as compared to the linear regime explored in Chapter 2 and 3, free from most of the approximations involved in the analytic approach presented in Chapter 3, the governing flow equations in this chapter are solved rather exactly (limited only by the finite spatial resolution) with explicit inclusion of multiple axial mode structure of downstreaming flow of both, the streaming driver and the confined dust. The approach to nonlinear solutions is shown to be nontrivial where even a numerical approach to them in 2-dimensions, as adopted in this work, must involve an iterative procedure. The vortex flow solutions for the identical set up in the low Reynolds number obtainable by both, the previous linear approach as well as the present nonlinear numerical approach, are comparable as the numerical solutions for standard parameters reduce in to the analytic (series) solutions in the appropriate low Reynolds number limit.

The emerging distinct nonlinear characteristics of the dust vortex flow are noted in numerical solutions where the circulation originally symmetric about z_0 in the low Reynolds number begins to turn asymmetric about z_0 in higher Reynolds number ($\text{Re} \gg 1$) regime. The flow structure in the nonlinear (high Re) regime is also found to be dependent on the aspect ratio (L_z/L_r) of the dust confinement domain, an effect which is analyzed in more detail in following Chapter 5. Among one of the most fundamental nonlinear characteristics which is quantitatively recoverable from the nonlinear vortex flow equilibrium solutions with decreasing μ (or increasing Re), the strength of the nonlinear term $-\mathbf{u} \cdot \nabla \omega / \mu$ is seen to increase and this nonlinear convection of the vorticity, in turn, is found duly balanced by the viscous diffusion represented by the term $\nabla^2 \omega$, introducing the convective mode of the vorticity transport in the set up. For small μ value cases presented, the most interesting variation is present in boundary regions of the solution which is produced entirely by the balance $\nabla^2 \omega - \mathbf{u} \cdot \nabla \omega / \mu \sim 0$ as the contribution of other terms remains nearly negligible. The boundary that provides the strongest source of vorticity which in the nonlinear regime can be dissipated orthogonal to streamlines much deeper in the domain volume at a relatively slower rate than linear case after being convected away in the interior along the streamlines.

Similar to observations of a dust torus where poloidal dust flow is recoverable with considerably uniform vorticity, the driven primary vortex in the present solutions is formed with almost uniform vorticity in the core, surrounded by region of a strong variation of vorticity value and oscillatory nature of streamfunction. The relationship between vorticity ω and product $r\psi$ is examined in the small and large Reynolds number regimes to recover independence of ω from $r\psi$ in the uniform vorticity core formed at large Reynolds number. In this limit the core vorticity follows the curvilinear form of an integral condition on the regions of closed streamlines where boundary conditions are no longer usable for determination of ω in high Reynolds number regime and its analytic value remains largely indeterminate.

In presence of 2D heterogeneous boundary conditions applied to dust flow in a curvilinear coordinate system, the major nonlinear effects cause the boundary layer to separate from the domain boundary. This causes the vorticity generated from the interaction with the no-slip, or frictional, boundaries to be convected away with strong flows of the primary vortices. The separation allows dynamic isolation of the regions scaling with the dimensions of small scale features of the boundary (e.g., spatial modulations or the sharp corners) and development of secondary vortices in these regions. The development of separated boundary layer is investigated as a structural bifurcation where the kinematic viscosity assumes role of the bifurcation parameter and the separation coincides with the bifurcation. The bifurcation is shown to occur when the vorticity profile approaches its first zero value along the boundary at the point where its minimum is located. This critical behavior and signatures of equivalent nonlinear vortex states in experiments indicates capacity of confined dusty plasma vortex structures to represent a class of systems that can self-stabilize by making a critical transition to a self similar state, for example, biophysical transition during cells undergoing mitosis. The nonlinear scaling of the boundary layer parameters with kinematic viscosity μ is obtained that shows a velocity independent linear estimate of kinematic viscosity to modify and additionally depend up on the flow velocity and its gradient scale length along the streamlines as $\mu = \Delta r_b^2 \frac{u}{L_{\parallel}}$. Similarly, existence of a critical values μ^* demarcating transition to nonlinear regime is identified. These two factors allow estimation of viscosity of charged fluids using appropriate scaling by identifying a structural change in flow patterns in experiments. The nonlinear dust vortex dynamics thus offers quantitative insight and analytic framework to a number of natural systems that dusty plasmas emulate.

5

Co-rotating multiple vortex equilibria in nonlinear regime

5.1 Introduction

A remarkable property of the nonlinear solutions presented in previous Chapter [4](#) has been that the geometry and dimensions of the dust-fluid vortex structure in nonlinear operating regime are asserted by the dynamics rather than governed by the boundary structure [\[26\]](#). Unlike the linear vortex flow solutions [\[24, 25\]](#), nearly circular multiple co-rotating vortices emerge in the nonlinear regime with virtual boundary separated from the domain boundary as the dust flow streamfunction (ψ) which is allowed to be multivalued in its dependence on the vorticity (ω). This partial freedom from the boundary geometry in a dust vortex is facilitated by the essential nonlinear effects that ensure a steady state transport of vorticity, via a newer convective mode of transport, from its sources to a homogeneous sink present in the form of the neutral fluid. The nonlinear dust flow dynamics achieves this by balancing the net source of vorticity to be diffused as well as convected flux of the

vorticity rather than pure diffusion across the streamlines in the nonlinear regime requiring a boundary layer having sharp gradient along the domain boundary.

The solutions corresponding to this newer set up develop branch-like regions in the interior where the gradient of the vorticity can have a projection on the normal to physical boundary with a positive sign. This means that the vorticity can now diffuse even in the direction directed exactly towards the the physical boundary rather than essentially away from it as allowed in the purely diffusive linear regime. The regime prior to this transition sees almost zero diffusive flux of vorticity normal to the physical boundary in the separation region and therefore no strong vortex activity in this region and dust flow that is almost stagnant. One therefore watches the sign of the normal component of the gradient of the vorticity at the separation location as a function of the parameter μ and identifies its critical value μ^* at the bifurcation point in the functional space corresponding to a change in sign. The solutions beyond the critical value μ^* serve as natural equilibria that must be approached asymptotically by beginning from any arbitrary initial flow field arrangement. The fact that these equilibria show a critical transition to maintain its stability represents a large class of system where a critical transition must occur and where the properties like the maximum structure size are determined by this critical limit. The factors determining the nonlinear solutions in the present nonlinear driven Navier-Stokes system are diffusivity and inertia that control the dimension of the vortex structure, presenting no possibility of equilibrium with larger or smaller structures.

In this chapter, the same driven-dissipative bounded dust flow system in an unbounded flowing plasma is reconsidered from previous Chapter 4 as shown schematically in Fig. 5.1. Then in Section 5.2 we first present the results with variation in the domain aspect ratio and its impact on the formation of vortices and their number. The case of bifurcating flow solutions with domain aspect ratio 2 is discussed first where vortex replication with nearly a dimension ratio 1:1 is recovered

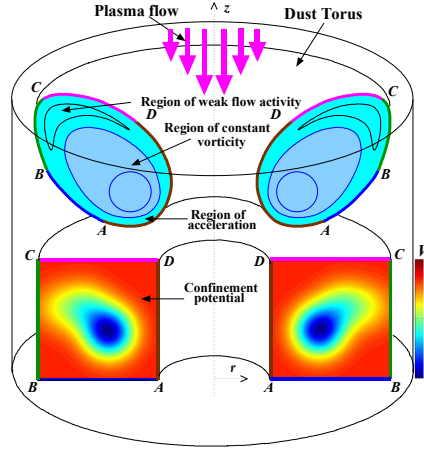


Figure 5.1: Schematic representation of the toroidal dust cloud with vortex motion and mapping of the boundary of its cross-section to a toroidal domain of rectangular cross-section accommodated in the cylindrical geometry of the present nonlinear solutions. Segments AB , BC , CD and DA , of the cloud map to the corresponding sides of the rectangle $ABCD$.

in comparison to $1 : (\sqrt{2} - 1)$ as recovered while analyzing flow in a square shaped domain in Chapter 4. Such a bifurcation predicted for a dusty plasma 2D flow cell is discussed in the light of its close resemblance to bifurcation transition in more complex biophysical processes, for example, in certain approaches to model the process of cell division or mitosis.

In Section 5.3 we examine more diverse aspect ratio values, including those exceeding 2 and smaller than unity. It is discussed that the cases with aspect ratio larger than 2 and more a complete sequence of identical corotating vortices is recovered with number of identical vortices equal to the value of aspect ratio. This result is discussed in the light of recovery of similar results in the dusty plasma experiments by M. Choudhary *et al.* [13] where a dust cloud with aspect ratio exceeding unity is indeed seen to develop a series of multiple corotating vortices at stronger drive, or larger Reynolds number. In the cases of aspect ratio smaller than unity, the vortices are seen to show a transition to a diffusion dominated single vortex state, even at much smaller kinematic viscosity values.

The solutions correspond to no exact balance between nonlinear convection and diffusive transport terms in the model. Summary and conclusion from the above studies are presented in Section 5.6.

5.2 Vortex flow at higher domain aspect ratio

While diffusion in a dust cloud under the model (4.4)-(4.5) is active in all the limits, the convection channel additionally becomes available in the nonlinear cases. The two effects compete in this regime and the convective transport gets to decide the flow topology when the flow velocity rises above a threshold. Below this threshold the diffusion across the streamlines is the dominant mechanism of the vorticity transport and the convection channel is secondary. The sharp gradients at the boundary that decay into the interior with a monotonic streamfunction (or vorticity) variation is therefore the characteristics of the linear solutions. In the nonlinear regime, on the other hand, a nonmonotonic spatial variation of the streamfunction characterizes development of localized regions where the vorticity transport along the streamline is stronger and therefore the vorticity brought, convectively, along the streamlines diffuses in both the directions about the carrier streamlines owing to the developed gradients with drop in vorticity in both the directions about them, as clear from the vorticity plots in Fig. 4.11 over this transition. The diffusive transport of the vorticity to core, or to the exterior region, is still small and most of the vorticity flux is dissipated by the means of sink (neutrals) well within in the separated boundary layer itself.

5.2.1 Vortex structure replication for domain aspect ratio

$$L_z : L_r = 2$$

Note that the central, uniform-vorticity circulation visible in the nonlinear limit, Fig. 4.11(d) is isolated from the boundaries. Given its isotropy, a single scalar parameter, or its radius, is limited by the radius of curvature of the flow that must reverse within minimum separation between two boundaries. With explicit presence of dust inertia, at larger flow velocity the turning of flow sets up a macroscopic mode of circulation scaling with separation between two boundaries in the incompressible dust flow. Interesting vortex flow structure develop following a BLS transition in case the axial dimension of the confinement domain is longer than the separation between the radial boundaries determining the turning radius of the inertial flow. A case with aspect ratio $L_z/L_r = 2$, driven with ion flow of $I = 1$, is examined in Fig. 5.2 with $\xi = 10^{-4}U_0/L_r$ and $\nu = 10^{-3}U_0/L_r$, for a wide range of Reynolds number $\text{Re} \simeq 0.01$ to 100. It is seen that a secondary vortex identical to the first forms in the region further upstream (of the driving ion flow) if the viscosity μ is reduced further. This results from the sharp separated boundary of the first vortex extending deeper in to the domain interior along the boundary of the primary vortex and beginning to act as a virtual domain boundary for the upper region, providing a vanishing flow velocity boundary condition identical to the original domain boundary. It can be well predicted that this might trigger formation of a sequence of identical vortices for even larger aspect ratios as discussed in more detail in Sec. 5.3.

The transition in terms of axial and radial flow velocity profiles is presented in Fig. 5.2(f) and (g), respectively. The impact of the nonlinearly developed extended virtual boundary can be seen deep into the interior where, in a quite counter-intuitive observation from Fig. 5.2(f), the magnitude of the dust flow velocity u_z begins to drop (red profile with $\mu = 3 \times 10^{-5}U_0L_r$) with decrease in the μ (increasing

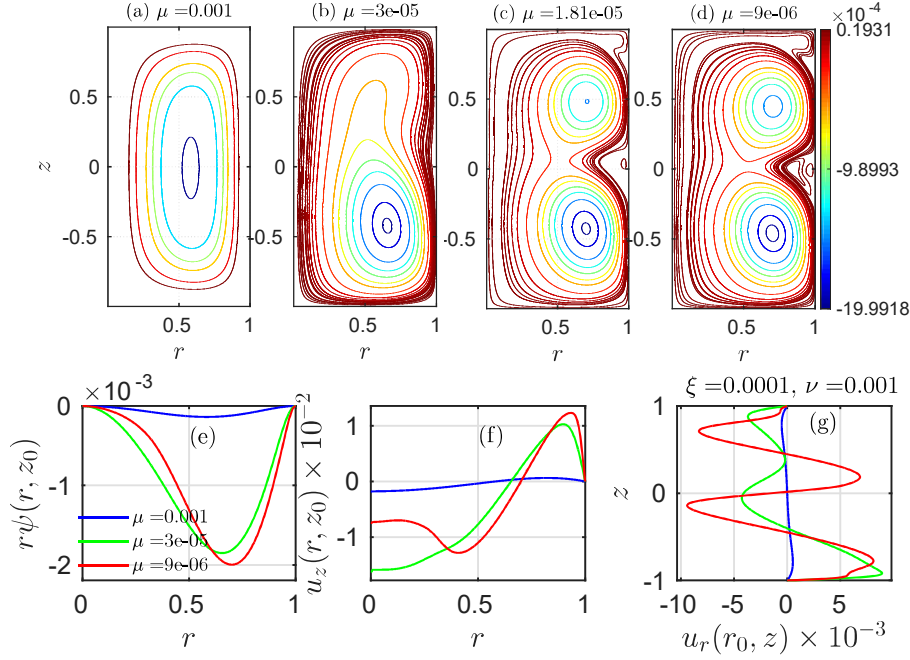


Figure 5.2: [Effect of varying viscosity at $L_z : L_r = 2$] Streamlines for the dust fluid flow in r - z plane for varying (a) $\mu = 10^{-3}U_0L_r$, (b) $\mu = 3 \times 10^{-5}U_0L_r$ (c) $\mu = 1.8 \times 10^{-5}U_0L_r$ and (d) $\mu = 9 \times 10^{-6}U_0L_r$ respectively having fixed other parameters $\xi = 10^{-4}U_0/L_r$, $\nu = 10^{-3}U_0/L_r$. The corresponding cross-section profiles for (e) $r\psi(r, z_0)$, (f) $u_z(r, z_0)$ and (g) $u_r(r_0, z)$ passing through the center of the primary vortex (r_0, z_0) .

Reynolds number) in the region close to $r \rightarrow 0$. The u_z value at $r = 0$ drops below its value in the interior despite that the driver strength approaches its maximum at $r = 0$. The downward directed dust flow velocity at $r = 0$ which thus shows a maximum as a function of μ at the critical value $\mu = \mu^* \sim 10^{-5}U_0L$ as seen in Fig 5.2(f). Similarly, the radial component of the dust flow velocity u_r is clearly seen in Fig. 5.2(g) to vanish at $z \sim 0$ such that the line $z = 0$ begins to resemble a domain boundary (at least for large r). Note that transition in a domain of aspect ratio $L_z : L_r = 1$, as addressed in Chapter 4, produced a dynamically identical structure only with a scale ratio of $1 : (\sqrt{2} - 1)$ as opposed to the scale ration nearly 1:1 as recovered in the case of domain aspect ratio 2. Whether this scale ratio 1:1 is general for all the values of the domain aspect ratio larger than unity

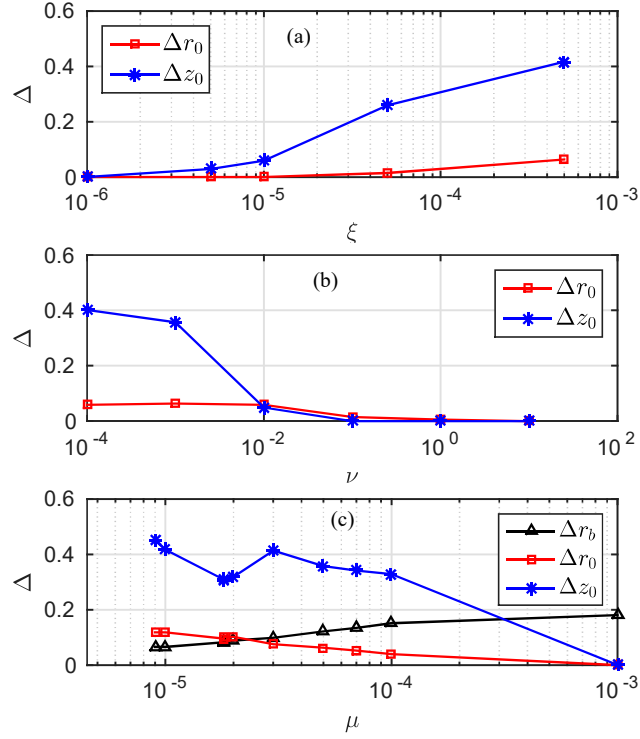


Figure 5.3: [Shifting effect in (r_0, z_0) with varying ξ , ν and μ] Shifting in center of circulation (r_0, z_0) with changes in (a) ion dragging co-efficient ξ , (b) neutral collision frequency ν . And (c) Shifting in center of circulation (r_0, z_0) , and changes in boundary layer thickness Δr_b with varying kinematic viscosity μ .

(2 or more) is investigated in the next section.

5.2.2 Critical topological modification of 2D vortex structures

We now examine the magnitude of topological change in the vortex flow structures during the critical BLS transition and present comparison between the modifications along axial and radial dimensions for the case of domain aspect ratio $L_z/L_r = 2$. The Fig. 5.3(a), (b) and (c) present the shift with respect to change in ξ , ν and μ , respectively, in the radial and axial locations of the primary vortex r_0 and z_0 , respectively. In the observed variations in each case, a larger shift is

generally noticed in the axial location z_0 of the vortex in comparison to the radial location r_0 with respect to change in all the parameters. The variation in both r_0 and z_0 are also relatively simpler and monotonic with respect to variation in ξ and ν . However, with respect to the viscosity μ the shift in z_0 shows a complex nonmonotonic behavior and shows that the system undergoes a critical change at about $\mu = 1.2 \times 10^5 U_0 L_r$ and shows a relaxation like behavior at a critical value μ^* comparable to this value. Among another noticeable effect, the amount of shift both in the dust boundary layer width and in the primary vortex center (triangles and boxes in Fig. 5.3(c) are found to be complementary to each other showing that the effect of critical BLS transition has been uniform and global rather than being limited to the boundary layer structure.

5.3 Generation of co-rotating vortex sequence for higher aspect ratio

The dust vortex flow analysis is extended further in this subsection to confinement domain aspect ratio $L_z/L_r > 2$. Variation in the vortex flow structure topology is analyzed with external driver flow vorticity mode index $I = 1$, $\xi = 10^{-4} U_0/L_r$, $\nu = 10^{-3} U_0/L_r$ and varying kinematic viscosity from $\mu = 10^{-3}$ to $10^{-5} U_0 L_r$ such that the corresponding effective Reynolds number varies up to the nonlinear regime from $Re \simeq 0.1$ to 100. The series of structural changes for wide range of Re or that of the kinematic viscosity μ is shown in Fig. 5.4(a) to (c), in term of streamlines of dust circulation in an r - z plane of the toroidally symmetric confined domain.

In the linear regime ($\mu = 10^{-3} U_0 L_r$ or $Re \ll 1$), dominated by pure viscous transport, the flow in the confined domain is characterized by single vortex with boundary aligned flow streamlines, and a boundary layer that runs along the no-slip boundary and has sharp velocity gradient in the direction orthogonal to the

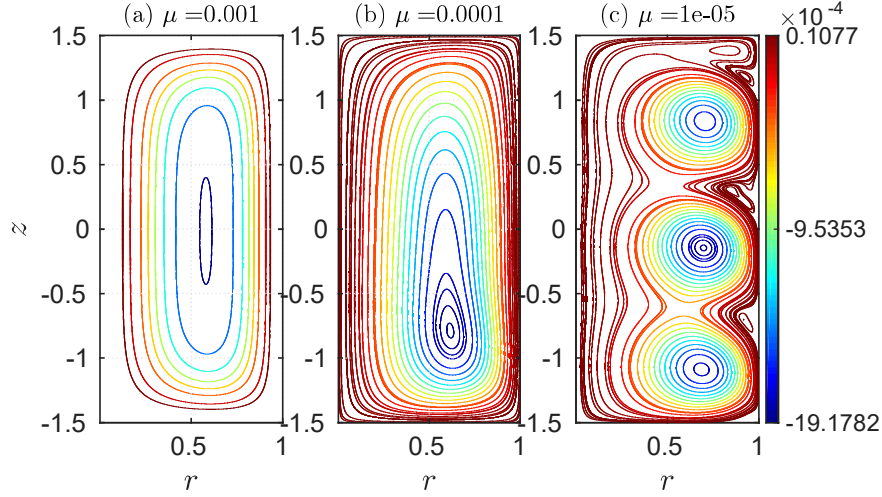


Figure 5.4: [Effect of varying viscosity at $L_z : L_r = 3$] Streamlines for the dust fluid flow in r - z plane, correspond to varying (a) $\mu = 10^{-3}U_0L_r$, (b) $\mu = 10^{-4}U_0L_r$, (c) $\mu = 10^{-5}U_0L_r$ respectively having fixed other parameters $\xi = 10^{-4}U_0/L_r$, $\nu = 10^{-3}U_0/L_r$.

boundary. The vortex flow follows these linear characteristics up to $\text{Re} \leq 5$ as shown in Fig. 5.4(a). However, upon increases in Re from 5 to 20, the flow patterns are no longer symmetric about the center-line of the confined region and the center of the vortex drifted axially downward and radially outward and the vortex flow converges to a new equilibrium flow structure as shown in Fig. 5.4(b). Further increase in Reynolds number or $\mu \approx 10^{-5}U_0L_r$ produced the spontaneous structural change by the nonlinear structural bifurcation at a critical kinematic viscosity μ^* [26]. As predicted and discussed in Sec. 5.2.1 the vortex flow pattern makes spontaneously transition to a sequence of three separated co-rotating vortices, each having a nearly uniform vorticity core region with dimension of the smallest scale available ($L_r \ll L_z$) in the system, and bounded by a virtual boundary and a shear region as shown in Fig. 5.4(c). For the confining system having aspect ratio of $L_z : L_r = 3$, the radial shear scale of the background streaming plasma (driver) flow remains L_r , but the axial interactions range of the driver with the confined dust is extended up to longer extension $L_z \gg L_r$. Thus the background ions transfer larger

momentum to the confined dust and nonlinear structural bifurcation is observed to take place at a relatively lower critical Reynolds number $\text{Re}^* \approx 60$, or at critical kinematic viscosity $\mu^* \approx 8 \times 10^{-5} U_0 L_r$, while $\text{Re}^* \approx 80$ or $\mu^* \approx 1 \times 10^{-5} [U_0 L_r]$ in case of confining system having aspect ratio of $L_z : L_r = 2$.

For the dimensions where $L_z > L_r$ but not an integer multiple of L_r , a partially developed vortex at the upstream ion-flow end of the cell is visible in addition to an integer number of fully grown vortex as seen in Fig. 5.4.

5.3.1 Recovery of multiple co-rotating vortices in the experiments

In many dusty plasma experiments displaying fluid-like dust phase and its relevant flow dynamics, the structure of the boundary of the confining domain is an important factor allowing to identify the dynamical regime of the flow. For example in many confinement domain with noncircular boundaries the boundary layer separation takes place as the separated boundary layer forms along a nearly circular boundary of a dominant vortex. Either a stagnant flow or a secondary vortex activity, similar to secondary vortex formed in solutions in Fig. 4.10, must be observed in such cases in the region between the separated and physical domain boundary. In a very close observation experimental results of M. Kaur *et al.* [12] showed that when the confinement domain is highly non-circular a nearly uniform vorticity circular vortex forms in the core of the domain while a clearly separated weaker flow activity is observed in the region between the boundary of the core vortex and noncircular boundary of the domain (see, for example, the dust cloud geometry in Fig. 2.1 and 5.5). Clearly with small volume of the region between vortex boundary and domain boundary the secondary vortex formed in such setup is inhibited by the strong viscous diffusion and the dimension of the secondary vortex formed remain smaller than the primary vortex, for example, the

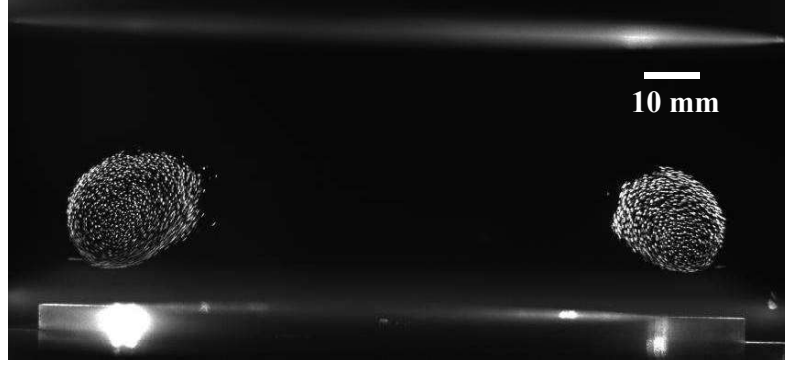


Figure 5.5: Uniform vorticity core region surrounded by very sharp and localized shear flows observed in toroidal dust cloud with poloidal circulation in the laboratory dusty plasma experiment by M. Kaur *et al.* Phys. Plasmas **22**, 033703 (2015)[12].

smaller dimensions of the secondary vortices forming in the corner of the square shaped domain of the solutions in Fig. 4.10. The large aspect ratio cases present special cases of domains where primary vortex formed may have adequate volume of the dust fluid outside the primary vortex boundary for another vortex of the similar dimension to form and develop into a corotating replica of the primary vortex, as represented by large domain aspect ratio solutions, for example, those for case $L_z/L_r = 2$ presented in Fig. 5.7 of the Sec 5.2.1 and its general form with $L_z/L_r = 3$ presented in Fig. 5.7 of the Sec. 5.3.

Interestingly, a recent experiment carried out by M. Choudhary *et al.* [13], who analyzed dust dynamics in domain of higher aspect ratio $L_z/L_r \sim 2-3$, has indeed shown a similar structural transition from a single dust vortex structure to a state of multiple co-rotating dust vortices. Transition by observed by Choudhary *et al.* resulting from a variation in input power to the plasma discharge and in the location of the dust cloud in the background plasma as described in Fig. 5.6 adopted from [13]. In another recent experimental work Kil-Byoung Chai *et al.* [106], reported recovery of dust grain poloidal vortices with two adjacent co-rotating poloidal vortices. The vortex formation in the observations by Chai *et al.* is

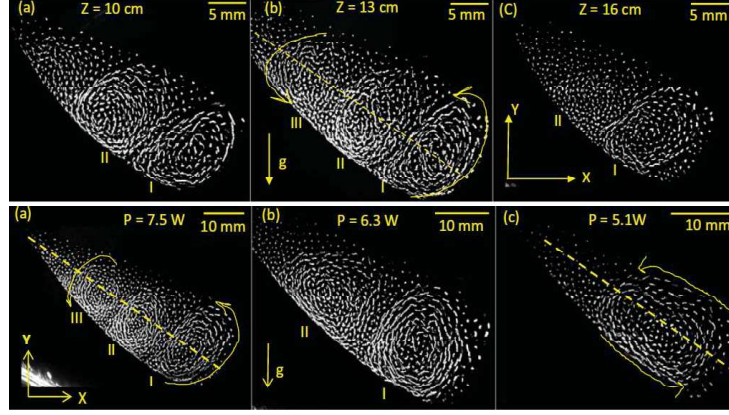


Figure 5.6: Steady equilibrium co-rotating vortices observed in dusty Phys. Plasmas **24**, 033703(2017) [13]. The number of vortex structures depends on the position of the observed cross-section away from the source region and the variation in input power as shown in upper and lower rows.

reported in presence of ion density gradient and the gradient of the magnitude of the ion ambipolar velocity.

The close agreement between the dust dynamics described by our nonlinear formulation and the driven dust flow dynamics experiments carried out quite independently by Choudhary *et al.* [13], incorporating also the complex phenomenon (critical transition) of development of multiple corotating vortices from a single vortex, indicate that the laboratory dusty plasma show strong signatures of flow activity with access to nonlinear regime of the dust flow. The agreement further motivates the idea that dusty plasma experiments can be one of the easily realizable prototypes for the study of the complex systems which additionally tend to follow a definite analytic prescription, although with a certain number of underlying simplifications.

5.4 Characteristics of driven dust flow with fractional domain aspect ratio

For the curvilinear setup as considered in the present studies, the characteristics of dust dynamics is very different when the aspect ratio of the confining system is less than unity, ($L_z/L_r < 1$). We once again examine such cases for the vertically streaming (z -directed) driving ions field having a monotonic shear consistent with $I = 1$ over the radial scale L_r , which however interacts with the confined domain only over a relatively much shorter axial length $L_z (\ll L_r)$. In such confined domains, even with stronger coupling ξ the ions might transfer a relatively very less momentum to the confined dust in comparison with the case of large aspect ratio $L_z > L_r$ and dust mainly requires to flow along a longer radial dimension of the domain $L_r \gg L_z$. The major effect in this regime is increasing dominance of diffusive transport of vorticity along the direction of drive when dust is flowing along radial direction rather than the axial direction. The regime sees a strong effect and interaction between the boundary layers forming along the radial boundaries (top and bottom boundaries in Fig. 5.1). Among one of the characteristics observations in this regime, the nonlinear structural bifurcation takes place at very high critical Reynolds number Re^* or small critical kinematic viscosity of the dust μ^* depending on the aspect ratio of the confinement domain.

5.4.1 Dependence on changing domain aspect ratio

The series of structural changes for wide range of Re or kinematic viscosity is shown in Fig. 5.7, in term of streamlines patterns of dust circulation in the r - z plane of confined domain. Although the fundamental dependence of flow structures on the variation of Reynolds number is very similar to the case of aspect ratio $L_z/L_r = 2$ as discussed in section 5.2.1, there is considerable difference in critical parameter

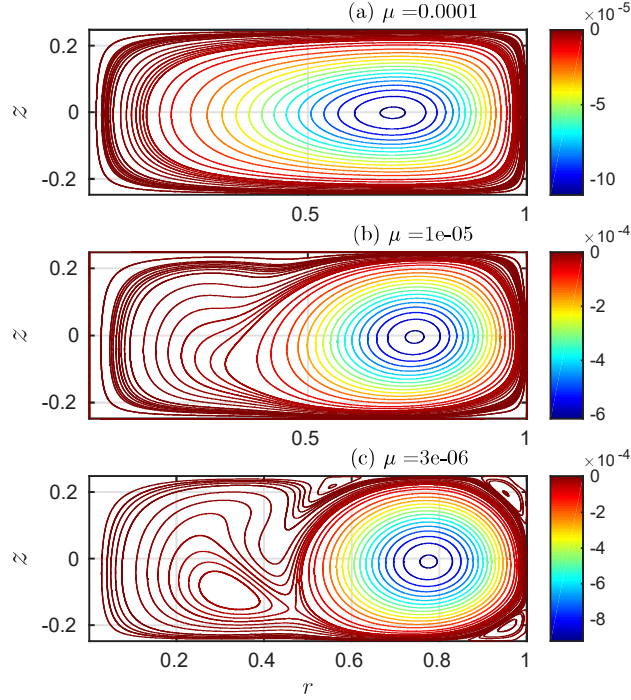


Figure 5.7: [Effect of varying viscosity at $L_z : L_r = 0.5$] Streamlines for the dust fluid flow in $r - z$ plane, correspond to varying (a) $\mu = 10^{-3}U_0L_r$, (b) $\mu = 10^{-5}U_0L_r$ and (c) $\mu = 3 \times 10^{-6}U_0L_r$ respectively having fixed other system parameters $\xi = 10^{-4}U_0/L_r$, $\nu = 10^{-3}U_0/L_r$.

values μ^* for the nonlinear structural bifurcation of the flow field in comparison to the large aspect ratio cases. In the case of viscous linear regime up to $\mu = 10^{-4}U_0L_r$ or $\text{Re} \approx 20$, the flow confirms with basic characteristics of the linear vortex flow as visible in Fig. 5.7(a). When the Re increases up to $30 - 100$, the flow patterns is no longer symmetric about $z = 0$ and the center of the vortex is shifted radially outward and develops an equilibrium structure with an almost uniform vorticity core, i.e., a region with $u \cdot \nabla \omega = 0$ and $\frac{\partial \omega}{\partial(r\psi)} = 0$, as shown in Fig. 5.7(b). Further rise in the Reynolds number up to $\text{Re} \approx 150$ by using $\mu = 3 \times 10^{-6}U_0L_r$, the shifting effect strengthens and a structural bifurcation take place through the critical μ^* ($\approx 5 \times 10^{-6}U_0L_r$), as visible from Fig. 5.7(c).

We now examine the effect of reduction in domain aspect ratio from 0.5 by

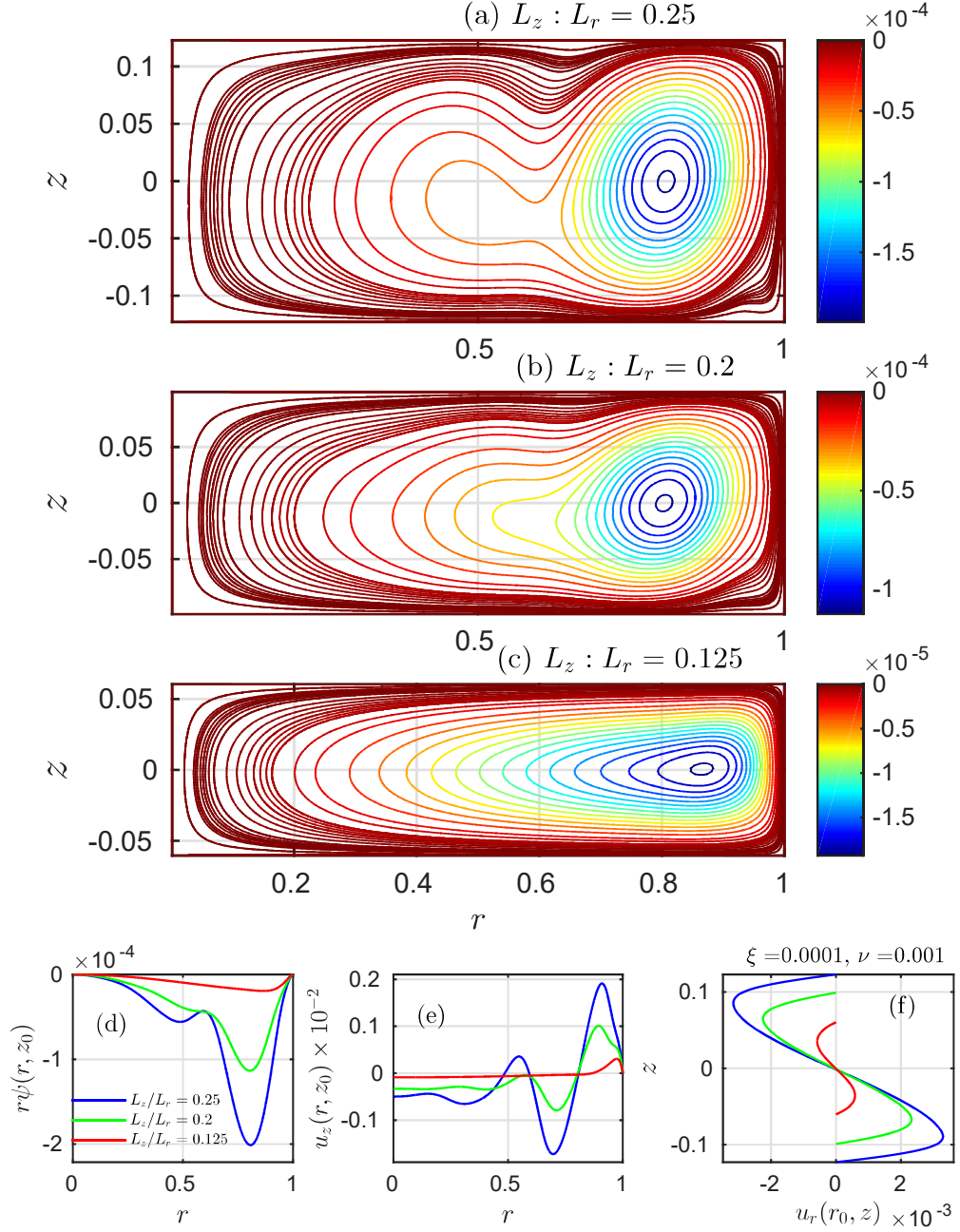


Figure 5.8: [Effect of varying system size $L_z : L_r$] Streamlines for the dust fluid flow in r - z plane, correspond to fixed $\mu = 3 \times 10^{-6} U_0 L_r$, $\xi = 10^{-4} U_0 / L_r$, $\nu = 10^{-3} U_0 / L_r$ and varying aspect ratio (a) $L_z : L_r = 0.25$, (b) $L_z : L_r = 0.2$ and (c) $L_z : L_r = 0.125$ respectively. The corresponding cross-section profile for (d) $r\psi(r, z_0)$, (e) $u_z(r, z_0)$ and (f) $u_r(r_0, z)$ passing through the center of primary vortex (r_0, z_0) .

fixing the kinematic viscosity to the value $\mu = 3 \times 10^{-6} U_0 L_r$ for which the nonlinear flow is already recovered with aspect ratio $L_z/L_r = 0.5$ in Fig. 5.7(c). When the aspect ratio is further reduced to values $L_z/L_r = 0.25, 0.20$ and 0.125 as shown in Fig. 5.8(a), (b) and (c), respectively, a transition back to almost a linear regime is recover for $L_z/L_r = 0.125$ because of dominance of diffusive transport along z , or in the direction orthogonal to the streamlines that are largely aligned to top and bottom boundaries.

This transition is presented in terms of and profiles of streamfunction plotted as function of r at $z = z_0$ and radial and axial profiles of the velocity components u_z and u_r , respectively, along the line segments passing through the center of the primary vortex as shown in Fig. 5.8 resulting from the variation in the values of the aspect ratio, $L_z/L_r=0.25$ (blue), 0.20 (green) and 0.125 (red). The transition is identified by a nonmonotonic streamfunction profile for $L_z/L_r=0.25$ and 0.2 becoming monotonic for $L_z/L_r= 0.125$ in Fig. 5.8(d). The velocity component u_z plotted in Fig. 5.8(e) similarly shows transition of the profile from a double bipolar structure to a single bipolar structure. The Fig. 5.8(f) shows a weakening flow velocity (reduction of Re) with the shrinking z dimension of the region with reducing aspect ratio.

5.5 Continued stability by structural bifurcation

Many complex systems operate with an underlying nonlinear mechanisms where the point in the parameter space at which the stability of one solution is lost is precisely the point where another solution bifurcates from it [84]. The structural bifurcation at μ^* highlighted in an electrostatically suspended dust vortex flow cell is one such phenomenon in a driven system that, apart from produc-

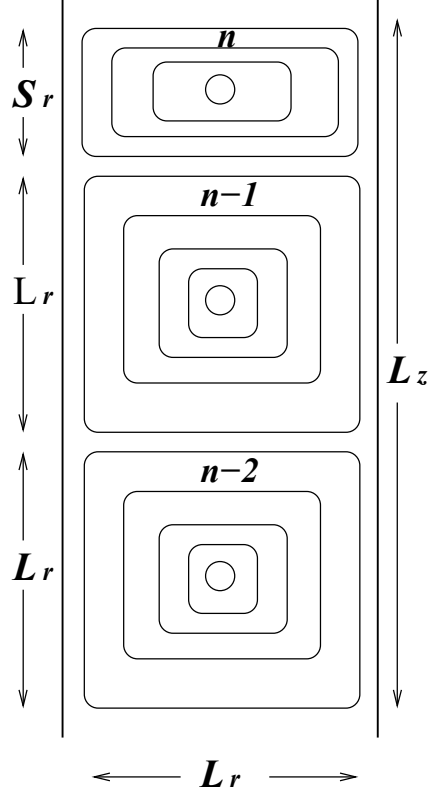


Figure 5.9: Schematic of an autonomous system with vortex nonlinearity controlled periodic replication and growth of vortex.

ing dynamically active and physically realizable 3D entities, generates physical near-replicas of parent entities which grow unstable by their changing physical attributes. From above analysis one notes that a dynamical system where the aspect ratio $L_z[V(r, z, t)]/L_r$ is a slowly varying function, via the confinement domain potential $V(r, z, t)$, of time, it is possible to recover a *frequency* of structural bifurcations and rate of generation of, say, the dusty plasma cells populating an axially elongating confinement domain.

In order to achieve a quantitative correlation with bifurcation based evolution of certain biophysical microsystems [28, 57] within the present approach, it might be of more interest to consider a rather complex but more realistic autonomous

state of the set-up. As described schematically in Fig. 5.9, this objective can formally be achieved by allowing dependence on time to enter only via a function of vortex area $A_c \sim L_r * S_z$ (where $S_z < L_r$ is the axial dimension of a growing vortex) of a growing of n^{th} vortex, given by a time integral over an area dependent (linear) rate α_0 of the change of axial dimension S_z ,

$$S_z(t) = \int_{t_{n-1}}^t \alpha_0 A_c[S_z(t')] dt' \quad (5.1)$$

with a results that a bifurcation must takes place periodically at,

$$L_z = (n - 1)L_r + S_z = nL_r. \quad (5.2)$$

where n is a positive integer. The model (5.1)-(5.2) provides a prescription for a partially developed cell which must grow until it undergoes a structural bifurcation, seeding another partially grown cell in the setup. A detailed characterization of the formal model (5.1)-(5.2) is however subject of a potential future work, involving computations of isothermally growing equilibria at prescribed rate α_0 , by treating S_z as a parameter.

5.6 Summary and conclusions

In this chapter, we presented the solutions of 2D nonlinear hydrodynamic formulation of confined, volumetrically driven dust cells with variation in the confinement domain's aspect ratio and its impact on the formation of vortices and their number. The case of bifurcating flow solutions with domain aspect ratio 2 is discussed first where vortex replication with nearly a dimension ratio 1:1 is recovered in comparison to $1 : (\sqrt{2} - 1)$ as recovered while analyzing flow in a square shaped domain in Chapter 4. Such a bifurcation predicted for a dusty plasma 2D flow cell is discussed in the light of its close resemblance to bifurcation transition in more

complex biophysical processes, in certain approaches, for example, to model the process of cell division or mitosis [28, 57].

In the context of pure laboratory dusty plasma experiments, the formulation predicted a class of nonlinear multiple-co-rotating vortex solutions which were experimentally recovered in almost simultaneously conducted laboratory dusty plasma experiments. The advanced numerical analysis done examined more diverse aspect ratio values, including those exceeding 2 and smaller than unity. It is discussed that in the cases with aspect ratio larger than 2 and more, a complete sequence of identical corotating vortices is recovered with number of identical vortices equal to the value of the aspect ratio. This result is discussed in the light of recovery of similar results in the dusty plasma experiments by M. Choudhary *et al.* [13] where a dust cloud with aspect ratio exceeding unity is indeed seen to develop a series of multiple corotating vortices with stronger drive, or larger Reynolds number. In the cases of domain aspect ratio smaller than unity, the vortices are seen to show a transition to a diffusion dominated single vortex linear state, even at much smaller kinematic viscosity values. The solutions correspond to no exact balance between nonlinear convection and diffusive transport terms in the model.

In the linear limit the diffusion across the streamlines is the dominant mechanism of the vorticity transport and the convection channel is secondary. The sharp gradients at the boundary that decay into the interior with a monotonic streamfunction (or vorticity) variation is therefore the characteristics of the linear solutions. In the nonlinear regime, on the other hand, a nonmonotonic spatial variation of the streamfunction characterizes development of localized regions where the vorticity transport along the streamline is stronger and therefore the vorticity brought, convectively, along the streamlines diffuses in both the directions about the carrier streamlines by means of the developed gradients, with drop in vorticity in both the directions, about them. The diffusive transport of the vorticity to core,

or to the exterior region, is still small and most of the vorticity flux is dissipated by the means of sink (neutrals) well within in the separated boundary layer itself. It is noted that while the transition in a domain of aspect ratio $L_z/L_r = 1$, as addressed in Chapter 4, produced a dynamically identical structure only with a scale ratio of $1 : (\sqrt{2} - 1)$ the structure scale ratio nearly 1:1 is recovered in the case of domain aspect ratio 2.

Critical topological modification of 2D vortex structures are noted where the variation in both r and z coordinates of vortex location show a monotonic shift with respect to variation in ξ and ν . However, with respect to the viscosity μ the shift in axial location of the vortex showed a complex non-monotonic behavior indicating that the system undergoes a critical change in dynamics at certain specific μ^* value and shows a relaxation like behavior at this value.

The close behavioral agreement between the dust dynamics described by our nonlinear formulation and the driven dust flow dynamics in a number of dusty plasma experiments, incorporating also the complex phenomenon (critical transition) of development of multiple corotating vortices from a single vortex, indicates that the laboratory dusty plasma show strong signatures of flow activity extending into the nonlinear regime of the fluid-like dust flow. The agreement further motivates the idea that dusty plasma experiments can be one of the easily realizable prototypes for the study of the complex systems which additionally tend to follow a definite analytic prescription, although with a larger number of underlying simplifications.

In the regime of fractional domain aspect ratio $L_z/L_r < 1$, the major effect is noted to be the increasing dominance of diffusive transport of vorticity along the direction of drive when dust is flowing along radial direction rather than the axial direction. This regime sees a strong effect and interaction between the boundary layers forming along the radially extended axial boundaries (or top and bottom boundaries). Among one of the characteristics observations in this regime, the

nonlinear structural bifurcation takes place at very high critical Reynolds number Re^* or small critical kinematic viscosity of the dust μ^* depending on the aspect ratio of the confinement domain.

Interesting vortex flow structure develop following a BLS transition in case the axial dimension of the confinement domain is longer than the separation between the radial boundaries determining the turning radius of the inertial flow. It is seen that a secondary vortex identical to the first forms in the region further upstream (of the driving ion flow) if the viscosity μ is reduced further. This results from the sharp separated boundary of the first vortex extending deeper in to the domain interior along the boundary of the primary vortex and beginning to act as a virtual domain boundary for the upper region, providing a vanishing flow velocity boundary condition identical to the original domain boundary.

As discussed in the final part of this chapter, we suggested an elementary prescription in order to correlate the present treatment to bifurcation based evolution of certain biophysical microsystems [28, 57]. A possible approach in this direction is to consider a rather complex but more realistic autonomous version of the present setup to formally replace non-self-consistent constraints in terms of prescribed confining potential and driving background plasma flow. Achieving a periodic frequency of bifurcation in autonomously growing vortex flow cells might be possible by introducing a dependence of the cell dimension via a time-integral relationship with the increasing area of an unsaturated vortex cell. Although an exact implementation and solution of the prescribed model remains subject of a future extension of the present computational analysis, the formally introduced model highlights a prescription for a partially developed cell which must grow until it undergoes a structural bifurcation, seeding another partially grown cell in the setup providing a nonlinearity controlled periodic sequence of physical structure generation.

6

Conclusion and future work

This thesis addressed the problem of flow structures in the spatially confined fluid-like phase of the dusty plasma, or the cloud of heavily charged dust particles electrostatically suspended in the plasma. Apart from systematically formulating and analyzing dust vortex flow dynamics recovered in many recent dusty plasma experiments, the studies presented in this thesis additionally focused on a special class of driven complex systems formally representable by the confined, steadily and volumetrically driven flow of the dust-fluid in the routine experiments and many natural circumstances. The central conclusion from this study highlights that, while microscopic characteristics of dusty plasma are well-known to resemble the crystalline [51–53] to viscoelastic fluid-like media [18, 54], the overall macroscopic dynamics of its fluid-like phase represents vortex activity in many volumetrically driven complex and biophysical fluids at much accessible scales.

The results obtained in the first half of the study, mainly done by numerical solutions in the linear limit of the developed 2D hydrodynamic formulation [24], successfully predicted and interpreted experimentally observed multiplicity of vortex in a series of observations by M. Kaur *et al.* [11, 24]. A more systematic and analytic approach to various advanced aspects of linear dust vortex dynamics also

outlines basic scaling of boundary effect at low to moderate Reynolds number [25]. The second half of the study similarly addressed a further advanced and complete nonlinear regime of the dust vortex flows. The nonlinear studies extended the limits of valuable analytic prescriptions of estimates and scaling recoverable from rather easily diagnosed flow dynamics of the dust, to high Reynolds number nonlinear regimes. The remarkable aspect of a continued stability of spatially extended vortex structures via a structural bifurcation is analyzed by means of finding and presenting nonlinear co-rotating multiple vortex solutions of the formulation, while also highlighting their recovery in a recent independent set of experiments where the recovered series of co-rotating structures additionally show an identical transition.

6.1 Main conclusions of the thesis

The following discussion further highlights various noticeable, observations, findings and conclusion from the entire length of the present study.

In **Chapter 1** it is shown that beginning from the conservation equations in 2D cylindrical setup a formulation can be developed for the dust streamfunction to yield the 2D dust flow field components. Reducible in to a set of multiple coupled first order partial differential equations, the model can be suitably solved for dust streamfunction, subject to appropriate boundary conditions that are transformed in terms of the dust streamfunction and its derivatives. Describing a number of possible sources, the solutions obtained here consider the vorticity supplied by a streaming sheared flow of ions, exerting a drag force on the dust, as a representative driving mechanism. Demonstrating the desired applicability to the dust vortex formation observed in a number of experimental conditions, this first characterization in terms of dust streamfunction solutions yielded the following characteristic observations and conclusions:

- The complete 2D profiles of the dust streamfunction $\psi(r, z)$ produce corresponding streamlines, represented, in the present curvilinear geometry, by the contours of the product $r\psi$ in the domain of the solutions.
- The no-slip boundary used at finite boundary section introduces friction between: the stationary dust medium it represents at the boundary, and the internal dust flow field, such that a strong shear develops allowing the velocity at the boundary to drop to small values at the corresponding boundary sections.
- This finite region adjacent to the resisting boundary where a strong viscous diffusive stress develops is seen extended up to certain characteristic width that can be identified as the boundary layer thickness.
- The net flux of confined dust across the vertical symmetry location $z = z_0$ remains zero since the dust flow, driven by the ion drag, undergoes only a circular flow in the volume as it is confined by the boundaries of the region satisfying the continuity equation.
- For the ion flow profile which is unidirectional, because of the confinement the dust flow is along the ion flow where ion flow is stronger and is capable of dragging the dust along. It however turns against the ion flow at the large r locations where the downward ion flow is rather weak, resulting in its steady circulation.
- At small values of drag coefficient ξ the radial profiles of dust flow at symmetry plane is almost uniform, it however tends to acquire the radial variation (or shear) almost identical to that of the driver fluid when a larger drag coefficient is present with appropriate modification near the external boundaries to satisfy imposed boundary conditions.

- For a small value of ion drag co-efficient ξ the dust circulation is negligible. However, the gradual strengthening of the dust circulation is observed with increasing ξ and fixed value of μ and ν .
- The weakening of strength of streamline patterns with increasing neutral collision frequency ν shows the characteristics change of dust circulations with varying neutral collision frequency. Dust dynamics can cease at extremely high neutral collision frequency.
- Increase in the dust viscosity coefficient μ although results only in a negligible reduction in the flow strength, it changes position of the center of circulation and increases the width, Δr_b , of the boundary layer developed on the resisting boundaries with increasing dust viscosity
- The dust flow at the boundary remains parallel to the boundary surface, however the flow velocity parallel to the boundary changes in magnitude depending on the nature of boundary.
- Since the velocity at the boundary with stationary dust must drop to zero (the no-slip boundary condition), a maximum value appears in the velocity profiles close to the boundary and the separation of this maximum from the boundary, Δr_b , can be a good measure of the boundary layer thickness in most cases of interest. As already noticed, this characteristic length scale increases with increasing viscosity μ .
- The dependence of Δr_b on ξ over a wide range of small values of ξ ($\sim 10^{-4}U_0/L_r$) is negligible. However, in the cases with large enough ξ values ($\sim 1 U_0/L_r$), the Δr_b value is sensitive to ξ and relatively smaller for higher ion drag coefficients ξ , and therefore smaller for larger dust flow velocities.
- The streamfunction solutions were presented in additional cases of nonmonotonic shear in the streaming plasma flow. When a narrow stream of plasma

$\Delta L = 0.1L_r$ is used as a driver localized at radial center $r = L_r/2$ of the domain, the dust streamfunction presents a solution that divides the domain in two separate zones, forming two counter-circulating dust flow vortices about the location of the stream.

- The flow characteristics recovered for the case of monotonic driver are found quite relevant to the vortices observed in the experimental setups where localized source of momentum is present, e.g, in the laser heated driven dust flow in a laboratory experiments [131]. This prediction of multiple vortices[24] also motivated the subsequent recovery of similar multiple counter-rotating vortices in laboratory dusty plasma experiment at IPR-India by M. Kaur *et al.* [12], up on introducing non-monotonic radial density profile of the background ions.
- Gradual development of a counter-rotating vortex was studied by introducing an increasing shift in the localized stream of ions. Transition from a single to multiple vortex regime is recovered where the upward moving dust flux balances the downward driven flux via two disjoint regions in the r - ϕ plane, producing two counter circulating vortex in the r - z plane.
- With respect to multiple vortex solutions it is generally noted that they must emerge when a complex source structure with multiple localized shear layers is used as external driver. For a fixed system size, however, the radial scale length of the vortices must reduce in such situation allowing the viscous dissipation or nonlinear effects of vorticity convection to become important at sufficiently larger k values, where a viscous cutoff, k_d , may exist and determine the smallest sustainable spatial scale of the observable vortex [132, 133].

In **Chapter 3**, the presented analytic treatment used the description of the vorticity of both the dust and of the driving plasma in terms of strength of eigenmodes

of a curvilinear bounded setup in the mode number space. The analytic solutions for the dust flow are obtained by treating the boundary value formulation as an eigenvalue problem, and using the linearly independent set of Bessel functions as eigenmodes that allows both driving and driven flows to follow valid flux conservation and have a multiple scale vorticity spectrum.

Following are among the main conclusions from this analytic description and its solutions, in terms of orthonormal set of radial basis functions.

- The expression of the driver flow field in the form of system eigenmodes (3.26) allows studying the dynamic equilibrium between the two flows with systematically increasing radial mode number of the driving field. This increase is observed to introduce smaller gradient scales in the dust flow and yield a corresponding limit on the smallness of the vortex flow scale, effectively because of the presence of finite dust viscosity.
- The variation of the dust velocity profile near the external no-slip boundary shows that the dust dynamics involved new scale introduced by the boundaries other than the driving external fields. The range of scales present in the system can be visualized from the corresponding intensity spectrum of the constituent modes of the driven dust flow vorticity profiles, $\text{Int}(m) = a_m^2$ (where a are the coefficients of the dust eigenmodes). This spectral dependence could be characterized in the analysis as a function of mode number m for increasing value of radial mode number of source vorticity I .
- In respect to the smallest scale analyzable by the largely macroscopic hydrodynamic formulation, very small length scales in the boundary layer, that are either comparable or finer than the average inter-dust-element separation, d , are obviously disallowed in the existing macroscopic model by the special conditions used for limiting the minimum scale of flow gradients in the present solution procedure. With finite possibility of finite stochastic at microscopic

(molecular) level, such finer scales are likely to be populated by modes with a power-law that in the some of the first-principle computer simulations have been predicted to follow a Kolmogorov-like turbulent scaling [135]. However, how these resulting finer-scales structures must interact with the boundary layer that forms at the similar scales, remains an interesting question for analytically determining the nature of the spectrum at such finer scales. Correctly addressing this region of spectrum under the hydrodynamic formulation would therefore require extending the present Navier-Stokes model to a generalized hydrodynamic model, by including the essential viscoelastic effects [116].

- The boundary layer thickness for a wide range of μ value is found to be almost independent of the coefficient of ion drag ξ such that profiles of $\Delta r_b(\mu)$ evaluated with various ξ values are seen to be overlapping. The shear scale length is, in turn, not sensitive to the ξ and the driver strength remains largely decoupled with the characteristics of the dust dynamics in the linear (low Re) flow regimes. This behavior shows the neutrality of the dust dynamics with respect to the driving mechanism and its strength.
- With the effect of increasing complexity in the driver setup resolved in the orthogonal eigenfunctions and characterized individually for increasing value of radial mode number, a scale independence of effects associated with boundary could be identified. Both the boundary layer thickness and the dust Reynolds number are shown to have definite exponents of variation with respect to the medium viscosity μ . While the effective boundary layer width is recovered to scale with $\mu^{1/3}$, the effective Reynolds number for the set-up is recovered to scale with $\mu^{-2/3}$. Both these orderings are seen to be obscured by an increasing spatial complexity of the driving mechanism. The degree of the impact of this complexity is estimated by systematically characterizing

the effect of individual driver flow modes in various cases with increasing value of the cylindrical mode number.

In **Chapter 4**, the obtained complete 2D nonlinear solutions are shown relevant to a large number of observations in dusty plasmas setups where a vigorous dust vortex flow dynamics is observed with flow velocities approaching the nonlinear limit. The nonlinear solutions are also in confirmation with a variety of characteristics observed in the experiments, for example observation by M. Kaur *et al.* [11], where localized dust vortex with relatively uniform core vorticity are seen surrounded by regions with strong variation, featuring very vigorous to relatively moderate or negligible dynamical activity.

Following are among the main conclusions from the analysis of the nonlinear structure of the problem and its 2D solutions.

- The emerging distinct nonlinear characteristics of the dust vortex flow are noted in numerical solutions where the circulation originally symmetric about z_0 in the low Reynolds number begins to turn asymmetric about z_0 in higher Reynolds number ($Re \gg 1$) regime. The flow structure in the nonlinear (high Re) regime is also found to be dependent on the aspect ratio (L_z/L_r) of the dust confinement domain.
- With decreasing μ (increasing Re) the strength of the nonlinear term $-\mathbf{u} \cdot \nabla \omega / \mu$ is seen to increase and this nonlinear convection of the vorticity, in turn, is found duly balanced by the viscous diffusion represented by the term $\nabla^2 \omega$, introducing the convective mode of the vorticity transport in the set up. For small μ value cases presented, the most interesting variation is present in boundary regions of the solution which is produced entirely by the balance $\nabla^2 \omega - \mathbf{u} \cdot \nabla \omega / \mu \sim 0$ as the contribution of other terms remains nearly negligible.
- The boundary that provides the strongest source of vorticity which in the

nonlinear regime can be dissipated orthogonal to streamlines much deeper in the domain volume at a relatively slower rate than linear case after being convected away in the interior along the streamlines.

- Similar to observations of a dust torus where poloidal dust flow is recoverable with considerably uniform vorticity, the driven primary vortex in the present solutions is formed with almost uniform vorticity in the core, surrounded by region of a strong variation of vorticity value and oscillatory nature of stream-function. The relationship between vorticity ω and product $r\psi$ is examined in the small and large Reynolds number regimes to recover independence of ω from $r\psi$ in the uniform vorticity core formed at large Reynolds number.
- In the above limit, the core vorticity follows the curvilinear form of an integral condition, originally indicated by Batchelor [27] for such flows, on the regions of closed streamlines where boundary conditions are no longer usable for determination of ω in high Reynolds number regime and its analytic value remains largely indeterminate.
- In presence of 2D heterogeneous boundary conditions applied to dust flow in a curvilinear coordinate system, the major nonlinear effects cause the boundary layer to separate from the domain boundary. This causes the vorticity generated from the interaction with the no-slip, or frictional, boundaries to be convected away with strong flows of the primary vortices. The separation allows dynamic isolation of the regions scaling with the dimensions of small scale features of the boundary (e.g., spatial modulations or the sharp corners) and development of secondary vortices in these regions.
- Advancing a somewhat recent identification of a strong nonuniformity of vorticity developed along the boundary discussed by M. Ghil *et al.* [137, 138] in the context of time dependent turbulent flows, the development of separated boundary layer is investigated as a structural bifurcation. It is

highlighted that in the confined dust vortex flows, the kinematic viscosity assumes role of the bifurcation parameter instead of time and the separation coincides with the bifurcation. The bifurcation is shown to occur when the vorticity profile approaches its first zero value along the boundary at the point where its minimum is located. This critical behavior and signatures of equivalent nonlinear vortex states in experiments indicates capacity of confined dusty plasma vortex structures to represent a class of systems that can self-stabilize by making a critical transition to a self similar state, for example, biophysical transition during cells undergoing mitosis [26].

- The nonlinear scaling of the boundary layer parameters with kinematic viscosity μ is obtained that shows a velocity independent linear estimate of kinematic viscosity to modify and additionally depend up on the flow velocity and its gradient scale length along the streamlines as $\mu = \Delta r_b^2 \frac{u}{L_{\parallel}}$. Similarly, existence of a critical values μ^* demarcating transition to nonlinear regime is identified. These two factors allow estimation of viscosity of charged fluids using appropriate scaling by identifying a structural change in flow patterns in experiments.

The nonlinear dust vortex dynamics thus offers quantitative insight and analytic framework to a number of natural systems that dusty plasmas emulate.

In **Chapter 5**, we presented the solutions of 2D nonlinear hydrodynamic formulation of confined, volumetrically driven dust cells with variation in the confinement domain's aspect ratio and its impact on the formation of vortices and their number. The structural bifurcation originally identified and predicted Chapter 4 for a dusty plasma 2D flow cell is discussed in the light of its close resemblance to bifurcation transition in more complex biophysical processes, in certain approaches, for example, to model the process of cell division or mitosis [28, 57].

Following are among the main conclusions from the studies presented in this part of the studies.

- In the context of pure laboratory dusty plasma experiments, the formulation predicted a class of nonlinear multiple-co-rotating vortex solutions which were experimentally recovered in almost simultaneously conducted laboratory dusty plasma experiments. It is shown that in the cases with aspect ratio larger than 2 and more, a complete sequence of identical corotating vortices is recovered with number of identical vortices equal to the value of the aspect ratio. This result is discussed in the light of recovery of similar results in the dusty plasma experiments by M. Choudhary *et al.* [13] where a dust cloud with aspect ratio exceeding unity is indeed seen to develop a series of multiple corotating vortices with stronger drive, or larger Reynolds number. In the cases of domain aspect ratio smaller than unity, the vortices are seen to show a transition to a diffusion dominated single vortex linear state, even at much smaller kinematic viscosity values. The solutions correspond to no exact balance between nonlinear convection and diffusive transport terms in the model.
- In the nonlinear regime of solution analyzed, a nonmonotonic spatial variation of the streamfunction characterizes development of localized regions where the vorticity transport along the streamline is stronger and therefore the vorticity brought, convectively, along the streamlines diffuses in both the directions about the carrier streamlines by means of the developed gradients, with drop in vorticity in both the directions, about them. The diffusive transport of the vorticity to core, or to the exterior region, is still small and most of the vorticity flux is dissipated by the means of sink (neutrals) well within in the separated boundary layer itself. It is noted that while the transition in a domain of aspect ratio $L_z/L_r = 1$, as addressed in Chapter 4, produced a dynamically identical structure only with a scale ratio of $1 : (\sqrt{2} - 1)$ the structure scale ratio nearly 1:1 is recovered in the case of domain aspect ratio 2.

- Critical topological modification of 2D vortex structures are noted where the variation in both r and z coordinates of vortex location show a monotonic shift with respect to variation in ξ and ν . However, with respect to the viscosity μ the shift in axial location of the vortex showed a complex non-monotonic behavior indicating that the system undergoes a critical change in dynamics at certain specific μ^* value and shows a relaxation like behavior at this value.
- The close behavioral agreement between the dust dynamics described by our nonlinear formulation and the driven dust flow dynamics in a number of dusty plasma experiments, incorporating also the complex phenomenon (critical transition) of development of multiple corotating vortices from a single vortex, indicates that the laboratory dusty plasma show strong signatures of flow activity extending into the nonlinear regime of the fluid-like dust flow. The agreement further motivates the idea that dusty plasma experiments can be one of the easily realizable prototypes for the study of the complex systems which additionally tend to follow a definite analytic prescription, although with a larger number of underlying simplifications.
- In the regime of fractional domain aspect ratio $L_z/L_r < 1$, the major effect is noted to be the increasing dominance of diffusive transport of vorticity along the direction of drive when dust is flowing along radial direction rather than the axial direction. This regime sees a strong effect and interaction between the boundary layers forming along the radially extended axial boundaries (or top and bottom boundaries). Among one of the characteristics observations in this regime, the nonlinear structural bifurcation takes place at very high critical Reynolds number Re^* or small critical kinematic viscosity of the dust μ^* depending on the aspect ratio of the confinement domain.
- Interesting vortex flow structure develop following a BLS transition in case

the axial dimension of the confinement domain is longer than the separation between the radial boundaries determining the turning radius of the inertial flow. It is seen that a secondary vortex identical to the first forms in the region further upstream (of the driving ion flow) if the viscosity μ is reduced further. This results from the sharp separated boundary of the first vortex extending deeper in to the domain interior along the boundary of the primary vortex and beginning to act as a virtual domain boundary for the upper region, providing a vanishing flow velocity boundary condition identical to the original domain boundary.

- The dynamical structure of the bifurcation suggests a quantitative correlation with bifurcation based evolution of certain self-replicating biophysical microsystems can be achieved by defining an autonomous evolution of the domain boundaries. This is indicated to be possible by allowing a slow dependence on time to enter only via a function of vortex area of a growing n^{th} vortex, given by a time integral over an area dependent (linear) rate of the change of axial dimension S_z .

6.2 Future work

Some of the immediately visible goals set by the existing conclusions of the present studies are enlisted as below.

1. As the next step of validation of the results by observation in the existing experiment, where predicted multiplicity (in linear regime) and sequence of co-rotating vortices (in nonlinear regime) were both successfully observed, a quantitative validation of the linear and nonlinear boundary layer scalings prescribed by the respective formulations is proposed as a useful future study in collaboration with dusty plasma experiments. Performing advanced PIV diagnostics of dust circulation for obtaining flow velocity and its gradients can

perhaps additionally identify the transition caused by structural bifurcation and validate respective scalings above and below such transition. Prediction of the kinematic viscosity from the experiments might allow exploring the microscopic/molecular level structure of the strongly charged dust medium.

2. A more self-consistent treatment of the steady-state dust vortex flows needs to incorporate an equivalent flow model for the driver of the vortex dynamics which presently has a prescribed form. Introducing a fluid equation based model for the sheared flow of ions, presently used as a passive driver of the dust dynamics, is proposed as the first possibility for a more self consistent study.
3. For extending the applicability of the result to strongly coupled regime of the complex dust-fluid, an advanced version of the formulation, based on a generalized fluid model might be implemented. The corresponding results should allow exploring a strong-coupling version of the boundary layer scalings in such conditions applicable to the strongly coupled media and their interaction along the interfaces.
4. The topology of the confined dust clouds in the present formulation is assumed to be simple rectangular where dust is confined by a uniform potential well. However, the more realistic topologies relevant to real natural systems or experimental setups are non-uniform irregular structures. A possible immediate extension is to end this geometrical restriction within present set of assumptions for the model to explore effects of a wider range of boundary structures on the existing solutions.
5. We have observed that steady equilibrium flow structure is rather sensitive to change in the parameter μ about its critical value in the nonlinear regime. The structural transition about this critical parameter and their stability in

this parameter region are yet to be understood more systematically. This constitutes a potential future study.

6. The steady-state dynamical equilibria recovered in terms of solutions essentially correspond to thermodynamic non-equilibrium states of the systems. Moreover, they are unique, irrespective of the initial conditions in terms of the relevant microscopic variables. The working principle for such driven-dissipative systems to converge to a unique solution must involve an associated statistical approach when a stochasticity or noise is involved. A critical level of this noise must affect the ability of the system to converge to the existing solutions that formally correspond to a thermodynamic limit. An associated stochastic treatment of our approach presents an interesting possibility in terms of a future study.

Finally, as discussed in the final part of Chapter 5, from the view point of a stronger applicability to driven complex systems, we suggested an elementary prescription in order to correlate the present treatment to bifurcation based evolution of certain biophysical microsystems [28, 57]. A possible approach in this direction is to consider a rather complex but more realistic autonomous version of the present setup to formally replace non-self-consistent constraints in terms of prescribed confining potential and driving background plasma flow. Achieving a periodic frequency of bifurcation in autonomously growing vortex flow cells might be possible by introducing a dependence on the cell dimension via a time-integral relationship with the increasing area of an unsaturated vortex cell. An exact implementation and solution of the prescribed model remains subject of a useful future extension of the present computational analysis. The formally introduced model highlights a prescription for a partially developed dust cell which must grow until it undergoes a structural bifurcation, seeding another partially grown cell in the setup providing a nonlinearity controlled periodic sequence of physical structure generation.



Introduction to relevant fluid and flow properties

A fluid is a state of matter which deforms continuously under the influence of shear stress, no matter how small. For example, liquids and gases. The applied shear stress is proportional to its strain rate giving shear stress $\tau_{yx} = \eta(\partial u_x / \partial y + \partial u_y / \partial x)$. Here, τ_{yx} is stress along x-direction and on surface perpendicular to y-direction, ($\partial u_x / \partial y$ is shear rate along y-direction) and η is proportional constant called viscosity. Those fluids having constant η are known as Newtonian fluids and those fluids with varying η are known as Non-Newtonian fluids. However, in case of solid state, the applied shear stress proportional to its strain (not the strain rate) giving $\sigma_{yx} = \epsilon(\partial x / \partial y + \partial y / \partial x) / 2$. Here ϵ is the elasticity or rigidity modulus of the system. The deformation stop at a critical fixed strain angle and return to its initial state when we remove the stress applied on it. In fluid dynamics the identity of individual particle is neglected and only the motion of fluid elements is considered assuming statical averaging in a fluid elements is already perform. This approximation is called **continuum hypothesis** and valid for those fluid having very small Knudsen number $\text{Kn} = (\lambda / L_r)$. The Knudsen number (Kn) is a

dimensionless number defined as the ratio of the molecular mean free path length λ to a representative physical length scale L_r . When the Knudsen number is small, say of the order of $\text{Kn} \leq 10^{-2}$, the fluid can be treated as a continuous medium and the associated macroscopic variables: velocity, density, pressure, and temperature etc can be treated as continuous fields (vector or scalar) in the flow system.

Now the dynamics of fluid system can be analyzed by tracking the motion of each fluid elements (small region of control mass) instead of following every individual particles. Every fluid elements are marked and followed in the flow domain. The independent variables are initial position of fluid particle and varying time. Most of the physical laws like Newton law of motion are applicable to see the dynamics of these fluid elements. This approach of flow analysis is called **Lagrangian approach**, but it has been very challenging to follow each of these fluid elements if it follows complicated trajectories. However, in case of experimental analysis of fluid flow observer is fixed at certain position and fluid allows to flow through various observation points. Considering various fixed point (small region of control volume) in space, and observed fluid flows passing these points can reflect the same characteristics of the flows. This approach is known as **Eulerian approach**, and very relevant to many experimental flow analysis. The independent variables are space coordinates and time. However, in general both the Lagrangian and Eulerian specification of the flow field can be applied in any observer's frame of reference, and in any coordinate system used within the chosen frame of reference. These two concepts are relate to each other by a relation called **Material Derivative** shown in equation (A.1).

$$\left(\frac{D\phi}{Dt}\right)_{Lagrangian} = \left(\frac{\partial\phi}{\partial t}\right)_{Euler} + \mathbf{u} \cdot \nabla\phi \quad (\text{A.1})$$

In the following thesis work, the Eulerian approach which is also very relevant to experimental observations is used throughout the flow analysis.

A.1 Equations for fluid dynamics

The whole theory of fluid dynamics are base on some fundamental laws of nature such as conservation of mass (continuum flow), conservation of momentum (Newton 2nd law of motion) and conservation of energy (1st law of thermodynamics) of an isolated system. Following these fundamental laws at a control volume of the fluid (Eulerian approach), one can derive governing differential equations that represent the whole dynamics of a fluid flow system. The set of equations are comes out as follows,

$$\frac{\partial \rho}{\partial t} + \nabla \cdot (\rho \mathbf{u}) = 0, \quad (\text{A.2})$$

$$\frac{\partial \mathbf{u}}{\partial t} + \mathbf{u} \cdot \nabla \mathbf{u} = g - \frac{\nabla p}{\rho} + \mu \nabla^2 \mathbf{u} - \frac{2}{3} \mu (\nabla \cdot (\nabla \cdot \mathbf{u}) \mathbf{I}) + \mathbf{f}_{frictions}, \quad (\text{A.3})$$

$$\rho \left(\frac{\partial \mathbf{e}}{\partial t} + \mathbf{u} \cdot \nabla \mathbf{e} \right) = k \nabla^2 T + \Phi - p \nabla \cdot \mathbf{u}. \quad (\text{A.4})$$

These set of differential equations which represent the whole fluid dynamics satisfying the above fundamental laws are known as the Navier-Stokes equations. In the above set of equations, it has more unknowns variables then the numbers of equations. So, it require more equations for closure the set of couple differential equations.

Generally density(ρ) can relate to pressure and temperature, and this relation is given by a special equation called equation of state $p = c\rho^\gamma$, $\gamma = c_p/c_v$. The simplest form is $p = \rho RT$ (ideal gas equation). And $dh = c_p dT$ or $de = c_v dT$ allows to express enthalpy or internal energy in terms of temperature. Now, overall we have 6 scalars unknowns variables (density, pressure, 3-velocity components and temperature T) and 6 scalar equations (conservation of mass, 3-components of conservation of momentum, conservation of energy and equation of state). All three conservation equations (conservation of mass, momentum and energy) and equation of state are coupled and closure, now all the equation can to be solved

simultaneously using proper boundaries or initial conditions base on the nature of flow system.

A.2 Viscoelastic fluids

For strongly couple complex fluids such as biological systems, dusty plasma having coupling parameter in the range ($100 \leq \Gamma \leq \Gamma_c$), the system behave like viscous-elastic fluid. For such flows, both the viscous and elastic effect are effectively involve in the flow characteristics. Thus, the momentum conservation equation is modified into more generalized manner including the elastic effect as a new time scale introduced by the elasticity called memory effect [139]. The generalized equation can be written as follows,

$$\left[1 + \tau_m \left(\frac{\partial}{\partial t} + \mathbf{u} \cdot \nabla\right)\right] \left[\left(\frac{\partial}{\partial t} + \mathbf{u} \cdot \nabla\right) \mathbf{u} + \frac{\nabla p}{\rho} - \nabla V\right] = \eta \nabla^2 \mathbf{u} + \left(\frac{\mu}{3} + \zeta\right) \nabla(\nabla \cdot \mathbf{u}) \quad (\text{A.5})$$

Here, ρ , u , p , V are dust density, velocity, pressure and potential of the dust flow field respectively. And τ_m is the newly introduced memory relaxation time scale due to elastic effect, μ is kinematic viscosity, ζ is bulk viscosity of the dusty plasma. In the limit $\tau_m \frac{\partial}{\partial t} < 1$, the equation is reduce to standard Navier-Stokes momentum equation shown in Eqn.(A.3). On the other limit $\tau_m \frac{\partial}{\partial t} > 1$, the equation is more complex with multiple time scales involve in the system.

A.3 Incompressible hydrodynamics

Incompressibility is an approximation which is well satisfied by slowly moving flows which are subsonic in nature, i.e., Mac number ($u/c_s \ll 1$). Here c_s is the acoustic velocity in the fluid medium. In other words, a flow is assumed to be incompressible if relative changes in density $\Delta\rho/\rho$ due to change in Δp is negligible.

This approximation can be represent by a general equation as follow,

$$\frac{\partial^2}{\partial t^2}(\nabla \cdot \mathbf{u}) = c_s^2 \nabla^2(\nabla \cdot \mathbf{u}), \quad c_s = \sqrt{\gamma p / \rho}. \quad (\text{A.6})$$

This equation demonstrates that any divergence in the flow field is part of sound wave, and will propagate away at the acoustic speed(c_s). Thus for flow without any sound waves ($u \ll c_s$),

$$\nabla \cdot \mathbf{u} = 0. \quad (\text{A.7})$$

Thus, the smaller is the Mach number ($M \approx u/c_s$), the better will be the approximation of incompressible flow nature. For incompressible flows, the density of a fluid elements has a known value (almost constant), i.e., it is no longer an unknown parameter. Therefor, there is no equation of state for incompressible flows that relate pressure in term of density. Considering this simplification together with isothermal viscosity (Newtonian fluid), then the set of equation Navier-Stokes equations becomes,

$$\nabla \cdot \mathbf{u} = 0, \quad (\text{A.8})$$

$$\frac{\partial \mathbf{u}}{\partial t} + \mathbf{u} \cdot \nabla \mathbf{u} = g - \frac{\nabla p}{\rho} + \mu \nabla^2 \mathbf{u} + \mathbf{f}_{frictions}, \quad (\text{A.9})$$

$$\rho c_v \left(\frac{\partial T}{\partial t} + \mathbf{u} \cdot \nabla T \right) = k \nabla^2 T + \Phi. \quad (\text{A.10})$$

Now for the incompressible flows, the continuity and momentum equation are decouple from the energy equation. This is the reason why the energy equation is not important in the incompressible ($u/c_s \ll 1$) flow system. Therefore we can first solve continuity and momentum equations to find the unknown velocity and pressure distribution without knowing the temperature. After finding the velocity and pressure fields, energy equation can be used to find the temperature distribution of the flow system. Heat transfer and therefore the energy equation is not always a primary concern in an incompressible flow. Thus, energy equation (and therefore

temperature) can be dropped for isothermal (constant temperature) incompressible flows and only the mass and momentum equations are solved to obtain the velocity and pressure fields. Therefore, incompressibility is an appropriate limit for simplifying almost all the modelling and characterization of fluid dynamics.

A.4 Vortex structures and vorticity

A **vortex** is a kind of flow fields in which the flow is swirling around an axis, which may be straight or curved line. Vortex motion occurs in a wide range of physical phenomena in nature. For examples, Smoke rings, whirlpools, tornadoes, hurricanes, the Great Red Spot of Jupiter and Saturn's hexagon formed at its north pole etc. It is important to distinguish between circular motions of fluid in a close orbit and the spinning of the fluid elements. For visualization, the spinning could be observed by placing a tiny object on the concern flow element, and observe how it move freely in the flow field. Therefore, vorticity($\vec{\omega}$) as well as concept of circulation (Γ_c) are used to characterize spinning of flows field. Here,

$$\Gamma_c = \oint_C \mathbf{u} \cdot d\mathbf{l} \simeq \iint_S (\nabla \times \mathbf{u}) \cdot d\mathbf{S} \simeq \iint_S \vec{\omega} \cdot d\mathbf{S}, \quad \vec{\omega} = (\nabla \times \mathbf{u}) \quad (\text{A.11})$$

Circulation is the line integral around a closed curve of the velocity field. And **vorticity** is defined as local rotation or spin of a fluid element about an axis through the element, i.e the circulation per unit area of the flow. Vortices are of two main kinds. If the vorticity or circulation is zero along any close loop away from the swirling axis, then such flow is called **irrotational vortices** or free vortices ($\omega = \mathbf{0}$). Circulation is always non-zero if inclose the center of vortex system. On the other, those flow having non-zero vorticity or circulation away from the swirling axis, are known as **rotation vortices** ($\omega \neq \mathbf{0}$). Thus, a flow with circular streamlines may have zero vorticity, and a flow with straight streamlines may have non-zero vorticity.

A.5 Potential flow and streamfunction.

The velocity field of a continuum flow, as discussed above, can have different characteristics in a flow system. Then base on Helmholtz's theorem also known as fundamental theorem of vector calculus, the velocity field can be decomposed into the sum of irrotational part ($\nabla \times \mathbf{u} = 0$), and a solenoidal part ($\nabla \cdot \mathbf{u} = 0$)[23]. Thus,

$$\mathbf{u} = \nabla\phi + \nabla \times \Psi. \quad (\text{A.12})$$

This is very general expression of a vector field in terms of some potential which are not unique and allows gauge transformations. Now for irrotational flow ($\nabla \times \mathbf{u} = 0$), this implies existence of a scalar potential ϕ such that $\mathbf{u} = \nabla\phi$. Considering a purely two-dimensional flow fields, in which velocity takes the form

$$\mathbf{u}(x, y, t) = \hat{\mathbf{i}} u_x(x, y, t) + \hat{\mathbf{j}} u_y(x, y, t). \quad (\text{A.13})$$

Again assuming the flow is irrotational, the velocity components in terms of scalar potential ϕ can be written as follows,

$$u_x(x, y, t) = \frac{\partial\phi}{\partial x} \quad \text{and} \quad u_y(x, y, t) = \frac{\partial\phi}{\partial y}. \quad (\text{A.14})$$

Moreover, if this potential flow is incompressible in nature ($\nabla \cdot \mathbf{u} = 0$), then the new condition for irrotational and incompressible flows becomes,

$$\begin{aligned} \nabla \cdot \mathbf{u} &= 0, \\ \nabla \cdot (\nabla\phi) &= 0, \\ \nabla^2\phi &= 0. \end{aligned} \quad (\text{A.15})$$

This equation must be supplemented by the boundary conditions of the flow domain.

APPENDIX A. INTRODUCTION TO RELEVANT FLUID AND FLOW PROPERTIES

Now, for a general incompressible flows $\nabla \cdot \mathbf{u} = 0$, this implies the existence of a vector potential $\mathbf{\Psi}$, such that $\mathbf{u} = \nabla \times \mathbf{\Psi}$. Then vorticity is given by,

$$\tilde{\omega} = \nabla \times \mathbf{u} \approx \nabla \times (\nabla \times \mathbf{\Psi}) \approx \nabla(\nabla \cdot \mathbf{\Psi}) - \nabla^2 \mathbf{\Psi} \quad (\text{A.16})$$

The streamfunction vector potential is quite complicated in real 3D space, however it is very useful specially for two dimension or axis symmetric three dimensional system where, $\mathbf{\Psi} \rightarrow (0, 0, \psi)$ and $\hat{\omega} \rightarrow (0, 0, \omega)$, giving $(\nabla \cdot \mathbf{\Psi}) = 0$ and $\mathbf{u} = (\nabla \psi \times \hat{\mathbf{z}}) \sim (\nabla \times \psi \hat{\mathbf{z}})$. Then the velocity components for incompressible flow in 2D flow can be express in terms of streamfunction as follows,

$$u_x(x, y, t) = \frac{\partial \psi}{\partial y} \quad \text{and} \quad u_y(x, y, t) = -\frac{\partial \psi}{\partial x}. \quad (\text{A.17})$$

Then the vorticity for the two dimensional incompressible flows become,

$$\omega = -\nabla^2 \psi \quad (\text{A.18})$$

Now, for irrotational incompressible flow, the equation is reduce to $\nabla^2 \psi = 0$, satisfying Laplacian as the case of velocity potential ϕ in Eqn.(A.15). The velocity potential and streamfunction give us the two alternatives representations of velocity as shown in Eqn.(A.14) and Eqn.(A.17). By comparing these expressions, we found that ϕ and ψ satisfy the following conditions.

$$u_x = \frac{\partial \phi}{\partial x} = \frac{\partial \psi}{\partial y} \quad \text{and} \quad u_y = \frac{\partial \phi}{\partial y} = -\frac{\partial \psi}{\partial x}. \quad (\text{A.19})$$

These relations are recognized as the Cauchy-Riemann conditions for a complex expression $w(z) = \phi(x, y) + i\psi(x, y)$ to be analytical function of the complex argument $z = x + iy$. Thus we can express a complex potential,

$$w(z) = \phi(x, y) + i\psi(x, y) \quad (\text{A.20})$$

which is a homomorphic function of complex argument $z = x + iy$, in a complex plain and it has a well defined derivative $(\partial w / \partial z)$, called the complex velocity which is independent of the direction of differentiation in the complex plane.

Equations in term of scalar potential are easier to solve than the nonlinear Euler or Navier-Stokes equations in vector field. Once we have solved for the potential ϕ , the characteristics of the flow system can be visualized in term of the velocity components recovered from Eqn.(A.17), and the pressure found using Bernoulli's Theorem. Moreover stream function can express many characteristics of a flow systems in term of streamlines patterns as well as mass flow rate of the system.

Streamlines :- Streamlines are lines that are instantaneously tangent to the velocity vector of the flow. Streamlines pattern shows the direction in which fluid element will travel at any instant point of time. Mathematically,

$$0 = (\mathbf{u} \times \hat{dl}) \sim (u_x dy - u_y dx) \sim \left(\frac{\partial \psi}{\partial y} dy + \frac{\partial \psi}{\partial x} dx \right) \sim d\psi \quad (\text{A.21})$$

Contours of stream function i.e lines of equal ψ values gives the streamlines in a two dimensional flows. Different streamlines in a flow, at a same instant time do not intersect, because a fluid particle cannot have two different velocities at the same location in a flow field.

Mass flow rate :- The rate of fluid flow passing through an area element per unit time is an important quantity in flow system. It can be express as ,

$$\dot{m}_{flux} = \int_a^b \rho \mathbf{u} \cdot \hat{n} dS = \int_a^b \rho (u_x dy + u_y dx) \simeq \int_a^b d\psi \simeq \psi_b - \psi_a. \quad (\text{A.22})$$

Hence, the mass flow rate or mass flux between any two streamlines is given by the different of their stream function values. Closer is the streamlines, smaller is the flow rate and vice versa.

B

Overview of complex (dusty) plasmas

Plasma is one of the four fundamental states of matter, the others being solid, liquid, and gas. Plasmas are considered as the forth state of matter with three different components, i.e, electrons, ions and neutrals. Literally plasmas are defined as partially or fully ionized medium which are electrically quasineutral and shows collective behaviors [60]. The plasma state of matter is generally characterized by certain parameters such as temperature T_j , that represent the equilibrium distribution of j -species with average kinetic energy $E_{ev} \sim K_B T_j$, and the number density n_j , the mass m_j associated with the different species in the system. However, instead of directly talking about these many parameters, someone can express certain length and time scales which depend on these parameters and represent the characteristic features of the plasma. Generally length scale such as Debye length $\lambda_{Dj} = (T_j/4\pi n_j e^2)^{1/2}$, time scale with respect to plasma frequency $\omega_j = (n_j e^2/m_j \epsilon_0)^{1/2}$, and acoustic speed $c_s = \lambda_{Dj} \omega_j$ are very useful scales of a plasma system. Here e is electronic charge, λ_{Dj} is Debye length which is measure of distance over which the influence of the electric field of an individual charged particle j -species is felt by other charged particles inside the plasma. Plasma

frequency indicates that the internal space charge potential of j -species oscillates with a characteristic frequency ω_j by virtue of its inertia. The other important characteristic frequencies are associated with the collisions of the plasma particles (electrons and ions) with stationary neutrals. The plasma oscillations will persist only when the collision frequency are smaller than plasma frequency, i.e. $\nu_{jn} < \omega_j$. Plasmas are of various kind base on the properties of constituent species electrons, ions and neutrals. When $T_e \sim T_i$ and $n_e \sim n_i$, those plasmas are classified as hot plasma (or thermal plasma) where the collisional rate between $e - e$, $ion - ion$ and $e - ion$ species are equal and maintain a common thermal equilibrium with $\lambda_{De} \sim \lambda_{Di}$. While for $T_e \gg T_i$ those plasmas are called cold plasma (or non-thermal plasma) where the collision rate among ions or among electrons ($e - e$, $ion - ion$) themselves is larger than the rate of collisions between an ion and an electron ($e - ion$) [60, 61].

Complex(dusty) plasmas are consider as the forth state of matter with four different components, which in addition to the usual plasma components i.e., electrons, ions and neutrals, it contain micron sized particles, also called grain or dust. The dust grains are intrinsically neutral, relatively heavy and large sized particles mostly dielectric or conducting in nature and so it introduce many peculiar phenomena in the system. Once the grains are introduced in conventional electron-ion plasma, it faces heavy flux of (highly mobile) electrons relative to ions over its surface and collect more electrons and gets negatively charged at most of the time [22]. In some occasions, when the dust particles undergo emission of electrons because of radiation sources like ultraviolet lights, secondary electron emission, thermionic emission, field emission etc., and the dust grains may also be found to be positively charged [62]. Thus, one has the possibility of charging dust grains both negatively and positively.

These particles acquire large electric charges and masses, and exhibit many collective behaviors through long-range coulomb interactions. The charges on dust species can be fluctuated because the electrons/ions may leave the surface of dust

grains in course of collision with other ions or dust grains specially in streaming plasma, or because of thermal effects, or other radiative processes in the plasma [63]. A dusty plasma is significantly different from a multi-ions plasma, because the presence of massive charged dust grains produces new collective phenomena on a different time and length scales. The inclusion of charged dust species makes the plasma becomes even richer with several additional new modes arising solely due to introduction of new scales or due to additional instabilities. Thus this extra component of macro-particles increases the complexity of the system even further. The dynamics of dusty plasma is very similar with many complex fluids that has multiple phases of particles that introduce multiple length and time scales in the system. This is why dusty plasma is sometime called as “complex plasma” [22, 64].

The new equilibrium quasi-neutrality condition for the ionized state in the presence of negatively charged dust grains is given by

$$Z_i n_i = n_e + Z_d n_d, \quad (\text{B.1})$$

where Z_i is the number of ion charge state, n_s is the unperturbed number density of the plasma species s (s equals i for ions, e for electrons and d for dust grains), and Z_d is the number of charges on the dust grain surface. When most of the electrons from the main plasma are attached onto the dust grain, i.e $Z_i n_i \approx Z_d n_d$, the dusty plasma may be regarded approximately as a two-component plasma composed of negatively charged dust grains and the ions, the latter shield the negative dust grains [140]. Such a situation is common in the Saturn rings as well as in low-temperature laboratory discharges. However in positive charged grain as in thermal or radiated dusty plasma, the shielding take place by electrons and hence at equilibrium we have $Z_d n_d \sim n_e$ since the ion number is completely depleted in the system.

For dusty plasma, the length scale and time scale which represent the characteristic features of the system are base on Debye length λ_{Dd} , plasma frequency $\omega_d = (n_d e^2 / m_d \epsilon_0)^{1/2}$, then corresponding acoustic speed supported in the system

is $c_{sd} = \lambda_{Dd}\omega_d$ etc. The dusty plasma Debye length λ_{Dd} is given by

$$\frac{1}{\lambda_{Dd}^2} = \frac{1}{\lambda_{De}^2} + \frac{1}{\lambda_{Di}^2}, \quad (\text{B.2})$$

where $\lambda_{De} = (T_e/4\pi n_e e^2)^{1/2}$ and $\lambda_{Di} = (T_i/4\pi n_i e^2)^{1/2}$ are the electron and ion Debye length respectively. T_e and T_i are the electron and ion temperature in the energy unit, n_e and n_i etc are the unperturbed electron and ion number density, and e is the magnitude of the electron charge. The other scales such as, dust radius (r_d), inter-dust separation (a_d) also have significant role for classification of dusty system into various groups. If $r_d \ll \lambda_D < a_d$, the dust grains get shielded by opposite charge species and do not participate in collective dynamics of dust. Such types of dust system are known as “Dust in plasma”, here one can treat the dust from a particle dynamics point of view [22, 141]. However for $r_d \ll \lambda_D \geq a_d$, the effect of neighboring dust particles are significant and interactions is very significant. When these additional species behave in a collective fashion the dust system is known as a “Dusty plasma”, here one can treat the system as fluid of dust grains because the rate of momentum exchange through interactions between the micro particles are much larger than that through other means like in between dust-neutral or dust-ions etc. The ratio a_d/λ_D which signify how dense is the shielded dust system in a plasma is called screening parameters κ . Smaller the value of screening parameter κ , the density of the dust system get increase and get more interactions with the neighboring dust particles. We know that potential on a shielded sphere is $\phi(r_d)/\phi_0 \approx \lambda_D/(r_d + \lambda_D)$, so the potential of the shield sphere will be greatly depressed from its vacuum value if $r_d \gg \lambda_D$. It indicates that being highly charged is not sufficient for a dust grain to have a large potential, it also require $r_d \ll \lambda_D$ [141].

Now instead of using all the multiples parameters such as the temperature T_j , the number density n_{j0} and various length scales and time scales, it is possible to represent the characteristic features of dusty plasma in term of only two param-

ters, screening parameter κ and Coulomb coupling parameter Γ . The ratio a_d/λ_D is known as screening parameter κ which takes care of density and shielding due to background plasma. Coupling parameter Γ measures the degree of interactions over the thermal motion of the ensemble of dust particles for fixed inter particle separation and background shielding κ [1, 22, 65, 66]. Mathematically Γ is given by the ratio of average coulomb potential energy (including the shielding effect) to average kinetic energy of particle in the dust system.

$$\Gamma = \frac{(Z_d e)^2}{4\pi\epsilon a_d K_b T_d} \exp\left(-\frac{a_d}{\lambda_D}\right), \quad (\text{B.3})$$

where $a_d = (3/4\pi n_d)^{1/3}$ is the Wigner-Seitz radius or mean inter-dust separation, n_d is the particle number density, $Q_d = Z_d e$ is the dust particle charge, and T_d is the equilibrium temperature. As Γ increases, the dust system changes from a nearly collisionless or only occasional binary collisions, gaseous regime for $\Gamma \ll 10$ continuously through an increasingly correlated, liquid-like regime $10 \leq \Gamma \ll 175$ to the Wigner crystallization into a lattice near $\Gamma_m \geq 175$ as shown in Fig. (1.3). The high dust charge (typically $Q \sim 10^5 e$) even at low dust temperature makes the coupling parameter $\Gamma > 1$ even at lower dust density. Thus the dusty plasmas could be found in gaseous, liquid as well as ordered crystalline phase. The phase transition occur under suitable physical conditions of the dust system. Staticly, the local density around a given particle as a function of the distance from this particle, is smooth in gases phase $\Gamma \ll 10$, and rapidly vanishes for small r because of the repulsions between the particles. As the Γ increases, positions of neighboring particles are more and more correlated, leading to a modulation of local density around a given particle. At $\Gamma \geq \Gamma_m$, the modulation or fluctuation in local density grows spontaneously into full long-range order, characteristic of a periodic crystalline structure [67, 68]. The kinematic viscosity which is system property of a fluid flows, can correlate with the coupling parameters Γ and screening parameter κ for a dust fluid flows [5, 69, 70]. It is very fortunate that most of dusty plasma are in fluid regime and thus well known fluid model can be used for flow dynamics

intuitively. As shown in Fig. (1.4), the regions where kinematic viscosity ν^* increase with decreasing Γ is in gases regime while the regions with ν^* increase with Γ is in liquid state of the dust fluid. Dusty plasma is attractive field of research because of its unique features, i.e., existence in various states of matter and the dynamics of dust particles can observed at kinetic level. This become a versatile medium which support various collective phenomena and useful for study of many fundamental physics of nature. Dusty plasma has been using as a strong medium (model system) to conduct computation and real experiments and visualized for many relevant flow process of complex flows of nature which are inherently difficult in the actual system.

B.1 Various forces on dust particles

The dynamics of charged dust clouds in a plasma are seem to account for the combined effects of various forces acting on the dust particles. Some of the dominant forces are the force due to gravity, the electrostatic and electromagnetic forces, the thermophoretic force and the ions and neutrals drag forces etc. As the scope of present thesis is to study the dynamics of a dust clouds in a shear plasma and thus the analysis of effect of various interactions with the background fields, the explicit analysis of the behavior of macroscopic particles under the action of various forces are important to characterized the dust dynamics. When several dust grains are inserted into the plasma, they are charged strongly and equally in polarity and thus repel each other. The situation, however, can be more complicated, it has been shown theoretically that at larger distances, there can be long range attractive force between the particles [6]. Thus there are a number of forces that control the dynamics of dust grains in a plasma. Some of the most important dominant forces are discussed briefly as follows.

B.1.1 Force of gravity

The dust grains introduced in plasma are relatively heavy and large sized particles compare to plasma components electrons, ions and neutral particles. Thus dust particles (with radius larger than micron $1\mu m$) in the plasma experience considerable gravity and grain to grain self-gravitational forces which are proportional to the mass density ρ_d of the dust grains. The gravity force can be written as

$$F_g = \frac{4}{3}\pi r_d^3 \rho_d g \quad (\text{B.4})$$

The force of gravity scales with the volume of the microparticle, and thus $F_g \propto r_d^3$. For a microparticle made of melamine-formaldehyde often used in complex plasma experiments with density ($\rho_d = 1510 \text{ kg/m}^3$) and radius ($r_d = 3.4 \mu m$), the strength of the force of gravity is $F_g = 2.49 \times 10^{-13} \text{ N}$ [142, 143]. The force of gravity is always directed toward the center of concern planets and conservative in nature. One way to eliminate the influence of gravity on Earth is letting the whole setup drop. Drop towers (like the one available at the University of Bremen) provide microgravity for about five seconds. Again On parabolic flights, a plane performs a flight maneuver resulting in tens of seconds of weightlessness. In Europe, an Airbus A300 is used to achieve up to 22 seconds of low gravity ($\pm 0.05 \text{ g}$). The best way to perform experiments eliminating the influence of gravity is to use the International Space Station(ISS), where good microgravity conditions are realized [3, 47, 144].

B.1.2 Thermophoretic Force

One of the possible ways to increase the upwards force against the gravity acting on the micro particles is to maintain a temperature gradient in the plasma system. In the presence of any temperature gradient ∇T of the neutrals or ions gas, the dust system feel a force F_T in the direction of $-\nabla T$, which is referred to as the thermophoretic force. The thermophoretic force acting on a spherical dust particle

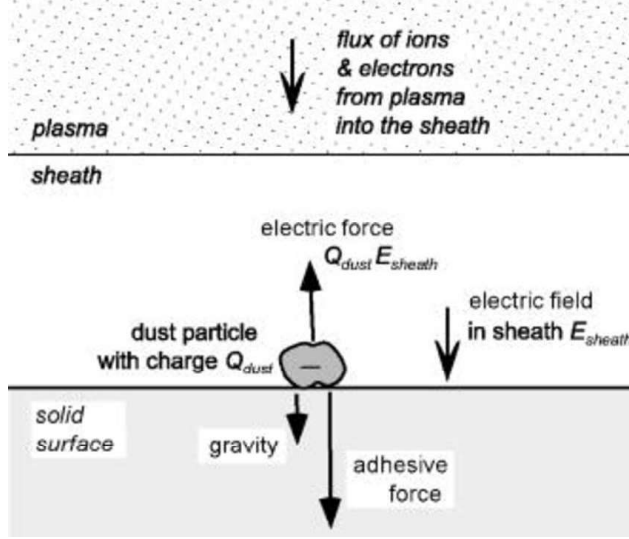


Figure B.1: Various forces on a dust particle [32].

in a monatomic gas can be written as

$$F_T = -\frac{8R^2\sqrt{2\pi}}{15v_{th}}a^2\kappa_T\nabla T_n, \quad (\text{B.5})$$

where $v_{th} = (T_n/m_n)^{1/2}$ is the average thermal speed of the neutral particles, κ_T is the translational part of the thermal conductivity. The thermophoretic forces experienced by the dust particles for a temperature gradient of $\nabla T_n \approx 1 \text{ K/cm}$ is of the order of $1.0 \times 10^{-13} \text{ N}$ [142, 143], which is bit weaker than the gravitational force. It is found that the thermophoretic force plays an essential role in the formation of different shapes of plasma-dust structures. The thermophoretic force can easily lift up micron-sized dust particles in plasmas under microgravity conditions.

B.1.3 Ion-Dragging Force

The ion-drag forces F_{di} in a plasmas arises due to collisions between (highly mobile) streaming ions and (weakly mobile) charged dust grains. The force basically describes the momentum transfer from the streaming ions to the dust particles.

Since the momentum transfer is in between the charged particles, the interactions cross section is larger than any other interactions such as charged-neutral or neutral-neutral interactions. Thus the ion-drag force is the sum of the collection and Coulomb forces, i.e $F_{di} = F_{di}^{collection} + F_{di}^{Coulomb}$. Assuming that the dust particles are at rest, the collection force is given by

$$F_{di}^{collection} = \pi b_c^2 \rho_i v_s u_i \quad (\text{B.6})$$

where $\rho_i = m_i n_i$ is the ion mass density, u_i is the ion streaming velocity, $v_s = (u_i^2 + 8T_i/\pi m_i)^{1/2}$ is the mean speed of ions approaching the dust particle, and $b_c = R(1 - 2Z_i e \phi_f / m_i v_s^2)^{1/2}$ is the maximum impact parameter for dust-ion collision from the orbital motion limited probe theory. And ϕ_f is the floating potential of the dust particles. The Coulomb force is written as

$$F_{di}^{Coulomb} = 4\pi b_{\pi/2}^2 \Gamma \rho_i v_s u_i \quad (\text{B.7})$$

where $b_{\pi/2} = q_d e / m_i v_s^2$ and $\Gamma = (1/2) \ln[(\lambda_D^2 + b_{\pi/2}^2) / (b_c^2 + b_{\pi/2}^2)]$ are the impact parameters for 90° deflection and Coulomb logarithm respectively. For a dust particle with charge $Q \sim 4 \times 10^4 e$, radius $r \sim 5 \mu m$ in plasma with $n_i \sim 10^9 \text{ cm}^{-3}$, $v_i \sim 10^4 \text{ m/sec}$, the ion dragging force is of the order of $1.0 \times 10^{-12} \text{ N}$ [142, 143]. This is among the dominant forces act on the dust clouds. This theory has been modified with more correction factors day by days.

B.1.4 Neutral-Collision Force

Assuming that the neutral molecules are at rest, the neutral drag force arises when the microparticles are moving relative to the neutral background gas, so that the momentum transferred from the grains to the neutral backgrounds. Thus the neutral drag force act as dissipating forces directed oppositely to the direction of motion of the microparticles. The neutral collision force for a Maxwellian

distribution of neutral gas molecules is approximated as follows.

$$F_{dn} = -\frac{8}{3}\sqrt{2\pi}R^2\rho_n v_{tn}(u_d - w_n) \quad (\text{B.8})$$

where $\rho_n = n_n m_n$ is the mass density of the neutral molecules, and w_n is the velocity of the neutral molecules. For a dust particle with velocity of 4 cm/sec , and neutral gas density of $3 \times 10^6 \text{ cm}^{-3}$ at a pressure of 134 Pa , the neutral friction is of the order of $1.4 \times 10^{-13} \text{ N}$ [142, 143] which is one order less than the ion dragging forces in most of the systems.

B.1.5 Electromagnetic Force

In the presence of an electric field E and magnetic field B in the plasma, the force acting on a conducting dust particle is

$$F_{em} = Q_d(E + v_d \times B) \quad (\text{B.9})$$

The charge of the microparticles is proportional to their radius, and therefore $F_{em} \propto r_d$. Inside the bulk of the discharge, the electric fields are much weaker, as they are screened by the plasma. However, the electric field is much larger in sheaths and pre-sheaths regions adjacent to the plasma wall boundaries. The electric force acting on a negatively charged dust grain is upward, away from the -ve electrodes that is on the bottom in the plasma sheath, and thus dust grains can be levitated on account of a balance between the upward electric force and downward various forces. The strength of the electrostatic forces can vary externally based on the requirement for dust confinement in the system.

For micron particles in a plasma, the dominant forces are electric forces, thermophoretic force, ion-drag force and gravity. A force balance is achieved in the plasma sheath above the electrodes where the electric field is strong enough to levitate the particles against the gravity as shown in Fig. (B.1). For larger electrodes, horizontal extended dust clouds are observed and allow to be localized by extra po-

tential such that the whole system behave like a potential well for dust system. For examples, arising a groove in the electrode[145], or electrode having a parabolic trough[146], the equipotential lines in the plasma sheath are distorted, thus yielding an additional horizontal component of the electric field force that leads to a confinement also in the horizontal plane. The self sustain plasma potential also support horizontal confinement of these negative charge particles in a plasma.

B.2 Descriptive methods for dusty plasma

The dusty plasmas, as described earlier could be found in gaseous, liquid or solid phase depending upon the combination of screening parameter κ and coupling parameter Γ . The weakly coupled dusty plasma regime ($\Gamma \ll 10$) are close to collisionless fluid(gases), the strongly couple dusty plasma with ($\Gamma \leq 100$) behave like dense fluids(liquid), and strong couple dusty plasma having ($100 \leq \Gamma \ll \Gamma_c$) behave like viscous-elastic fluid, then elastic dust crystalline for ($\Gamma \gg \Gamma_c$). At strongly coupling regime the collective motions are more often important than individual dynamics. As the state of dusty plasma is changing for different screening parameter κ and coupling parameter Γ , the system characteristics has to analysis in various possible ways. Therefor, it is important to choose appropriate model for analysis the characteristics of the dust flows depending ranges of κ and Γ and nature of studies. There are certain positive significance as well as limitations in all descriptive model.

In **Molecular Dynamic (MD) simulations** model, the exact dynamics of each particles in a system is analyzed assuming that electrons and ions are inertia less compare to heavy dust, that produce only shielding background to the dust particles. Thus dust are considered to be interacting each other through Yukawa potential[4].

$$V(r) = \frac{(Z_d e)^2}{r} \exp\left(-\frac{r}{\lambda_D}\right) \quad (\text{B.10})$$

This model is useful in all state of dusty plasma, however it is very significant for

strongly couple regimes $\Gamma \sim \Gamma_c(175)$, where dust crystalline are formed and affect of streaming ions are not much concerned in the system. There is no other model or methods better than Molecular Dynamic (MD) simulations in these regimes. However a typical dusty plasma density might be $n_d \sim 10^9$ per cm^3 . It will require few thousands of dust particles and hence are expensive in computation. Moreover, it would be very difficult or nearly impossible to see dynamics of all the constituent particles if dust particles follows a complicated nonlinear trajectories.

In few analysis where the effect of background plasma (streaming ions or neutrals) are very effective, **Particle In Cell (PIC) simulations** model is used assuming the background plasma is system of a number of fluid-elements. The charge and mass of these fluid-elements are proportionally larger than that of original plasma particles, but the ratio of charge to mass remains the same. In this model, the resolution of time scales, length scales suitable for all the multicomponent species having different mass and size are very challenging.

Fortunately, most of the dusty plasma observed in real experiments and in nature are in fluid regime, and can be explained intuitively by **Generalized Hydrodynamics** model. In the fluid model, identity of individual particle is neglected, and only the motion of fluid elements is taken into account. For dust system having wide range of coupling parameter $\Gamma \ll \Gamma_c$, the simple fluid model is applicable, even up to visco-elastic regime $100 < \Gamma < \Gamma_c$, where the solid like elastic properties have been coupled with viscous nature of dust fluid. It has been assumed that complex plasma is composed of two or more inter-penetrating fluids, one for each concern species. Each fluid will interact each other through collisions or Coulumbic interactions. Fluid model is explicitly used in this thesis work. So more detail description of this model and application in dusty plasma is explicitly discussed as follows.

Bibliography

- [1] H. Thomas, G. E. Morfill, V. Demmel, J. Goree, B. Feuerbacher, and D. Möhlmann. Plasma crystal: Coulomb crystallization in a dusty plasma. *Phys. Rev. Lett.*, 73:652–655, Aug 1994.
- [2] A. Melzer, V. A. Schweigert, I. V. Schweigert, A. Homann, S. Peters, and A. Piel. Structure and stability of the plasma crystal. *Phys. Rev. E*, 54:R46–R49, Jul 1996.
- [3] G. E. Morfill, H. M. Thomas, U. Konopka, H. Rothermel, M. Zuzic, A. Ivlev, and J. Goree. Condensed plasmas under microgravity. *Phys. Rev. Lett.*, 83:1598–1601, Aug 1999.
- [4] T. Saigo and S. Hamaguchi. Shear viscosity of strongly coupled yukawa systems. *Physics of Plasmas*, 9(4):1210–1216, 2002.
- [5] S. Hamaguchi, R. T. Farouki, and D. H. E. Dubin. Triple point of yukawa systems. *Phys. Rev. E*, 56:4671–4682, Oct 1997.
- [6] V. E. Fortov, O. S. Vaulina, O. F. Petrov, V. I. Molotkov, A. V. Chernyshev, A. M. Lipaev, G. Morfill, H. Thomas, H. Rothermel, S. A. Khrapak, Yu. P. Semenov, A. I. Ivanov, S. K. Krikalev, and Yu. P. Gidzenko. Dynamics of macroparticles in a dusty plasma under microgravity conditions (first experiments on board the iss). *Journal of Experimental and Theoretical Physics*, 96(4):704–718, 2003.
- [7] O. S. Vaulina, A. A. Samarian, O. F. Petrov, B. James, and F. Melandso. Formation of vortex dust structures in inhomogeneous gas-discharge plasmas. *Plasma Physics Reports*, 30(11):918–936, 2004.
- [8] Yoshifumi Saitou and Osamu Ishihara. Dynamic circulation in a complex plasma. *Phys. Rev. Lett.*, 111:185003, Nov 2013.
- [9] H M Thomas, G E Morfill, V E Fortov, A V Ivlev, V I Molotkov, A M Lipaev, T Hagl, H Rothermel, S A Khrapak, R K Suetterlin, M Rubin-Zuzic, O F Petrov, V I Tokarev, and S K Krikalev. Complex plasma laboratory pk-3 plus

- on the international space station. *New Journal of Physics*, 10(3):033036, 2008.
- [10] V N Tsytovich, G Morfill, U Konopka, and H Thomas. Collision-dominated dust sheaths and voids - observations in micro-gravity experiments and numerical investigation of the force balance relations. *New Journal of Physics*, 5(1):66, 2003.
- [11] Manjit Kaur, Sayak Bose, P. K. Chattopadhyay, Devendra Sharma, J. Ghosh, and Y. C. Saxena. Observation of dust torus with poloidal rotation in direct current glow discharge plasma. *Physics of Plasmas*, 22(3):033703, 2015.
- [12] Manjit Kaur, Sayak Bose, P. K. Chattopadhyay, D. Sharma, J. Ghosh, Y. C. Saxena, and Edward Thomas Jr. Generation of multiple toroidal dust vortices by a non-monotonic density gradient in a direct current glow discharge plasma. *Physics of Plasmas*, 22(9):093702, 2015.
- [13] Mangilal Choudhary, S. Mukherjee, and P. Bandyopadhyay. Experimental observation of self excited co-rotating multiple vortices in a dusty plasma with inhomogeneous plasma background. *Physics of Plasmas*, 24(3):033703, 2017.
- [14] Lukas Holzer, Jochen Bammert, Roland Rzehak, and Walter Zimmermann. Dynamics of a trapped brownian particle in shear flows. *Phys. Rev. E*, 81:041124, Apr 2010.
- [15] Siegfried Grossmann. The onset of shear flow turbulence. *Rev. Mod. Phys.*, 72:603–618, Apr 2000.
- [16] E. Lauga and T. R. Powers. *Rep. Prog. Phys.*, 79, 2008.
- [17] Charles W. Wolgemuth. Collective swimming and the dynamics of bacterial turbulence. *Biophysical Journal*, 95(4):1564 – 1574, 2008.
- [18] L. Pan, A. Morozov, C. Wagner, and P. E. Arratia. Nonlinear elastic instability in channel flows at low reynolds numbers. *Phys. Rev. Lett.*, 110:174502, Apr 2013.

- [19] Edwards Thayne Helton Kristen Yager, Paul and Bernhard H. Microfluidic diagnostic technologies for global public health. *Nature (London)*, 442:412–418, July 2006.
- [20] Todd M. Squires and Stephen R. Quake. Microfluidics: Fluid physics at the nanoliter scale. *Rev. Mod. Phys.*, 77:977–1026, Oct 2005.
- [21] Abraham D. Stroock, Stephan K. W. Dertinger, Armand Ajdari, Igor Mezić, Howard A. Stone, and George M. Whitesides. Chaotic mixer for microchannels. *Science*, 295(5555):647–651, 2002.
- [22] P.K. Shukla and A.A. Mamun. *Introduction to Dusty Plasma Physics*. Series in Plasma Physics. CRC Press, 2015.
- [23] L.D. Landau and E.M. Lifshitz. *Fluid Mechanics*. Number v. 6. Elsevier Science, 2013.
- [24] Modhuchandra Laishram, Devendra Sharma, and Predhiman K. Kaw. Dynamics of a confined dusty fluid in a sheared ion flow. *Physics of Plasmas*, 21(7):073703, 2014.
- [25] Modhuchandra Laishram, Devendra Sharma, and Predhiman K. Kaw. Analytic structure of a drag-driven confined dust vortex flow in plasma. *Phys. Rev. E*, 91:063110, Jun 2015.
- [26] Modhuchandra Laishram, Devendra Sharma, Prabal K. Chattopdhyay, and Predhiman K. Kaw. Nonlinear effects in the bounded dust-vortex flow in plasma. *Phys. Rev. E*, 95:033204, Mar 2017.
- [27] G. K. Batchelor. On steady laminar flow with closed streamlines at large reynolds number. *Journal of Fluid Mechanics*, 1(2):177–190, 1956.
- [28] Benjamin Pfeuty and Kuniyoshi Kaneko. Minimal requirements for robust cell size control in eukaryotic cells. *Physical Biology*, 4(3):194, 2007.
- [29] S. Mitic, R. Sütterlin, A. V. Ivlev H. Höfner, M. H. Thoma, S. Zhdanov, and G. E. Morfill. Convective dust clouds driven by thermal creep in a complex plasma. *Phys. Rev. Lett.*, 101:235001, Dec 2008.

- [30] M. A. Fink, S. K. Zhdanov, M. H. Thoma, H. Höfner, and G. E. Morfill. Pearl-necklace-like structures of microparticle strings observed in a dc complex plasma. *Phys. Rev. E*, 86:065401, Dec 2012.
- [31] Ashwin R. Vasavada, Andrew P. Ingersoll, Don Banfield, Maureen Bell, Peter J. Gierasch, Michael J.S. Belton, Glenn S. Orton, Kenneth P. Klaasen, Eric DeJong, H.Herbert Breneman, Todd J. Jones, James M. Kaufman, Kari P. Magee, and David A. Senske. Galileo imaging of jupiter’s atmosphere: The great red spot, equatorial region, and white ovals. *Icarus*, 135(1):265 – 275, 1998.
- [32] T. M. Flanagan and J. Goree. Dust release from surfaces exposed to plasma. *Physics of Plasmas*, 13(12):123504, 2006.
- [33] N. N. Bogoliubov. Kinetic equations. *Journal of Physics USSR*, 10(3):265, 1949.
- [34] John G Kirkwood. The statistical mechanical theory of transport processes i. general theory. *The Journal of Chemical Physics*, 14(3):180–201, 1946.
- [35] Max Born and HS Green. A general kinetic theory of liquids. i. the molecular distribution functions. *Proceedings of the Royal Society of London. Series A, Mathematical and Physical Sciences*, pages 10–18, 1946.
- [36] N.A. Krall and A.W. Trivelpiece. *Principles of plasma physics*. Number v. 0-911351 in International series in pure and applied physics. McGraw-Hill, 1973.
- [37] H. Grad. *Thermo-dynamik der Gase/Thermodynamics of Gases*. Springer, Berlin, 1958.
- [38] S. Chapman and T.G. Cowling. *The Mathematical Theory of Non-uniform Gases: An Account of the Kinetic Theory of Viscosity, Thermal Conduction and Diffusion in Gases*. Cambridge Mathematical Library. Cambridge University Press, 1970.
- [39] S. I. Braginskii. *Rev. Plasma Phys.*, 1:205, 1965.

- [40] Narendra Singh and Amit Agrawal. Onsager’s-principle-consistent 13-moment transport equations. *Phys. Rev. E*, 93:063111, 2016.
- [41] Edward Thomas Jr. Direct measurements of two-dimensional velocity profiles in direct current glow discharge dusty plasmas. *Physics of Plasmas*, 6(7):2672–2675, 1999.
- [42] Edward Thomas Jr. Measurements of spatially growing dust acoustic waves in a dc glow discharge plasma. *Physics of Plasmas*, 13(4):042107, 2006.
- [43] Prigogine and R. Balescu. *Acad. Roy. Belg. Bull. Clin. Sci.*, 41:917, 1955.
- [44] P. Glansdorff and I. Prigogine. Sur les propriétés différentielles de la production d’entropie. *Physica*, 20, 1954.
- [45] J-M. Andr. What is life: non-equilibrium thermodynamics, dissipative structures, bifurcations, chaos, and evolution. *Revue des Questions Scientifiques*, 177:323–346, 2006.
- [46] A. Einstein. Über die von der molekularkinetischen theorie der wärme geforderte bewegung von in ruhenden flüssigkeiten suspendierten teilchen. *Annalen der Physik*, 322(8):549–560, 1905.
- [47] Anatoli P Nefedov, Gregor E Morfill, Vladimir E Fortov, Hubertus M Thomas, Hermann Rothermel, Tanja Hagl, Alexei V Ivlev, Milenko Zuzic, Boris A Klumov, Andrey M Lipaev, Vladimir I Molotkov, Oleg F Petrov, Yuri P Gidzenko, Sergey K Krikalev, William Shepherd, Alexandr I Ivanov, Maria Roth, Horst Binnenbruck, John A Goree, and Yuri P Semenov. Pke-nefedov: plasma crystal experiments on the international space station. *New Journal of Physics*, 5(1):33, 2003.
- [48] Gregor E. Morfill, Milenko Rubin-Zuzic, Hermann Rothermel, Alexei V. Ivlev, Boris A. Klumov, Hubertus M. Thomas, Uwe Konopka, and Victor Steinberg. Highly resolved fluid flows: “liquid plasmas” at the kinetic level. *Phys. Rev. Lett.*, 92:175004, Apr 2004.
- [49] Milenko Rubin-Zuzic, Hubertus M Thomas, Sergej K Zhdanov, and Gregor E Morfill. Circulation’ dynamo in complex plasma. *New Journal of Physics*, 9(2):39, 2007.

BIBLIOGRAPHY

- [50] Jean-Marie Andr  . What is life: non-equilibrium thermodynamics, dissipative structures, bifurcations, chaos, and evolution. *Revue des Questions Scientifiques*, 177(3-4):323–346, 2006. Publication code : RES. ACAD.
- [51] H. Thomas, G. E. Morfill, V. Demmel, J. Goree, B. Feuerbacher, and D. Mohlmann. *Phys. Rev. Lett.*, 73:652–655, 1994.
- [52] H. Ikezi. Coulomb solid of small particles in plasmas. *The Physics of Fluids*, 29(6):1764–1766, 1986.
- [53] O. Arp, D. Block, M. Klindworth, and A. Piel. Confinement of coulomb balls. *Physics of Plasmas*, 12(12):122102, 2005.
- [54] P. K. Kaw and A. Sen. In G. J. Kalman, J. M. Rommel, and K. B. Blagoev, editors, *Strongly Coupled Coulomb Systems*. Plenum, New York, 1998.
- [55] KN Margaritis and Richard Anthony Black. Modelling the lymphatic system: challenges and opportunities. *Journal of The Royal Society Interface*, 9(69):601–612, 2012.
- [56] Marcus and Philip S. Numerical simulation of jupiter’s great red spot. *Nature (London)*, 331:693–696, Feb 1988.
- [57] Wallace F. Marshall, Kevin D. Young, Matthew Swaffer, Elizabeth Wood, Paul Nurse, Akatsuki Kimura, Joseph Frankel, John Wallingford, Virginia Walbot, Xian Qu, and Adrienne HK Roeder. What determines cell size? *BMC Biology*, 10(1):101, 2012.
- [58] Jonathan  J. Turner, Jennifer  C. Ewald, and Jan  M. Skotheim. Cell size control in yeast. *Current Biology*, 22(9):R350 – R359, 2012.
- [59] Nicole Meyer-Vernet and Jean-Pierre Rospars. Maximum relative speeds of living organisms: Why do bacteria perform as fast as ostriches? *Physical Biology*, 13(6):066006, 2016.
- [60] F.F. Chen. *Introduction to Plasma Physics and Controlled Fusion*. Springer International Publishing, 2015.

- [61] J.A. Bittencourt. *Fundamentals of Plasma Physics*. Springer New York, 2004.
- [62] Susmita Sarkar and Saumyen Maity. Role of positively charged dust grains on dust acoustic wave propagation in presence of nonthermal ions. *Physics of Plasmas*, 20(8), 2013.
- [63] Chunshi Cui and J Goree. Fluctuations of the charge on a dust grain in a plasma. *IEEE Transactions on plasma science*, 22(2):151–158, 1994.
- [64] André Melzer and John Goree. 6 fundamentals of dusty plasmas, 2008.
- [65] P. Bandyopadhyay, G. Prasad, A. Sen, and P.K. Kaw. Driven transverse shear waves in a strongly coupled dusty plasma. *Physics Letters A*, 372(33):5467 – 5470, 2008.
- [66] M. S. Murillo. Using fermi statistics to create strongly coupled ion plasmas in atom traps. *Phys. Rev. Lett.*, 87:115003, Aug 2001.
- [67] Marc Baus and Jean-Pierre Hansen. Statistical mechanics of simple coulomb systems. *Physics Reports*, 59(1):1 – 94, 1980.
- [68] T. S. Strickler, T. K. Langin, P. McQuillen, J. Daligault, and T. C. Killian. Experimental measurement of self-diffusion in a strongly coupled plasma. *Phys. Rev. X*, 6:021021, May 2016.
- [69] T. Saigo and S. Hamaguchi. Shear viscosity of strongly coupled yukawa systems. *Physics of Plasmas*, 9(4), 2002.
- [70] V. E. Fortov, O. F. Petrov, O. S. Vaulina, and R. A. Timirkhanov. Viscosity of a strongly coupled dust component in a weakly ionized plasma. *Phys. Rev. Lett.*, 109:055002, Aug 2012.
- [71] C. J. Mitchell, M. Horányi, O. Havnes, and C. C. Porco. Saturn’s spokes: Lost and found. *Science*, 311(5767):1587–1589, 2006.
- [72] Colleen A. McGhee, Richard G. French, Luke Dones, Jeffrey N. Cuzzi, Heikki J. Salo, and Rebecca Danos. {HST} observations of spokes in saturn’s b ring. *Icarus*, 173(2):508 – 521, 2005.

BIBLIOGRAPHY

- [73] Vadim N Tsytovich and J Winter. On the role of dust in fusion devices. *Physics-Uspekhi*, 41(8):815, 1998.
- [74] K. Narihara, K. Toi, Y. Hamada, K. Yamauchi, K. Adachi, I. Yamada, K.N. Sato, K. Kawahata, A. Nishizawa, S. Ohdachi, K. Sato, T. Seki, T. Watari, J. Xu, A. Ejiri, S. Hirokura, K. Ida, Y. Kawasumi, M. Kojima, H. Sakakita, T. Ido, K. Kitachi, J. Koog, and H. Kuramoto. Observation of dust particles by a laser scattering method in the jippt-iiu tokamak. *Nuclear Fusion*, 37(8):1177, 1997.
- [75] J Winter. Dust in fusion devices - experimental evidence, possible sources and consequences. *Plasma Physics and Controlled Fusion*, 40(6):1201, 1998.
- [76] Andrea Malizia, Luigi Antonio Poggi, Jean-François Ciparisse, Riccardo Rossi, Carlo Bellecci, and Pasquale Gaudio. A review of dangerous dust in fusion reactors: from its creation to its resuspension in case of loca and lova. *Energies*, 9(8):578, 2016.
- [77] Editors. *Nucl. Fusion*, 39:2137, 1999.
- [78] XZ Tang and GL Delzanno. Dust divertor for a tokamak fusion reactor. *Journal of fusion energy*, 29(5):407–411, 2010.
- [79] BV Kuteev, V Yu Sergeev, SV Krylov, VG Skokov, and VM Timokhin. Conceptual analysis of a tokamak reactor with lithium dust jet. *Nuclear Fusion*, 50(7):075001, 2010.
- [80] LaËrfa Boufendi and AndrÄl Bouchoule. Industrial developments of scientific insights in dusty plasmas. *Plasma Sources Science and Technology*, 11(3A):A211, 2002.
- [81] Robert L Merlino. Dusty plasmas and applications in space and industry. *Plasma Physics Applied*, 81:73–110, 2006.
- [82] AV Ivlev, GE Morfill, V Nosenko, R Pompl, M Rubin-Zuzic, and HM Thomas. Fluid complex plasmas—studies at the particle level. In *COMPLEX SYSTEMS: 5th International Workshop on Complex Systems*, volume 982, pages 577–583. AIP Publishing, 2008.

- [83] Pei-San Tu, Chia-Ling Chan, Lee-Weng Teng, Wei-Yen Woon, and Lin I. 2d dusty plasma liquids in mesoscopic channels. *Physica Scripta*, 2004(T107):98, 2004.
- [84] G. Iooss and D.D. Joseph. *Elementary Stability and Bifurcation Theory*. Undergraduate Texts in Mathematics. Springer New York, 2012.
- [85] John C Rutledge, AE Mullick, G Gardner, and IJ Goldberg. Direct visualization of lipid deposition and reverse lipid transport in a perfused artery. *Circulation research*, 86(7):768–773, 2000.
- [86] Adel M Malek, Seth L Alper, and Seigo Izumo. Hemodynamic shear stress and its role in atherosclerosis. *Jama*, 282(21):2035–2042, 1999.
- [87] M. Puttscher and A. Melzer. Dust particles under the influence of crossed electric and magnetic fields in the sheath of an rf discharge. *Physics of Plasmas*, 21(12):123704, 2014.
- [88] Predhiman K. Kaw, Kyoji Nishikawa, and Noriyoshi Sato. Rotation in collisional strongly coupled dusty plasmas in a magnetic field. *Physics of Plasmas*, 9(2):387–390, 2002.
- [89] Noriyoshi Sato, Giichiro Uchida, Toshiro Kaneko, Shinya Shimizu, and Satoru Iizuka. Dynamics of fine particles in magnetized plasmas. *Physics of Plasmas (1994-present)*, 8(5):1786–1790, 2001.
- [90] Felix Cheung, Alex Samarian, and Brian James. The rotation of planar-2 to planar-12 dust clusters in an axial magnetic field. *New Journal of Physics*, 5(1):75, 2003.
- [91] Jan Carstensen, Franko Greiner, Lu-Jing Hou, Horst Maurer, and Alexander Piel. Effect of neutral gas motion on the rotation of dust clusters in an axial magnetic field. *Physics of Plasmas (1994-present)*, 16(1):013702, 2009.
- [92] Edward Thomas Jr., Uwe Konopka, Brian Lynch, Stephen Adams, Spencer LeBlanc, Robert L. Merlino, and Marlene Rosenberg. Quasi-discrete particle motion in an externally imposed, ordered structure in a dusty plasma at high magnetic field. *Physics of Plasmas*, 22(11):113708, 2015.

BIBLIOGRAPHY

- [93] E. Thomas, U. Konopka, D. Artis, B. Lynch, S. Leblanc, S. Adams, R. L. Merlino, and M. Rosenberg. The magnetized dusty plasma experiment (mdpx). *Journal of Plasma Physics*, 81(2), 2015.
- [94] Giichiro Uchida, Satoru Iizuka, Tetsuo Kamimura, and Noriyoshi Sato. Generation of two-dimensional dust vortex flows in a direct current discharge plasma. *Physics of Plasmas (1994-present)*, 16(5):053707, 2009.
- [95] M. Klindworth, A. Melzer, A. Piel, and V. A. Schweigert. Laser-excited intershell rotation of finite coulomb clusters in a dusty plasma. *Phys. Rev. B*, 61:8404–8410, Mar 2000.
- [96] Tobias Miksch and André Melzer. Fluorescent microspheres as tracer particles in dusty plasmas. *Phys. Rev. E*, 75:016404, Jan 2007.
- [97] V. I. Vladimirov, L. V. Deputatova, A. P. Nefedov, V. E. Fortov, V. A. Rykov, and A. V. Khudyakov. Dust vortices, clouds, and jets in nuclear-induced plasmas. *Journal of Experimental and Theoretical Physics*, 93(2):313–323, 2001.
- [98] DA Law, WH Steel, BM Annaratone, and JE Allen. Probe-induced particle circulation in a plasma crystal. *Physical review letters*, 80(19):4189, 1998.
- [99] OS Vaulina, AA Samarian, AP Nefedov, and VE Fortov. Self-excited motion of dust particles in a inhomogeneous plasma. *Physics Letters A*, 289(4):240–244, 2001.
- [100] OS Vaulina, AA Samarian, OF Petrov, BW James, and VE Fortov. Self-excited motions in dusty plasmas with gradient of charge of macroparticles. *New Journal of Physics*, 5(1):82, 2003.
- [101] A Samarian, O Vaulina, W Tsang, and BW James. Formation of vertical and horizontal dust vortexes in an rf-discharge plasma. *Physica Scripta*, 2002(T98):123, 2002.
- [102] M Schwabe, LJ Hou, S Zhdanov, AV Ivlev, HM Thomas, and GE Morfill. Convection in a dusty radio-frequency plasma under the influence of a thermal gradient. *New Journal of Physics*, 13(8):083034, 2011.

- [103] V. N. Tsytovich, S. V. Vladimirov, O. S. Vaulina, O. F. Petrov, and V. E. Fortov. Theory of dust self-organized convection in cylindrical discharges. i. the model and stationary nonlinear dust structures. *Physics of Plasmas*, 13(3):032305, 2006.
- [104] S Mitic, R Sütterlin, AV Ivlev H Höfner, MH Thoma, S Zhdanov, and GE Morfill. Convective dust clouds driven by thermal creep in a complex plasma. *Physical review letters*, 101(23):235001, 2008.
- [105] Tim Bockwoldt, Oliver Arp, Kristoffer Ole Menzel, and Alexander Piel. On the origin of dust vortices in complex plasmas under microgravity conditions. *Physics of Plasmas (1994-present)*, 21(10):103703, 2014.
- [106] Kil-Byoung Chai and Paul M. Bellan. Vortex motion of dust particles due to non-conservative ion drag force in a plasma. *Physics of Plasmas*, 23(2):023701, 2016.
- [107] Michael A Dopita, Charlene Heisler, Stuart Lumsden, and Jeremy Bailey. Probing the dusty accretion torus of seyfert galaxies. *The Astrophysical Journal*, 498(2):570, 1998.
- [108] CK Goertz. Dusty plasmas in the solar system. *Reviews of Geophysics*, 27(2):271–292, 1989.
- [109] Juan P. Hernandez-Ortiz, Christopher G. Stoltz, and Michael D. Graham. Transport and collective dynamics in suspensions of confined swimming particles. *Phys. Rev. Lett.*, 95:204501, Nov 2005.
- [110] Nivedita Nivedita and Ian Papautsky. Continuous separation of blood cells in spiral microfluidic devices. *Biomicrofluidics*, 7(5):054101, 2013.
- [111] Jacopo Biasetti, Pier Giorgio Spazzini, Ulf Hedin, and T. Christian Gasser. Synergy between shear-induced migration and secondary flows on red blood cells transport in arteries: considerations on oxygen transport. *Journal of The Royal Society Interface*, 11(97), 2014.
- [112] James P Gleeson. Transient micromixing: examples of laminar and chaotic stirring. *Physics of Fluids (1994-present)*, 17(10):100614, 2005.

BIBLIOGRAPHY

- [113] Siddhartha Tripathi, Y. V. BalaVarun Kumar, Amit Agrawal, Amit Prabhakar, and Suhas S. Joshi. Microdevice for plasma separation from whole human blood using bio- physical and geometrical effects. *Scientific Reports*, 6:26749, 2016.
- [114] A Salih. Conservation equations of fluid dynamics. 2011.
- [115] Dan S Henningson. Martin berggren august 24, 2005. 2005.
- [116] P. K. Kaw and A. Sen. Low frequency modes in strongly coupled dusty plasmas. *Physics of Plasmas*, 5(10):3552–3559, 1998.
- [117] Mohsen Jahanmiri. Particle image velocimetry: Fundamentals and its applications. Technical report, Chalmers University of Technology, 2011.
- [118] Gregor E. Morfill and Alexei V. Ivlev. Complex plasmas: An interdisciplinary research field. *Rev. Mod. Phys.*, 81:1353–1404, Oct 2009.
- [119] N.N. Rao, P.K. Shukla, and M.Y. Yu. Dust-acoustic waves in dusty plasmas. *Planetary and Space Science*, 38(4):543 – 546, 1990.
- [120] S. Mitic, B. A. Klumov, U. Konopka, M. H. Thoma, and G. E. Morfill. Structural properties of complex plasmas in a homogeneous dc discharge. *Phys. Rev. Lett.*, 101:125002, Sep 2008.
- [121] M. A. Fink, S. K. Zhdanov, M. Schwabe, M. H. Thoma, H. HÄufner, H. M. Thomas, and G. E. Morfill. Autowaves in a dc complex plasma confined behind a de laval nozzle. *EPL (Europhysics Letters)*, 102(4):45001, 2013.
- [122] O. Arp, D. Block, M. Klindworth, and A. Piel. Confinement of coulomb balls. *Physics of Plasmas*, 12(12), 2005.
- [123] Yingxi Zhu and Steve Granick. Limits of the hydrodynamic no-slip boundary condition. *Phys. Rev. Lett.*, 88:106102, Feb 2002.
- [124] Michael S. Barnes, John H. Keller, John C. Forster, James A. O’Neill, and D. Keith Coultas. Transport of dust particles in glow-discharge plasmas. *Phys. Rev. Lett.*, 68:313–316, Jan 1992.

- [125] S. A. Khrapak, A. V. Ivlev, G. E. Morfill, and H. M. Thomas. Ion drag force in complex plasmas. *Phys. Rev. E*, 66:046414, Oct 2002.
- [126] A. V. Ivlev, S. A. Khrapak, S. K. Zhdanov, G. E. Morfill, and G. Joyce. Force on a charged test particle in a collisional flowing plasma. *Phys. Rev. Lett.*, 92:205007, May 2004.
- [127] S.S. SASTRY. *INTRODUCTORY METHODS OF NUMERICAL ANALYSIS*. PHI Learning, 2012.
- [128] E. Balagurusamy. *Numerical methods*. TATA McGraw-Hill, 1999.
- [129] William H Press. *The art of scientific computing*. Cambridge university press, 1992.
- [130] Gwenaël Salin and Jean-Michel Caillol. Transport coefficients of the yukawa one-component plasma. *Phys. Rev. Lett.*, 88:065002, Jan 2002.
- [131] Yan Feng, J. Goree, and Bin Liu. Observation of temperature peaks due to strong viscous heating in a dusty plasma flow. *Phys. Rev. Lett.*, 109:185002, Oct 2012.
- [132] Yue-Kin Tsang, Edward Ott, Thomas M. Antonsen, and Parvez N. Guzdar. Intermittency in two-dimensional turbulence with drag. *Phys. Rev. E*, 71:066313, Jun 2005.
- [133] Robert H. Kraichnan. Inertial ranges in two-dimensional turbulence. *Physics of Fluids*, 10(7), 1967.
- [134] B. D. Scott. In A. Dinklage, Thomas Klinger, Garrit Marx, and L. Schweikhard, editors, *Plasma Physics, Confinement, Transport and Collective Effects*, chapter 8. Springer, Berlin Heidelberg, 2005.
- [135] Mierk Schwabe, Sergey Zhdanov, Christoph R  th, David B. Graves, Hubertus M. Thomas, and Gregor E. Morfill. Collective effects in vortex movements in complex plasmas. *Phys. Rev. Lett.*, 112:115002, Mar 2014.
- [136] O. A. Oleinik and V. N. Samokhin. Mathematical models in boundary layer theory. *Chapman and Hall, London*, 1999.

BIBLIOGRAPHY

- [137] Michael Ghil, Jian-Guo Liu, Cheng Wang, and Shouhong Wang. Boundary-layer separation and adverse pressure gradient for 2-d viscous incompressible flow. *Physica D: Nonlinear Phenomena*, 197(1&A2):149 – 173, 2004.
- [138] Shouhong Wang Michael Ghil, Tian Ma. Structural bifurcation of 2-d incompressible flows. *Indiana Univ. Math. J.*, 50:159–180, 2001.
- [139] Akanksha Gupta, Rajaraman Ganesh, and Ashwin Joy. Kolmogorov flow in two dimensional strongly coupled yukawa liquid: A molecular dynamics study. *Physics of Plasmas*, 22(10):103706, 2015.
- [140] P. K. Shukla. A survey of dusty plasma physics. *Physics of Plasmas*, 8(5), 2001.
- [141] P. M. Bellan. A model for the condensation of a dusty plasma. *Physics of Plasmas*, 11(7), 2004.
- [142] A Barkan and RL Merlino. Confinement of dust particles in a double layer. *Physics of Plasmas*, 2(9):3261–3265, 1995.
- [143] Mikhail A. Belyaev and Roman R. Rafikov. The dynamics of dust grains in the outer solar system. *The Astrophysical Journal*, 723(2):1718, 2010.
- [144] Hubertus M. Thomas, Gregor E. Morfill, Alexei V. Ivlev, Anatoli P. Nefedov, Vladimir E. Fortov, Hermann Rothermel, Milenko Rubin-Zuzic, Andrey M. Lipaev, Vladimir I. Molotkov, and Oleg F. Petrov. Pke-nefedov — complex plasma research on the international space station. *Microgravity - Science and Technology*, 16(1):317–321, 2005.
- [145] Bin Liu, K. Avinash, and J. Goree. Characterizing potentials using the structure of a one-dimensional chain demonstrated using a dusty plasma crystal. *Phys. Rev. E*, 69:036410, Mar 2004.
- [146] A. Melzer. Mode spectra of thermally excited two-dimensional dust coulomb clusters. *Phys. Rev. E*, 67:016411, Jan 2003.